Models, Algorithms and Architectures for Cooperative Manipulation with Aerial and Ground Robots

Nicolas Staub

THÈSE

En vue de l'obtention du

DOCTORAT DE L'UNIVERSITÉ DE TOULOUSE

Délivré par : *l'Université Toulouse 3 Paul Sabatier (UT3 Paul Sabatier)*

Présentée et soutenue le *17/01/2018* **par :**

Nicolas STAUB

Models, Algorithms and Architectures for Cooperative Manipulation with Aerial and Ground Robots

---

JURY

Anibal OLLERO	Professeur	Rapporteur
Philippe FRAISSE	Professeur	Rapporteur
Sandra HIRCHE	Professeur	Examinateur
Simon LACROIX	Directeur de Recherche	Examinateur
Paolo ROBUFFO GIORDANO	Directeur de Recherche	Examinateur
Antonio FRANCHI	Chercheur CNRS	Directeur de thèse

École doctorale et spécialité :
EDSYS : Robotique 4200046

Unité de Recherche :
Laboratoire d'Analyse et d'Architecture des Systèmes (LAAS–CNRS)

Directeur de Thèse :
Antonio FRANCHI

Rapporteurs :
Anibal OLLERO et *Philippe FRAISSE*

Acknowledgments

First, I would like to express my sincere gratitude to Dr. Antonio Fanchi, my thesis supervisor, for his guidance and availability during the course of my PhD. His work dedication and enthusiasm was a daily inspiration. A warm thanks also go to the LAAS–CNRS, my hosting lab, and its people, in particular to the RIS group for making this research possible and providing a fantastic work environment.

I would like to thank the jury members for taking part in my defense and providing stimulating questions and discussions about my work and its perspectives. In particular, I am most grateful to the two reviewers, Pr. Anibal Ollero and Pr. Philippe Fraisse, for their invaluable feedbacks on my work.

I would like to express my deepest gratitude to Pr. Dongjun Lee, for hosting me six months at Seoul National University in South Korea. This stay was a life experience both from the research perspective and from the personal one. I would also thank all the students from the INROL lab for their warm welcome and their help to settle. In particular Hyunsoo and Changsu for their kindness and guidance.

This journey would not have been the same without all the people around. A warm thanks goes to Matthieu Herrb and Anthony Mallet for their constant support and guidance. My warmest thanks go to Marco, for all the insightful discussions but also for all the moments in and out the lab that we shared. I am deeply in debt to Burak as well, for his guidances and enthousiam during our joint work at the beginning of my PhD life and for his warm friendship. My gratitude also goes towards Davide for is invaluable work and support during our joint project, especially the insane rush toward Hanover. I want to thank Quentin for sharing French humor with me during the most stressful part of my PhD and for his dedication to making things work. I would also like to express my gratitude to all the other students met other the years, for more or less serious discussions. Special thanks go to Kevin, Cécile and Aïva for the invaluable coffee breaks and discussions.

I would take the opportunity to thank everyone from the KUKA 2017 Innovation Award, which made the Tele-MAGMaS demonstration possible. The KUKA IA team for their unwavering support during the installation week in Hanover. All the members of the Tele-MAGMaS team for being part of it and for their contributions. Especially those present in Hanover for the installation and demonstration. My sincere gratitude goes to Mostafa who managed to finish is PhD concurrently to being heavily involved in the project.

Lastly, I would like to express my deepest gratitude to my family and friends for their support and encouragements in this journey. My parents for their unconditional love and for transmitting me this eagerness toward sciences and techniques, always supporting it. My brother for the jokes and discussions we shared along the way. My friends, in and out of the lab, who were around and oversaw my PhD life, their constant support and encouragements proved invaluable. I would like to thank my flatmates for being there every day, especially Pierrick with whom I navigated the PhD life.

And of course the last word for *Franzi*, who provides sparkles in my life and an oasis of calm when it is most needed, thank you for being on my side.

Abstract

In recent years, the subject of *physical interaction for aerial robots* has been a popular research area with many new mechanical designs and control approaches being proposed. The *aerial robotics* community is currently observing a paradigm shift from classic guidance, navigation, and control tasks towards more unusual tasks, for example requesting *aerial robots* to physically interact with the environment, thus extending the manipulation task from the ground into the air. This thesis contributes to the field of *aerial manipulation* by proposing a novel concept known has *Multiple Aerial-Ground Manipulator System* or *MAGMaS*, including what appears to be the first experimental demonstration of a MAGMaS and opening a new route of research.

The motivation behind associating ground and aerial robots for cooperative manipulation is to leverage their respective particularities, ground robots bring strength while aerial robots widen the workspace of the system. The first contribution of this work introduces a meticulous system model for MAGMaS. The system model's properties and potential extensions are discussed in this work. The planning, estimation and control methods which are necessary to exploit MAGMaS in a cooperative manipulation tasks are derived. This works proposes an optimal control allocation scheme to exploit the MAGMaS redundancies and a general model-based force estimation method is presented. All of the proposed techniques reported in this thesis are integrated in a global architecture used for simulations and experimental validation. This architecture is extended by the addition of a tele-presence framework to allow remote operations of MAGMaS. The global architecture is validated by robust demonstrations of bar lifting, an application that gives an outlook of the prospective use of the proposed concept of MAGMaS. Another contribution in the development of MAGMaS consists of an exploratory study on the flexibility of manipulated loads. A vibration model is derived and exploited to showcase vibration properties in terms of control.

The last contribution of this thesis consists of an exploratory study on the use of elastic joints in aerial robots, endowing these systems with mechanical compliance and energy storage capabilities. Theoretical groundings are associated with a nonlinear controller synthesis. The proposed approach is validated by experimental work which relies on the integration of a lightweight variable stiffness actuator on an aerial robot.

Keywords

Cyber-physical systems – Aerial manipulation systems – Shared control – Non-linear control and estimation – Manipulation with compliant actuators

Résumé

Les dernières années ont vu le développement de recherches portant sur l'interaction physique entre les robots aériens et leur environnement, accompagné de l'apparition de nombreux nouveaux systèmes mécaniques et approches de régulation. La communauté centrée autour de la robotique aérienne observe actuellement un déplacement de paradigmes des approches classiques de guidage, de navigation et de régulation vers des tâches moins triviales, telle le développement de l'interaction physique entre robots aériens et leur environnement. Ceci correspond à une extension des tâches dites de manipulation, du sol vers les airs. Cette thèse contribue au domaine de la manipulation aérienne en proposant un nouveau concept appelé MAGMaS, pour « Multiple Aerial Ground Manipulator System ».

Les motivations qui ont conduites à l'association de manipulateurs terrestres et aériens pour effectuer des tâches de manipulation coopérative, résident dans une volonté d'exploiter leurs particularités respectives. Les manipulateurs terrestres apportant leur importante force et les manipulateurs aériens apportant leur vaste espace de travail. La première contribution de cette thèse présente une modélisation rigoureuse des MAGMaS. Les propriétés du système ainsi que ses possibles extensions sont discutées. Les méthodes de planning, d'estimation et de régulation nécessaire à l'exploitation des MAGMaS pour des tâches de manipulation collaborative sont dérivées. Ce travail propose d'exploiter les redondances des MAGMaS grâce à un algorithme optimal d'allocation de forces entre les manipulateurs. De plus, une méthode générale d'estimation de forces pour robots aériens est introduite. Toutes les techniques et les algorithmes présentés dans cette thèse sont intégrés dans une architecture globale, utilisée à la fois pour la simulation et la validation expérimentale. Cette architecture est en outre augmentée par l'addition d'une structure de télé-présence, afin de permettre l'opération à distances des MAGMaS. L'architecture générale est validée par une démonstration de levage de barre, qui est une application représentative des potentiels usages des MAGMaS. Une autre contribution relative au développement des MAGMaS consiste en une étude exploratoire de la flexibilité dans les objets manipulés par un MAGMaS. Un modèle du phénomène vibratoire est dérivé afin de mettre en exergue ses propriétés en termes de contrôle.

La dernière contribution de cette thèse consiste en une étude exploratoire sur l'usage des actionneurs à raideur variable dans les robots aériens, dotant ces systèmes d'une compliance mécanique intrinsèque et de capacité de stockage d'énergie. Les fondements théoriques sont associés à la synthèse d'un contrôleur non-linéaire. L'approche proposée est validée par le biais d'expériences reposant sur l'intégration d'un actionneur à raideur variable léger sur un robot aérien.

Mots Clés

Systèmes cyber-physiques – Système de manipulation aérienne – Commande partagée – Commande et observateur non-linéaires – manipulation avec actionneur souple

Contents

List of Figures

List of Tables

List of Multimedia

[video 1–2015] **video 1**. *Total Thrust Modeling and Identification with Onboard Accelerometer and Battery*. https://youtu.be/RdL3adVm6sA. May 2015 (cited on pages 59 and 60).

[video 2–2016] **video 2**. *Aerial Robots with Rigid/Elastic-joint Arms: Controllability Preliminary Experiments*. https://youtu.be/Gtojd5AyxtY. Oct. 2016 (cited on pages 103 and 108).

[video 3–2017] **video 3**. *Towards Robotic MAGMaS: Multiple Aerial-Ground Manipulator Systems*. https://youtu.be/ZW9M4YXLsXw. May 2017 (cited on pages 73 and 74).

[video 4–2017] **video 4**. *Tele-MAGMaS Hanover System Presentation*. https://vimeo.com/217252361. Apr. 2017 (cited on pages 88 and 154).

[video 5–2017] **video 5**. *Tele-MAGMaS Hanover Demonstration*. https://youtu.be/GRnGSvJGUKk. Apr. 2017 (cited on pages 76, 88 and 154).

[video 6–2017] **video 6**. *Aerial-ground Cooperative Manipulation of Long Bars*. https://youtu.be/TrrPEP3CNlY. July 2017 (cited on pages 87, 153 and 154).

[video 7–2018] **video 7**. *OTHex Bar Lifting*. https://youtu.be/AikN3_PgYU4. May 2018 (cited on page 81).

List of Acronyms

AM Aerial Manipulation

APhI Aerial Physical Interaction

AR Aerial Robot

AV Aerial Vehicle

BLDC Brushless Direct Current

CoG Center of Gravity

CoM Center of Mass

DoF Degree of Freedom

EE End-Effector

ESC Electronic Speed Controller

FFT Fast Fourrier Transform

FPV First Person View

FSM Finite State Machine

HMI Human-Machine Interface

IMU Inertial Measurement Unit

LBR-iiwa "Leichtbauroboter", German for lightweight robot, intelligent industrial work assistant

LQR Linear-Quadratic Regulator

MAGMaS Multiple Aerial-Ground Manipulator System

MAV Micro Aerial Vehicle

MoCap Motion Capture System

NED North-East-Down

OTHex Open Tilted Hexarotor

PVTOL Planar Vertical Take-off and Landing Vehicle

PWM Pulse Width Modulation

ROS Robot Operating System

SQP Sequential Quadratic Programming

TCP Tool Center Point

Tele-MAGMaS Human in the Loop MAGMaS

UAV Unmanned Aerial Vehicle

USAR Urban Search and Rescue

VSA Variable Stiffness Actuator

VTOL Vertical Take-off and Landing Vehicle

Part I

Preliminaries

Chapter 1

Contribution and Overview

Contents

1.1 Contributions

Nowadays free-flying Micro Aerial Vehicle (MAV) are a mature technology which has obtained several commercial successes, *e.g.*, crop/structure visual inspection and drone hobby racing. The next frontier for aerial robotics is symbolized by Aerial Physical Interaction (APhI), where MAV are embodied with the capability to physically interact with their environment. This opens the way to many applications, *e.g.*, contact inspection and cooperative manipulation. In recent years, many incremental contributions have been made leading to Aerial Robot (AR) development, *i.e.*, Aerial Vehicle (AV) with the ability to physically interact with the environment. Motivated by the recent advances in the field of aerial robotics, this thesis proposes to extend the field of Aerial Manipulation (AM) by presenting the first general study of collaborative manipulation between ground manipulator(s) and aerial manipulator(s). The proposed system is called MAGMaS, which stands for Multiple Aerial-Ground Manipulator System and is based on the vision that AR can be beneficial to manipulation tasks in the form of *flying companions*. In particular, the motivation to combine ground and aerial manipulators resides in the desire to alleviate their respective shortcomings. This thesis showcases the first experimental demonstration of a Multiple Aerial-Ground Manipulator System (MAGMaS), opening a new route of research.

The first study on a MAGMaS is presented in [Staub–2017], which covers the modeling, control synthesis, simulation and preliminary experiments. The fact that the proposed multi-robots system is heterogeneous is carefully addressed in the control synthesis. Preliminary experiments are conducted, validating the proposed MAGMaS concept and the mechanical design of the AR. From this foundation, further work on MAGMaS is conducted, fostered by the participation to the KUKA 2017 Innovation Award[1]. The MAGMaS concept is enriched with a tele-presence framework, for operation in remote or hazardous environments. The associated work, from theoretical developments to successful demonstration at the

[1] `https://www.kuka.com/en-de/technologies/research-and-innovation/kuka-innovation-award/kuka-innovation-award-2017`

Hanover Fair 2017, was lead by LAAS–CNRS in cooperation with INIRIA/IRISA Rennes, University of Siena and Seoul National University. The focus on the efforts developed during this challenge were towards integration and demonstration of a MAGMaS with tele-operation capabilities; results are detailed in [Staub–2018] and [Staub–]. In particular, I was in charge of the global architecture and integration of the system, of the ground manipulator control and of the logistics. I also participated in the task planning and AR control framework developments. The last direction explored in the study of MAGMaS consisted in studying the flexibility in the manipulated load. This work was conducted in cooperation with Seoul National University and lead to an extension of the MAGMaS model by considering the flexibility in a co-manipulated beam. Further theoretical work was conducted in the form of a thorough system analysis and the exhibition of the flexibility properties; the corresponding results are to be found in [Yang–2018].

Based on the observation that force estimation capabilities are of paramount importance for APhI applications, in order to ensure both safe and stable operations. A preliminary work on external force estimation was conducted before focusing on the MAGMaS. The proposed approach relies on a class of simple models and the identification of their parameters, as presented in [Staub–2015].

Another contribution of this thesis in the field of APhI, consists in the study of elastic joints for AR. This direction of work has been explored with the main motivations of paving the way for safe APhI with the environment, thanks to the mechanical compliance induced by elastic joints. Additionally elastic joints also allow for velocity amplification, which proves useful for dynamic tasks, *e.g.*, throwing. This vast topic, which is at date still almost completely unexplored in the literature, was partially addressed in [Yüksel–2016b] in cooperation with the Max Planck Institute for Biological Cybernetics in Tübingen, Germany.

Levels of Maturity of the Presented Works

The careful reader will realize that the maturity of the experimental works presented is uneven. Choices have been made to maximize the research outcomes with the unavoidable limited time and resources. The MAGMaS concept presented in this work is a novel approach that needed solid theoretical foundation. Moreover, developing and conducting experiments with multi-robot systems composed of an industrial manipulator and an AR proved to be challenging and time intensive. In particular, the imposed change, during the thesis course, of industrial manipulator and AR required an extra integration work. Considering the different constraints, priority had to be given to demonstrate results, hence some directions which seemed promising in terms of research work had to be put on hold. Overall, experimental work is always presented, even if in preliminary form, to validate the proposed ideas. the possible future directions for further developments on both MAGMaS and Variable Stiffness Actuator (VSA) for AR are presented in the corresponding chapters.

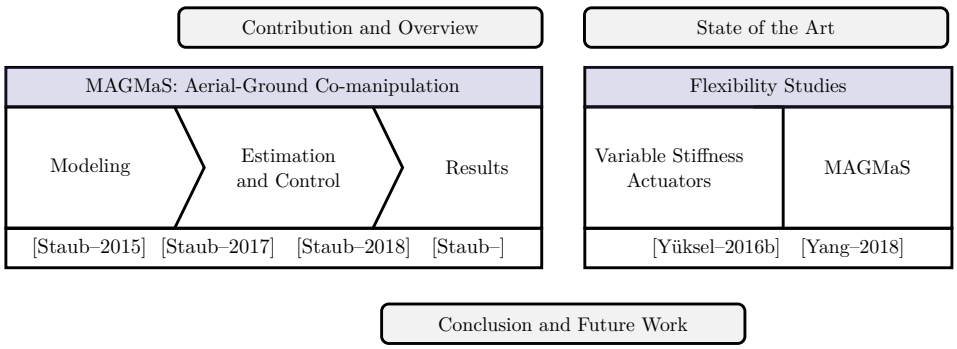

Figure 1.1 – Graphical overview of the chapters, the main topics, and the relation to the publications.

1.2 Organization

An in-depth state of the art is conducted in Chapter 2, presenting the motivations behind APhI in general and focusing on AM. A comprehensive review of all components needed for AM is conducted, including mechanical design, control and estimation, and the latest results in AM and cooperation between AR.

The following developments are centered around the concept of Multiple Aerial-Ground Manipulator System (MAGMaS); a totally new concept for aerial-ground cooperative manipulation developed throughout the presented work. The motivations behind MAGMaS and the associated models are presented in Chapter 3. In particular, the observations leading to the concepts of MAGMaS are listed along with possible use cases. In a second part, the rigorous modeling of the MAGMaS is derived through modeling of the sub-components. An emphasis is given to the control and estimation methods in Chapter 4. Two low level control schemes for AR are discussed and the importance of force estimation is underlined. Based on these developments, an overall control architecture for MAGMaS is proposed. The MAGMaS study is concluded by the description of MAGMaS real designs and presentation of both experimental and simulation results in Chapter 5.

Lastly, two exploratory and ongoing works on flexibility are presented in the last part of this thesis. In Chapter 6, the influence and exploitation of elasticity in the AR manipulator is introduced and studied in the general AM case, accompanied with discussions on intrinsic mechanical compliance benefits for AM. A parallel preliminary study on the flexibility in a beam manipulated by a MAGMaS is presented in Chapter 7. A model of MAGMaS including flexibility in the beam is derived and the system properties are exhibited based on the model analysis.

Ultimately the contributions are summarized in Chapter 8. Discussions about open research directions and future possible works are presented along the results review.

Chapter 2

State of the Art in Aerial Physical Interaction

Contents

Abstract

This chapter presents the fields of APhI and AM, the latter being a special case of the former. Sec. 2.1 outlines the motivation and the historical foundations of the APhI field, while Sec. 2.2 presents an overview of the field at large. The next two sections develop the field of AM from the mechanical design, Sec. 2.3, to the associated control theory, Sec. 2.4. The final section, Sec. 2.5, explores the thrilling topic of collaborative physical interactions for AV.

2.1 Motivations

Since August 1849 and the first use by Austrian forces of an UAV to target enemy positions. The field of UAV remained heavily fostered by military interests, from

(a) [NASA] (b) [Wikimedia Foundation] (c) [Wikimedia Foundation]

Figure 2.1 – Collections of MAV platforms: from left to right a fixed wing aircraft, an helicopter and a multi-rotor Unmanned Aerial Vehicle (UAV).

providing practice target for training, to long endurance surveillance of remote or sensible areas and combat engagement. From this military background came the name "drone" given due to the resemblance of sound of early UAV motors and the male bee. In the following developments, the emphasis is on MAV, understood as "small enough to be practical for a single-person transport and use" (see [Galinsky–2007]), practically this maps to a weight up to 5 kg to 6 kg and a span of around 1.2 m, see Fig.B.1.

In the recent decades, due to price drops in small consumer electronics, MAV became available to the research community and industries outside heavily subsidies military projects. Leading the path to other MAV usages and designs, for both fixed-wing aircraft and rotor-crafts. In particular rescue services and agricultural industries are interested in monitoring capacities. Academia and industry, were shortly followed by the general public in the MAV market, hobbyist being focused on MAV racing and airborne photography. Seeing the success and research results for free-flight UAV operations, see [Mahony–2012] for a tutorial on multi-rotor AV, new research field on Aerial Physical Interaction (APhI) emerged in the last 15 years. The goal of this field is to provide MAV with the capability of physically interacting with the environment, ranging from simple surfaces pocking to more complex cooperative load manipulation.

Aerial Physical Interaction

Aerial Physical Interaction (APhI) is a generic term to design all physical interactions between one AV and its environment. A very early example can be the in-flight refueling maneuver, demonstrated as early as June 1923. As of today this procedure is still not fully automated and requires the dexterity of an aircraft pilot or a boom operator in the case of rigid boom, while the probe-and-drogue system is close to be automated, see [Wilson–2015].

The following developments are going to focus on to APhI for unmanned aircraft, whether it be for probing the environment, react to collision or manipulate objects. In order to perform APhI with MAV a few requirements are set and will be developed at length in Sec. 2.2. The first two simple tasks of APhI, that come to mind, are pocking the environment, *i.e.*, exerting force trajectories on surfaces and perching, *i.e.*, allowing the MAV to perch on the environment in order to recharge battery or acquire data, see Fig. B.2. Another conceptually simple APhI tasks consists in linking a MAV to the ground by mean of a tether. These tasks will be described more in depth in Sec. 2.2. The whole work of this thesis fits under the umbrella of APhI.

In Europe the research efforts towards APhI are fostered by the European Commission via funding of major cooperation projects. AIRobots[1] from 2010 to 2013 funded under FP7 and targeted at developing a new generation of service robots, ARCAS[2] from 2011 to 2015 funded under FP7 and targeted at aerial transporta-

[1] `http://airobots.dei.unibo.it/`
[2] `http://www.arcas-project.eu/`

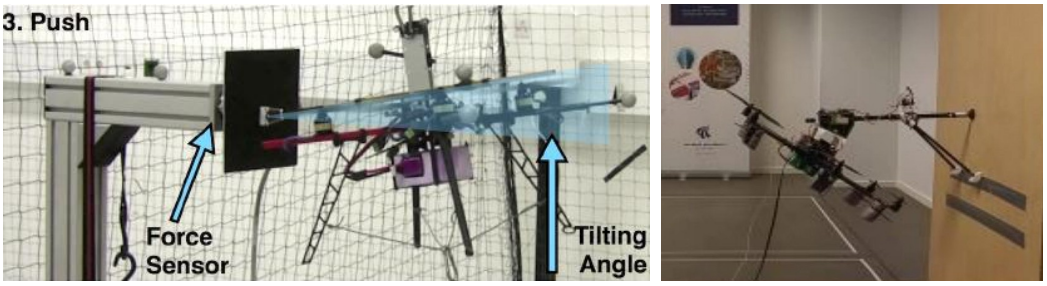

(a) [Gioioso–2014a] (b) [Wopereis–2017a]

Figure 2.2 – Examples of Aerial Physical Interactions: (a) pocking a surface and (b) perching on a wall.

tion and assembly, AeroWorks[3] targeted at enabling an Aerial Robotic worker and Aeroarms[4] from 2015 on, under H2020 fundings, which objectives are toward validation of APhI for industrial inspection and maintenance.

Aerial Manipulation

A subfield of APhI can be recognized for Aerial Manipulation (AM), being the use MAV to complete complex manipulation tasks. in the literature there is a confusion between transportation and manipulation, the latter being a special case of transportation including a dexterity component inherent to manipulation. In the following, transportation might be used as an illustration of basic manipulation capabilities. As such, AM regroups all the tasks where an object has to be transported or manipulated by one or a group of MAV, see Fig. B.4. In order to do so, developments in mechanical design of Aerial Manipulators, control and estimation techniques and collaboration framework are necessary. Mechanical design for AV are explored in Sec. 2.3, both for APhI and AM, with a special focus on some unconventional designs. Usually, these designs coupled with the physical interaction rise new problems for the control of the AV, presented in Sec. 2.4. Going even further in complexity, there is the realization of collaborative APhI tasks, like cooperative manipulation with other AR, Humans or Ground Robots, this topics is surveyed in Sec. 2.5. The work of this thesis is oriented towards AM paradigms.

Perception

Finally while perception of the environment is of paramount importance for the realization of autonomous APhI tasks, it is not the scope of the works presented in this thesis, as it covers a very wide and active area of research in itself. In particular in the followings the perception problem to acquire UAV state are always considered as solved in order to focus on the control theory aspects.

[3] `https://www.aeroworks2020.eu/`
[4] `https://aeroarms-project.eu/`

(a) [Nguyen–2015] (b) [Mellinger–2010]

Figure 2.3 – Examples of Aerial Manipulation: (a) drawer opening/closing and (b) collaborative load transportation.

2.2 Aerial Physical Interaction Paradigms

In this section, a review of the principal challenges faced and applications of APhI is presented. An overview of APhI designs, with special emphasis on 'un-conventional' AV solutions is proposed. The main applications of APhI are detailed and discussed, including perching, force exertion on surfaces and tethered AV.

2.2.1 Original Mechanical Designs

Typical off-the-shelf MAV are not mechanically fit for APhI tasks, often the propellers volume is open to collision and they don't have specific termination for contact with the environment. Therefor to pave the way to APhI and AM the first modification of standard MAV concerns mechanical design to enable APhI capacities. An in-depth review of the different mechanical design for Aerial Manipulator is presented in Sec. 2.3, the taxonomy presented there also applies for the simplest APhI tasks. For sake of completeness some mechanical designs only fit for APhI that does not involve manipulation are presented here, with a selection depicted in Fig 2.4.

A primary target of APhI mechanical design is to protect the propeller volume from intrusions and alleviate collision contact disturbances *w.r.t.* the flying behavior. One approach proposed by [Briod–2014] is to mount to passive rotating spherical shell around the main frame of a classical Vertical Landing and Take-Off Vehicle (VTOL), this mechanism enables the UAV to collide with obstacles without compromising its flight stability. This design allows to bounce on the environment, a refinement is presented in [Salaan–2017] using hemispherical shells, thus leaving an aperture for an End-Effector (EE) to reach outside of the shell. Lately this approach of shelling MAV in spherical structure was developed for package delivery in [Kornatowski–2017]. Another AV concept, the AIrBurr, is presented in [Klaptocz–2013] and [Briod–2013], the emphasis is on proposing a design significantly reducing the effect on impacts with the environment on the flying behavior, ultimately providing a recovery procedure if the system falls on the ground. This

(a) [Klaptocz–2013] (b) [Disney Research]

Figure 2.4 – Two Original Designs: (a) the AIrBurr capable of falling to the ground without breaking and upright itself to take-off again, and (b) the Vertigo capable of climbing walls.

allows 'blind' exploration of cluttered environments. Some research are exploring the possibility to climb wall, as in [Pope–2017] where a standard quadrotor is augmented with a kind of locomotion mechanism for vertical walls. Or this project, Vertigo[5], with a cart like vehicle actuated by two orientable propellers, even though this one is not an AV it represents and interesting use of propeller actuation. Other systems are developed for custom applications, like the large quadrotor presented in [Tsukagoshi–2015], fitted with a door handle opening mechanism and using the propellers to push door open. Or the quadrotor, in [Molina–2017], fitted with a sawing mechanism for perching and cutting tree branches near power lines.

2.2.2 Applications

The applications of APhI, not embraced by AM, consist of perching, when a MAV attaches itself temporarily to the environment, or force exertion on a surface, by pushing on a point or sliding while pushing. Collision recovery is not detailed, even though collisions are physical interactions, because the recovery happens when there is no more physical interaction, *i.e.*, in free flight.

Perching

Perching is investigated in the field of APhI, as a mean to increase the endurance of MAV. Indeed once perched and fastened the MAV do not need to resist gravity with their propellers, hence reducing their power consumption. Perching can be useful for sensor network, being temperature sensor or cameras used for environment monitoring, *e.g.*, for crowd monitoring, or working as radio relays in post-disaster environment. Another usage of the perching maneuver is solar battery recharging,

[5] https://www.disneyresearch.com/publication/vertigo/

a MAV with low battery terminal voltage can perch and use solar panel to recharge its battery before continuing the mission. In [Wopereis–2017a] the authors investigate perching for multi-rotor AV, they proposed an associated design for perching on vertical walls. The results presented in [Pope–2017] go even further and propose a solution to perch and climb on vertical surfaces. In [Thomas–2016b] aggressive flight maneuver for perching on inclined surface is investigated. Perching capabilities have also been successfully demonstrated for fixed-wing MAV, *i.e.*, small airplanes, as in [Mehanovic–2017] and [Desbiens–2011].

Force Exertion on Surface

Another often described task in the literature of APhI is the exertion of forces on a surface while following a force trajectory. This description translates to pocking/pushing were the goal is to exert a desired force on some location, either for sensing with contact sensor or trigger mechanism, *e.g.*, switches, and to sliding along a surface while maintaining contact, *e.g.*, for ceiling painting. Examples can be found in [Gioioso–2014a] with a near-hovering controller used to exert 3D forces on a vertical surface via a passive tool-tip, in [Ryll–2017] a multi-directional thrust AV is used for pipe contact inspection, applying forces on the measurements points, in [Yüksel–2017] where a rigid tool is used to slide on an uneven ceiling or in [Alexis–2013] for pushing along a vertical surface with feedback from pressure sensor. Another interesting design is proposed in [Papachristos–2014a], focusing on exerting a large force on the surface by re-orienting the propellers. Another approach, proposed in [Wopereis–2017b], for applying contact forces on the environment that are comparable to the MAV's weight relies on LQR control to achieve substantial force application on a specific contact point.

Tethered Aerial Vehicle

The last APhI task reviewed consists of linking an AV to the ground by mean of a cable. They can be used to transport energy or data increasing the AV autonomy, see Fig. B.3. Moreover the tether can be used to enhance the flight performances, as in [Sandino–2014a], for hovering, or to guide the landing, as in [Sandino–2014b]. And even to perform maneuvers impossible without the tether, like smooth and safe landing on a sloped surface as in [Tognon–2016b]. Tethered AV are now available as a product in France[6], with application to area surveillance with visual sensor or air quality monitoring.

2.3 Design of Aerial Manipulators

In this section an exhaustive taxonomy of aerial manipulator designs is conducted. The designs proposed in the literature can be ordered considering three main cri-

[6] `http://elistair.com/`


(a) [Elistair]


(b) [Kondak–2009]

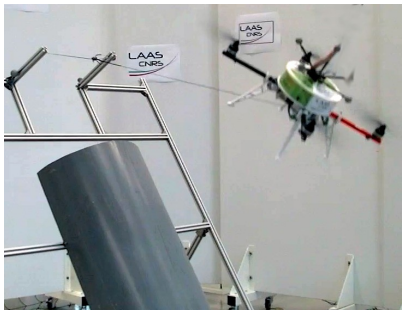

(c) [Tognon–2016b]

Figure 2.5 – Tethered Aerial Physical Interaction: (a) commercial solution for enduring monitoring, (b) collaborative load transportation and (c) exploitation of tether to land on a sloped surface.

teria: *i)* the flying platform design, *ii)* the manipulation mechanism and *iii)* the prehension mechanism. Each of them being developed hereafter.

2.3.1 Flying Platform Designs

In both APhI and AM, the AV design is of paramount importance. Indeed the design of the AV bears underlaying system properties that facilitate or inhibit the APhI tasks. By mean of control certain properties can be smartly leveraged but it is often easier to start with an adequate mechanical design. Here are regrouped the main design ideas present in the vast literature of APhI.

Under-actuated Design

Among the different aerial manipulator systems present in the literature a vast majority can be grouped by their under-actuation characteristic. That means that their translational and rotational dynamics are not fully decoupled, *i.e.*, they can not follow an arbitrary 6D trajectory in $SE(3)$. The under-actuation property arises from the mechanical design of the platforms, where the propeller(s) are physically arranged so that the total thrust is always exerted along one direction in the body frame of the AV, typically along the z-axis, thus lateral motion of the AV requires some tilting of the whole body to re-orient the total thrust in the desired direction of motion.

Collinear propellers: a design in which all propeller rotation plane are coplanar. This is the case for the most well know MAV platform, the planar quadrotor, which consist of four propellers distributed along the edge of a rectangle (regular or not), all oriented in the same direction. The simplicity of the mechanical design comes at the cost of under-actuation. Its simplicity and robustness also made it famous among hobbyists. Rotational motion is achieved via differential commands

of the propellers. One can group in the same family hexa- and octo-rotors, following the same propeller layout rule but with regular hexagon and octagon patterns, respectively. The benefit of such a design is usually an increase of payload which proves to be capital for heavy load transportation. This multiplication of propellers does not result in a one to one increase of the payload has it usually also results in a power consumption increase which needs to be balanced by additional battery. Overall the design is still beneficial and is used to carry heavy loads, *e.g.*, dual arm manipulator of 1.8 kg, as in [Suarez–2017a], or sensors in non-AM scenarios like the ALTA8 from *Free Fly Systems*[7] capable of lifting a 9.1 kg payload for an empty weight of 6.2 kg. The general model of multi-rotor MAV is developed in depth in Sec. 3.2, with emphasis on the collinear case, and a possible control strategy for APhI is detailed in Sec. 4.2.

Ducted-fan: a design in which propeller are encased in a duct. The principle of this design is, as its name suggests, that the airflow is produced by two propellers encased in a duct, *i.e.*, a small pipe, they are counter rotating to allow yaw control. Rotational motion is achieved via actuated flaps in the airflow. The main advantage of this design is the inherent safety from already encased propellers, which is paramount for interaction with human users. Also the ducted fan design exploits aerodynamics properties to increase the lift produced by propellers by guiding the airflow in the duct. One application is presented in [Fumagalli–2014].

Helicopter: a design in which a main propeller produces the actuation thrust while a smaller one acts as a stabilizer. This design is well know and also suited for big AV as produced by aircraft industries. An example of large helicopter with industrial manipulator can be found in [Kondak–2014]. While research on AM are also conducted with smaller helicopter as in [Pounds–2014].

Multi-directional Thrust Design

A recent trend in the aerial manipulator design is the emergence of multi-directionnal thrust AV, meaning that their total thrust can be oriented in several directions in the body frame. This allows for their translational and rotational dynamics to be fully decoupled (up to the actuation limits), *i.e.*, they are fully actuated. To guarantee the full actuation the mechanical design imposes non-collinear layout of the propellers. Due to that, full actuation comes at a cost of internal force, *i.e.*, loss of energy efficiency. One can choose to start from a well known under actuated structure and modify it, like the work present in [Rajappa–2015][Ryll–2017] on hexarotors. A similar idea is proposed for quadrotor in [Odelga–2016], based on a parallelogram principle to reorient the propellers. Or one can even think about designs encompassing more novelty, aimed at automatically optimize the full actuation, as the design described in [Park–2016] or aimed at allowing the exertion of

[7] `http://freeflysystems.com/alta-8/specs`

given wrenches applied by the EE via automated design in [Nikou–2015]. A judicious choice in the layout leads to a multi-directional platform, while keeping the control input allocation simple and minimizing the internal forces. These platforms can follow an arbitrary trajectories in $SE(3)$. But more importantly as lateral force exertion do not require any orientation change, they can withstand external force perturbations while following 6D trajectories. Another work in this direction is presented in [Brescianini–2016], where an eight-rotor configuration that maximizes the vehicle's agility in any direction is derived based on a static force and torque analysis for generic actuator configurations.

Mixed Design

Interestingly, some design try to exploit the advantages of both under- and full actuation, refereed to as mixed design hereafter. It is the case of the design presented in [Ryll–2016] where the platform can change in flight the propeller orientation, allowing power efficient free-flight and perturbation resistant physical interaction. This versatility comes at the cost of mechanical complexity and let the need of extra-actuation (to tilt the propeller) arise. Similar solution is proposed by the Voliro[8] project with one tilting motor for each propeller, allowing more flexibility in global configuration. Another more basic solution consist in taking an under-actuated quadrotor and add a propeller with spinning axis in the direction of the force exertion, as in [Albers–2010] or [McArthur–2017]. With this additional propeller the system gains some actuation degree but remains under-actuated. Some design just use quadrotors as orientable thrust generator fixed on a structure, *e.g.*, [Nguyen–2015] with three quadrotors attached via passive rotational joints on a triangular structure holding a gripper or a tool.

Fixed Wing Design

Fixed wing design are purposely omitted in this taxonomy as there inherent flight behavior is not fit for AM. From the APhI point of view this design can be used in perching, as reviewed in Sec. 2.2.2.

2.3.2 Embedded Manipulation Mechansim Designs

In order to pass from APhI to AM, a manipulator or at least a prehension mechanism needs to be embedded on AV. With this extension AV can be properly called Aerial Robot (AR). In the literature, several different design approaches for manipulator were identified, see Fig. B.5. The main idea remaining that a manipulator increases the dexterity of the AR for manipulation tasks, eventually compensating for under-actuated AV.

[8] `https://www.voliro.ethz.ch/`

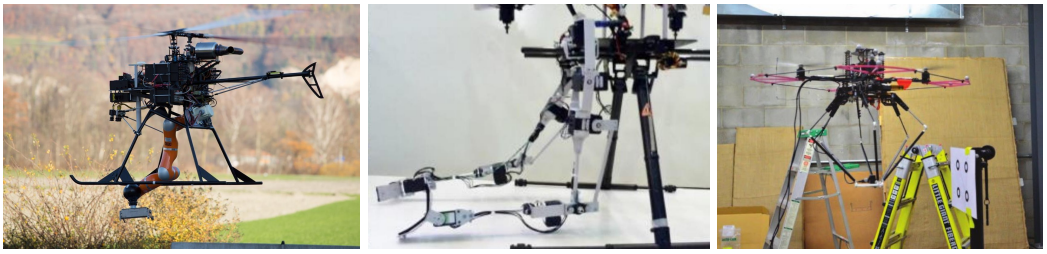

(a) [Kondak–2014] (b) [Suarez–2017a] (c) [Danko–2015]

Figure 2.6 – Different kind of aerial manipulators: (a) industrial 7-DoFs, (b) dual arm manipulator and (c) parallel manipulator mounted below a MAV.

Joint-Actuated Manipulator

The simplest approach consist in taking off-the-shelf serial manipulator solutions and attached them below a AV . This as been proposed with top grade industrial manipulators in [Kondak–2014]. But also with smaller lightweight manipulator based on classical design as in [JimenezCano–2013]. As the manipulator is mounted on the AV, there exists a strong mechanical coupling between their respective dynamics, usually compensated by means of control. An interesting approach concerning this is proposed in [Ruggiero–2015], where moving the battery as a counterweight is experimented. In general, the solution of bluntly strapping two pre-existing systems together does not provide good performances as the manipulator workspace is significantly reduced by the AV actuation limits and the flying performances degrade due to the strong coupling.

Deported Actuation Manipulator

A way to reduce the dynamical coupling is to reduce the inertia of the manipulator, typically by using cable or transmission-belt mechanism. With this kind of mechanism the motors moving the joints can all be located close to the AV platform and its center of mass (CoM). Thus reducing the dynamical coupling as the norm of the inertia tensor of the manipulator remains small. An example can be found in [Tognon–2017].

Parallel Manipulator

Another kind of manipulator design for AM, is the parallel design which allows dexterous manipulation. In [Keemink–2012] a delta design mixing actuated and passive DoF is used to propose a robust and lightweight aerial manipulator, which as been enhanced in [Fumagalli–2016]. The parallel design is also used in [Steich–2016] in order to inspect tree cavities and a full-body controller is presented in [Kamel–2016]. Finally [Danko–2015] present a large parallel manipulator design mounted below a quadrotor, in order to compensate for MAV motion during pickup.

Another parallel manipulator design is presented in [Six–2017], where instead of embedding a parallel manipulator on a MAV, quadrotors are used as actuators of a parallel manipulator, *i.e.*, their are linked by a rigid articulated passive chain, and their respective motion induce displacement of the EE.

Passive Manipulator

For certain constrained manipulation tasks, or when multi-directional thrust platform are used, an active manipulator might not be necessary. This means that the actuated Degrees of Freedom (DoF) of the aerial manipulator are already matching the DoFs of the tasks: this is the main idea behind the use of passive joint manipulator. The passive joint can also be seen as a way to decouple the behavior of the manipulator EE and the flying platform. For example a full 3D passive revolute joint allows to decouple the rotational dynamics of the EE and the AV , this proves useful if the rotation actuation capacity of the AV are small as in [Nguyen–2015].

Cables Links are a special case of passive manipulators: in the sense that, when the cable is taut, they can be thought as a one link manipulator attached via a passive joint to the AV. AM accomplished by a group of AR taut to a platform is presented in [Manubens–2013]. Experimental results with helicopters were presented in depth in [Kondak–2009] and [Bernard–2011].

Compliant Manipulator

Compliant manipulators have made a recent apparition in AM field and are composed of joints that are actuated but with an additional capacity to be elastic around their setpoint. This is often achieved through the use of elastic components in the design of the manipulator, *e.g.*, springs, as in [Yüksel–2015] and [Suarez–2015a] [Suarez–2015b] [Suarez–2016] [Suarez–2017b]. The main motivation is to ensure soft collisions with the environment, thus preventing the AR to become unstable on collision, see [Bartelds–2016] for direct impact experiments. The addition of elastic behavior in the manipulator increases significantly the complexity of the mechanism and the associated control algorithms.

Multiple Arms Manipulator

Another manipulator structure which needs to be mentioned in this taxonomy is the multiple arms manipulator, where the manipulator appendage is constituted of several arms. The first successful description and validation can be found in [Suarez–2015a] [Suarez–2017b]. These demonstrations were followed by a human operated commercial products[9] by another organization. A recent work, [Orsag–2017], presents a detailed analysis of the coupling between dual-arm AR and the environment during manipulation, proposing to focus on three different coupling descriptions (momentary-loose-strong) to benchmark performances. Another approach found is the literature, see [Yeol–2014], aims at having three tentacle-like

[9] `https://www.prodrone.jp/en/products/`

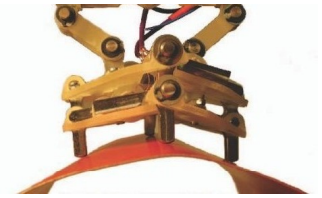

(a) [Gawel–2017]

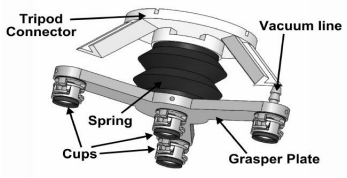

(b) [Kessens–2016]

(c) [Mohammadi–2016]

Figure 2.7 – Different prehensors for AM: (a) magnetic mechanism to grasp non flat ferrous objects, (b) vacuum based prehensor working with an airborne pump and (c) swarm grasping of a cylindrical object.

mechanism below an AR to grasp an object or perch on the environment, also enabling the system with locomotion capabilities. This mechanism is a bridge between a manipulator and a prehensor.

No manipulator

One approach to circumvent the use of embedded manipulators and their drawbacks, or when manipulators DoFs are not needed to conduct the task, is to attach a prehension mechanism or a dedicated tool rigidly to the AV, either directly on it or on a rigid arm. This approach as been investigated in [Ryll–2017] with for tools and in [Lindsey–2011] for grippers. Another approach proposed recently, in [Zhao–2017], is to have an AV re-configurable geometry, allowing to encircle the load by a ring of propellers. More details on the prehension mechanisms are to be given in the next section.

2.3.3 Prehension Mechanism Designs

To complete this aerial manipulator design section, a review of the main prehension mechanisms used in the field of AM is introduced, see Fig. B.6 for some examples.

Mechanical Claws

This is the standard gripper mechanism of robotics, composed of two (or more) claws or fingers actuated by one (or more) electrical motor located in the gripper. The motion can either be linear or rotational, *e.g.*, [Thomas–2016a][Backus–2014]. The grasping is realized by encircling part or all of the object to be manipulated. This kind of design are standard and quite robust, hence their use. Their main advantage is their compactness and versatility coupled with their weight/grasping force ratio. Moreover as the actuator are electrical there is no need for power conversion, *i.e.*, they can be plugged directly on the battery.

Vacuum Based Prehensor

Another way to attach to an object or surface is to use vacuum based mechanisms. They can be passive mechanism composed of suction cup, like the one proposed in [Wopereis–2017a]. The main advantage being their light weight, while the suction force can not be controlled and suction on surface is not guaranteed. Moreover an additional mechanism for releasing is necessary. An effort to overcome the latest two drawbacks can be seen in the design of a vacuum pump based gripper in [Kessens–2016], sticking/unsticking consist then in switching on/off the pump. Thanks to careful design, the weight from the pump is minimized, making AM practical. In a recent work on blimp like[10] AR the grasping system is also based on difference of pressure to realize suction.

Magnetic Prehensor

For completeness magnetic prehension is introduced. Obviously this approach only works on ferrous objects, or objects previously equipped with ferrous receptors. As for the vacuum case one can use passive magnets, which consume no energy but necessitate high force exertion to release the object. Electro-magnet can be used to circumvent this issue, their power consumption remaining modest. This has been proposed in [Gawel–2017] or for a simpler design [Bähnemann–2017]. The use of magnetic prehensor has been fostered by the 2017 MBZIRC Challenge[11] requirements to pick objects with ferrous surface.

MAV Swarm Prehension

An interesting approach to reduce the design complexity of the AR is to use a swarm or a group of them to grasp and object, ensuring firm grasp by multiples simple contacts. This approach is studied in [Gioioso–2014b] and [Mohammadi–2016], where the authors use MAV to mimic the behavior of fingers and coin their solution as “flying hand”. Another, lately emerging design as been proposed in [Zhao–2017] where the geometry of the AV can be re-arranged in flight, giving the possibility to surround objects.

2.4 Control and Estimation Techniques for Aerial Manipulator

From control point of view, APhI is way more challenging and demanding than free flight. Not only geometric pose controllers are needed to allow the AV to track desired pose trajectories, but also force based controllers to ensure intrinsically stable behavior while in contact with the environment. In order to allow feedback force

[10] https://www.festo.com/group/en/cms/11957.htm
[11] http://www.mbzirc.com/challenge/2017

control, measurements or estimation of the external forces are necessary. Finally tele-operation frameworks used in case of human supervision are briefly introduced.

2.4.1 Geometric Pose Control

Geometric control of AVs aims at stabilizing the system in free flight and allowing trajectory tracking. The pose of the AV is expressed by a position in $\mathbb{R}^3$ and a 3-DoF rotation, thus the pose is in the Special Euclidean group $SE(3)$. In the literature several different orientation representation are present, Euler angles which are prone to Gimbal Lock, see [Mistler–2001][Spedicato–2016], quaternion which have a redundant representation of $SO(3)$, see [Mayhew–2011] and rotation matrix which do not suffer the two previous drawbacks but are a non-compact representation, see [Lee–2010]. The first approach encounter in the literature consists in applying classical synthesis techniques to an approximate linear model of the vehicle dynamics. In [Castillo–2005], the linear controller sequentially stabilize the thrust and then the orientations, this sequential approach is also used in [Spedicato–2016].

The call for increasing performances and maneuverability led to the use nonlinear control strategies. They rely on dynamical feedback linearization, see [Mistler–2001], to bring the system in a linear form where linear control techniques can be applied. In [Raffo–2010] an approach based on model predictive control and $\mathcal{H}_\infty$ controller is proposed as nonlinear robust control strategy. A popular nonlinear tracking controller is developed on the special Euclidean group $SE(3)$ in [Lee–2010], with almost global stability. Note that non-linear control approaches are typically more computationally intensive, which might be an issue for embedded deployment. But nowadays small computers, *e.g.*, intel NUC series[12], are powerful enough to run model predictive control algorithm and some additional optimization problem in real-time, see *e.g.*, [Baca–2016].

2.4.2 Force Based Control

To perform safe APhI, trajectory tracking control is not sufficient and additional control strategies addressing the force interaction are necessary. Indeed in such applications, a flying robot is required to exert certain forces and torques to the environment, while maintaining a stable flight. A classic techniques rely on admittance/impedance framework as in [Augugliaro–2013] for admittance and [Lippiello–2012] [Gioioso–2014a] [Ruggiero–2014] for impedance. Other approaches relies on energetic considerations. For example in [Mersha–2011] relying on port-Hamiltonian modeling and bond graphs. Or [Yüksel–2014b] relying on an Interconnection and Damping Assignment Passivity Based Control (IDA–PBC) scheme.

2.4.3 External Forces Estimation

The subject of external forces estimation is of paramount importance for MAV as this information is useful to improve flight behavior (reaction to wind and/or

[12] `https://www.intel.com/content/www/us/en/products/boards-kits/nuc.html`

collision) and to allow quality APhI with force feedback. Hereafter the term external forces is used to refer to 6D general forces or 6D wrench indifferently.

Necessity of Force Estimation

The reason to privilege estimation of external forces over actual sensor measurements, despite the better quality of the measurements, mainly comes from the issue to integrate force sensors and their associated electronics on MAV. Indeed, despite the recent years advances in 6D Force/Torque sensors (F/T-sensor) miniaturization of the associated electronics usually suffer from poor form-factor and weight unsuitable for MAV applications, meaning that at the same time the volume of the electronics and its weight make the sensor solution unusable in practice. The weight is especially an issue as, at the same time, it reduces the flight endurance and the exploitable actuation bandwidth for the APhI tasks. Even though, an interesting development in miniaturized 6D F/T-sensor is the mini sensor[13], with fitting electronics, specially designed at IIT to fit the iCub robot. The power consumption of such a device can also be an issue, as it would drain the battery and hence reduce the flight endurance of the overall system. Finally a strong argument against F/T-sensor is the fact the measurements are localized, *e.g.*, [Alexis–2013], hence the external force information only describes what happens at the measurement points, whereas the estimation approach provide information on force applied in any point of the structures. Another drawback of F/T-sensor is their cost, which often amount for as much as the rest of the MAV if not more, compared to the ever decreasing cost of embedded computing driven by the cellphone market.

To overcome these drawbacks force estimation is used. The force estimation methods also come with limitations, the main one being the aggregation of a lots of phenomena in the same estimate. Namely all wrenches applied on the AR are combined like contact(s) with the environment and wind, on top of that model inaccuracy and raw measurements bias and noise are merged in the estimate. Thankfully these effects can be mitigated through calibration of the the different sensors and parameter identification routine for the model(s) used. The addition of contact detection mechanisms, as in [Rajappa–2017], allows to separate the contribution from physical interaction and wind.

Flight Behavior Improvements

External force estimation can be beneficial to free-flight MAV, especially outdoor where the wind, an external force, is often neglected in the control synthesis. Indeed by taking the wind into account the flight performances can be significantly improved for MAV [Alexis–2010], other schemes to do so have been proposed in [Tomić–2016] (and previous) and [Rodriguez–2016][Rodriguez Salazar–2017] for gliders. Inside operations are not exempted from wind effects, as the airflow produced by the propeller generates aerodynamic perturbations which can be related

[13] `wiki.icub.org/images/a/a7/FTSens.pdf`

to wind. More toward APhI, external force estimation can be used to detect collision with the environment, as in [Tomić–2015] and trigger recovery procedure. This can prove extremely useful in cluttered and unstructured environments, finding its application in unknown or damaged buildings exploration.

Physical Interactions

In order to perform APhI the force based control strategies detailed in Sec. B.1.6 require a force feedback. Making the force estimation component mandatory for their implementation. In [Ruggiero–2014] a momentum based external generalized force observer is presented, which requires to measure the whole dynamical system state, the control torques and the thrust to produce an estimate of the external wrench. The methods has been proven to work indoor by using a precise off-board motion capture tracking. In [Augugliaro–2013] a classical Unscented Kalman Filter is presented to estimate the external force and torque acting on a quadrotor. This approach has also been tested with the use of an off-board motion capture system. An external wrench estimation based on momentum-based observer was used in [Ryll–2017] to demonstrate force exertion by a multi-directional thrust AV. Another approach is described, in [Yüksel–2014a] with a Lyapunov based nonlinear observer. Another estimation scheme based on the system dynamic model is proposed in [Tomić–2014]. In [Rajappa–2017] the external wrench estimation is based on a residual estimator.

A static mapping between commanded thrust and actual force has been proposed by [Bellens–2012]. A more accurate, yet static, mapping of the force produced by a typical brushless motor for AV has been proposed by [Spica–2013], based on discretized force measurements for desired commands.

2.4.4 Tele-operation Framework

Tele-operation refers to control frameworks in which remote human operators are supervising systems of various autonomy levels, often providing high level control thanks to their reasoning abilities or manually driving robots, hence the operator side is referred as master and the remote robotic system as slave, see [Niemeyer–2008] and [Passenberg–2010]. In order to provide the human operator with situational awareness about the system and its surroundings tele-presence paradigm are used, employing either visual feedback or haptic feedback.

Visual feedback is conceptually simple, a camera (or several) is placed in the slave side, to provide the master side with a view of the environment and robotic system. Haptic feedback consists in providing the master side with force or position/velocity feedback from the slave side and are detailed hereafter. Haptic feedback associated with tele-operation is named bilateral tele-operation and is provided via an haptic device which is a robot. The typical commands for both master and slave robotics systems are force and position/velocity ones. A bilateral tele-operation framework is described by its number of channels, *i.e.*, the number of

commands exchanged between the master and slave. For example if the slave robot receives a single type of command and the master side receive only one type of feedback, the architecture is named 2-channel bilateral tele-operation. In [Son–2013] the human operator's performances, in terms of maneuverability and perceptual sensitivity, through bilateral tele-operation for multiple robots are investigated. In particular, force cues are used to transcribe the proximity of obstacles in the remote environment and velocity cues to transcribe the velocity mismatch of the robots.

Based on the type of commands accepted by the slave robots and the kind of commands accepted by the master, impedance and admittance framework are used. All combination of commands type for the master and slave side are possible and there is no *a priori* best choice, combination shall be tested and evaluated based on robustness (*w.r.t.* communication, model uncertainty, external disturbances, ...), task performance, tele-presence (as felt by the operator) and transparency (dynamic cancellation of master and slave systems). Evaluation of the impact of different haptic cues on UAV operators can be found in [Son–2013]. Comparison of transparency as defined by control theory and felt by user is investigated in [Hirche–2012].

There are two additional ways of using tele-operation from and high level control perspective. Haptic cues can be used to render virtual fixtures or virtual fences to the operator, the former helping guiding some task relevant motions and the later shielding some area of the environment, *e.g.*, to avoid collision. Also the tele-operation can be used in a shared control paradigm, where the slave system autonomously carries out a task, and the master is used to generate local trajectory modifications. Either spatial, *i.e.*, altering the trajectory to avoid and obstacle, or temporal, *i.e.*, slowing down the motion to reduce dynamical efforts. These two kind of modifications allow the operator to provide update on the system or the environment without triggering re-planning.

2.5 Collaborative Aerial Physical Interaction

From a semantic stand point, collaboration (working jointly with other toward a common goal) and cooperation (operating together to realize a task) are considered equivalent. A collaboration denotes a joint work, it does not necessary involve physical interaction, with the environment or with the other collaborators, that is to say heterogeneous robots, ground and AV, mapping/monitoring an area is a collaboration task but not relevant in the scope of APhI.

Collaboration between Aerial Vehicles

A few works considering swarm, or team of AR, performing APhI with the environment or inside the swarm have been presented, see Fig. 2.8. Most notably, swarm of AR are used for collaborative construction, as in [Augugliaro–2014], to build a tower structure out of bricks or to build tensile structures, *e.g.*, bridge, as in [Augugliaro–2015], or to assemble cubic structure in [Lindsey–2011] or more complex structure

(a) [Lindsey–2011] (b) [Bernard–2011] (c) [Augugliaro–2013]

Figure 2.8 – Aerial Robot collaborations, (a) collaborative structure assembly by a team of ARs, (b) collaborative load transportation via tether and (c) human-AR collaboration for assembly tasks.

with a dedicated construction planning in [Sempere–2014] [MunozMorera–2015]. In this case the physical interaction is not affected by the other members of the swarm. Or in the well developed case of cooperative load transportation, by team of AR. This results in a group of AR tasked to transport a load in a coordinated fashion, the loading being a bar directly grasped [Kim–2017](and previous) or attached by cables [Gassner–2017] or some structure [Wu–2014][Michael–2009]. One can also mention the work presented in [Nguyen–2015] where three quadrotors are attached to a rigid structure via passive rotational joints, the task is to coordinate the structure motion to use a tool attached to the structure. Another interesting work is presented in [Ritz–2012], where three quadrotors are attached to a net by mean of rope and they trow and catch balls with the net, the trowing is particularly interesting in the scope of collaborative physical interaction.

Collaboration with Ground Vehicles

An exciting topic in APhI, is the interaction with ground robot in order to alleviate some drawbacks of AR, *e.g.*, the autonomy/payload. The work going in that direction mostly showcase simulation results. In [Tognon–2016a] and [Papachristos–2014b] a cable is taut between the ground vehicle and the AV, this can be a solution to enhance power endurance of the MAV. The former focus on the trajectory control of the MAV, while the latest in focused on the autonomous navigation and mapping. Some autonomous landing on moving robot as been demonstrated outdoor in [Vlantis–2015]. Other occurrences of Aerial-Ground cooperation can be found in [Spica–2012] and [Gawel–2017], where an AR picks-up a object from a moving ground robot and in [Nguyen–2016] where the foundations for associating a ground mobile vehicle and an AV to transport an object are sketched.

Collaboration with Human

Despite the vast literature on human-robot collaborative tasks, it seems that few works in the direction of physical collaboration between human and AR have been presented so far in a conclusive way. Choice has been made not to consider collision detection and recovery as a cooperative interaction, as it is not collaborative. A work in the collaborative direction can be found in [Mueller–2011], AV juggling balls with human or other AV. In [Augugliaro–2013] a human-robot physical interaction is tested, relying on admittance control scheme, see Fig. 2.8c.

In a recent work [Rajappa–2017] a framework and MAV for human-UAV interactions are presented and lay the foundation of possible safe human-UAV cooperation. Another framework for human-UAV safe interaction is presented in [Tomić–2014] and relies on impedance control. The safe interaction control is a first step toward collaboration between human and AR.

Part II

MAGMaS: Aerial-Ground Co-manipulation

Chapter 3

MAGMaS: Aerial-Ground Co-manipulation
Motivations and Modeling

Contents

Abstract

This chapter presents the motivations leading to the MAGMaS concept and the associated modeling. Sec. 3.1 introduces the MAGMaS concept, from its motivations and potential applications. The next two sections focus on the modeling, first the modeling of AR in Sec. 3.2, and then the global modeling of MAGMaS in Sec. 3.3. The final section, Sec. 3.4, proposes a discussion on the presented models assumptions and their possible extensions.

3.1 Motivations

The idea of a Multiple Aerial-Ground Manipulator System (MAGMaS) comes from the practical limitations of both ground and aerial manipulators, a simple – yet still mostly unexplored – solution to mitigate their drawbacks is two combine them in a unique system.

Typically, for robotic object handling, two approaches are independently studied, on one hand the use of (mobile) ground manipulators and on the other hand the use of AR. The rich literature on ground manipulators proposes use cases with single robot or multi-robot systems for object handling, in particular for cooperative transportation [Dumora–2013][Cehajic–2017a], of possibly large objects [Machado–2016][Dumora–2012], or robotic sensing and manipulation offshore [Pfeiffer–2011], or for cooperative assembly [Knepper–2013] and manufacturing [Cherubini–2016]. However two major drawbacks to the use of ground robots can be identified. Firstly, typical small industrial manipulators have limited joint torque limits resulting in poor maximal admissible Cartesian torque at the EE. Secondly ground manipulators, mobile or not, have a rather small workspace around their base, inhibiting their

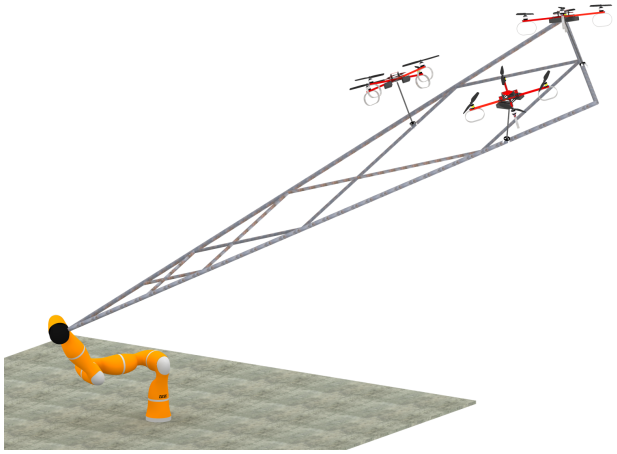

Figure 3.1 – Schematic view of a MAGMaS composed of one ground manipualtor (7 DoF) and three underactuated AR attached to the load via 3D passive revolute joints.

manipulation capabilities, especially along the vertical direction. This can prove particularly problematic for long objects handling. Indeed, if the ground manipulator can not grasp them by their Center of Mass (CoM) due to workspace limitations, the manipulation would require high torque at the ground manipulator's EE. Moreover long objects manipulation is often subject to re-grasping maneuvers in order to overcome workspace limitations, this hinders the execution performances. A rising approach is the use of AR for construction and large load handling. This as been made possible by the last decades developments in UAV, especially toward AR, being AV with physical interaction capabilities. Their use as been demonstrated as group to carry load via tether as early as 2009 in [Kondak–2009], splitting the overall payload among members. An interesting and recent use of AR can also be seen in multi-robot construction or assembly [Augugliaro–2014] [Lindsey–2012] or aerial manipulation as presented in [Kim–2013] and [Suarez–2015b]. A major drawback of these platforms is the limited actuation range, resulting in limited payload capacity.

The originality of the MAGMaS approach is to consider a *heterogeneous* multi-robot system composed of both ground and aerial manipulators, see Fig. B.8, to leverage their individual flaws as introduced in [Staub–2017]. The small payload of the AR is compensated by the strength of the ground manipulator, while the limited workspace and small torque at the EE of the ground manipulator is balanced by the virtually unlimited workspace and the favorable lever provided by AR. Thanks to their large workspace AR can exert force on the load in order to reduce the torque induced at the EE of the ground manipulator by the load weight. With this teaming, AR can act as *flying companions* helping the ground manipulator to carry long loads by grasping them on another extremity and mitigating torque at

(a) (b)

Figure 3.2 – Potential use cases for MAGMaS of different composition. Left (a) in a USAR scenario with a mobile base and an underactuated AR cooperatiely cleaning buldings remains. Right (b) in a decomissioning scenario with a fixed ground robot and a multi-directionnal thrust AR cooperatively manipulating a pipe.

the ground manipulator EE while it carries the object, thus allowing manipulation of the load in a *cooperative* way.

Another advantage resulting from the use of *flying companions*, compared to a ground manipulator alone, is the oscillation damping in the transported load. In the studied use-case, of a ground manipulator grasping an object far from its CoM, the oscillations in the case of alone ground manipulator transportation can be quite important. Thanks to the AR, oscillations in the load can be suppressed by mean of control. This is also achieved by cooperative transportation of loads by ground manipulators team or aerial manipulators team, which are both ruled out due to their respective drawbacks.

3.1.1 Applications

The field of applications for MAGMaS is vast and encompasses all manipulation tasks of long or weird shaped objects, moreover if it has to be realized in environments potentially hazardous for human the robotic solution is even more justified.

Manipulation of long objects is a common task for robotics systems, for illustration one can think about, scaffold or transmission tower construction, maintenance of several pipe plants like chemical or gas plants. These are example where the MAGMaS could be used for construction like tasks, see Fig. B.9. Another kind of tasks identified for MAGMaS, is their usage to extend manipulator reach, creating an extended and dexterous last link of the ground manipulator. Typically for high off the ground operations, like, *e.g.*, painting, hole drilling, bulb changing. Finally, a last kind of operation identified for MAGMaS is taking place in unstructured environments and consists in ruins cleaning after a catastrophe, *e.g.*, an earthquake, where the remains of building are often weirdly shaped pieces and structures. This application is denoted as Urban Search and Rescue (USAR) and is illustrated in Fig. B.9a.

The interest toward robotics solution is motivated by hazard-level for humans.

The described manipulation tasks can take place in potentially hazardous environments as, but not limited to, *i)* post natural or human disaster situations, *e.g.*, post-earthquake or industrial catastrophe, where the lives of rescuers are at risks due to structure collapse, *ii)* high altitude or secluded locations, like mountain construction sites, South Pole camps or off-shore platforms, where risk are multiplied for workers due to scarce access to medical care, and *iii)* environments with radiations due to nuclear activities, *e.g.*, nuclear plant decommissioning. Some of these environments are also hazardous for the platform as described in the experimental Chapter 5 and their usage would require further hardening of the system like ATEX compliance for explosive atmosphere or Radiation Hardening for nuclear environments.

Among the presented applications, the most promising one is the nuclear plant decommissioning for fully autonomous MAGMaS, especially because nuclear plants are highly structured environment, thus simplifying perception requirements.

3.2 Modeling of Aerial Robots

This section introduce the modeling of AR, starting from the classical modeling of multi-rotor AV, based on their design two categories of platforms are considered and their dynamics models are derived. The addition of a manipulator, and its modeling, leads to a complete model for AR.

3.2.1 Multi-rotor Vehicle Dynamics and Standard Motor Model

In this section, the dynamics model of a general multi-rotor AV is developed as it will be of use. This model is generic, it can be used in the case of collinear multi-rotor but also in the case of thrust orientable multi-rotors.

The inertial frame, also referred as world frame, is denoted $\mathcal{F}_W$ and defined by its origin O_W and three unit vectors along the main axes denoted $\{\mathbf{x}_W, \mathbf{y}_W, \mathbf{z}_W\}$, the compact notation for this definition yields $\mathcal{F}_W : O_W - \{\mathbf{x}_W, \mathbf{y}_W, \mathbf{z}_W\}$. The body frame of the multi-rotor is $\mathcal{F}_B : O_B - \{\mathbf{x}_B, \mathbf{y}_B, \mathbf{z}_B\}$, where O_B is located at the center of mass (CoM) of the AV. The position of O_B expressed in $\mathcal{F}_W$ is denoted by $\mathbf{p}_B \in \mathbb{R}^3$, see Fig. 3.3 for illustration. The orientation of $\mathcal{F}_B$ can be chosen arbitrarily without lost of generality, in practice $\mathbf{x}_B$ is aligned with a forward direction that might be obvious from mechanical design, *e.g.*, a part of the multi-rotor structure like a bar supporting a motor in the quadrotor case. The North-East-Down (NED) convention, *i.e.*, $\mathbf{z}_B$ pointing downwards when the AV is hovering, can be chosen but is not necessary. Orientation are described via rotation matrices in $SO(3)$, where $\mathbf{R}_{\triangle}^{\blacklozenge} \in SO(3)$ expresses the rotation of frame $\mathcal{F}_{\triangle}$ *w.r.t.* frame $\mathcal{F}_{\blacklozenge}$. Omissions of $\blacklozenge$ are intended as $\blacklozenge = W$. In a similar manner, $\boldsymbol{\omega}_{\triangle} \in \mathbb{R}^3$ denotes the angular velocity of $\mathcal{F}_{\triangle}$ *w.r.t.* $\mathcal{F}_W$, expressed in $\mathcal{F}_{\triangle}$. Given these definitions, the orientation kinematics of the body is expressed by

$$\mathbf{R}_B = \mathbf{R}_B \left[\boldsymbol{\omega}_B\right]_{\times} \tag{3.1}$$

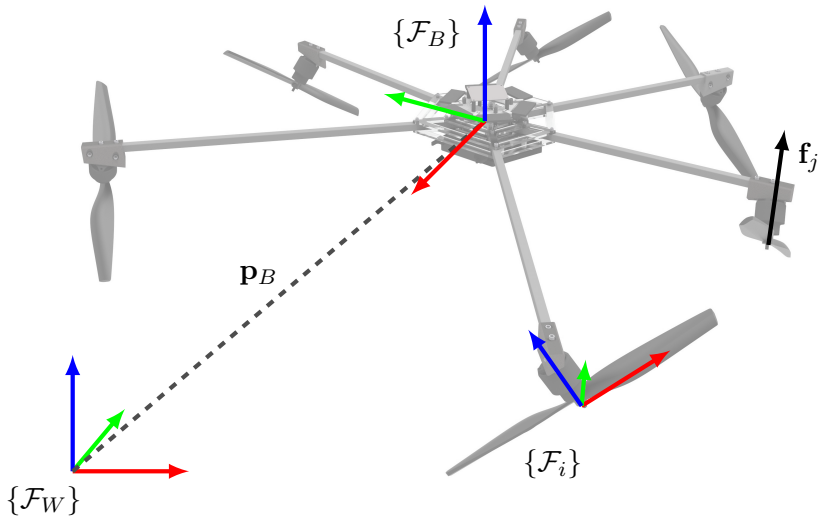

Figure 3.3 – Illustration of the principal frame used for the modeling of a multi-rotor's dynamics, superimposed on a tilted hexarotor. The axes $\mathbf{x}_*, \mathbf{y}_*, \mathbf{z}_*$ are represented in red, green and blue respectively. The inertial frame is denoted $\mathcal{F}_W$ and the body frame centered on the AV's CoM is denoted $\mathcal{F}_B$. For readability only one propeller frame $\mathcal{F}_i$ is represented. A propeller thrust is depicted as $\mathbf{f}_j$, on another propeller, to highlight the thrust direction.

where $[\star]_\times \in SO(3)$ represents the skew symmetric matrix associated to any vector $\star \in \mathbb{R}^3$.

Denote with N the number of propellers of the vehicle, collinear or not. Each propeller is associated with a frame $\mathcal{F}_i : O_i - \{\mathbf{x}_i, \mathbf{y}_i, \mathbf{z}_i\}$ defined by its origin O_i the center of the propeller, the main axis are oriented so that their spinning plane is defined by $\mathbf{x}_i - \mathbf{y}_i$ and the spinning axis is $\mathbf{z}_i$. The orientation of a propeller in $\mathcal{F}_B$ is defined by $\mathbf{R}_i^B$. In the special case of a collinear multi-rotor, all propellers are spinning in the same plane, which is typically $\mathbf{x}_B - \mathbf{y}_B$, thus around axes collinear to $\mathbf{z}_B$.

Translational Dynamics

In the Newton-Euler formalism, the translational dynamics in $\mathcal{F}_W$ can be expressed as

$$m\ddot{\mathbf{p}}_B = -mg\mathbf{z}_W + \mathbf{R}_B \left(\mathbf{f}^B + \mathbf{f}_e^B\right), \tag{3.2}$$

where $m \in \mathbb{R}_+$ is the mass of the vehicle, $-g\mathbf{z}_W$ is the gravity acceleration, $\mathbf{f}^B \in \mathbb{R}^3$ is the total actuation force acting on the vehicle, or *total thrust*, expressed at the CoM of the vehicle and $\mathbf{f}_e^B \in \mathbb{R}^3$ is the external forces expressed in $\mathcal{F}_B$. In *contact-free* flight and without the presence of wind $\mathbf{f}_e^B \equiv \mathbf{0}$.

The dominant aerodynamics of each rotor i, for $i = 1, \dots, N$, produces a force (thrust) $\mathbf{f}_i^B$ in the body frame, $\mathbf{f}_i^B = \mathbf{R}_i^B \mathbf{z}_i \mathrm{f}_i$. In the special case of collinear multi-rotor it simplifies to $\mathbf{f}_i^B = \mathrm{f}_i \mathbf{z}_B$ (see, e.g., [Mahony–2012]). In order to take into account the spatial disposition of the propellers, define $\mathbf{B}_1 \in \mathbb{R}^{3\times N}$ as the mapping between the single propeller forces and the overall actuation force in body frame, influenced by their respective orientations. One can write

$$\mathbf{f}^B = \mathbf{B}_1 \begin{bmatrix} \mathrm{f}_1 \\ \vdots \\ \mathrm{f}_N \end{bmatrix} + \boldsymbol{\delta}, \tag{3.3}$$

where $\boldsymbol{\delta}$ comprises second order aerodynamic forces mainly due to flapping and drag effects, that are typically neglected in nominal working conditions [Mahony–2012]. In the collinear case the expression can be further simplified as the total thrust is applied along $\mathbf{z}_B$,

$$\mathbf{f}^B = \sum_{i=1}^{N} \mathrm{f}_i \mathbf{z}_B + \boldsymbol{\delta} = \mathrm{f}_F \mathbf{z}_B + \boldsymbol{\delta}, \tag{3.4}$$

It can be assumed, as first approximation see [Mahony–2012], that the thrust produced by the rotor i is instantaneously related to its spinning velocity ϖ_i by the following relation

$$\mathrm{f}_i = c_{F,i} \varpi_i^2, \tag{3.5}$$

where $c_{F,i} > 0$ are *aerodynamic constants* that depends on the specific properties of the propeller used and the airflow around it. A common assumption consists in assuming that for a given propeller type, c_F is unique. Taking (3.5) into account (3.3) ca be rewritten

$$\mathbf{f}^B = \mathbf{F}_1 \begin{bmatrix} \varpi_1^2 \\ \vdots \\ \varpi_N^2 \end{bmatrix} + \boldsymbol{\delta}, \tag{3.6}$$

where $\mathbf{F}_1 \in \mathbb{R}^{3\times N}$ is the force control matrix and is function of the propellers orientation and location in $\mathcal{F}_B$ and of the aerodynamic coefficients c_F.

Rotational Dynamics

Equivalently, in the Newton-Euler formalism, the rotational dynamics in $\mathcal{F}_B$ can be expressed as

$$\mathbf{J}\dot{\boldsymbol{\omega}} = -\boldsymbol{\omega} \times \mathbf{J}\boldsymbol{\omega} + \boldsymbol{\tau} + \boldsymbol{\tau}_e, \tag{3.7}$$

where $\mathbf{J}$ denotes the Inertia matrix of the AV, the term $-\boldsymbol{\omega} \times \mathbf{J}\boldsymbol{\omega}$ represents the contribution of the Coriolis and centripetal forces and $\times$ denotes the cross-product, $\boldsymbol{\tau} \in \mathbb{R}^3$ is the actuation torque produced, also called total torque, expressed at the CoM and $\boldsymbol{\tau}_e \in \mathbb{R}^3$ is the external torque expressed in $\mathcal{F}_B$. Again, in *contact-free* flight and without the presence of wind $\boldsymbol{\tau}_e \equiv \mathbf{0}$. Similarly to the translational dynamics, each propeller produces a reaction torque $\boldsymbol{\tau}_i$ due to the rotor drag, this reaction is exerted along the rotation axes of the propeller so $\boldsymbol{\tau}_i = \mathbf{R}_i^B \tau_i \mathbf{z}_i$, which leads in the special case of collinear multi-rotor to $\boldsymbol{\tau}_i = \tau_i \mathbf{z}_B$. In general, the actuation torque produced $\boldsymbol{\tau}$ is composed of the addition of the drag torques $\boldsymbol{\tau}_i$ and of the moment produced by single propeller thrust $\mathbf{f}_i$ under

$$\boldsymbol{\tau} = \sum_{i=1}^{N} \left(\boldsymbol{\tau}_i + \boldsymbol{p}_i^B \times \mathbf{f}_i^B \right), \tag{3.8}$$

where $\boldsymbol{p}_i^B$ is the position of the propeller in $\mathcal{F}_B$. Note that, the total torque span is clearly influenced by the spatial distributions of the propellers. Similarly to the thrust case, the drag torque can be approximated by

$$\tau_i = c_{\tau,i} \varpi^2 \tag{3.9}$$

where $c_{\tau,i} > 0$ are *aerodynamic constants*, often assumed equal for a set of propellers with the same geometry, *i.e.*, $c_{\tau,i} = c_\tau \quad \forall i \in [1...N]$. Introducing the torque control matrix $\mathbf{F}_2$, a compact notation of (3.8) can be written

$$\boldsymbol{\tau} = \mathbf{F}_2 \varpi^2 \tag{3.10}$$

where $\mathbf{F}_2$ is function of the propellers orientation and location in $\mathcal{F}_B$ and of the two aerodynamic coefficients c_F and c_τ.

Full Dynamics

The previous translational and rotational dynamics can be grouped to express the full body dynamic in a compact way

$$\begin{bmatrix} m\ddot{\mathbf{p}}_B \\ \mathbf{J}\dot{\boldsymbol{\omega}} \end{bmatrix} = \begin{bmatrix} -mg\mathbf{z}_W \\ -\boldsymbol{\omega} \times \mathbf{J}\boldsymbol{\omega} \end{bmatrix} + \begin{bmatrix} \mathbf{R}_B \mathbf{F}_1 \\ \mathbf{F}_2 \end{bmatrix} \begin{bmatrix} \varpi_1^2 \\ \vdots \\ \varpi_N^2 \end{bmatrix} + \begin{bmatrix} \mathbf{R}\mathbf{f}_e \\ \boldsymbol{\tau}_e \end{bmatrix}. \tag{3.11}$$

Which is the compact form of the Euler-Newton dynamics for multi-rotor AV. Based on the propeller physical implementation in the design of AV two situation arises, either the AV is said underactuated or it is said to have multi-directional thrust actuation, both property are reflected by the control matrices, $\mathbf{F}_1$ and $\mathbf{F}_2$, expression.

The dynamics (3.11) can be rewritten in a more compact form by considering $\mathbf{q}_{av} \in \mathbb{R}^6$ as vector of generalized coordinates for the AV, which concatenates the

position and orientation. This leads to the expression

$$\mathbf{M}_{av}\mathbf{q}_{av} + \mathbf{c}_{av}(\mathbf{q}_{av}, \dot{\mathbf{q}}_{av}) + \mathbf{g}(\mathbf{q}_{av}) = \mathbf{G}_{av}\boldsymbol{u} + \mathbf{f}_{ext}, \tag{3.12}$$

where $\mathbf{M}_{av} \in \mathbb{R}^{6\times6}$, $\mathbf{c}_{av}(\mathbf{q}_{av}, \dot{\mathbf{q}}_{av}) \in \mathbb{R}^6$ and $\mathbf{g}(\mathbf{q}_{av}) \in \mathbb{R}^6$ represents the AV inertia matrix, the Coriolis/centripetal and the gravity terms respectively. the control inputs are denoted $\boldsymbol{u} = \left[\varpi_1^2 \dots \varpi_N^2\right]^\top \in \mathbb{R}^N$ and the control matrix $\mathbf{G}_{av} \in \mathbb{R}^{6\times N}$ maps their impact on the AV dynamics. The total external forces exerted on the AV are denoted $\mathbf{f}_{ext}$ and are expressed at the CoM.

Underactuated Aerial Vehicles

Underactuation is used to characterize vehicles which have less actuation DoFs than motion DoFs, which implies that they cannot follow arbitrary trajectories in their configuration space. In particular for multi-rotor AV all collinear designs, *i.e.*, when the propeller spinning axes are all collinear, are underactuated and the thrust direction is fixed in the body frame of the AV as perpendicular to the propellers rotation plane. Indeed, for these designs, *e.g.*, typical quadrotors, lateral motion cannot be achieved without a change of orientation, this strong coupling between the rotational and translational dynamics traduces the underactuation property and is reflected in the expression of $\mathbf{F}_1$, where the terms corresponding to the lateral motion have dependencies on the AV orientation. Note that the increase of propellers number, if keeping the same collinear design, does not resolve the underactuation.

Multi-Directional Thrust Aerial Vehicles

Another popular class of multi-rotor AV are described as multi-directional thrust platforms, meaning that the thrust orientation in body frame is not fixed and can be chosen by mean of control. In this case, the total thrust is exerted in a 3D polytope, as opposed to the underactuated case where it is exerted along a line, see Fig. 3.4. This is made possible by the non collinear positioning of the propellers. Also, this is only possible when there are at least six propellers, *i.e.*, $N \geq 6$, when one considers that also the total moment has to be multi-directional and controllable independently from the total force. This useful property comes at the cost of internal forces, *i.e.*, loss of energetic efficiency. Resulting in a trade-off between the total thrust polytope shape and the internal forces. In this case the AV can follow any arbitrary trajectory not violating the propellers actuation constraints, otherwise the AV is also hindered by a coupling between its translational and rotational dynamics. For more insights about these kind of design [Rajappa–2015], [Ryll–2016] and [Michieletto–2017] are recommended reads.

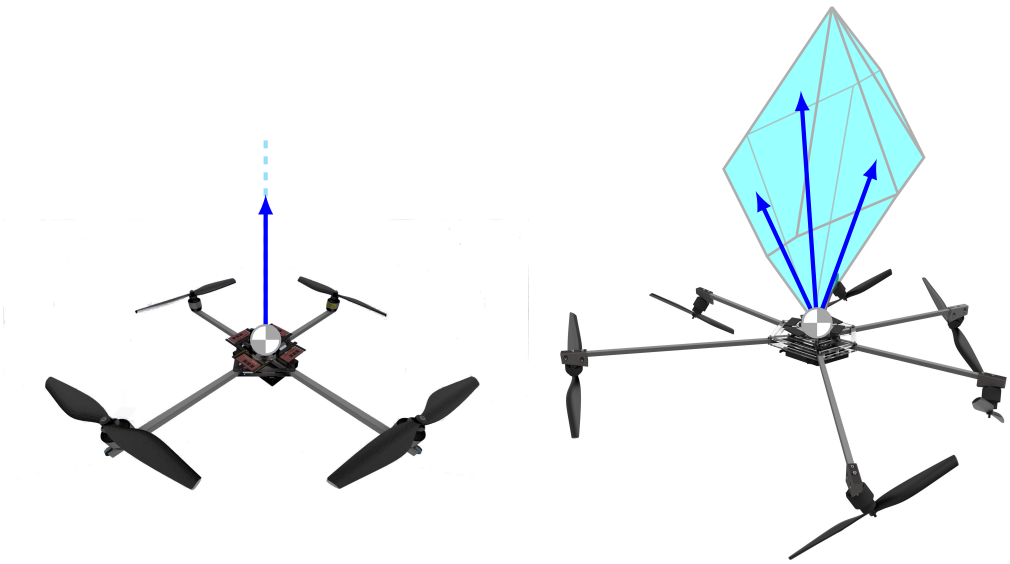

(a) (b)

Figure 3.4 – Illustration of the total thrust exertion space for both (a) underactuated and (b) multi-directional thrust AV. In the underactuated case the total thrust can only be exerted along a line in the body frame (1D), while in the multi-directional thrust case the total thrust can be exerted inside a polytope (3D).

3.2.2 From Aerial Vehicle to Aerial Robot

Aerial Robot denomination is used to denote the capability of not only perceiving the environment an moving through it, but also acting on it by physical means. To endow AV with physical interaction capabilities the solution is to equip them with a manipulator.

Consider a m-DoF manipulator to be embedded on the AV and denote $\mathcal{F}_{am,0}$: $O_{am} - \{\mathbf{x}_{am}, \mathbf{y}_{am}, \mathbf{z}_{am}\}$ the base frame of the manipulator, centered in O_{am} the base of the manipulator, see Fig. 3.5. The vector $\mathbf{p}_{am}^{B} \in \mathbb{R}^3$ denotes the position of the base in the AV body frame, $\mathcal{F}_B$. The Tool Center Point (TCP) of the manipulator EE is located in $O_{am,ee}$ which has an associated frame, $\mathcal{F}_{am,ee}$: $O_{am,ee} - \{\mathbf{x}_{am,ee}, \mathbf{y}_{am,ee}, \mathbf{z}_{am,ee}\}$. The coordinates associated with each link are written $\mathbf{q}_j$ with $j \in \{1, \ldots, k\}$ and concatenated in $\mathbf{q}_{am}$ yield for the manipulator dynamics

$$\mathbf{M}_{am}\ddot{\mathbf{q}}_{am} + \mathbf{C}_{am}(\mathbf{q}_{qm}, \dot{\mathbf{q}}_{am}) + \mathbf{g}(\mathbf{q}_{qm}) = \boldsymbol{\tau}_{am} + \mathbf{J}_{am}^{\top}\mathbf{f}_{ext} + \mathbf{J}_{ar}^{\top}\mathbf{f}_{ar}, \tag{3.13}$$

where $\mathbf{M}_{am} \in \mathbb{R}^{m\times m}$, $\mathbf{C}_{am}(\mathbf{q}_{qm}, \dot{\mathbf{q}}_{am}) \in \mathbb{R}^m$ and $\mathbf{g}(\mathbf{q}_{qm}) \in \mathbb{R}^m$ represents the manipulator's inertia matrix, the Coriolis/centripetal and the gravity terms respectively. The vector $\boldsymbol{\tau}_{am} \in \mathbb{R}^m$ denotes the actuation torque and $\mathbf{f}_{ext} \in \mathbb{R}^6$ and $\mathbf{f}_{ar} \in \mathbb{R}^6$ are the external wrench applied to the manipulator respectively at the EE

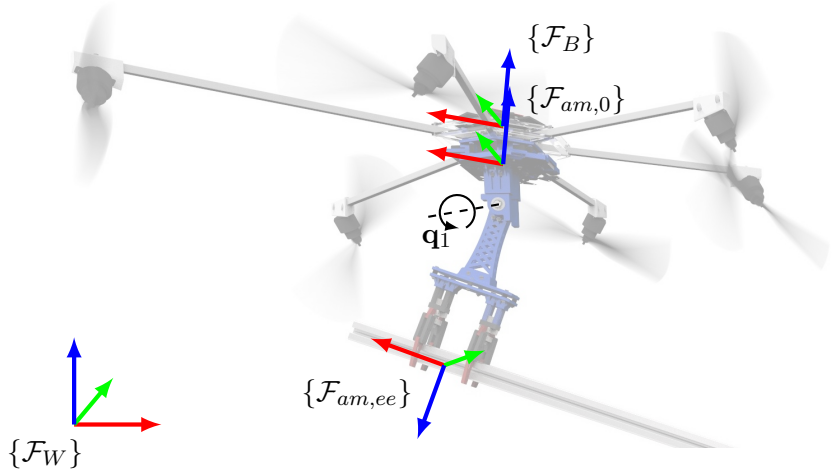

Figure 3.5 – Illustration of the principal frames used for the modeling of an AR dynamic, superimposed on a custom AR with a single joint manipulator. The axes $\mathbf{x}_*, \mathbf{y}_*, \mathbf{z}_*$ are represented in red, green and blue respectively. The inertial frame is denoted $\mathcal{F}_W$, the body frame centered on the AV's CoM is denoted $\mathcal{F}_B$, the embedded manipulator's base frame is denoted $\mathcal{F}_{am,0}$ and its TCP frame is denoted $\mathcal{F}_{am,ee}$. The manipulator joint coordinates, $\mathbf{q}_1$, is also represented for illustration.

and the base. Finally the matrices $\mathbf{J}_{am} \in \mathbb{R}^{6\times k}$ denote the manipulator geometric Jacobian and $\mathbf{J}_{ar} \in \mathbb{R}^{6\times k}$ the dynamical coupling term between the AV and the aerial manipulator.

By merging (3.12) with (3.13) and considering as generalized coordinate $\mathbf{q} = \begin{bmatrix}\mathbf{q}_{av}^\top & \mathbf{q}_{am}^\top\end{bmatrix}^\top \in \mathbb{R}^{6+k}$ one can write the full AR dynamical model as

$$\begin{bmatrix}\mathbf{M}_{av} & \mathbf{J}_{ar} \\ \mathbf{J}_{ar}^\top & \mathbf{M}_{am}\end{bmatrix} + \begin{bmatrix}\mathbf{c}_{av}(\mathbf{q}_{av}, \dot{\mathbf{q}}_{av}) \\ \mathbf{c}_{am}(\mathbf{q}_{qm}, \dot{\mathbf{q}}_{am})\end{bmatrix} + \begin{bmatrix}\mathbf{g}_{av(\mathbf{q}_{av})} \\ \mathbf{g}(\mathbf{q}_{qm})\end{bmatrix} = \begin{bmatrix}\mathbf{G}_{av} & \mathbf{0} \\ \mathbf{0} & \boldsymbol{I}_k\end{bmatrix}\begin{bmatrix}\boldsymbol{u}_{av} \\ \boldsymbol{\tau}_{am}\end{bmatrix} + \begin{bmatrix}\mathbf{f}_{ext,av} \\ \mathbf{J}_{am}^\top \mathbf{f}_{ext,am}\end{bmatrix}, \tag{3.14}$$

The coupling between the AV and the aerial manipulator appears explicitly through the term $\mathbf{J}_{ar}$ and is also present in the expressions of the Coriolis/centripetal and gravity terms. Note that the control matrix is totally decoupled between the AV and the aerial manipulator. And that both the external wrench $\mathbf{f}_{ext,av}$ applied to the AV and the external wrench $\mathbf{f}_{ext,am}$ applied to the arm EE are considered.

Passive or Actuated Joints for Aerial Manipulators

The first reflex that can be seen in the design of new AR is to take both an existing AV and a lightweight manipulator, stitch them together and hope for the best. But having a manipulator attached to a floating base rises several mechanical and control challenges, moreover the main limitation to this solution is the static and dynamic

coupling between the manipulator and the AV and the actuation limits of the AV. This coupling can prove destabilizing in general for the AR, as wrench applied at the manipulator's EE maps to torques at the AV CoM, which has typically pretty low torque actuation limits, around 0.2 N m to 0.5 N m. From their capabilities, MAV multi-rotors are more suited for force input and can also be seen as thrusters for AM. Hence instead of a complex manipulator one can, in practice, focus on simpler one link design.

As for underactuated AV the thrust can only be exerted along their **z**-axis in body frame, to have orientable thrusters the rotational dynamics of the AR should be decoupled from the one of the load. This results in the choice of 3D passive rotational joints in our first MAGMaS prototype. With the three centers of rotation coinciding with the AR CoM so that force at the EE of the manipulator does not generate torque on the flying platform. Note that this decoupling property is only achieved in the mechanical limits of the passive joint itself.

The multi-directional thrust AV can in principle exert an orientable thrust while rigidly attached to a load, then again inside a certain polytope constrained by the propeller physical implementation. However in practice the choice to use passive revolute joint, to decouple the AR rotation from the one of the manipulated load, can be legitimate as to allow the completion of certain manipulation task or enlarge the set of possible orientation of the thrust.

3.3 Modeling of MAGMaS

The considered MAGMaS is composed by a n-DoF ground manipulator, and k AR that cooperatively manipulate an object, see Fig. B.8.The system modeling when the object is not grasped is omitted, as well documented in the literature of robotic navigation. The EE of the ground manipulator is equipped with a gripper in order to rigidly grasp the object. Each AR is equipped with a *grasping link* attached to the CoM by means of a passive spherical joint. At the other end, the grasping link is equipped with a gripper. This mechanism allows to grasp the object while leaving the AR attitude unconstrained. In this first approach on MAGMaS the choice was made to consider a passive joint in the manipulator for one main reason: the relatively limited torque actuation of multi-rotor AV. Indeed multi-rotor can exert a reasonable force, around 28 N for a small quadrotor, but significantly less torque, around 0.2 N m for the same platform. From this observation it is clear that forces and torques applied by the environment on the AR EE should be minimized in order to prevent destabilization of the AR. Hence the passive spherical joint, a 3D passive revolute joint, efficiently decoupling rotational dynamics of the AV and its attached manipulator.

Recall $\mathcal{F}_W : O_W - \{\mathbf{x}_W, \mathbf{y}_W, \mathbf{z}_W\}$ denote the world frame, an let the manipulated object body frame be denoted with $\mathcal{F}_O : O_O - \{\mathbf{x}_o, \mathbf{y}_o, \mathbf{z}_o\}$, where O_O is the object CoM. Without loss of generality it can be assumed that $\mathcal{F}_O$ is parallel to the ground manipulator EE frame, as depicted in Fig. 3.6. The body frame of the i–th AR

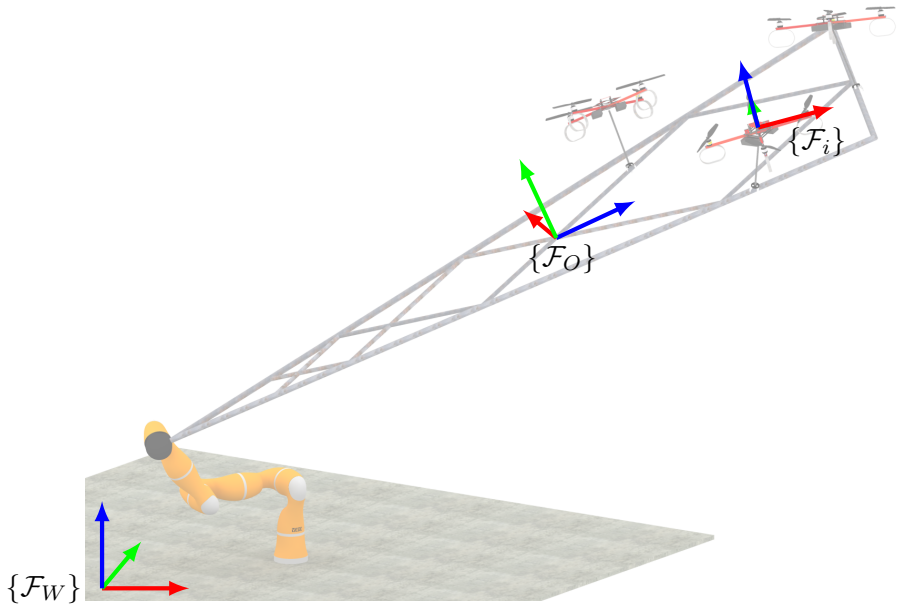

Figure 3.6 – Illustration of the principal frames used for the modeling of a MAGMaS, superimposed on one composed of a single ground manipulator and three underactuated AR. The axes $\mathbf{x}_*, \mathbf{y}_*, \mathbf{z}_*$ are represented in red, green and blue respectively. The inertial frame is denoted $\mathcal{F}_W$, the object body frame centered on the object's CoM is denoted $\mathcal{F}_O$. The AR body frame are denoted $\mathcal{F}_i$ and are centerd on their respective CoM.

(with $i \in \{1, \dots, k\}$) is denoted with $\mathcal{F}_i : O_i - \{\mathbf{x}_i, \mathbf{y}_i, \mathbf{z}_i\}$ where O_i is the AR CoM, denoted $\mathcal{F}_B$ in section 3.2 and renamed for compactness.

The position of O_O and O_i in $\mathcal{F}_W$ are denoted $\boldsymbol{p}_o,\ \boldsymbol{p}_i\ \in \mathbb{R}^3$ and $\mathbf{R}_o,\ \mathbf{R}_i \in SO(3)$ are the rotation matrices expressing the orientation of $\mathcal{F}_O$ and $\mathcal{F}_i$ *w.r.t.* $\mathcal{F}_W$. The matrices $\mathbf{R}_o$ and $\mathbf{R}_i$ are parameterized by a set of roll/pitch/yaw angles $\boldsymbol{\eta}_o = [\phi_o\ \theta_o\ \psi_o]^\top \in \mathbb{R}^3$ and $\boldsymbol{\eta}_i = [\phi_i\ \theta_i\ \psi_i]^\top \in \mathbb{R}^3$, respectively. Although singular this parametrization can be used as the AR are assumed to remain away from the parametrization singularities. The angular velocities of $\mathcal{F}_O$ and $\mathcal{F}_i$ *w.r.t.* $\mathcal{F}_W$, expressed in the corresponding body frame, are denoted with $\boldsymbol{\omega}_o,\ \boldsymbol{\omega}_i \in \mathbb{R}^3$, respectively. Furthermore, let $m_o,\ m_i \in \mathbb{R}^+$ and $\mathbf{J}_o,\ \mathbf{J}_i \in \mathbb{R}^{3\times3}$ be the mass and inertia matrix of the object and i–th AR.

The i–th AR exerts a thrust force $\boldsymbol{u}_t^i$ applied at its CoM. In the underactuated AV case, $\boldsymbol{u}_t^i = u_t^i \mathbf{z}_i$ with u_t^i is a controllable magnitude and $\mathbf{z}_i$ specified by the AR orientation, which is regulated by the control torque vector $\boldsymbol{u}_r^i = [u_{r_x}^i\ u_{r_y}^i\ u_{r_z}^i]^\top \in \mathbb{R}^3$. In the multi-directional thrust case both the magnitude and the orientation of $\boldsymbol{u}_t^i = [u_{t_x}^i\ u_{t_y}^i\ u_{t_z}^i]^\top \in \mathbb{R}^3$ can be controlled directly and independently.

Then (3.11) can be re-written as

$$m_i\ddot{\boldsymbol{p}}_i - m_i g\mathbf{z}_W = \mathbf{R}_i\boldsymbol{u}_t^i - \mathbf{h}_i \tag{3.15}$$

$$\mathbf{J}_i\dot{\boldsymbol{\omega}}_i + \boldsymbol{\omega}_i \times \mathbf{J}_i\boldsymbol{\omega}_i = \boldsymbol{u}_r^i \tag{3.16}$$

where $\mathbf{h}_i \in \mathbb{R}^3$ is the load of the system on i-th AR and the inputs introduced in Sec. 3.2.1 are related to $\boldsymbol{u}_t^i$ and $\boldsymbol{u}_r^i$ via

$$\begin{bmatrix}\boldsymbol{u}_t^i \\ \boldsymbol{u}_r^i\end{bmatrix} = \begin{bmatrix}\mathbf{F}_1 \\ \mathbf{F}_2\end{bmatrix}\begin{bmatrix}\varpi_1^2 \\ \vdots \\ \varpi_N^2\end{bmatrix} \tag{3.17}$$

for the i-th AR with N propellers.

Similarly than in Sec. 3.2.1, from (3.16), recalling the relationship between $\boldsymbol{\omega}_i$ and the derivative the Euler angles $\dot{\boldsymbol{\eta}}_i$ as $\boldsymbol{\omega}_i = \mathbf{E}_i(\boldsymbol{\eta}_i)\dot{\boldsymbol{\eta}}_i$, the rotational dynamics of the i–th AR is

$$\mathbf{M}_i\ddot{\boldsymbol{\eta}}_i + \boldsymbol{c}_i(\boldsymbol{\eta}_i, \dot{\boldsymbol{\eta}}_i) = \boldsymbol{u}_r^i \tag{3.18}$$

in which $\mathbf{M}_i \in \mathbb{R}^{3\times3}$ is the rotational part of the i–th AR's Inertia matrix, $\boldsymbol{c}_i(\boldsymbol{\eta}_i, \dot{\boldsymbol{\eta}}_i) \in \mathbb{R}^3$ is the Coriolis/centripetal term. Moreover the position of O_i in $\mathcal{F}_O$ is denoted by $\mathbf{r}_i \in \mathbb{R}^3$. Thus the relationship $\boldsymbol{p}_i = \boldsymbol{p}_o + \mathbf{R}_o\mathbf{r}_i$ olds for $i \in \{1, \ldots, k\}$.

The dynamical model of the ground manipulator is

$$\mathbf{M}_m(\mathbf{q}_m)\ddot{\mathbf{q}}_m + \boldsymbol{c}_m(\mathbf{q}_m, \dot{\mathbf{q}}_m) + \boldsymbol{g}_m(\mathbf{q}_m) = \boldsymbol{u}_m - \mathbf{J}_m^\top(\mathbf{q}_m)\mathbf{h}_o \tag{3.19}$$

where $\mathbf{q}_m = [q_1 \ \ldots \ q_n]^\top \in \mathbb{R}^n$ is the joint angle coordinate vector, $\mathbf{h}_o \in \mathbb{R}^6$ is the wrench applied by the manipulator to the {object–AR} system, expressed in the EE frame, $\mathbf{M}_m(\mathbf{q}_m) \in \mathbb{R}^{n\times n}$ is the inertia matrix, $\boldsymbol{c}_m(\mathbf{q}_m, \dot{\mathbf{q}}_m) \in \mathbb{R}^n$ and $\boldsymbol{g}_m(\mathbf{q}_m) \in \mathbb{R}^n$ represent the Coriolis/centripetal and gravity terms, respectively, $\mathbf{J}_m(\mathbf{q}_m) \in \mathbb{R}^{6\times n}$ is the geometric Jacobian of the manipulator and $\boldsymbol{u}_m = [u_m^1 \ldots u_m^n]^\top \in \mathbb{R}^n$ gathers the n joint torques of the manipulator.

From this point on, the modeling considers the use of underactuated AR with full passive rotational joints and a one link aerial manipulator in order to exhibit a set of properties for this case. In particular the 3D revolute joint is designed so that the 3 axes of rotation are passing through the AR CoM. This means that the rotational dynamic of the AR is efficiently decoupled from the one of the manipulated object and the thrust is exerted along the $\mathbf{z}$-axis in body frame of the AR, *i.e.*, $\boldsymbol{u}_t^i = u_t^i\mathbf{z}_i$. This particular case is especially useful in practice to overcome torque actuation limits for simple quadrotors.

Considering as generalized coordinates $\mathbf{q} = [\mathbf{q}_m^\top \ \mathbf{q}_a^\top]^\top \in \mathbb{R}^{n+3k}$, where $\mathbf{q}_a = [\boldsymbol{\eta}_1^\top \ \ldots \ \boldsymbol{\eta}_k^\top]^\top \in \mathbb{R}^{3k}$, the position of the AR is not part of the generalized coordinates as it is constrained by the object position once rigidly grasped and $\boldsymbol{u} = [\boldsymbol{u}_m^\top \ \boldsymbol{u}_r^\top]^\top \in \mathbb{R}^{n+3k}$ in which $\boldsymbol{u}_r = [\boldsymbol{u}_r^{1\top} \ldots \boldsymbol{u}_r^{k\top}]^\top \in \mathbb{R}^{3k}$. The dynamical model of the whole

system can be written as

$$\mathbf{M}(\mathbf{q})\ddot{\mathbf{q}} + \boldsymbol{c}(\mathbf{q}, \dot{\mathbf{q}}) + \boldsymbol{g}(\mathbf{q}) = \boldsymbol{u} - \mathbf{J}^{\top}(\mathbf{q})\mathbf{h}, \tag{3.20}$$

in which

$$\begin{aligned}
\mathbf{M}(\mathbf{q}) &= \operatorname{diag}\left(\mathbf{M}_m(\mathbf{q}_m), \mathbf{M}_1(\boldsymbol{\eta}_1), \ldots, \mathbf{M}_k(\boldsymbol{\eta}_k)\right) \\
\boldsymbol{g}(\mathbf{q}) &= \left[\boldsymbol{g}_m(\mathbf{q}_m)\ \mathbf{0}_{3k\times 1}\right]^{\top}, \\
\boldsymbol{c}(\mathbf{q}, \dot{\mathbf{q}}) &= \left[\boldsymbol{c}_m(\mathbf{q}_m, \dot{\mathbf{q}}_m), \boldsymbol{c}_1(\boldsymbol{\eta}_1, \dot{\boldsymbol{\eta}}_1), \ldots, \boldsymbol{c}_k(\boldsymbol{\eta}_k, \dot{\boldsymbol{\eta}}_k)\right]^{\top}, \\
\mathbf{J} &= \operatorname{diag}\left(\mathbf{J}_m(\mathbf{q}_m), \mathbf{0}_3, \ldots, \mathbf{0}_3\right).
\end{aligned}$$

The term $\mathbf{h} \in \mathbb{R}^{6+3k}$ is defined as $\mathbf{h} = [\mathbf{h}_o^{\top}\ \mathbf{h}_t^{\top}]^{\top}$, where $\mathbf{h}_t = [\mathbf{h}_1^{\top}, \ldots, \mathbf{h}_k^{\top}]^{\top}$, $\mathbf{h}_i \in \mathbb{R}^3$ expresses the particular load felt by each AR. The structure of $\mathbf{J}$ arises from the fact that the passive joints efficiently decouple the AR rotational dynamics. The dynamic equation of motion for the rigid body object completes the dynamic model of the system

$$\mathbf{M}_o(\mathbf{x})\ddot{\mathbf{x}} + \boldsymbol{c}_o(\mathbf{x}, \dot{\mathbf{x}}) + \boldsymbol{g}_o(\mathbf{x}) = \mathbf{h}_e \tag{3.21}$$

where $\mathbf{x} = [\boldsymbol{p}_o^{\top}\ \boldsymbol{\eta}_o^{\top}]^{\top} \in \mathbb{R}^6$ is the object pose vector, $\mathbf{M}_o \in \mathbb{R}^6$, $\boldsymbol{c}_o \in \mathbb{R}^6$, and $\boldsymbol{g}_o \in \mathbb{R}^6$ are inertial matrix, Coriolis/centripetal and gravity vectors, respectively, and $\mathbf{h}_e$, called external wrench, is the resultant force of the ground manipulator and all the AR, that moves the object and can be calculated as follows

$$\mathbf{h}_e = \mathbf{G}\mathbf{h} \tag{3.22}$$

where the grasp matrix $\mathbf{G}$ is defined as $\mathbf{G} = [\mathbf{T}_m\ \ \mathbf{G}_t(\mathbf{q})]$ in which $\mathbf{T}_m \in \mathbb{R}^{6\times 6}$ transforms $\mathbf{h}_o$ from the EE frame to the world frame and $\mathbf{G}_t(\mathbf{q}) \in \mathbb{R}^{6\times 3k}$ describes the influence of the AR thrust vectors on the object motion. It is straightforward to obtain them as follows

$$\mathbf{T}_m = \begin{bmatrix} \mathbf{R}_o^{\top} & \mathbf{0} \\ \mathbf{S}(\mathbf{R}_o^{\top}\mathbf{r}_e) & \mathbf{R}_o^{\top} \end{bmatrix} \tag{3.23}$$

$$\mathbf{G}_t(\mathbf{q}) = \begin{bmatrix} \mathbf{I}_3 & \ldots & \mathbf{I}_3 \\ \mathbf{S}(\mathbf{R}_o^{\top}\mathbf{r}_i) & \ldots & \mathbf{S}(\mathbf{R}_o^{\top}\mathbf{r}_k) \end{bmatrix} \tag{3.24}$$

where $\mathbf{r}_e \in \mathbb{R}^3$ is the ground manipulator EE position in $\mathcal{F}_O$ and $\mathbf{S}(\cdot)$ the the skew-symmetric operator on a vector. Now consider (3.22), the grasp matrix $\mathbf{G}$ is full-row rank by construction, thus for a given $\mathbf{h}_e$ the inverse of (3.22) can be written as follows

$$\mathbf{h} = \mathbf{G}^{+}\mathbf{h}_e + \mathbf{V}\mathbf{h}_n = \mathbf{h}_E + \mathbf{h}_I \tag{3.25}$$

where $\mathbf{G}^{+}$ is a pseudo-inverse of $\mathbf{G}$ and $\mathbf{V}$ is a full-row rank matrix spanning

the null-space of $\mathbf{G}$ and $\mathbf{h}_n$ is an arbitrary vector of appropriate dimension that parameterizes the solution sets [Prattichizzo–2008]. Concatenated wrench vector $\mathbf{h}_E$ are wrenches that can result in motion, while $\mathbf{h}_I$ are known as internal wrenches, and their directions are such that they do not contribute to a motion.

3.3.1 System Constraints

The ground manipulator joint torques and force vector of each AR must comply with the following system constraints.

- The limited orientation of the thrust produced by the i–th AR, either due to rotations of spherical joints constrains (underactuated case) or by the polytope boundaries (multi-directional thrust case).

$$\chi_i(\boldsymbol{\eta}_i) = \sqrt{(h_i^x)^2 + (h_i^y)^2} - \tan(\alpha_i) h_i^z \leq 0 \tag{3.26}$$

  where $\mathbf{h}_i = [h_i^x, h_i^y, h_i^z]^\top$ is the force vector and $\alpha_i \in \mathbb{R}^+$ shows the allowed cone angle of either the spherical joint or an approximation of the polytope envelope;
- the ground manipulator joints have limited rotation range,

$$q_i^{\min} \leq q_i \leq q_i^{\max} \quad i = 1, ..., n \tag{3.27}$$

  where $q_i^{\min}, q_i^{\max} \in \mathbb{R}^+$ are scalar values representing the upper and lower joint bounds;
- the robot manipulator torques are limited,

$$u_m^{i^{\min}} \leq u_m^i \leq u_m^{i^{\max}} \quad i = 1, ..., n, \tag{3.28}$$

  where $u_m^{i^{\min}}, u_m^{i^{\max}} \in \mathbb{R}$ represent the upper and lower torque bounds for the manipulator;
- each AR has a bounded thrust,

$$\|\mathbf{h}_i\| \leq h_i^{\max} \quad i = 1, ..., k \tag{3.29}$$

  where $h_i^{\max} \in \mathbb{R}^+$ is the maximum applicable thrust.

3.4 Discussion

As the work on MAGMaS is still young a large set of open research directions can still be investigated, in particular with respect to the constitution of the MAGMaS and the tasks at hand.

Moving base

In the work presented in this thesis the ground manipulator is mounted on a base remaining fixed during the cooperative manipulation. An interesting direction would be to study the case of a moving ground manipulator during the cooperative manipulation. Interesting topics being; leveraging the mobile base motion in the task, accounting for all the system constraints in the planning and the control allocation, optimally exploiting the null space of the overactuated system.

Degree of Freedom of the System

A open direction of research consists in studying the rationals behind the choice of the number DoF for the systems, their nature (passive/active) and their impact on the performances. The number of required DoFs for the ground manipulator and the number of AR as their manipulator DoFs and nature, all have an impact on the system performance but also on its complexity impacting not only the system procurement and maintenance costs but also computational and cognitive power necessary to operate the system.

Several Aerial Robots

As depicted in Fig. B.8, MAGMaS are not limited to a single AR, as described so far in this thesis, but are meant to be composed of several AR. In this case, the choice of the number and kind (under- or fully actuated) of AV remains to be investigated, criterion for the choice might range from single AV autonomy, affordability and complexity, to overall system complexity and operational configuration gain, for example.

Load Grasping

Also an engaging topic, arising from the use of several manipulators, is the automatic grasping locations choice for all manipulators, both ground and aerial, based on their actuation constraints and *a priori* or estimated information of the load parameters. Additionally for weird shaped load, the grasping location should be optimized to both facilitate the load cooperative handling and to allow control of the vibrations in the load.

Load Parameters

The last potential future work direction is related to the load kinematic and dynamic parameters. As the kinematic parameters play an important role in robust cooperative manipulation it is important to be able to retrieve them, see [Erhart–2013] [Erhart–2015] for approach relying on 6D wrench at the grasping points and [Erhart–2015] for modeling and analysis of cooperative manipulation dynamics. Load parameters estimation strategy without explicit communication is proposed in [Marino–2017], while a completely decentralized estimation method has been

firstly proposed in [Franchi–2014] and then extended with a robust control approach in [Petitti–2016].

Chapter 4

MAGMaS: Aerial-Ground Co-manipulation Force Estimation and Control

Contents

Abstract

This chapter presents the global control framework used for MAGMaS, from the planning to the low-level control. The general planning and control allocation scheme is reviewed in Sec. 4.1 for MAGMaS in general. Followed by the description of the geometric control for AR, Sec. 4.2. The next three sections focus on the forces estimation for APhI: motivating it in Sec. B.2 and detailing two parallel approaches, in Sec. 4.4 and Sec. 4.5, which are discussed in Sec. 6.6. The knowledge of the external force applied on the AR is then leveraged in by a force based controller presented in Sec. 4.7.

4.1 Planner and Control Allocation

The high level supervision of the task is handled by a task planner, which monitors the system state and generates trajectories accordingly and a control allocation stage, which, from the desired trajectory of the manipulated load, can infer the trajectories and/or control efforts for each subsystem, see Fig. 4.1. The proposed scheme is very general in the sense that it is generating trajectories in all stage of the cooperative manipulation, *i.e.*, when the object is grasped or not, taking into account the different constraints. In order to match with the low-level controllers used, the output can be chosen to match their requirements, *e.g.*, possibility to control the ground manipulator in Cartesian or joint space.

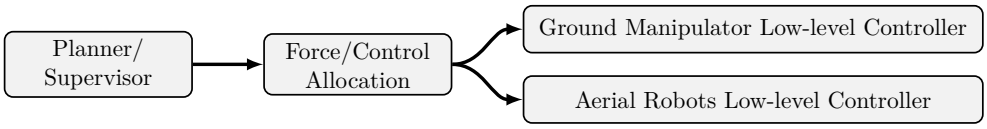

Figure 4.1 – High level view of the full control architecture, from the Task Planner to the low-level controllers, each detailed in Chaper 4.

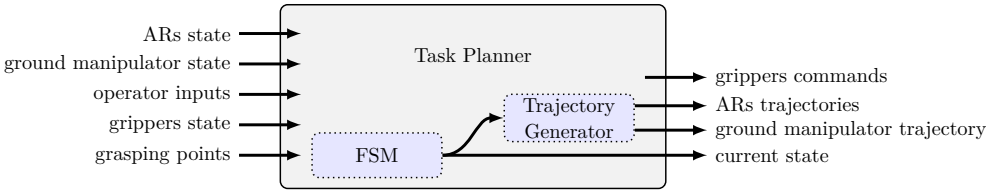

Figure 4.2 – Generic task planner overall structure, with inputs and outputs, as implemented for our MAGMaS experiment.

4.1.1 Task Planning

For supervision of the MAGMaS a generic high level planner was devised, composed of: *i)* a task planner, *ii)* a basic Finite State Machine (FSM) and *iii)* a trajectory generator with different policy for each state of the FSM, see Fig. 5.15.

It is generic in the sense that it can generate reference trajectories for either the manipulated object or for the two manipulators based on the FSM status. The planner is aware of the system state and can trigger FSM evolution based on the system sensors and human operator inputs. The actual content of the task planner and its strategies are experiment dependent and are presented more in depth with the experimental results, Chapter 5.

Note that due to the novelty of MAGMaS the emphasis of the presented work is more on the system design and control than on the use of advanced planning techniques, for example there is no collision detection or obstacle avoidance implemented, yet.

4.1.2 Full MAGMaS Control Allocation

This section details the control architecture, derives the feedback linearization, formalizes the force allocation optimization problem, also uncertainties handling is introduced. The overall control architecture is summarized in Fig. 4.3.

Consider the trajectory tracking in operational workspace as the task associated to the manipulation of the object. The task is described by a set of variables $\boldsymbol{t} \in \mathbb{R}^{\sigma}$, since the object is a rigid body $\sigma \leq 6$. On the other hand, the object configuration only depends on the arm joint angles $\boldsymbol{q}_m$, thus the task is function of the sole $\boldsymbol{q}_m$ and can be written $\boldsymbol{t} = \boldsymbol{f}(\boldsymbol{q}_m)$, where $\boldsymbol{f} : \mathbb{R}^n \to \mathbb{R}^{\sigma}$ is a differentiable map assumed to be known for a given manipulator. A prerequisite for a generic reference to

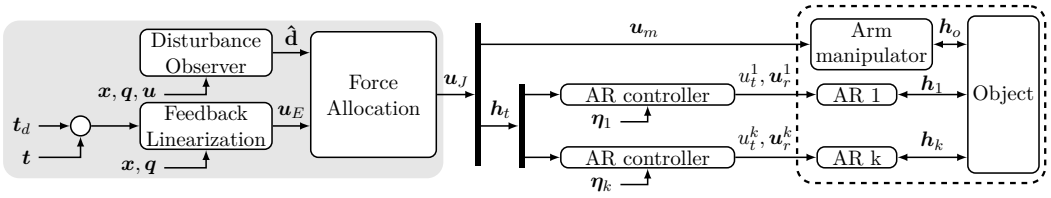

Figure 4.3 – Proposed control scheme for MAGMaS (dashed rectangle) with 3D passive rotational connections, composed of a feedback linearization controller, a disturbance observer to deal with uncertainties, and an optimization-based force allocation scheme, for the control allocation part (gray area), see Sec. 4.1.2. Indiviual attitude controller are devised for each AR, the ground manipulator is considered to be directly torque controlled.

be trackable is that the map $\boldsymbol{f}$ is surjective, which, in turns, implies $\sigma \leq n$. In conclusion, $\sigma \leq \min\{6, n\}$. Furthermore, the task is assumed planned such as to comply with the robot manipulator joint limits (3.27). The problem addressed in this work is to let the task $\boldsymbol{t}$ track a desired reference $\boldsymbol{t}_d$ while taking advantage of the MAGMaS redundancy and heterogeneity.

The trajectory tracking task control is done through input-output exact linearization, via static feedback, see [Isidori–1995]. Recall, in order to design a static feedback linearization control law, each output is differentiated until at least one input appears and the obtained differential map must result invertible. In the presented case, the first differentiation of the task w.r.t. time yields

$$\dot{\boldsymbol{t}} = \frac{\partial \boldsymbol{f}}{\partial \boldsymbol{q}_m}\dot{\boldsymbol{q}}_m = \mathbf{J}_t(\boldsymbol{q}_m)\dot{\boldsymbol{q}}_m = [\mathbf{J}_t(\boldsymbol{q}_m)\ \mathbf{0}_{\sigma_t \times 3k}]\,\dot{\boldsymbol{q}} \tag{4.1}$$

where $J_t \in \mathbb{R}^{\sigma \times n}$ is known as task Jacobian. A second time differentiation is necessary to make the control inputs appear,

$$\ddot{\boldsymbol{t}} = \frac{\partial \boldsymbol{f}}{\partial \boldsymbol{q}_m}\dot{\boldsymbol{q}}_m + \mathbf{J}_t(\boldsymbol{q}_m)\ddot{\boldsymbol{q}}_m = \boldsymbol{f}_t(\boldsymbol{q}_m, \dot{\boldsymbol{q}}_m, \ddot{\boldsymbol{q}}_m) + \mathbf{G}_u(\boldsymbol{q})\boldsymbol{u}_J \tag{4.2}$$

where

$$\begin{aligned}
\boldsymbol{f}_t(\boldsymbol{q}_m, \dot{\boldsymbol{q}}_m, \ddot{\boldsymbol{q}}_m) = \frac{\partial \dot{\boldsymbol{f}}}{\partial \boldsymbol{q}_m}\dot{\boldsymbol{q}}_m - \mathbf{J}_t\mathbf{M}_m^{-1}\left(\mathbf{c}_m(\boldsymbol{q}_m, \dot{\boldsymbol{q}}_m) + \mathbf{G}_m(\boldsymbol{q}_m)\right) - \\
\mathbf{J}_t\mathbf{M}_m^{-1}\mathbf{J}_m^{\top}\boldsymbol{t}_m^{-1}\left(\mathbf{M}_o(\boldsymbol{x})\ddot{\boldsymbol{x}} + \mathbf{c}_o(\boldsymbol{x}, \dot{\boldsymbol{x}}) + \mathbf{G}_o(\boldsymbol{x})\right) \\
\mathbf{G}_u(\boldsymbol{q}) = \mathbf{J}_t(\boldsymbol{q}_m)\mathbf{M}_m^{-1}(\boldsymbol{q}_m)\underbrace{\left[\mathbf{I}_n \quad \mathbf{J}_m^{\top}\boldsymbol{t}_m^{-1}\mathbf{G}_t(\boldsymbol{q})\right]}_{\mathbf{A}}
\end{aligned}$$

and $\boldsymbol{u}_J = [\boldsymbol{u}_m^{\top} \quad \boldsymbol{h}_t^{\top}]^{\top}$. Given the modeling assumptions, the matrix $\mathbf{G}_u$ is full row-rank whenever $\mathbf{J}_t$ is full row-rank, because by construction $\mathbf{A}$ is the projection

of $\boldsymbol{u}_J$ on the manipulator joints and $\mathbf{M}_m^{-1}$ is full rank by definition. From the structure it is also clear that the inputs directly related with the task dynamics are the manipulator torques, $\boldsymbol{u}_m$, and the concatenated force vector $\boldsymbol{h}_t$, generated by the thrust magnitudes $\boldsymbol{u}_t$ and the moments $\boldsymbol{u}_r$ of the AR, through (3.15)-(3.16). Task trajectory tracking can be enforced by a control action $\boldsymbol{u}_E \in \mathbb{R}^\sigma$ such that

$$\boldsymbol{u}_E = \ddot{\boldsymbol{t}}_d + \mathbf{K}_D\dot{\mathbf{e}} + \mathbf{K}_P\mathbf{e} - \boldsymbol{f}_t \tag{4.3}$$

where $\mathbf{e} = \boldsymbol{t}_d - \boldsymbol{t}$, $\mathbf{K}_D \in \mathbb{R}^{\sigma\times\sigma}$ and $\mathbf{K}_P \in \mathbb{R}^{\sigma\times\sigma}$ are diagonal positive definite matrices. To implement $\boldsymbol{u}_E$, $\boldsymbol{u}_J$ has to verify

$$\hat{\mathbf{G}}_u\boldsymbol{u}_J = \boldsymbol{u}_E, \tag{4.4}$$

in order to be plugged in (4.2) to ensure the tracking of a desired trajectory $\boldsymbol{t}_d$. Thanks to redundancy there are infinite possible input allocations, $\boldsymbol{u}_J$, for a given $\boldsymbol{u}_E$. Note that this modeling is similar to the problem of kinematic control for nonholonomic mobile manipulators, see [De Luca–2010], where the redundancy is exploited to locally maximize manipulability, while ensuring velocity damping of the high order dynamics of the considered model.

To do so, the control problem is formulated as a programming problem to minimize the cost function $\mathcal{J} : \mathbb{R}^{(n+3k)} \mapsto \mathbb{R}$ defined as $\mathcal{J}(\boldsymbol{u}_J) = \boldsymbol{u}_J{}^\top\mathbf{P}\ \boldsymbol{u}_J$, where $\mathbf{P} \in \mathbb{R}^{(n+3k)\times(n+3k)}$, defined as $\mathbf{P} = \text{diag}\left(\mathbf{J}_t\mathbf{J}_t^\top, \mathbf{P}_t\right)$, is a weighting matrix to allocate the forces according to the maximum torque of the ground manipulator motors and AR thrusters and in order to increase the force manipulability ellipsoid described by the matrix $\mathbf{J}_t\mathbf{J}_t^T$. The matrix $\mathbf{P}_t \in \mathbb{R}^{3k\times3k}$ allows to weight the ARs differently from each other and from the ground manipulator. The solution of the optimization problem is constrained by $\boldsymbol{u}_J \in \mathcal{F}$, where $\mathcal{F}$ is the feasible solutions set defined by the inequalities (3.26), (3.28) and (3.29), plus $\boldsymbol{u}_J$ should satisfy (4.4) which yields the constraint, $\xi(\boldsymbol{u}_J) = \mathbf{G}_u\boldsymbol{u}_J - \boldsymbol{u}_E = 0$, where $\xi : \mathbb{R}^{n+3k} \mapsto \mathbb{R}^\sigma$.

Note that the constraint (3.27) is addressed by the task choice. In summary, the control allocation problem is

$$\begin{aligned}
\boldsymbol{u}_J^* = \arg\min_{\boldsymbol{u}_J} \quad & \mathcal{J}(\boldsymbol{u}_J) \\
\text{s.t.} \quad & \chi_i(\boldsymbol{\eta}_i) \le 0 \quad i = 1, ..., k \\
& \|\boldsymbol{h}_i\| \le h_i^{\max} \quad i = 1, ..., k \\
& \min(u_m^i) \le u_m^i \le \max(u_m^i) \quad i = 1, ..., n \\
& \xi(\mathbf{u_J}) = 0.
\end{aligned} \tag{4.5}$$

All constraints, equalities and inequalities, are affine functions of the optimization variable $\boldsymbol{u}_J$ and since $\mathcal{J}(\boldsymbol{u}_J)$ is convex quadratic, (4.5) is a convex programming problem. A wide range of efficient methods can be used to solve the problem, as described in literature of convex optimization. The devised control allocation problem is not unique and other considerations could be taken into account, like

a parsimonious motion approach to limit the overall motion of actuated DoFs, as in [Gonçalves–2016].

Feedback Linearization techniques are relying on implicit model inversion. as such they are very sensitive to uncertainties. They can arise for several reasons, parametric uncertainties such as imprecise weight and length measurements, unmodeled dynamics, such as motor dynamics or the existence of unmodeled external disturbances.

All these uncertainties can also be coped with by the system redundancy by reformulating the optimization problem (4.5) and the trajectory tracking control $\boldsymbol{u}_E$ in the case of disturbances. Let and $\hat{\mathbf{G}}_u$ and $\hat{\boldsymbol{f}}_t$ be the nominal values of $\mathbf{G}_u$ and $\boldsymbol{f}_t$ that represent the existence of a lumped bounded uncertainty in the model. A disturbance term, $\mathbf{d} = \hat{\mathbf{G}}_u^+(\ddot{\boldsymbol{t}} - \hat{\boldsymbol{f}}_t) - \boldsymbol{u}_J$, can be introduced and the second order task dynamics (4.2) can be rewritten as

$$\ddot{\boldsymbol{t}} = \hat{\boldsymbol{f}}_t(\boldsymbol{q}_m, \dot{\boldsymbol{q}}_m, \ddot{\boldsymbol{q}}_m) + \hat{\mathbf{G}}_u(\boldsymbol{q})\left(\boldsymbol{u}_J - \mathbf{d}\right). \tag{4.6}$$

A common approach to estimate the disturbance is to use the following disturbance observer

$$\dot{\hat{\mathbf{d}}} = -\mathbf{L}\hat{\mathbf{d}} + \mathbf{L}\left(\hat{\mathbf{G}}_u^+(\ddot{\boldsymbol{t}} - \hat{\boldsymbol{f}}_t) - \boldsymbol{u}_J\right) \tag{4.7}$$

where $\mathbf{L} \in \mathbb{R}^{(n+3k)\times(n+3k)}$ is positive diagonal observer gain and $\hat{\mathbf{d}}$ is the output of the disturbance observer. This means that (4.4) rewrites as $\boldsymbol{u}_E = \hat{\mathbf{G}}_u\left(\boldsymbol{u}_J - \hat{\mathbf{d}}\right)$, and hence the optimization problem (4.5) as to be updated with

$$\xi(\boldsymbol{u}_J) = \hat{\mathbf{G}}_u(\boldsymbol{u}_J - \hat{\mathbf{d}}) - \boldsymbol{u}_E \tag{4.8}$$

to take into account the disturbances. Using this control scheme task trajectory tracking is guaranteed, while the system redundancies are exploited to satisfy the system constraints and reject possible disturbances.

4.2 Geometric Control for AR

In this section classical pose control based on [Lee–2010] is presented for two situations; the case where 3D passive spherical joints are used on underactuated AV, called the *pure thruster case*, and the case where 1D passive rotational joints are used in combination with multi-directional thrust AV, called the *constrained orientation case*.

4.2.1 AR Control – Pure Thruster Case

The special case of AR composed of underactuated flying platform with an arm mounted on a 3D passive spherical joint is studied in this section, this corresponds to the preliminary results on MAGMaS presented in [Staub–2017]. The position of such platform is constrained by the motion of the grasped object, but the rotational

dynamics is left free to orient the thrust in any desired direction, hence the name *Pure Thruster*. The low-level control law for the i^{th} AR can be written

$$u_t^i = \mathbf{z}_i^\top \mathbf{R}_i^\top \left(m_i g \mathbf{z}_W + \boldsymbol{h}_i\right) \tag{4.9}$$

$$\boldsymbol{u}_r^i = -\mathbf{K}_R \mathbf{e}_R^i - \mathbf{K}_\omega \mathbf{e}_\omega^i + \boldsymbol{\omega}_i \times \mathbf{J}_i \boldsymbol{\omega}_i \tag{4.10}$$

where $\mathbf{K}_R, \mathbf{K}_\omega \in \mathbb{R}^{3\times3}$ are diagonal gain matrices with positive elements, chosen to guarantee stability of the system, $\mathbf{e}_R^i$ is orientation matrix error defined by

$$\mathbf{e}_R^i = \frac{1}{2}\mathbf{S}^-(\mathbf{R}_d^{i\top}\mathbf{R}_i - \mathbf{R}_i^\top \mathbf{R}_d^i) \tag{4.11}$$

where $\mathbf{S}^-(\cdot)$ is the inverse operation of $\mathbf{S}(\cdot)$, *i.e.*, extracts the generating vector from a skew symmetric matrix, and $\mathbf{e}_\omega^i$ is the angular velocity error defined as

$$\mathbf{e}_\omega^i = \boldsymbol{\omega}_i - \mathbf{R}_i^\top \mathbf{R}_d^i \boldsymbol{\omega}_d^i \tag{4.12}$$

where $\boldsymbol{\omega}_d^i \in \mathbb{R}^3$ is the desired angular velocity. The desired rotation matrix $\mathbf{R}_d^i$ is simply obtained by calculating any rotation matrix that transforms $\mathbf{z}_W$ to $\boldsymbol{h}_i/\|\boldsymbol{h}_i\|$, *i.e.*, aligning the thrust direction to the load of the system on the corresponding AR.

4.2.2 AR Control – Constrained Orientation Case

The special case of AR composed of multi-directional thrust platform with arm mounted on a 1D passive revolute joint is studied in this section. The position of such platform is constrained by the motion of the grasped object and the rotational dynamic is only left free around one axis, hence the name *Constrained Orientation*. However, thanks to the multi-directional thrust property the thrust can still be oriented without changing the orientation of the AR. In this case the pose controller is of paramount importance to exploit the multi-directional thrust capabilities of the platform. From an arbitrary Cartesian reference trajectory, $(\mathbf{p}_B^r, \mathbf{R}_B^r) : \mathbb{R} \to SE(3)$, it generates the propellers control inputs $\boldsymbol{u}$, via dynamic inversion of the AR dynamics, that let $\mathbf{p}_B$ and $\mathbf{R}_B$ track at best the reference trajectory. The pose Controller is build around an inner control loop (*position controller*) and an outer control loop (*attitude controller*). The final stage of the controller is a *force-torque mapper* that computes the actual propeller spinning velocity $\boldsymbol{u}$. This controller has been detailed in [Ryll–2016] and will only be outlined here for completeness.

Position Controller

This stage receives as input the reference trajectory for the AR CoM coming from the planner $(\mathbf{p}^r, \dot{\mathbf{p}}^r, \ddot{\mathbf{p}}^r, \mathbf{R}_B^r)$ and the measured state $(\mathbf{p}_B, \dot{\mathbf{p}}_B)$, producing as output a reference control force $\mathbf{f}^r \in \mathbb{R}^3$ sent to the wrench mapper and a desired feasible orientation $\tilde{\mathbf{R}}_B^r$ (a priori different from the reference one, see below) which will feed the attitude controller. Note that the actuators limits are accounted for in

this computation. Given the position tracking errors $\mathbf{e}_p$ and $\mathbf{e}_v$, the reference force vector is expressed as

$$\mathbf{f}^r = m\left(\ddot{\mathbf{p}}^r + g\mathbf{e}_3 - \mathbf{K}_p\mathbf{e}_p - \mathbf{K}_v\mathbf{e}_v\right), \tag{4.13}$$

with $\mathbf{K}_p$ and $\mathbf{K}_v$ two positive definite gain matrices. The new reference orientation $\tilde{\mathbf{R}}_B^r$ is introduced as it can be different from $\mathbf{R}_B^r$ given by the planner. Indeed, due to actuation limits, the total thrust $\mathbf{f}^r$ has to remain in the pseudo-cone illustrated in Fig. 3.4b. If the reference control force, computed with the reference orientation, lies outside the pseudo-cone, then $\tilde{\mathbf{R}}_B^r$ is computed as the closest desired rotation matrix respecting the input constraints. In other words, $\tilde{\mathbf{R}}_B^r$ minimizes the distance with $\mathbf{R}_B^r$ in $SO(3)$ with $\mathbf{f}^r$ inside the actuation limits. This prioritizes the tracking of the position over the orientation, while trying to follow the best attitude trajectory.

Attitude Controller

This part produces as output the reference control torque $\boldsymbol{\tau}^r \in \mathbb{R}^3$, based on the desired rotation $\tilde{\mathbf{R}}_B^r$ provided by the position controller, the other reference input $\boldsymbol{\omega}^r$ and the measured state ($\mathbf{R}_B$, $\boldsymbol{\omega}_B$) under

$$\boldsymbol{\tau}^r = \boldsymbol{\omega}_B \times \mathbf{J}\boldsymbol{\omega}_B - \mathbf{K}_R\mathbf{e}_R - \mathbf{K}_\omega\boldsymbol{\omega}_B \tag{4.14}$$

with $\mathbf{K}_R$ and $\mathbf{K}_\omega$ being positive definite gain matrices and the orientation error $\mathbf{e}_R$ computed in $SO(3)$. The vector $\boldsymbol{\tau}^r$ is then fed to the force-torque mapper.

Force-torque Mapper

This final stage takes as input the reference wrench ($\mathbf{f}^r$, $\boldsymbol{\tau}^r$), computed by the two previous stages and provides as output a feasible set of control inputs $\boldsymbol{u}$ to be sent to the motors

$$\boldsymbol{u} = \begin{bmatrix} \mathbf{R}_B\mathbf{F}_1 \\ \mathbf{F}_2 \end{bmatrix}^{-1} \begin{bmatrix} \mathbf{f}^r \\ \boldsymbol{\tau}^r \end{bmatrix}. \tag{4.15}$$

This stage concludes the *Pose Controller* flow description.

The motor control inputs $\boldsymbol{u}$ can be a setpoints or a pseudo-setpoints for the motor input voltage or proper velocities to be tracked by the motors, based on the motor characteristics and control modalities. In particular, the matrix $\mathbf{F}_1$ and $\mathbf{F}_2$ embodied dynamic and aerodynamic parameters related to the motor and propellers used. The importance of the knowledge of these for fine force control is motivated and stressed in the following sections.

4.3 Force Estimation for Aerial Physical Interaction

4.3.1 Motivations

As outlined in Sec. 2.4.3 the knowledge of the force exerted on the environment by the aerial robot is of paramount importance to achieve a precise interaction force control. Furthermore, it can also be used in free flight to retrieve external disturbance forces like, *e.g.*, due to the wind or collision. For the reason already mentioned in Sec. 2.4.3, recall *i)* performance over weight and compactness ratio, *ii)* located measurements and *iii)* costs, 6D F/T-sensor are not suitable to be embedded in multi-rotors in the low/mid-cost range. Some work are exploring the combination of simple switch with model based force reconstruction, *e.g.*, [Rajappa–2017] or consider simpler force measurement mechanism along only one direction. These resolve the cost and weight drawbacks, but not the issue raised by localized measurements. This leads to the choice of investigating estimator based approaches, they depend highly on the system model and the propeller force exertion knowledge. Then based on the system model and states and the force exerted one can derive the external forces to which the AR is subjected. The crucial part here, is to determine the force and drag torque generated by the propellers. The requirements for such an observer are *i)* low computation burden and *ii)* ease of reproduction; these two requirements are set to enforce usability of this approach. The models used in the estimation process should remain as simple as possible to limit computational cost but still capture all the essential dynamics of the system in order to produce a trustworthy estimate. Once the models are set, their parameters estimation should be highly reproducible to be performed quickly after any modifications of the systems. The standard model of co-planar multi-rotor is presented hereafter and two solutions for the propeller force estimation are proposed, one based on model identification and the other one based on spinning velocity fine control. Note that another approach for force control considers aerodynamic power, see [Bangura–2014].

4.3.2 Proposed Solutions

In the following, two approaches developed at LAAS–CNRS are introduced, both aim at tackling the challenge of force exertion and force feedback for APhI.

The first approach relies on model identification for the propeller force generation. The main idea is to rely on dynamical measurements in order to model the propeller force exertion dynamics and also integrate the battery terminal output voltage to improve the model performances. The approach, detailed in Sec. 4.4, is generic and proposes a class of models based on simple observation rather than physics. Thanks to this abstraction the proposed models are simpler and the usage for low costs platforms using set-point commands instead of velocity command for the propeller is made easier.

The second approach is based on fine spinning velocity control of the propellers. On low/middle cost platforms, propeller spinning velocity closed loop control is

usually not proposed as there is not speed feedback signal available. This solution, detailed in Sec. 4.5 and Appendix A, is based on efficient speed measurement and aggressive spinning velocity control relying on adaptive control, this allows to neglect the propeller spinning velocity change dynamics. Associated with statically identified aerodynamics coefficients from the propellers, it has been demonstrated as a reliable way to perform force control for AR.

4.4 Force Estimation: Model Identification Approach

The work described in this part has been presented at
2015 IEEE Int. Conf. on Robotics and Automation [Staub–2015]

This section introduces an early work conducted on force estimation, in which a new class of models for the total thrust generation in multi-rotor MAVs is proposed and experimentally validated. This works focuses low- and middle-end co-planar platforms, where sensory and computation capabilities are limited. This works is original in the sense that it doens't relo on the typical model assumptions that the rotor spinning velocity is instantaneously controller, which neglects the dynamics of the spinning propellers and their associated Brushless Direct Current (BLDC) motor. In the proposed class of models it is considered that the total thrust has its own dynamics and its final value explicitly depends both on the pseudo-setpoint commands given to the motor driver and the measurement of the battery terminal voltage as explained in Sec. 4.4.2. The different model instances are compared within the class using a principled experimental setup in which the total thrust is precisely measured using a motion capture system as ground truth, instead of relying on a setup based on noise-prone force sensors. In Sec. 4.4.5, it is exhibited that the use of a dynamical model that includes also the battery terminal voltage significantly improves the prediction ability of the model in terms of accuracy. Finally, in the same section, experimental results show how the proposed model can be identified using on-board only acceleration measurements, achieving a surprisingly good accuracy when compared with the ground truth case. The use of the proposed model is expected to be important both in case of precise flight control and in the case of aerial physical interactive tasks.

4.4.1 Possible Drawbacks of the Standard Model

First consider the model of the translational dynamics (3.2) and used in many of the previous works, see *e.g.*, [Mahony–2012], assume that ϖ_i is the control input of the system and that c_F is known. Under these two assumptions the f_i, for $i = 1 \dots N$, can be considered as control inputs, which makes the control problem simpler. However, these assumptions are hard to be met in reality for the following reasons. First of all, the aerodynamic coefficient c_F is in many cases unknown, it depends on the propeller type, and even vary within the same type because of normal large-scale production variations. Second of all the motor has its own dynamics. Therefore ϖ_i,

spinning velocity, cannot be changed instantaneously acting on the torque applied by the motor.

In fact, in the best case, the motor control input is usually a *setpoint* for ϖ_i, which is tracked by the motor driver with a certain dynamics and accuracy. The control accuracy of f_i depends then on the accuracy in the knowledge of the parameter c_F (needed in order to generate the setpoint for the motor driver) and on the accuracy of the Electronic Speed Controller (ESC) in tracking the velocity setpoint. For typical multi-rotor platforms, especially in the low/mid-cost range, *e.g.*, the mikrokopter[1], the CrazyFlie[2], the asctec[3] and many other platforms [Li–2012]. It is not possible to send a setpoint for the spinning velocity to the motor drivers, but rather a pseudo-setpoint, *e.g.*, a Pulse Width Modulation (PWM) signal, which is monotically related to the steady state spinning velocity, if all the other flight conditions are constant.

In both cases (for setpoint and for pseudo-setpoint) the battery voltage level has an impact on the behavior of the motor controller, as noted, *e.g.*, in [Sa–2012]. In particular, the battery voltage decreases as long as the battery discharges due to the increase of the internal resistance. This measurement can be found among all the type of platforms. During contact-free flight, the dependence to the battery voltage can be overcome by using an adaptive term in the control law which compensates the discharge of the battery. Such a method can take the form of a mass estimator or an integral term [Spica–2013][Grabe–2013], which increases the average of the commands sent to the motors, thus compensating the voltage drop. This approach is working because the only force acting on the system are the weight and the thrust generated by the propellers. For physical interaction this technique can not be used since the interaction force involved in the balance is typically unknown.

In a first step, in order to have a good control of the force exerted by the system it is instead important to have control on the total thrust $\mathbf{f}^B$ exerted by the rotors. Therefore another viable approach, presented here, is to take into account the battery voltage influence and the motor dynamics directly in an input-output nonlinear model. In the next section, the process of thoughts leading to a class of models encompassing the direct relation between the (pseudo)-setpoints and the battery terminal voltage as inputs and the force as output, is presented.

4.4.2 Model Based on (Pseudo-)Setpoint and Battery Level

This section presents the reasoning leading to the proposed model class. The mode construction makes abstraction from the physics at play and rather focuses on simple observations of the system behaviors to extract its main features. This simplifies a lot the obtained model and captures the essential dynamics of the system {battery+ESC+BLDC+propeller} producing the actuation force. To do so denote $u_i \in [u_{min}, u_{max}]$, with $u_{min} > 0$ the control input of the motor driver,

[1] http://www.mikrokopter.de/
[2] http://www.bitcraze.se/category/crazyflie/
[3] http://www.asctec.de/en/

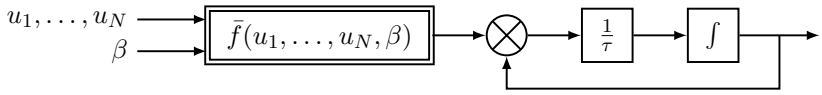

Figure 4.4 – Block diagram of the proposed model

which may represent either a setpoint or a pseudo-setpoint for the driver of the i^{th} motor of the vehicle. Denote with β the battery terminal voltage level, that can be assumed to be measured. The goal is then to propose a modeling of the relation between u_i and β and f_i that is as simple as possible but captures all the relevant dynamics.

Based on the analysis of experimental data, see *e.g.*, [Spica–2013] or [Sa–2012], the following observations have been made:

O 1: *if u_i is kept constant for a time window of the order of magnitude of ≈ 1 second then f_i reaches a constant value that is monotonically increasing w.r.t. u_i and monotonically decreasing w.r.t. β.*

Motivated by the previous observation the following simple model for the force exerted by one propeller is proposed

$$\dot{\mathrm{f}}_i = \frac{1}{\tau_i}\left(\overline{\mathrm{f}_i}(u_i, \beta) - \mathrm{f}_i\right) \tag{4.16}$$

where $\overline{\mathrm{f}_i}(u_i, \beta)$ is an unknown nonlinear map and τ_i is an unknown time constant, this model can be represented as a nonlinear block and a linear first order system, see Fig.4.4.

In order to provide a simple expression of f_T let us consider the following reasonable assumptions:

A 1: *$\overline{\mathrm{f}_i}(u_i, \beta)$ and τ_i are the same across all motor controllers, i.e., for $i = 1 \ldots N$*

A 2: *$\overline{\mathrm{f}_i}(u_i, \beta)$ is a smooth function that can be well approximated by a finite polynomial of a suitable order in the region of interest $u_i \in [u_{min}, u_{max}]$ and $\beta \in [\beta_{min}, \beta_{max}]$*

Assumption 1 is standard and translates to consider a unique time constant and a unique c_F and equivalent motors dynamics. This might be the first assumption to relax in an extension work.

Assumptions 1 and 2 yield

$$\tau_i = \tau, \qquad \forall\ i = 1 \ldots N \tag{4.17}$$

$$\overline{\mathrm{f}_i}(u_i, \beta) = \bar{\mathrm{f}}(u_i, \beta) \approx \sum_{j=0}^{n_u} \sum_{k=0}^{n_\beta} (\alpha_{jk} u_i^j \beta^k), \qquad \forall\ i = 1 \ldots N \tag{4.18}$$

where $n_u, n_\beta \in \mathbb{N}$ have to be chosen taking into account the desired model complexity and α_{jk}, with $j = 1 \dots n_u$, $k = 1 \dots n_\beta$, are $n_u \cdot n_\beta$ parameters to be estimated.

Using (3.4),(4.16),(4.17),(4.18) the dynamic of the total thrust f_T can be written as

$$\dot{\mathrm{f}}_T \approx \sum_{i=1}^{N} \frac{1}{\tau_i} \left(\sum_{j=0}^{n_u} \sum_{k=0}^{n_\beta} (\alpha_{jk} u_i^j \beta^k) - \mathrm{f}_i \right) \tag{4.19}$$

$$= \frac{1}{\tau} \left(\sum_{j=0}^{n_u} \sum_{k=0}^{n_\beta} (\alpha_{jk} \beta^k \sum_{i=1}^{N} u_i^j) - \mathrm{f}_T \right) \tag{4.20}$$

$$= \frac{1}{\tau} \left(\sum_{j=0}^{n_u} \sum_{k=0}^{n_\beta} \alpha_{jk} v_{jk} - \mathrm{f}_T \right) \tag{4.21}$$

where the compact notation $v_{jk} = \beta^k \sum_{i=1}^{N} u_i^j$ is used.

The equation (4.21) is describing a class of sufficiently simple nonlinear dynamic models for the total thrust of a multi-rotor platform using only the (pseudo)-setpoint and the battery voltage, both information that can bee found on nearly every, if not all, platforms.

The model class size is only limited by the choice of n_u and n_β, among the models present in the class some have better performance than others. The goal is to find the simplest model (*i.e.*, the one with the lowest number of parameters) that provides a sufficient prediction performance compared to more complex models.

4.4.3 Identification Procedure

Model (4.21) represents a class of models, depending on the values of the parameters n_u, n_β. In this class of models, three quantities are needed in order to estimate the parameters τ and the α_{jk}'s: the model inputs, *i.e.*, the (pseudo)-setpoint u_i and the battery voltage β and the model's output, *i.e.*, the total thrust f_T. The information on f_T can be replaced by acceleration information, given that the mass m of the system is known. In practical situations two cases, detailed in the following, can happen.

The case in which $\ddot{\mathbf{p}}_B$ can be precisely measured (*e.g.*, using a motion capture system). In this case the thrust force in the inertial frame $\mathcal{F}_W$, $\mathbf{f}^W = \mathbf{R}_B \mathbf{f}^B$, can be computed by directly employing (3.2). The total thrust f_T is then computed as $\|\mathbf{f}^W\|$. This way is used to provide ground truth measurements.

The second case is when the vehicle is equipped with a calibrated IMU which measures the proper acceleration of the vehicle expressed in the body frame $\mathcal{F}_B$, *i.e.*,

$$\bar{\mathbf{a}} = \mathbf{R}_B^T (\ddot{\mathbf{p}}_B + g \mathbf{z}_W) + \boldsymbol{\eta}_{IMU}, \tag{4.22}$$

where $\boldsymbol{\eta}_{IMU}$ is some additive noise with zero mean. This case will be used in the experiments to show that the model can be effectively identified using only onboard

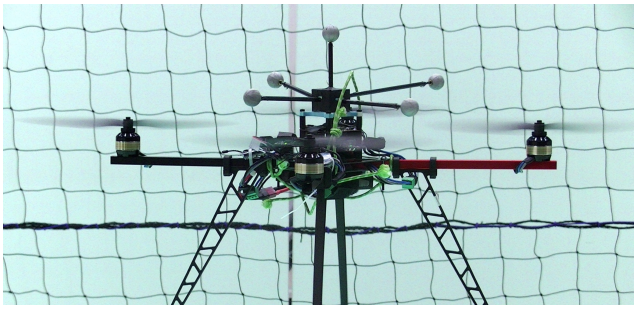

Figure 4.5 – The multi-rotor platform used at LAAS–CNRS

measurements. Using (3.2),(3.4) in (4.22) one gets

$$\bar{\mathbf{a}} = \frac{\mathrm{f}_T}{m}\mathbf{z}_B + \frac{1}{m}\boldsymbol{\delta} + \boldsymbol{\eta}_{IMU}. \tag{4.23}$$

In typical conditions (*i.e.*, at low speed and at a certain distance from the ground) f_T is much larger than the third component of $\|\delta\|$. Therefore, one can write

$$\mathrm{f}_T = m{\mathbf{z}_B}^T\bar{\mathbf{a}} + \eta_F \approx m\bar{a}_z. \tag{4.24}$$

Where η_F represents a negligible contributions of both the aerodynamic effects and the IMU noise. Assuming that the mass m of the vehicle can be measured before the flight, (4.24) shall be used as an onboard measurement of the total thrust.

Use of Estimated Model in Contact Tasks

Notice that (4.24) is valid only in contact-free flight, *i.e.*, when the non-gravitational forces acting on the vehicle can be expressed by (3.4). During contact, (3.4) includes also the interaction forces $\mathbf{f}_e^B$, thus it can be rewritten as

$$m\ddot{\mathbf{p}}_B = -mg\mathbf{z}_W + \mathbf{R}_B\left(\mathbf{f}^B + \mathbf{f}_e^B\right). \tag{4.25}$$

The estimation of f_T can be performed in the same way as before if $\mathbf{f}_e^B$ is known.

If instead the estimation of τ and $\bar{\mathrm{f}}$ is performed using measurements taken during contact-free flight phases, the identified model can then be used to estimate $\mathbf{f}_e^B$ in contact phases since both τ and $\bar{\mathrm{f}}$ are constant over time. This claim still requires experimental validation, which as not been carried out because the proposed method is finally not used in the subsequent work on cooperative manipulation.

4.4.4 Experiment Design

In order to estimate the parameters of the model introduced in (4.21) an experimental set up has been designed, see [video 1–2015], based on the Telekyb framework [Grabe–2013] and composed by a Motion Capture System (MoCap), a control computer and a quadrotor, see Fig. 4.5. The MoCap provides the tracked object

position at 100 Hz with millimeter-scale accuracy. A very accurate estimation of the velocity and acceleration is obtained post-processing the measured position with a non-causal Savitzky-Golay filter [Savitzky–1964].

The quadrotor mechatronics is based on the Mikrokopter platform, whereas the flight control software has been replaced by the Telekyb [Grabe–2013] one.

Two Xbee radio transmitters are used to send commands to the quadrotor and to record the telemetry data, respectively. Two of them are needed because Zigbee protocol is a half duplex channel, with a data rate of 80 kbits/s (not considering the packet overhead). So in order to send and receive the desired data at high frequency one is dedicated to sending the other one to receiving. The data recorded are: the battery voltage, a timer for synchronization, the four motors pseudo-setpoints (PWM signals) sent by the flight controller to the brushless controllers and the onboard acceleration measurements provided by the threee 3D LIS344alh accelerometers ($0.0057\, g_0 \mathrm{kg\,m\,s^{-2}}$ resolution and $\pm 2\, g_0 \mathrm{ms^{-2}}$ range). The accelerometers are calibrated following the procedure detailed in [Spica–2013]. The control computer runs the Telekyb control framework under the middleware Robot Operating System (ROS). The flight controller used for the quadrotor is a near-hovering scheme which allows to follow trajectories where the roll and pitch of the quadrotor remain within $\pm 30°$.

The produced thrust is then computed twice using *(i)* the acceleration measurement from the motion capture (ground truth) and *(ii)* the accelerometer reading, following the relations detailed previously in Sec. 4.4.3.

Trajectories for the Identification

Any trajectory that spans the the battery range and the pseudo-setpoint range of interest can be used for the identification. The former requirement asks for a flight duration that discharges the battery enough and the latter one asks for a sufficiently rich acceleration content of the tracked trajectory. To meet the arena-size constraint as well, a vertical trajectory has been chosen providing enough space to reach high accelerations while remaining near the hovering attitude. One drawback of this choice is the limitation imposed to the torque commands, as the command input where used predominantly for vertical acceleration, the margin left to adjust the attitude of the quadrotor was quite small and potentially leading to unstable behavior if the attitude was perturbed. Thus a balance had to be found empirically between the maximal acceleration on the trajectory and the stability of the system, see [video 1–2015] for flight records. To ensure the spectral richness of the acceleration the vertical trajectory is composed of five sinusoids with different pulsations:

$$z(t) = \rho + \sum_{i=1}^{5} a_i \; sin(\omega_i t + \phi_i), \tag{4.26}$$

ID of the model	1	2	3	4	5	6	7	8	9	10
n_u	0	0	1	1	0	2	1	2	2	2
n_β	0	1	0	1	2	0	2	1	2	2
Numb. of param.	2	3	3	4	4	5	7	7	10	10

Table 4.1 – Different models considered in the identification.

where $\rho = 2$ is a position offset, to avoid collision with the ground, and

$$
\begin{aligned}
[\omega_1, \ldots, \omega_5] &= 2\pi \cdot [0.3,\, 0.2,\, 0.1,\, 0.5,\, 0.6] \\
[a_1, \ldots, a_5] &= 0.3 \cdot [\omega_1^{-2},\, 0.95\omega_2^{-2},\, 0.9\omega_3^{-2},\, 0.8\omega_4^{-2},\, 0.7\omega_5^{-2}] \\
\phi &= \pi \cdot \left[\frac{1}{2}, \frac{1}{3}, \frac{1}{4}, \frac{1}{5}, \frac{1}{6}\right]
\end{aligned}
$$

are the pulsations, the amplitudes, and the phase shifts of the sinusoids, respectively. With this choice the input is then persistently exciting with order 10, making us able to identify of up to 10 parameters in (4.21), see, *e.g.*, [Ljung–1999].

With this approach the phase between the two sinusoids and their respective amplitude has to be carefully considered. In fact it has to be chosen so that the maximum amplitude of the input stays in a certain range and such that one sinusoid can not get hidden in the IMU's noise surrounding the other, leading to a situation where the IMU reading only describes one sinusoid, the other being hidden by noise.

4.4.5 Experimental Results

To estimate the parameters in the model of the class described by (4.21) a predictive error method coupled with a grey-box model are used. This method is a numerical optimization with a cost function based on the norm of the prediction [Soderstrom–1989]. Three different analyses have been conducted on the data and are described hereafter.

Model Order Choice and Mocap-based Identification

The number of parameters in (4.21) is $(n_u + 1) \cdot (n_\beta + 1) + 1$, thus it depends on the chosen value of n_u and n_β. The goal is to find n_u and n_β such that the system dynamics is well described by the estimated model but with the smallest number of parameters.

As explained in Sec. 4.4.4 the maximum number of parameters that can be identify with the described experimental setup is 10. Therefore one can consider $n_u, n_\beta \in \{0, 1, 2\}$. The 10 resulting models are summarized in Table 4.1, where models 9 and 10 have the same structure but the parameters are estimated with a different initial guess as explained in the following. Model 1 is discarded since the

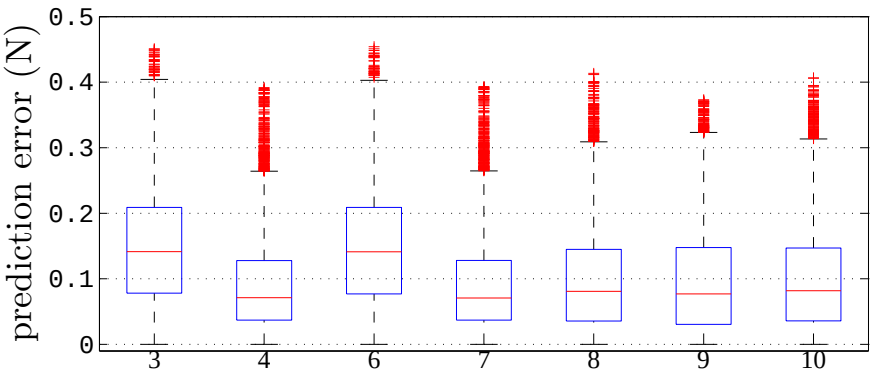

Figure 4.6 – Boxplot of the prediction error for the proposed models (see Tab. 4.1), the parameters are estimated with the ground truth and the prediction is compared against the ground truth.

system dynamics can not be described just by a constant. Models 2 and 5 are also discarded as they do not contain information on the (pseudo)-setpoint, but only about the battery state. The initial guess for the estimation of the parameters of more complex models is provided by the solution of the antecedent in the model class, thus creating the following orders: $3 \to 4 \to 7 \to 9$ and $3 \to 6 \to 8 \to 10$.

First the parameters are estimated using a set of data from the MoCap (the estimation using onboard-only sensor is detailed in Sec. 4.4.5). The estimated parameters are then validated against another set of data from the MoCap. To better validate the ability of prediction of the proposed models *w.r.t.* the battery effect, the battery voltages in the 2 sets span completely different values. Boxplots graphs of the absolute value from the prediction error are presented in Fig. 4.6, the prediction error is the absolute value of the error between the prediction and the ground truth. Overall the predictions are quite good, with a prediction error median around or under 0.1 N, which is remarkable considering that the range of the recorded force during the experiment is [7.5 N, 12.2 N]. This demonstrates that the proposed class of models is able to predict the total thrust accurately. The complete set of estimated parameters can be found in [Staub–2015] for the interested reader.

Discussion on Battery Influence

From the previous model performances, one can investigate the importance of the battery. Models 3 and 6, where battery voltage information are not used, are both outperformed (higher median, wider dispersion) by the models containing both pseudo-setpoint and battery information, *i.e.*, 4, 7, 8, 9 and 10. As models 3 and 4 have the same number of inputs the use of battery data is the only changing factor that can explain the better fitting of 4 with respect to 3. Moreover, one can notice that despite of the fact that model 6 has more inputs than model 4, its prediction ability is worse. In general one can conclude that the models in which $n_\beta \neq 0$ can

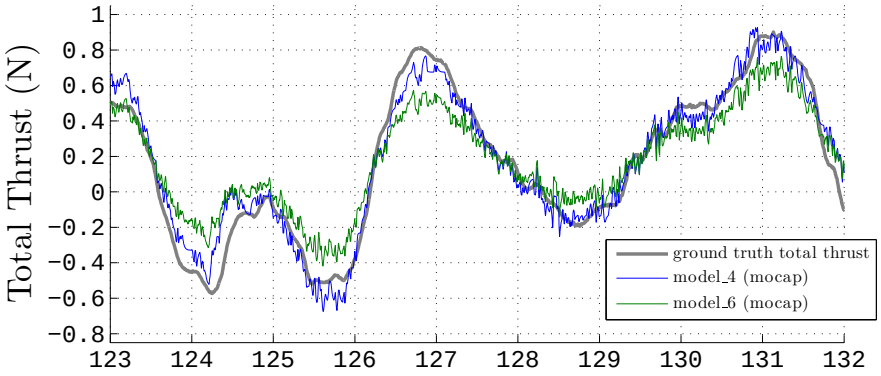

Figure 4.7 – Comparison of two estimated model. One not including battery info (model 6) and one including battery info (model 4). Both models have the same number of parameters, the one containing battery information is clearly better performing.

better predict the system behavior by taking into account the battery voltage drop along the flight. This fact removes, *e.g.*, the need for an adaptation term in the flight controller. This result confirms that the use of the battery voltage information improves 'substantially' the quality of the prediction. A direct comparison between model 4 and 6 on a chunk of the validation set is shown in Fig. B.7.

Accelerometer-based Identification

An analysis was conducted to determine the validity of parameters estimation based only on the onboard accelerometer measurements. Then the quality of the prediction of these models has been compared to ground truth (*i.e.*, the validation set used in the MoCap case). The prediction error is presented in Fig. 4.8 for all considered models. The prediction error is the absolute value of the error between the prediction and the ground truth, the MoCap.

The comparison of Fig. 4.6 and Fig. 4.8 shows that the parameter estimation process can also be conducted without a MoCap at the cost of minimal variation of the prediction error, allowing the proposed force prediction framework to be deployed without a MoCap. The complete set of estimated parameters can be found in [Staub–2015] for the interested reader.

Choice of the Best Model

From this analysis, model 4 results to be the best compromise between accuracy and complexity. In fact, this model resulted able to describe the dynamics of the system with the same level of prediction ability of models with more parameters. Furthermore, model 4 is computationally lightweight and therefore can be easily im-

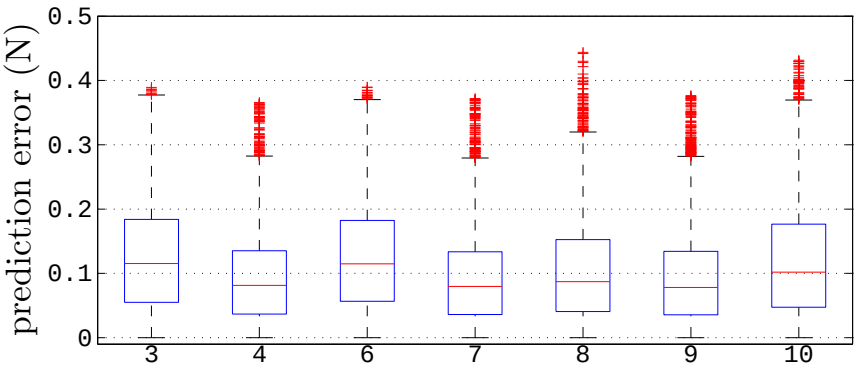

Figure 4.8 – Boxplot of the prediction error for the proposed models (see Tab. 4.1), the parameters are estimated with onboard acceleration and the prediction is compared against the ground truth

plemented, *e.g.*, on a microcontroller. Furthermore, this model keeps substantially the same the prediction ability if the estimation of the parameters is conducted using onboard accelerometer data.

4.4.6 Discussion

In this work a class of dynamic models is proposed to predict the force (total thrust) generated by an underactuated multi-rotor system. The major contributions have been to consider the motor dynamics, include battery terminal voltage information in the prediction model and to identify the model parameters using only onboard accelerometer measurements. An experimental investigation has been conducted to find the best model among the simplest ones in this class using the acceleration retrieved from MoCap measurements as ground-truth, to exploit (4.24). By comparing the prediction error for a set of possible inputs, it has been shown that the addition of the battery voltage information in the model provides a manifest better force prediction. From the experimental results it was also clear that the usage of only onboard acceleration measurement for identification does not result in a significant degradation of the prediction when compared to the use of ground truth for the same purpose.

Nevertheless the assumption is made that the only force acting on the system during the record of the data for parameter estimation are the weight force and the total thrust, thus an outdoor estimation of the parameters in windy conditions is not possible. However, the proposed models can be used for an outdoor estimation of external forces acting on the system, like *e.g.*, wind.

In parallel to this work, a concurrent method was developed at LAAS–CNRS for force estimation, relying on precise motor spinning velocity and static propeller parameters identification. This method is presented hereafter.

4.5 Force Estimation: Close Loop Spinning Velocity Control

This section introduces a work conducted at LAAS–CNRS, by other authors, which is detailed in [Franchi–2017b] and Appendix A. We highlight here the two main steps of such a force estimation approach, for the sack of completeness, as the work presented later in Chapter 5 is exploiting this approach.

4.5.1 ABAG Speed Controller

The biggest flaw of many low/middle-cost ESC, used in multi-rotor platforms for APhI, is that setpoints or pseudo-setpoints are used to command propeller spinning velocity in a open loop fashion. This relies on the use of look-up table and is clearly not fast nor robust, moreover the pre-calibration effort is non negligible. To address these drawbacks a method based on adaptive bias and adaptive gain, called ABAG, was developed at LAAS–CNRS, see [Franchi–2017b]. The solution developed is different from the classical ESC software presented earlier, as *i)* it does not require any pre-calibration phase, *ii)* it is extremely robust and applicable to a wide set of motor/propeller without the need of gain tunning, *iii)* it can achieve performances that are independent of the battery terminal voltage, the mechanical wearing, the temperature and so on, *iv)* it is amenable to extremely low complexity implementation even when compared with 'supposedly simple' classical controllers.

4.5.2 Force Controller at Propeller Level

Once the propeller spinning velocity is efficiently regulated, a last step is necessary for force control, identify the maps between spinning velocity and the wrench produced by the propeller (thrust force and drag moment). Relying on the simplified models presented in Sec. 3.2.1, this translates in identifying two aerodynamic coefficients; the aerodynamic thrust coefficient, c_F, and the drag coefficient, c_τ. This is done by mounting the motor/propeller pair on a *static* 6D F/T-sensor; and is presented here for completeness as it was investigated in [Bicego–2015]. The main drawback of this method are the extensive pre-calibration phase necessary for each kind of propeller and the fact that the wrench measurements are done in static conditions, which are theoretically different than in-flight condition from an aerodynamics point of view. Nevertheless this method has been proven good enough, and robust to these two implicit assumptions, to conduct successful precise force control experiments, see [Tognon–2016b][Ryll–2017] and Chapter 5.

4.6 Force Estimation: Discussion

The two approaches presented in Sec. 4.4 and Sec. 4.5 aim at improving the force control performance for APhI, with emphasis on complexity reduction, pre-calibration

operations minimization and robustness to parameters change. In the end, the second method has been chosen by LAAS–CNRS research group at large, as the best performing for the criteria highlighted. In particular its low computational cost and the versatility *w.r.t.* motor/propeller combination has been proven essential in practice. This choice do not suppress totally the need for pre-calibration methods. It has been shown that the speed control did not require a tuning of its parameter to perform well among a variety of motor/propeller combination. However in order to device precise force controller the mapping (linear or not) between the propeller spinning velocity and the wrench produced is still necessary. This is done by measurements campaign conducted on a *static*, *i.e.*, not flying, {motor+propeller} mounted on a 6D F/T-sensor. The exploitation of the data retrieved, leads to identification of relationship between the propeller spinning velocity and the wrench produced. This knowledge allows fine force control as demonstrated in several work, *e.g.*, [Tognon–2016b] or [Ryll–2017], and part of this thesis.

An open challenge for the speed control is the efficient tracking of low-speed, which is particularly relevant for speed change of sign, *i.e.*, inversion of the sense of rotation. The speed inversion is of particular concern for omni-directional AR, as it allows an increase of the actuation set with both positive and negative rotational speed. With the hardware used in [Franchi–2017b] the speed measurement information degrades with low rotation speed, since no encoder is used. So the inversion of sense of rotation needs to be done in open-loop, *i.e.*, with less accuracy. One solution would be to replace the zero-crossing speed information by an encoder, at cost of increased weight, mechanical complexity and onboard electronics (mostly cabling). Another original approach is to propose the use of variable pitch propellers, this solution as equivalent drawbacks but come with the possibility for finer force exertion control as the wrench generated by propeller can be modified by two control parameters; the spinning velocity and the pitch angle. Another remaining challenge is the proper calibration of the aerodynamic coefficients, the procedure described uses expensive F/T-sensor. Work on the identification/update of the control matrix is an interesting direction, as, at the same time, it estimates the aerodynamics coefficients and alleviate parametric uncertainties in the geometrical model used to build the control matrix, *e.g.*, displacement of the CoM due to additional mass or mounting imperfections. However this procedure could only be conducted in *free-flight*, to ensure the absence of external wrench applied on the AR.

4.7 Force Based Control

In the case of AR composed of multi-directional thrust platform with arm mounted on a 1D passive revolute joint, presented in Sec. 4.2.2, it is important to have some compliance in order not to break the mechanical system hitting its the physical constrains. In order to do so, a classical scheme based on external wrench observer, relying on the results provided in Sec. 4.5, and an admittance filter has

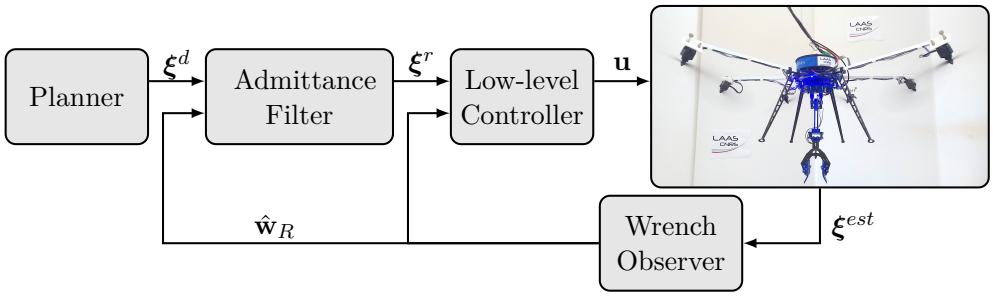

Figure 4.9 – Block-diagram of the full control architecture implemented for the Open Tilted Hexarotor (OTHex), an experimental plaftorm of the constrained orientation case. Let $\xi = (\mathbf{p}_B, \dot{\mathbf{p}}_B, \ddot{\mathbf{p}}_B, \mathbf{R}_B, \boldsymbol{\omega}_B, \dot{\boldsymbol{\omega}}_B)$ be a compact notation for the full state of the system, superscripts ^{d} and ^{r} denoting the desired and the reference trajectory, respectively. The state estimator is fed with pose measurements, *e.g.*, by a MoCap, which can be replaced by a visual-inertial estimator when a MoCap is not available (*e.g.*, in an outdoor context).

been implemented to introduce software compliance, see Fig. 4.9. This guarantees a stable and safe behavior of the system in presence of disturbances and parameters uncertainties.

4.7.1 Wrench Observer

The wrench observer is based on a dynamics model of the wrench generated by the propellers, in particular it contains an identified model of the aerodynamic effects at play for propellers in quasi-static flight and of the geometrical model of the AR. Via the expression of the AR dynamics in the Lagrangian form, a generalized momentum observer is designed, taking advantage of the inertia matrix particular structure in the Lagrangian formalism. This results in the expression of $\hat{\mathbf{w}}_R$ as first order low-pass dynamical system of the real wrench, with gain denoted K_I, where the tuning of this parameter regulates the convergence velocity of the estimator and the reduction of high-frequency noise. For a detailed explanation the reader is addressed to [Ryll–2017].

4.7.2 Admittance Filter

In order to perform safe physical interactions with the environment, a compliant behavior of the aerial manipulator should be ensured. Denote with $(\mathbf{p}_R^d, \mathbf{R}_R^d, \mathbf{v}_R^d, \dot{\mathbf{v}}_R^d)$ the desired trajectory of the interaction point, *i.e.*, the center of the revolute joint O_R. This reference is given by an off-line planner and represents the input of the admittance filter. The admittance filter computes a new reference trajectory $(\mathbf{p}_R^r, \mathbf{R}_R^r, \mathbf{v}_R^r, \dot{\mathbf{v}}_R^r)$ mimicking the following dynamics

$$\mathbf{M}_R \Delta\dot{\mathbf{v}}_R + \mathbf{D}_R \Delta\mathbf{v}_R + \mathbf{K}_R \mathbf{e}_R = \hat{\mathbf{w}}_R + \mathbf{w}_R^d, \tag{4.27}$$

which is the equation of a 6-DoF mass-spring-damper system described by inertia $\mathbf{M}_R$, damping $\mathbf{D}_R$ and stiffness $\mathbf{K}_R$. These three positive-definite matrices are chosen to enforce an over-damped behavior of the system, thus granting the stability of the AR when in contact with the environment. The other quantities of (4.27) are the acceleration and velocity error vector $\Delta\dot{\mathbf{v}}$ and $\Delta\mathbf{v}$and the pose error $\mathbf{e}_R$. The introduced admittance filter generates a 6D reference trajectory for O_R, both position and orientation, which will be turned into a 6D trajectory for O_B using rigid body transformations and their derivatives.

Chapter 5

MAGMaS: Aerial-Ground Co-manipulation Experimental Results

Contents

Abstract

This chapter highlights the results obtained on MAGMaS. To validate the concept of MAGMaS extensive simulations and proof of concepts experiments are presented in Sec. 5.1. Sec. 5.2 describes the follow up work on MAGMaS with the design of a dedicated AR and the addition of a tele-presence framework, Sec. 5.3. These two additions experimental validation and performances are presented in Sec. 5.4. The final section, Sec. 5.5, proposes a discussion on the possible improvements and research directions to increase the maturity level of MAGMaS.

5.1 Underactuated Aerial Robot

The work described in this Section has been presented at
2017 IEEE Int. Conf. on Robotics and Automation

[Staub–2017]

Based on the models and control algorithms developed for MAGMaS in the previous sections, a first MAGMaS composed of a ground manipulator and a underactuated AR is investigated. Both platforms are common in robotics and can be found off-the-shelves, the only missing part for the realization of such a MAGMaS consists in a 3D passive spherical joint to effectively decouple the rotation dynamics of the AR from the one of the manipulated object. This section present the simulation of such a MAGMaS and a set of experiments validating both the concept of MAGMaS and the proposed 3D passive spherical joint design.

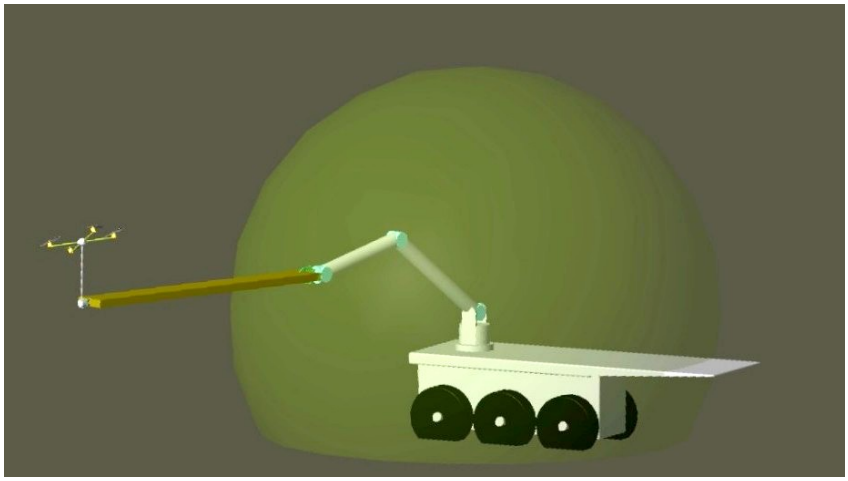

Figure 5.1 – Simulation environment in SimMechanics Toolbox, the ground manipulator is mounted on a mobile platform (with its EE workspace superimposed), the aerial manipualtor is a quadrotor underactuated multi-rotor and they cooperatively manipulate a beam.

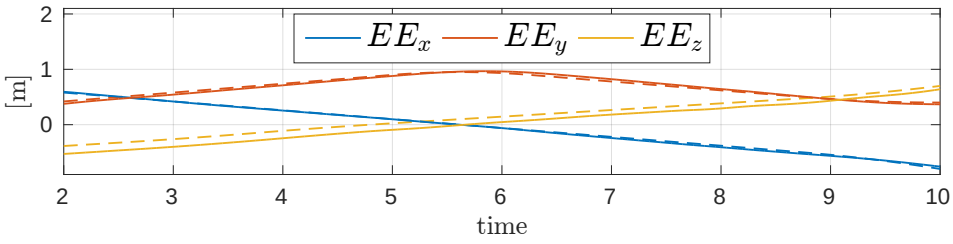

Figure 5.2 – Simulation case study, a ground manipulator and a AR cooperatively manipulating an object. Associated desired and actual position of the EE with respect to the arm base are plotted.

5.1.1 Simulation Results

Extensive and realistic numerical simulations were conducted for a 6 DoFs ground manipulator (anthropomorphic arm and a spherical wrist) cooperating with one quadrotor UAV, see Fig. 5.1. The goal is to both show and validate the feasibility and effectiveness of MAGMaS and the control scheme presented in Chapter 4. The simulation has been performed in Matlab/Simulink environment with the SimMechanics modeling toolbox. With this method the plant dynamical model is derived by the toolbox based on the specified geometry and mass repartition. This approach guaranties that the model used in the controller and the one used for the dynamics simulation are derived independently. For the control allocation, see Sec. 4.1.2, the optimization problem is solved via Sequential Quadratic Programming (SQP) method. The simulation sample time is 1 ms and the control loop one is 10 ms. The simulated ground manipulator is a Universal Robot UR5, with links length

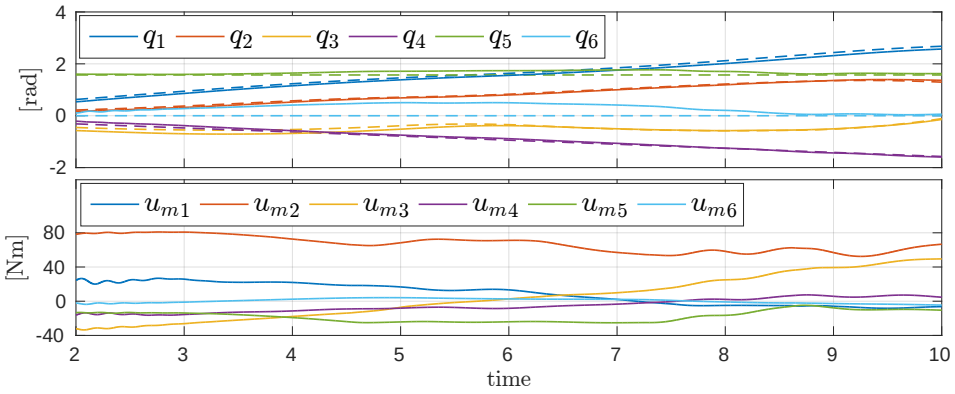

Figure 5.3 – Ground manipulator side. On top, both desired and actual joint angles. The desired angles are from inverse kinematics of the task trajectory. On bottom, associated manipulator input torques.

of 1.0 m and 0.7 m, total arm's mass of 18.4 kg, maximum rated payload is 5 kg and maximum joint torques are [150 150 150 28 28 28] N m, from base to EE. For the first simulation studies we decided to focus our interest on UR5 manipulator, mainly because its strength is such that the interest of cooperative manipulation can be exhibited with smaller/lighter object than for more powerful manipulators. Also the dynamics parameters of the UR5 have been publicly available in the literature, which is not the case for all industrial manipulators. The model developed in Sec. 3.3 can be derived the same way for any chosen manipulator. The simulated AR is a quadrotor of 0.50 m circumference actuated by four motor-propeller sets, each one can generate up to 10 N, and the length of the arm holding the gripper is 40 cm. The spherical joints limit is considered to be described by a cone of $\pi/4$ half cone angle. All the motors are modeled as a second order linear system with a 10 ms rise time. The cooperative task studied corresponds to a trajectory tracking task with the load being a 5 kg bar of dimension 0.05 m $\times$ 0.2 m $\times$ 1 m. The loading of the bar on the back of a mobile platform on which the ground manipulator is mounted is explored, see Fig. 5.1. The UR5 grasps the bar from one end and the quadrotor from the other end. The task consists to follow an appropriate trajectory (generated through way-points and cubic-spline-based trajectory generator) to put the bar on the back of the mobile base. Such a scenario could be of interest in robotic search and rescue missions. The control system is implemented considering a highly uncertain model, some terms of the controller inverse dynamic are neglected, the Inertial matrices are assumed diagonal and the Coriolis/centripetal terms are omitted. Furthermore 10% uncertainty is considered for the contact points, in order to highlight the robustness of the control approach, as the model used in the controller is highly uncertain.

The results of the trajectory tracking task are depicted in Fig. 5.2, with the ground manipulator EE position measured with respect to its base. As it is evident from this figure the given trajectory is tracked sufficiently well, even though the

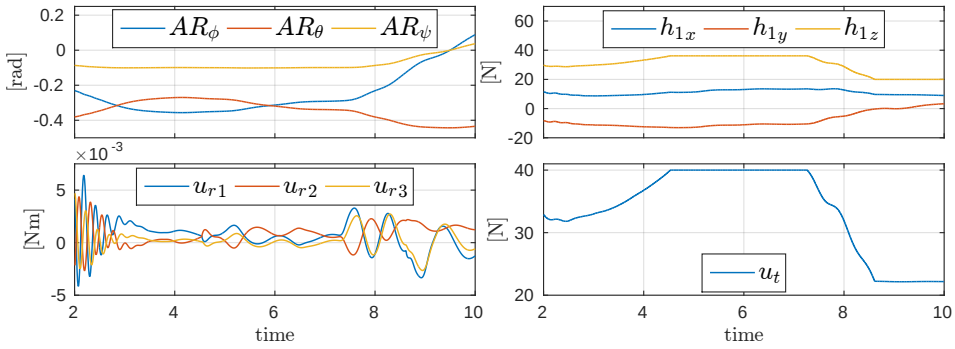

Figure 5.4 – AR side. Left, AR orientation and associated control torques, $\boldsymbol{u_r}$. Right, output of AR force allocation $\boldsymbol{h_t}$ and the AR thrust magnitude generated along AR's **z**-axis.

dynamics of the system is partially unknown, error in position are comprised in ± 7 cm range. Note that the ground manipulator alone is not able to perform this task, because of the torque constraints. Indeed the object weight is at the limit of the ground manipulator payload and the weight-generated torque at its EE does not satisfy the joints torque limits. For this reason, the ground manipulator alone is not able to perform the task, without grasping the bar far from its CoM. The MAGMaS core idea is to mitigate this requirement thanks to the use of an AR acting as a *flying companion* to reduce weight-generated torque on the ground manipulator EE.

The ground manipulator desired and actual joint angles are plotted in Fig. 5.3, with the desired joint angles obtained through inverse kinematics for the task trajectory. The weakness of the wrist joints generates larger errors in $\boldsymbol{q}(4, 5, 6)$, as the desired position can not be attained without violating the joint torque limits even with the help of the AR. However, thanks to the AR support the tracking task is performed sufficiently well. The control torques of the ground manipulator, shown in Fig. 5.3, remain within their actuation limits ([176 176 100 100 100 38 38] N m, respectively).

Fig. 5.4 shows the quadrotor states and control inputs in the simulation. Fig. 5.4 top left shows the orientation of the quadrotor which remains far away from the spherical joint limit and Fig. 5.4 bottom left shows the associated control torques. Fig. 5.4 top right illustrates the output of the optimal force allocation algorithm for the quadrotor, that is a desired force vector $\boldsymbol{h_t}$. This force vector is then generated by $\boldsymbol{u_r}$ and $\boldsymbol{u_t}$ which are the moments and thrust of the AR, shown in Fig. 5.4 bottom right and left, respectively, and again they all satisfy the system constraints. Note that in order to overcome the ground manipulator limits, from approximately $t = 5$ s to $t = 7$ s, the AR is pushed to its maximum total thrust by the control allocation algorithm.

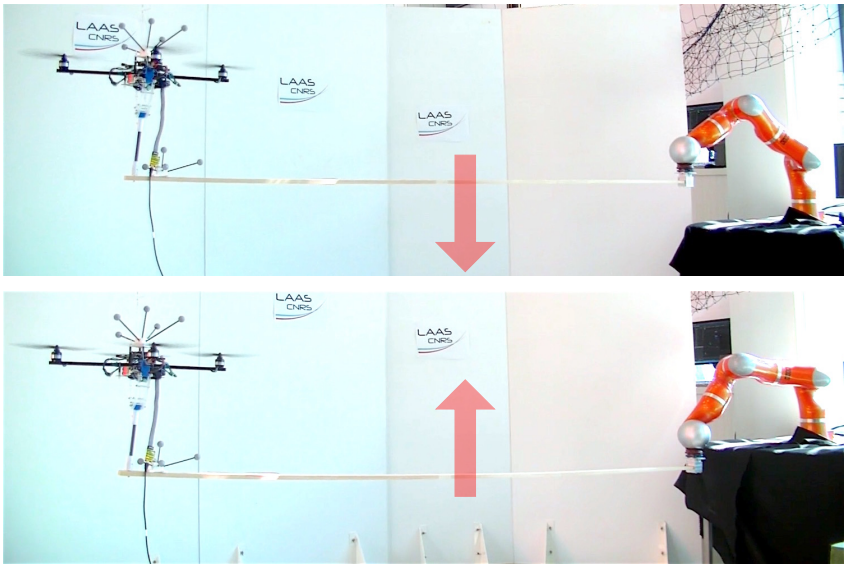

Figure 5.5 – Experimental setup: a KUKA LWR4 arm, a classical underactuated quadrotor and an in-house designed passive rotational joint. The two extreme configurations of the up-down trajectory with the bar hold horizontally are depicted.

5.1.2 Proof of Concept Experiments

The preliminary experimental work associated with MAGMaS aims at demonstrating the feasibility of MAGMaS and validating the proposed passive rotational joint design. The experimental setup relies on a KUKA LWR4 arm as ground manipulator and a single quadrotor as AR. Note that the ground manipulator is chosen different from the simulation, for practical reason, including the availability of an industrial manipulator for our experiments and the possibility for manipulation of longer object. Hence comparison between the simulation and preliminary experiments can not be directly conducted, but the experiment validate the feasibility and gains of using MAGMaS. The quadrotor is in-house-developed with a 1.2 kg payload, fitted with a custom passive rotational joint. This passive rotational joint ensures that the center of mass of the {AR+joint} system and the rotation center of the joint are coinciding, modulo manufacturing imperfections. This is of paramount importance as the AR can not sustain high torque disturbances. From the design, the rotational joint has the following angular constraints, two rotations are limited to $\pm 40°$ and $\pm 80°$ respectively and the last one is free, note that contrary to the simulation part the base of the joint cone is not a circle, but an ellipse, as the two rotations constraints are not symmetric. The object to be manipulated is a wooden bar of length 2.5 m and mass 0.61 kg. Also the grasping of the object is omitted, all sub-systems are rigidly attached together, this was done to simplify the system complexity in a first step. The full system is depicted in Fig. 5.5 and Fig. 5.8, for a close-up on the AR, additionally actual operations are featured in [video 3–2017].

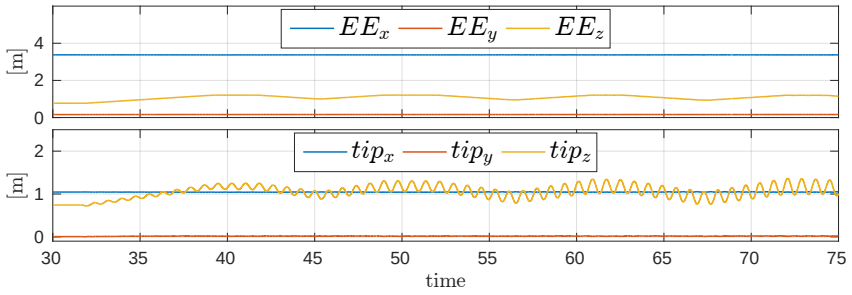

Figure 5.6 – The arm EE follows a vertical trajectory, as in Fig. 5.5, without the help of an AR. The tip position vibrates a lot due to the flexibility of the bar and is not able to track the EE **z**-trajectrory.

MAGMaS Approach Validation

As a first validation of the MAGMaS concept, the handling of a bar is considered with and without the help of an ARwas investigated, see [video 3–2017]. The ground manipulator's EE is moved up and down along the **z**-axis, see Fig. 5.5. Note that this comparison is possible because the bar characteristics are not violating the LWR4 payload/torques limits, this would not have been the case with UR5 manipulator, used for the simulation. For the case where the ground manipulator acts alone, see Fig. 5.6, it is clear that the bar tip is vibrating a lot while globally following the same trajectory as the manipulator's EE. The same experiment is performed with a AR attached at the tip of the bar, the relevant quantities are plotted in Fig. 5.6–5.7. Clearly the addition of the AR allows the bar tip to better follow the arm trajectory, the residual difference comes from the simple way the bar flexibility is handled in this preliminary experiment. This observation triggered further studies on the flexibility in a manipulated beam which are presented in Chapter 7. The careful modeling of the flexibility and its analysis show that the flexibility mode are controllable for the configuration used in this experiment, validating empirical observations.

Passive Joint Validation

A second experiment aims at validating the proposed design of the passive rotational joint, the AR is commanded to remain hovering, the bar tip is then moved in order to exhibit the rational decoupling between the bar tip and the QR, see Fig. 5.8 and Fig. 5.9 for orientation's monitoring of both tip of the bar and AR. In this experiment the orientation of the bar varies in a large range whereas the pitch of the AR remains in $\pm 3.5°$ range, which corresponds to its nominal range while hovering, hence validating the efficiency of the presented passive rotational joint.

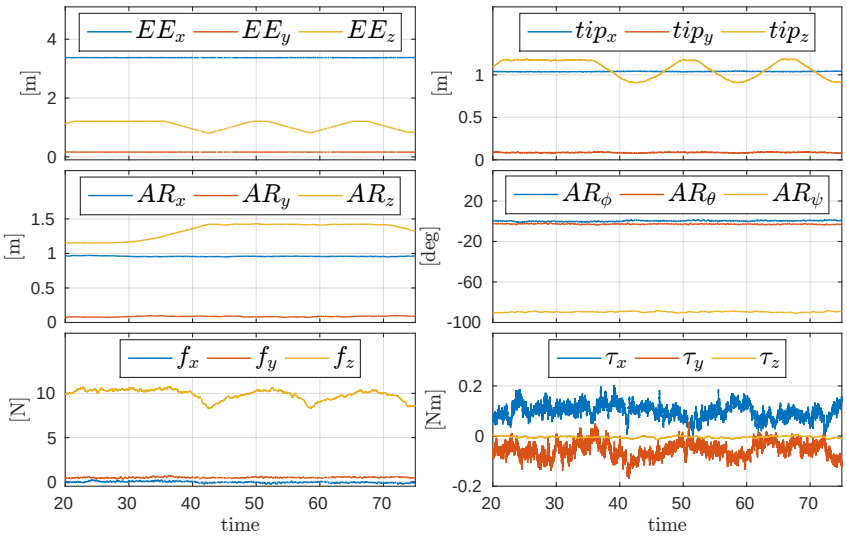

Figure 5.7 – The arm EE follows a vertical trajectory, as in Fig. 5.5, in cooperation with a AR. The tip of the bar follows the **z**-trajectory of the EE thanks to the AR stabilizing action.

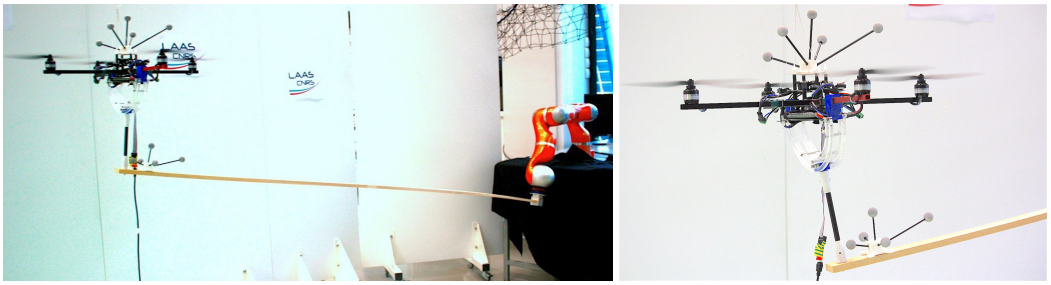

(a) (b)

Figure 5.8 – Second experiment (a) with the bar tilted, where the AR is hovering while the ground manipulator tilts the bar in order to exhibit the decoupling induced by the passive rotational joint. A closeup on the passive joint in action is pictured in (b).

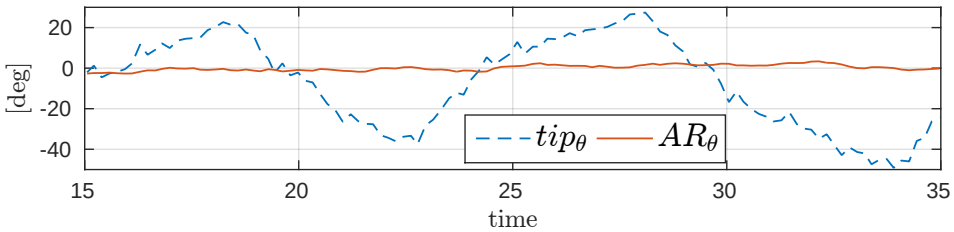

Figure 5.9 – orientation of the AR when subject to bar orientation changes, the passive rotational joint efficiently decouples the rotation of the AR and its EE attached to the tip of the bar.

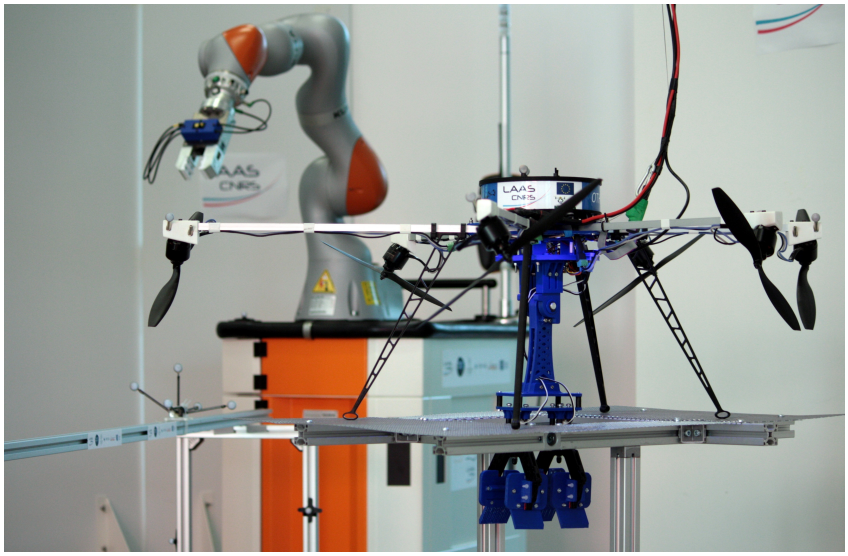

Figure 5.10 – State of the art industrial manipulator and in-house developped AR ready to be employed as a MAGMaS at LAAS–CNRS.

5.2 Multi-directional Thrust Aerial Vehicle

The work described in this Section has been accepted to the Robotic and Automation Magazine

[Staub–]

The work presented in this section corresponds to the first live demonstration of a MAGMaS for a cooperative manipulation task between a ground industrial manipulator and an AR. In particular the presented experimental results were conducted using a KUKA "Leichtbauroboter", German for lightweight robot, intelligent industrial work assistant (LBR-iiwa) and an in-house developed multi-directional thrust AR called OTHex, see Fig. 5.10. The LBR-iiwa is a state of the art industrial manipulator, which required extra work to integrate in our research software framework. Moreover the MAGMaS concept is augmented with a tele-presence framework. The successful combination of a MAGMaS and a tele-presence framework, took place in an internal project called Human in the Loop MAGMaS (Tele-MAGMaS). This project was demonstrated during the Hanover Fair 2017, see [video 5–2017].

5.2.1 Sytem Design, Architecture and Implementation

The MAGMaS presented in this section is composed of 3 main robotic components, *i)* the LBR-iiwa, *i)* the Open Tilted Hexarotor (OTHex) aerial manipulator and *i)* the Omega.6 haptic interface, a necessary component of the tele-presence framework. Additionally a simulator and visualizer have been developed to ease the integration of the system and provide visual feedback to the operator.

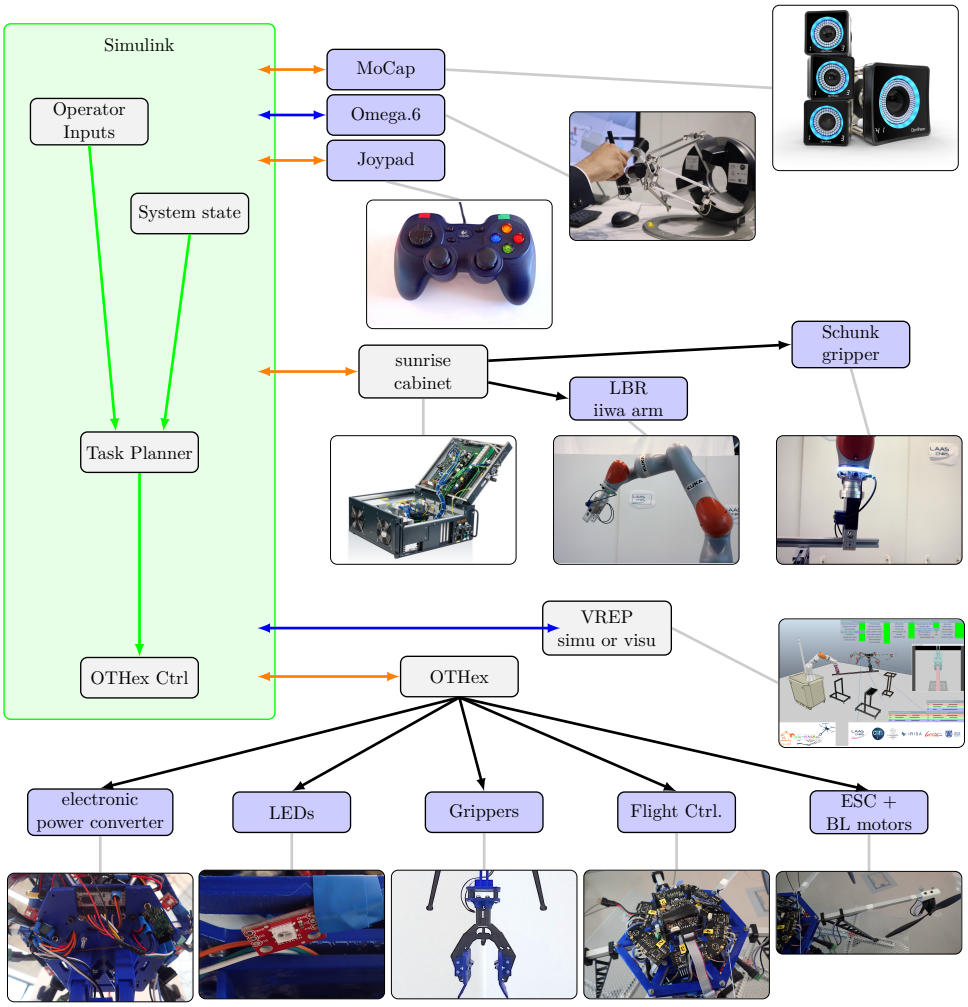

Figure 5.11 – Description of the software architecture used in the Tele-MAGMaS project, first implementation and demonstration of a Flying Companion concept. In green Matlab-Simulink links, in blue C S-function links, in orange Genom3 links and in black low-level links.

The experimental framework relies on the Genom3[1] abstraction layer, which allows to define middleware independent software components for robotics, the middleware can then be chosen at compilation time. Genom3 components can be controlled via tcl-shell, Matlab command line, Matlab-Simulink or middleware specific means, which allows high flexibility in the development and usage of the components.

The software architecture is shown in Fig. B.10. The high-level control of the full system is realized in Matlab-Simulink, linked to the hardware via Genom3 components or Matlab S-function drivers. This approach was chosen because the

[1] `https://git.openrobots.org/projects/genom3/wiki`

development and test of controller in Matlab-Simulink can be way faster than in pure C/C++, on the over hand Matlab-Simulink is far from real-time, hence the hardware has to be commanded via Genom3 components.

In the proposed architecture the Matlab-Simulink is running at 500 Hz, the task/path planner, the human input interpreter and the OTHex controller are running in Matlab-Simulink. The Matlab-Simulink process is linked with the haptic device via a custom S-function and to the simulator/visualizer via other S-functions. The Matlab-Simulink is also interfaced with joystik, Optitrack MoCap system, the OTHex hardware and the LBR-iiwa via Genom3 components. These Genom3 components are essentially drivers for the hardware as most of the algorithmic part is implemented in Matlab-Simulink. Except for the LBR-iiwa components. Indeed in order to satisfy the hard real-time constrains of the communication with the LBR-iiwa, inverse kinematics and other related utilities are performed in the Genom3 component.

Moreover this component based architecture allows easy repartition of the load between process and machines. In the presented experiments, ROS is chosen as middleware, which provides sufficient 'real-timeness' for the intended purpose. The component based design also allows seamless change of the operator inputs, perception components or of the MAGMaS hardware, as each of these are separated from the main algorithmic part and provide standard interfaces which are not hardware specific.

5.2.2 Aerial Manipulator – Open Tilted Hexarotor

The work described in this Section has been presented to
2018 IEEE Int. Conf. on Robotics and Automation
[Staub–2018]

The Open Tilted Hexarotor (OTHex) is an aerial manipulator developed at LAAS–CNRS and tailored to perform physical interaction tasks with the environment. It results from a custom design aimed at maximizing the platform APhI capabilities.

The OTHex is a multi-directional thrust platform as introduced in Sec. 3.2.1, *i.e.*, propellers are not collinear, see Fig. 5.12 with the tilting adapters (1). This design results in an important feature of the platform, the set of admissible control forces is not anymore a half-line as in the collinear case but is a polytope shaped like a double pyramid, the two halves being connected by their bases. This means that the robot can exert lateral forces without the need for re-orienting itself, as opposed to under-actuated multi-rotors, thus being able to track a decoupled reference trajectory in position and orientation, within the physical limits of the actuators. Aerial robots like the OTHex are starting to gain notoriety in the literature [Rajappa–2015][Ryll–2016]. These robots turn out to be particularly suitable for physical interaction tasks, since they can exert a decoupled set of forces and torques on another body, whatever the position of the contact point.

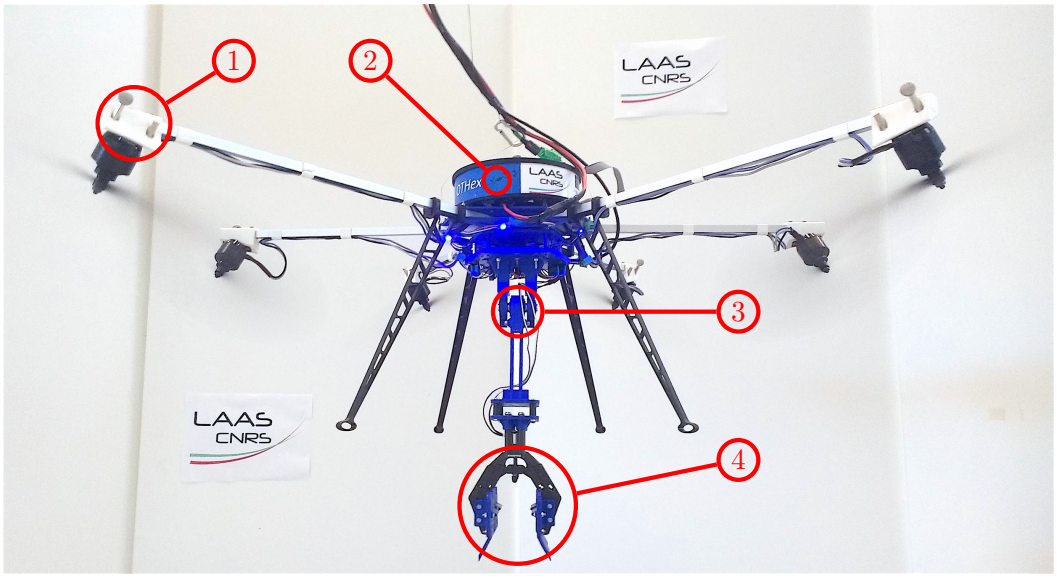

Figure 5.12 – Picture of the OTHex hovering. The main components of the OTHex are: (1) the tilting angles of the propeller allowing the multi-directionnal thrust property, (2) the electronics case containing flight controller and ESC, (3) the passive joint efficently decoupling the rotational dynamics of the load and (4) the grippering mechanism mounted on damper for compliance and with claw geometry facilitating the grasp.

The second particularity of the presented flying platform, like the adjective *open* suggests, consists of an aperture of 85° between two poles of the robot skeleton, see Fig. 5.13 . This configuration has been chosen over the regular hexagon positioning of the actuation units to facilitate the manipulation of a long object, *e.g.*, a beam. In this way the object can pass through the aperture, allowing a wider variety of beam manipulation tasks.

The third and last feature of the OTHex is a mechanical system composed of a passive 1-DoF passive revolute joint with two grippers, which endows the OTHex with grasping and manipulation capabilities required to perform physical interaction. A passive joint has been preferred over an actuated ones, to save the complexity of the system and because in the studied use case the OTHex acts as a *flying companion* following the ground manipulator motion. In particular, passive joint choice is motivated by the fact that most of the weight of the load is supported by the ground robot, while the role of the *flying companion* is to actively help the motion in order to reduce the needed torque at the ground robot's EE. Therefore, in this case there is no need to actuate this DoF. The design of the system emphasizes payload and robustness constraint, using 3D-printed part and carbon fiber materials. Moreover two grippers are used in parallel to limit rotation around the grasping point. Both grippers are controlled with an *arduino nano* board via a motor driver interfaced on the OTHex main power supply by a DC/DC converter.

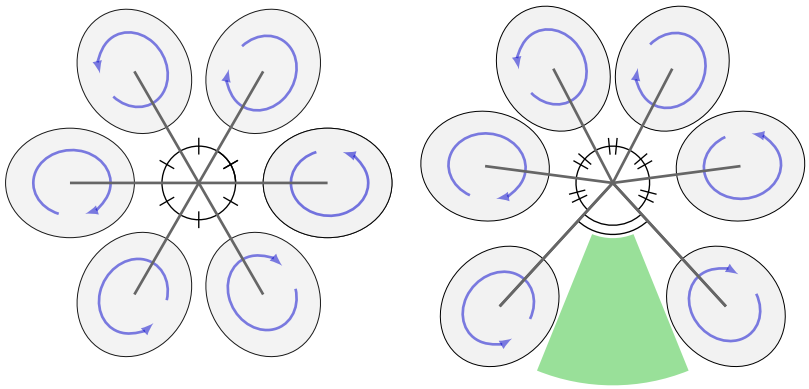

Figure 5.13 – Comparison of the spatial location of the propellers for a standard hexarotor configuration and the OTHex. The OTHex configuration is such that an aperture of 85° is left to facilitate the manipulation of a long object (green area).

The control board is controlled over serial via Matlab-Simulink.

The OTHex control architecture is articulated over three main components: a low-level controller, a wrench estimator and an admittance filter, as detailed in Chapter 4, and briefly recalled hereafter. A sketch of their inter-connection can be found in Fig. 4.9. The low-level control takes as input the OTHex state and a full 6D pose reference trajectory (the attitude is expressed by a rotation matrix) and gives as output the force that each propeller should produce to track the assigned position and orientation. The controller, presented in [Franchi–2017a], is a geometric control in SE(3) with a prioritized tracking of position over orientation. Which means that if the desired orientation is such that the reference thrust lies outside the pseudo-cone of admissible forces, then the closest orientation that lets the pseudo-cone include the assigned force is computed by solving an optimization problem and tracked. In other words, the controller ensures the tracking of the position and the closest rotation matrix satisfying the actuator constraints. To perform physical interaction tasks, the aerial robot needs some force sensory capabilities.

Parameter	**Value**	**Units**
weight (without battery)	2.48	[kg]
extra payload	2.9	[kg]
actuation unit 1st tilt angles	35	[°]
actuation unit 2nd tilt angles	-10	[°]
autonomy (on battery)	15	[min]
max. lateral force (hovering)	8	[N]

Table 5.1 – Key physical parameters related to OTHex.

To this purpose a model-based wrench estimator has been preferred to an on-board force/torque sensor, in order to preserve a bigger net payload for the UAV and to not restrain the force measurement only to the sensor location. The estimated force and torque is then the input of the admittance filter, which is re-computing a reference 6D pose from the desired one, acting like a mass-spring-damper system with rest point on the trajectory, under the influence external force. An appropriate tuning of the gains of this sub-system is required to give the robot the proper stiffness/compliance depending on the task to be performed. For the interested reader, the main characteristics of the OTHex are summarized in Table 5.1 and the experimental validation of the design and control architecture for bar lifting is performed in [video 7–2018].

5.3 Tele-Presence Framework

In the real world, MAGMaS might work in different environments, depending on the application, ranging from well-structured fully-known environments, *e.g.*, a factory or a warehouse, to completely unstructured and unknown environments, such as a disaster scene in a robotic search and rescue mission. Thus, depending on the environment and complexity of the task, the high level control of the system might change to match the conditions. While for a well-structured and fully known environment a fully autonomous MAGMaS might work sufficiently well, in unknown or partially known environment and for complex tasks the presence of one or more human operators could improve the robot team (working in the remote environment) in various aspects. Human operators can improve the precision of the task execution and enhance the task performance by reducing the execution time. Moreover the human intelligence could be of utmost importance in decision making, planning and run-time re-planning of the task in case of unpredicted situations; and thus increasing the reliability and safety level of the proposed system. The combination of the MAGMaS system and the human operator(s) tele-operating the MAGMaS in the remote environment is called Tele-MAGMaS.

The Tele-MAGMaS has three distinctive degrees of autonomy: *i) fully autonomous*, *ii) tele-operated* and *iii) shared-control*. The degree of autonomy of multi-robots systems should be tuned by considering the task at hand. For simple, predictable, tasks full autonomy system is often appropriate as human supervision is not required. But, in general, the use of semi-autonomous system, supervised or partially controlled by one or more human operators, is the only viable solution to deal with the complexity and unpredictability of real-world scenarios, see [Franchi–2012]. In the following the different approaches are reviewed, to underline how the human operator can assist or intervene in each approach by mean of a haptic device.

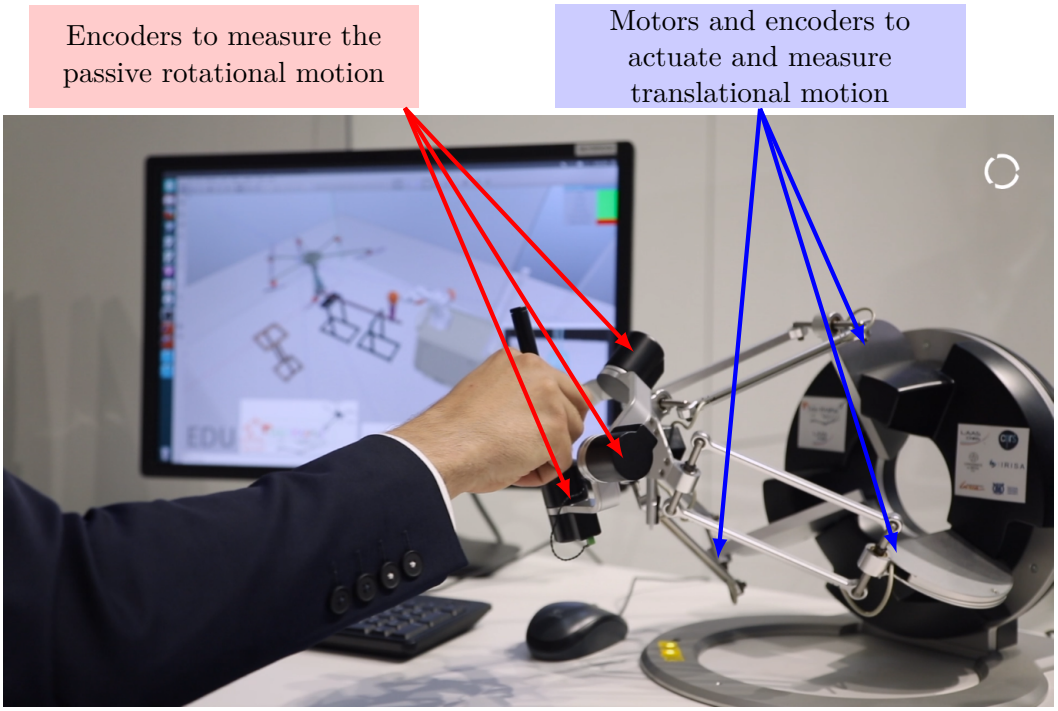

Figure 5.14 – Omega.6, the haptic device used in the presented testbed.

Haptic Interface

The human operator can assist the robot team using different interfaces, such as touch displays, game-pads and haptic devices. A haptic device (or haptic interface) is a robot with serial or parallel structure that works in the master side of a tele-operation system. The human operator can move the master robot by applying force to its handle and the master robot can also apply forces to the human operator, called "haptic cues" or "haptic feedback". Haptic feedback informs the human operator about the situation of the remote system.

In the LAAS–CNRS testbed, an Omega.6 was used as haptic device (manufactured by force dimension[2]), as shown in Fig. 5.14. The Omega.6 device has six Degrees of Freedom (DoF), the three translations are actuated by independently controlled DC motors and the three rotations are passive. The device communicates through USB 2.0 with the main PC and can be controlled at up to 4 kHz (the faster the control loop, the better the force rendering).

Fully autonomous MAGMaS

The fully autonomous operation mode of the MAGMaS is the simplest control modality. In this case the robots work in a well-structured fully known environment.

[2] http://www.forcedimension.com/

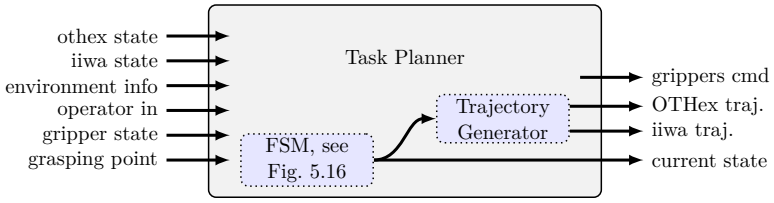

Figure 5.15 – Task planner inputs and outputs for a possible peg-in-hole task performed by a MAGMaS.

The described task-planner specifies the various stages of the task operation and associated trajectories, see Fig. 5.15. The outputs of the task planner are as follow,

- commands for robots' motion, for all robots during the whole execution time to be sent to their low-level controller
- commands for the robots' grippers
- state of the system: as a Finite State Machine (FSM), see Fig. 5.16, that specifies for the robots' local controller which command must be executed in each moment and how the robot trajectories should be computed.

On the other hand the task planner inputs are:

- the robots' motion feedback
- pose feedback of the environment
- desired contact points on the object
- the state of the grippers.

These inputs allow the task planer to react with simple policies on the environment and the task evolution.

The types of commands for the manipulators motion, that the they independently or cooperatively perform, depend on the local controller of the manipulators. These motion commands could be desired paths, trajectories, or forces/torques for the AR, grounded manipulator EE (or joints) and for the manipulated object. For example, if the ground manipulator local controller is accepting the desired joint angle values (and possibly their derivatives), then the output of the task planner must have the same type and the EE desired trajectory must be transformed into joint angle trajectories using the robot Inverse-Kinematics inside the trajectory generator.

The finite state machine, Fig. 5.16, defines the policy used by the task planner to generate the robot motion trajectories and triggers the grippers' actions, based on the robots and environment informations and the operator(s).

The autonomous cooperative manipulation phase can be implemented in centralized or decentralized manners. In centralized cooperative manipulation manner both robots are commanded based on the manipulated object position. A detailed description of this approach can be found in [Staub–2017]. While in decentralized approaches, such as leader-follower approach, during the cooperative manipulation, the ground manipulator manipulates the object and the flying manipulator is assisting the ground manipulator following its lead and producing additional upward

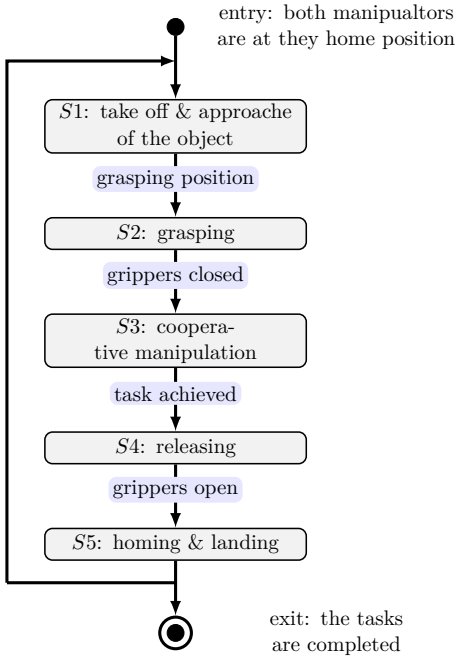

Figure 5.16 – the simple Finite State Machine (FSM) implemented in the proposed task planner. The fives states have their own trajectory generation policy and the transitions are based on the co-manipulation task status.

force on the bar. The autonomous cooperative manipulation of a bar is depicted in Fig. B.12, this was the strategy chosen for the bar lifting in the KUKA 2017 Innovation Award.

Tele-operated MAGMaS

In many real scenarios, such as search and rescue, MAGMaS must work in a partially or even completely unknown environment. The bilateral tele-operation approach is suggested to cope with unknown environment and uncertainties and also to facilitate the complex tasks. In bilateral tele-operation approach skilled human operator(s) drive the robots in a precise and safe manner. Moreover, the human operator(s) are provided with force feedback in order to improve their tele-presence [Sheridan–1992] and to increase their situational awareness from the remote side. In fact, in the bilateral tele-operation approach, the human intelligence performs the task planning with the help of visual and haptic feedback. If direct visual feedback is not possible, First Person View (FPV) cameras can be mounted on the robots. In the non-cooperative parts human operator(s) drive the robots, while in the cooperative part the operator(s) command the bar and the robots cooperatively manipulate the bar to perform the human command, *e.g.*, see [Sieber–2015]. Gripper and state change are manually triggered by the operator. In this case the human intelligence decides how to move the robot, what are the suitable contact points, how to move

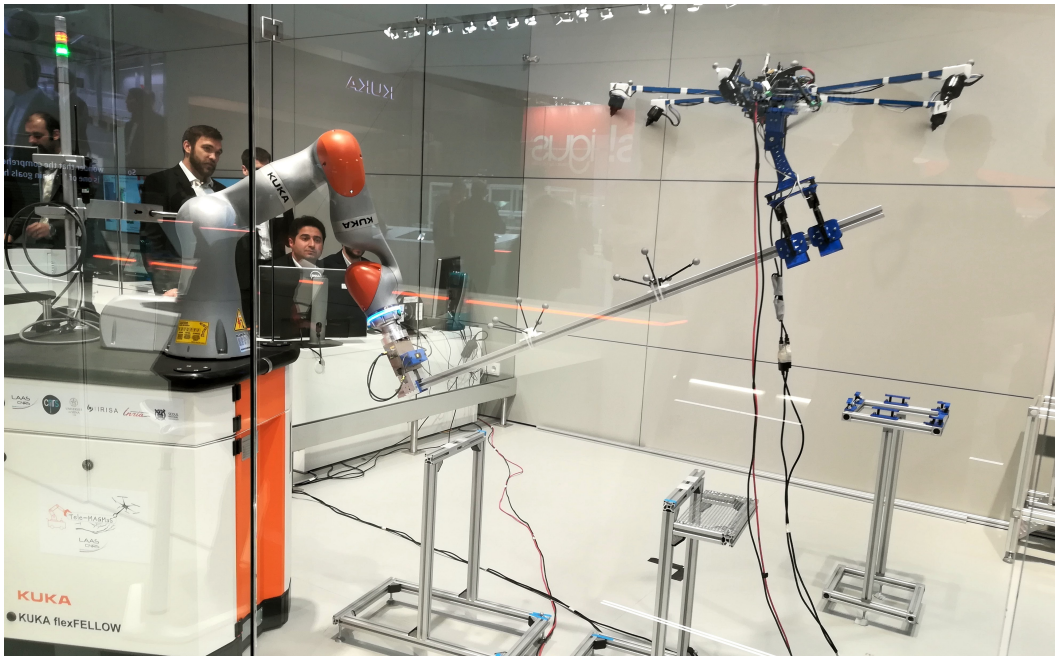

Figure 5.17 – A snapshot of the cooperative manipulation state of Tele-MAGMaS using bilateral tele-operation approach performed in KUKA 2017 Innovation Award at the Hanover Fair, with 4 operators in the background.

the bar and from which path the robot should come back to their home position. Bilateral tele-operation is a practically reliable approach to perform cooperative manipulation with MAGMaS in unknown and unstructured environments.

The most challenging state in this approach is the cooperative manipulation in which the robots must cooperatively manipulate the bar. In the proposed bilateral tele-operation control scheme, the desired object pose is generated online by the human operator through an haptic device.

The desired object pose and the current object state are sent to the object pose controller which computes low-level inputs for the robot controller. Either ideal wrench to be applied by each robot as in [Staub–2017], or robot pose necessary to reach object pose, which is better suited for the manipulators low-level interface.

On the backward channel of the bilateral tele-operation scheme, the operator receives a force feedback that depends on the inertia of the whole system and on a repulsive viscoelastic virtual force generated with the purpose of letting the operator feel the obstacles in the environment.

The bilateral tele-operation approach was chosen for the KUKA 2017 Innovation Award, hence the name *Tele-MAGMaS*. However as can be seen in Fig. B.12, the setup relied on direct (visual) connection between the robots and the operator(s), thus the connection quality was not taken into account. For further deployments of MAGMaS over longer distances, scheme of haptic data reduction shall be studied, *e.g.*, based on operator deadband and psychophysical properties, see *e.g.*,

[Vittorias–2010][Chaudhari–2011][Brandi–2011].

Shared-Control MAGMaS

The third control modality, shared control, deals with the case of the MAGMaS working in a semi-structured environment, *i.e.*, partially mapped environment or fully mapped but with possibility to have unpredicted events happening, *e.g.*, construction site or industrial environment where humans, robots and other machines work together. The shared control approach is in fact the combination of the previous two approaches. An automatic task planner plans the motion commands and changes of states and the human operator(s) can modify the planned trajectories. human operator(s) can locally change the trajectories or change the time law of the trajectories to react to the environment changes. For instance, the grasping point can be modified to accommodate environment evolution, the trajectory planner reflecting this change in the autonomous control part. Also the time law can be virtually increased/decreased to speed up/down the task execution, while the manipulators stay on their respective planned paths.

In the shared control approach, the human operator(s) is also provided with haptic feedback that allow to increase the situational awareness and tele-presence of the human operator(s). For example, consider that the robots are cooperatively transporting the object and the human operator feels a force feedback that shows the error of position and velocity of the object is high (for example due to erroneous weight information of the object in the planner, or external disturbances such as wind), here the human operator can slow down the planned trajectory. Another example could be the case when there is an obstacle on the planned path for a robot, in this case the human operator could modify the path locally to avoid collision. Changing the states could be done both automatically when the condition for changing the state is met, or could be done manually by the human operator(s), especially if the grippers are not equipped with sensors to detect their correct grasp/release actions.

5.4 Experimental Results

A set of experiments was conducted with a successful co-manipulation of a 2.5 m long bar. The desired task consist in cooperatively lifting a bar as illustrated in Fig. B.11, at first the OTHex is manually flown to grasp the bar from one of its ends, while the ground robot grasps the other end autonomously. Once both manipulators are attached to the bar, the co-manipulation is fully autonomous, they lift the bar from its supports, move it twice along a line in the horizontal plan (blue part in the data plots) and then synchronously lift the bar up to 30° (green part in the data plots). Then the two manipulators bring the bar back to its starting position. This experiment highlights both the vibration stabilization induced by the OTHex and the practical use of MAGMaS concept.

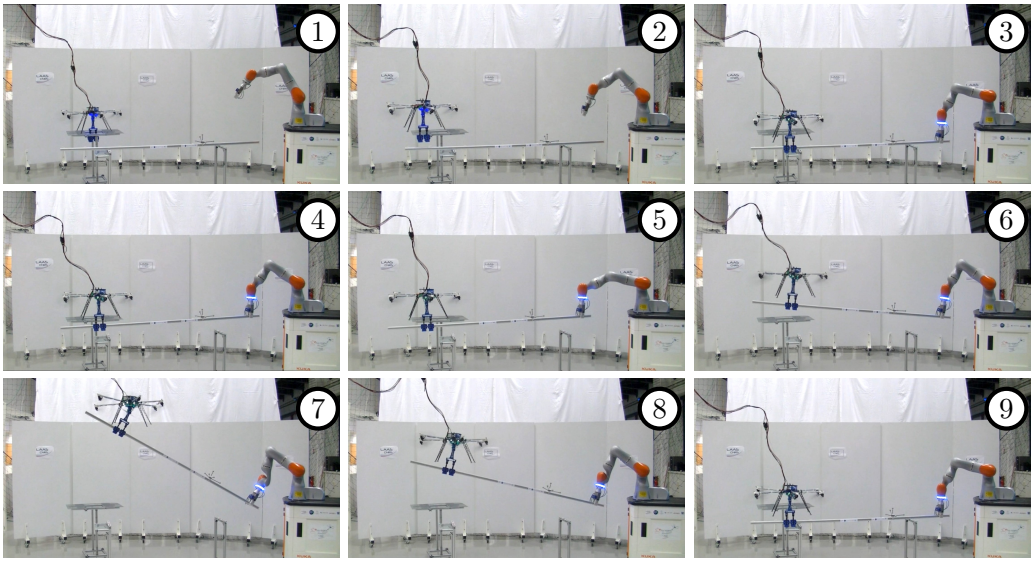

Figure 5.18 – Time-lapse of a MAGMaS cooperative manipulation task. Both robots are at their initial position (1), approach of the bar (2), grasping of the bar (3), cooperative lifting of the bar (4), cooperative lateral motion of the bar (5), cooperative lifting of the bar up to 30° (6-7-8) and release of the bar (9). See [video 6–2017] for the corresponding video of the experiment.

During this experiments the external wrench at the ground manipulator EE is recorded, see Fig. 5.19 for their evolution during the task. The joint torques for the ground manipulator, see Fig. 5.20, all stay within their limits during the task. The OTHex position and orientation is plotted in Fig. 5.21, notice that before (b) and after (d) the OTHex is flown manually, while in between the system is fully autonomous. Fig. 5.22 depicts the evolution of the passive joint angle during the task, the evolution of the angle is equivalent to the bar orientation and allows the OTHex to remain flat, *i.e.*, with almost constant pitch and roll while lifting the bar.

Key quantities of the system are plotted on Fig. 5.19- 5.22. The experiment sequence is depicted in Fig. B.11 and [video 6–2017], this highlights both the vibration stabilization induced by the OTHex and the feasibility of MAGMaS.

KUKA Innovation Award

The Tele-MAGMaS concept has been successfully demonstrated at the Hanover Fair 2017, as finalist of the KUKA 2017 Innovation Award, Advanced Challenge in Mechatronics. This occasion displayed the performing Tele-MAGMaS in front of industrials from all around the world. It was the occasion to demonstrate the robustness and reliability of the system, by performing demonstrations outside of a laboratory environment and as much as 10 times per day for over a week. During this demonstration the system was both tele-operated and autonomous to illustrate

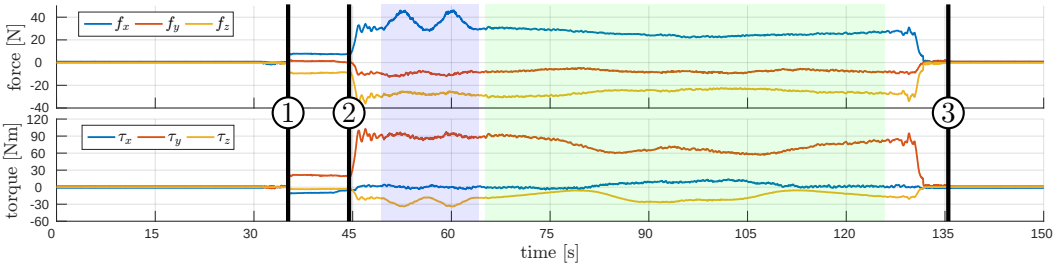

Figure 5.19 – external wrench as sensed from the joint sensor and projected in Cartesian space. The three instants highlighted are LBR-iiwa grasping (1), cooperative lifting (2) and LBR-iiwa releasing (3). The blue part highlights the horizontal motion and the green part the bar tilting.

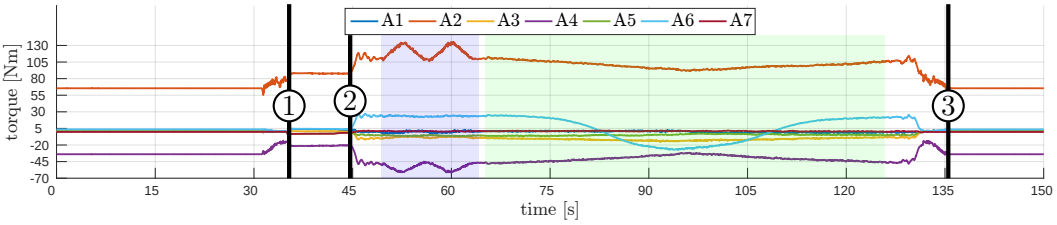

Figure 5.20 – joint torques for each articulation of the LBR-iiwa. The three instants highlighted are LBR-iiwa grasping (1), cooperative lifting (2) and LBR-iiwa releasing (3). The blue part highlights the horizontal motion and the green part the bar tilting.

both possibilities of the control framework note that due to booth constraint the bar manipulated was significantly shorter *w.r.t.* the experiments conducted at LAAS–CNRS. Videos highlighting the key-features of the demonstration can be found online in [video 4–2017] and [video 5–2017].

5.5 Discussion

The presented work covers both simulations and preliminary experiments conducted to validate the MAGMaS concept and then the world first demonstration of a MAGMaS with tele-operation capabilities. The preliminary results validate the individual bricks necessary to pave the way for MAGMaS deployment, from the theory to the mechanical design. The demonstration of the Tele-MAGMaS led to a further integration of the MAGMaS concept, in particular with a tele-presence framework and with the design of an AR tailored for cooperative bar manipulation. This was possible thanks to the participation to the KUKA 2017 Innovation Award which allowed to gather a lot of data and several feedbacks on the MAGMaS concept. Nevertheless MAGMaS are still in their infancy, among the future works four directions should be investigated in priorities: *i)* control and planning methods, *ii)* human-MAGMaS

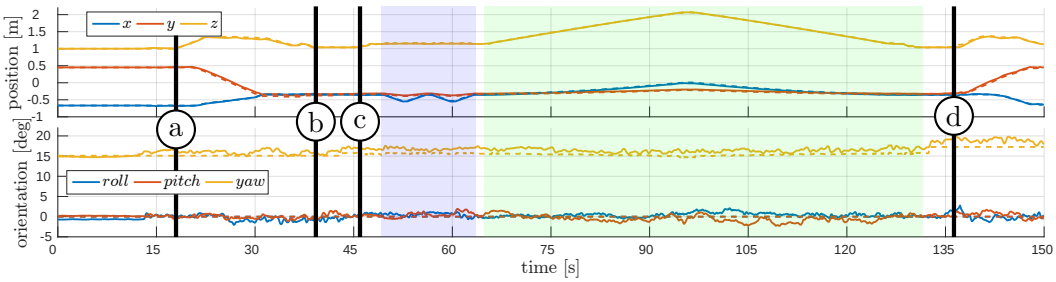

Figure 5.21 – position and orientation of the OTHex aerial manipulator. The four instants highlighted are take-off (a), OTHex grasping (b), cooperative lifting (c) and releasing (d). The blue part highlights the horizontal motion and the green part the bar tilting.

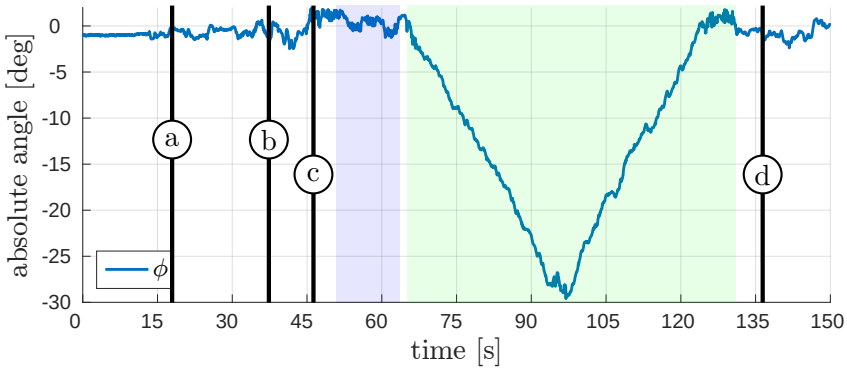

Figure 5.22 – evolution of the OTHex passive joint angle, during a typical task with free-flight, horizontal motion and object tilting. The four instants highlighted are take-off (a), OTHex grasping (b), cooperative lifting (c) and releasing (d). The blue part highlights the horizontal motion and the green part the bar tilting.

cooperation, *iii)* mechanical design solutions and *iv)* perception methods.

Control and Planning

The proposed high-level control schemes are embryonic in their design as the main focus was to first validate the MAGMaS concept and design. Now that a MAGMaS has been successfully demonstrated more emphasis can be put to the higher level control and to supervision development. In general the trajectory generation and planning techniques employed in the described work are not very elaborate and rely on educated guess and trial-and-error. A more autonomous and resilient framework should be implemented and could be the material of another PhD thesis. Hereafter a few possible directions to explore are detailed.

In order to account for the actuation heterogeneity in MAGMaS, further study on the load sharing should be conducted. In particular, frameworks, as the one

presented in [Zambelli–2015], are of interest. Another challenge in the load sharing comes from the high redundancies present in MAGMaS, techniques to limit internal wrenches should be investigated, *e.g.*, based on kinematic constraints [Erhart–2015].

At the moment the system is rather agnostic to its environment, in particular no checks for collision with the environment are conducted. Trajectories and environment layout are chosen heuristically to prevent collision from occurring. An advisable development for MAGMaS would be to devise a planning framework taking into account collision detection and avoidance with static or dynamic environment, the framework should be generic enough to cover both the cooperative manipulation part of the task and the separated motion part.

An intersecting direction of research would be to go toward sharing space between MAGMaS and human, by improving the environment awareness of the system and the system autonomy in term of reaction to the environment. Especially collision avoidance while pursuing the cooperative manipulation should be investigates in a framework allowing safe operation without system constraints violations.

Human-MAGMaS Cooperation

Human cooperation is a particularly thriving potential use of MAGMaS, sharing the space with human raises many questions, such as safety and communication paradigms. So far the OTHex used as a *flying companion* is equipped with a set of LEDs to reflect the state machine state, for sure this can be improved based on state of the art Human-Machine Interface (HMI). In this area, extensive is the literature that explores social, cognitive, or behavioral aspects of human-robot interaction [C Breazeal–2008]. Developments in the direction of Human-MAGMaS, or of Human-Flying Companion, physical interactions, are foreseen. The basis of which are present but will require refinement of the low-level controllers and developments of physical interaction control and planning strategies.

First of all, it is of paramount importance to ensure safety of the physical interaction, for example by balancing compliance with ISO10218 regulation and performances, see [Navarro–2017], or by considering a dynamic safety region around human in a invariance control framework, see [Kimmel–2015][Kimmel–2017].

A second objective for the system would be to interpret the haptic cues from the operator to interact smoothly in cooperation via non verbal communication. It has be shown that wrench information are not sufficient to detect operator's intention of motion, see [Dumora–2012], but that the addition of operator position makes it possible. Moreover the wrench sensed by the system also comprises the object dynamics, thus it is important to precisely estimate it, to remove that bias from the human motion recognition. In [Cehajic–2017a] the redundancy of the system is exploited to conduct this identification in the null-space of the operator grasp. A key factor also resides in the prediction of the operator behavior/motion uncertainty in order to perform predictive haptic assistance, decreasing operator discomfort, see [Medina Hernández–2015][Medina–2017]. Once the intention of the human is understood, the system can react to guide the operator via motion

primitives, see [Dumora–2013].

Strategy to make the system behavior intuitive for the operator are also to be investigated, *e.g.*, see [Navarro–2017] for mobile manipulator. The ability of the understanding the operator intentions can also allow the system to steer the operator toward a preferred behavior. A way of controlling the operator is to let the system use functional electrical stimulation to control the operator arm, see [Adorno–2015], possibly enhancing the human-robot interaction. Or to provide vibrotactile feedback to guide the operator arm motion, see [Cehajic–2017b].

Mechanical Design

Based on the experimental work presented a few possible design amelioration arose from usage of the system.

The OTHex Flying Companion was developed under 6 months, thanks to the high expertise of the team involved in the Tele-MAGMaS project. The first obvious improvement resides in the gripping mechanism at the EE of the AR. Indeed, due to time constraints off-the-shelves solution was chosen and integrated in the OTHex, even if the recorded performance were satisfactory a further work could reduce the weights of the mechanism and propose a locking mechanism for the closed position of the gripper.

Another point of design which could be improved is the propeller location and orientation. It appeared that in the actual layout, during a bar lifting task some propellers where perfectly oriented with the task direction and thus "overly" used. Based on the recent advances in the (optimal) design of multi-directional thrust, an iteration on the propeller layout might prove beneficial especially to allow lifting of heavier bar.

As the work was conducted with state of the art industrial manipulators from the ground side, the hardware was already satisfactory from a mechanical design point of view.

Lastly, in the presented work the system has limited computational power and the setup was lacking radio-frequency transmission of the perception information, at the beginning of the integration the perception was seen as less important to demonstrate the capacity of a MAGMaS and reliable wireless communication was an issue in the demonstration environment, this point is now solved by parallel developments and the integration of computational power by adding an onboard computer is foreseen. The payload of the OTHex allows to carry an small powerful computer like an Odroid-XU[3]. This architecture will call for further development of the control algorithm to enable a decentralize control framework, with at least a computer on the AR and one on the ground robot and with eventually a supervision station and/or a remote station for tele-operation. This will require work mostly on the OTHex platform and the control algorithms.

[3] `http://www.hardkernel.com/main/products/prdt_info.php?g_code=G137510300620`

Perception

The last possible direction for development of MAGMaS consists in improvements in the perception framework. At the moment the system relies on MoCap, for state estimation of the AR and environment awareness. Further works need to be carried on the perception for MAGMaS leading to more system autonomy. Work should be aimed at system state recovery, environment monitoring and grasping improvement. The AR control architecture is highly dependent to a good state estimate, The addition of sensors to MAGMaS in order to reconstruct the environment should be considered in order to identify autonomously unplanned obstacle and potential danger, thus removing the necessity of constant human supervision. Visual sensor for monitoring the environment can also provide queues to switch interaction policy, see, *e.g.*, [Cherubini–2015]. The last improvement that can be provided by perception enhancements for MAGMaS resides in the grasping of the load, using techniques known as eye-in-hand visual servoing, see *e.g.*, [De Luca–2007][Robuffo Giordano–2008].

Part III

Ongoing Studies on Flexibility and Conclusion

Chapter 6

Variable Stiffness Actuators for Aerial Vehicles

Contents

Abstract

This chapter briefly introduces new paradigms associated with VSA and contextualizes them for APhI applications, see Sec. 6.1. A 2D study is presented where the nonlinear model is derived in Sec. 7.1 and an exact feedback linearization scheme is proposed, see Sec. 6.3. Once the system is exactly linearized, a linear controller is synthesized, in Sec. 6.4, and validated through simulations, Sec. 6.5.1, and preliminary experimental results using an actuated joint with variable stiffness on a quadrotor platform, Sec. 6.5.2.

6.1 Variable Stiffness Actuators, Overview and Motivations

The recent trends of APhI research have been detailed at length in Chapter 2. This chapter focuses on the promising yet confidential use of VSA for APhI. Indeed in almost all the current designs, AR are equipped with rigid-joint arms. On the other hand, compliant-joint manipulators are widely considered in ground robots like humanoids and manipulators physically interacting with humans, as fostered by SaPHARI European project[1]. They are also effective tools for fast motion tasks, exploiting the elasticity of the joint to perform explosive tasks, such as throwing an object or hammering on a surface, which requires large velocities that rigid-joint arm can not provide [Braun–2013].

[1] `http://www.saphari.eu/`

Yet, their usage in aerial robotics and APhI is not fully investigated. Recent works started to consider the use of elasticity for AR, like, *e.g.*, [Yüksel–2015] for a single joint manipulator and [Suarez–2015b][Suarez–2017b] for dual arm manipulator.

In particular, in case of APhI the variable stiffness property can be exploited for explosive motion but also and more importantly to ensure mechanical compliance of the airborne manipulator. Indeed, using the stiffness tuning it is possible to impose a very stiff behavior to the manipulator, typically for tasks where EE precision is needed, *e.g.*, picking, while a compliant behavior can be implemented in the case of motion in an unknown or unstructured environment. In this case unforeseen collision's effects can be attenuated by the compliant behavior of the arm. Meaning that if the arm collides with the environment substantial part of the impact force will be stored in the VSA spring instead of being applied directly on the AV, this mechanical property reduces drastically the system failure rate. Lastly, by introducing mechanical compliance the VSA should represent an additional level of safety for human-robot interactions.

The implementation of VSA on AV faces two main challenges, *i)* the mechanical design and *ii)* the control analysis and synthesis.

Off-the-shelf VSA designs are meant for ground robots and, as such, are not fitting the lightweight and low power consumption required by AR designs. Nevertheless, one outcome of the SaPHARI project was the creation of *qb robotics*[2], a company producing a small and lightweight VSA that can be integrated on a quadrotor, although AM was not their targeted use case. Another solution to explore the VSA possibilities is too design from scratch a VSA matching the AR's constraints, as in [Yüksel–2015]. This approach comes with full control of the VSA system, but comes at high development costs and skill requirements.

The second main challenge, arises from the control analysis and synthesis. In order to accommodate for the complex and non-linear dynamics of such a system composed of an underactuated flying vehicle and a manipulator composed of elastic joints, differential flatness of the system is investigated. The literature presents analysis of the general case for a grounded mixed manipulator, *i.e.*, consisting of both rigid and elastic joints, and demonstrates their differential flatness [De Luca–1996]. But no result is readily available for floating base manipulators, here floating base refers to the case in which the base of the arm is not connected to the mechanical ground, *i.e.*, is suspended in the air. The only results available is presented [Thomas–2013], the authors prove that AR with a single rigid joint are exactly linearizable via a dynamic feedback and therefore are differentially flat, under the assumption that the center of thrust actuation coincides with the CoM of the system. This occults a large class of design and also totally eludes the elastic joint case. More results on differential flatness for AR can be found in both [Tognon–2017] and [Yüksel–2016a], with results on multi-link manipulators.

[2] `http://www.qbrobotics.com/`

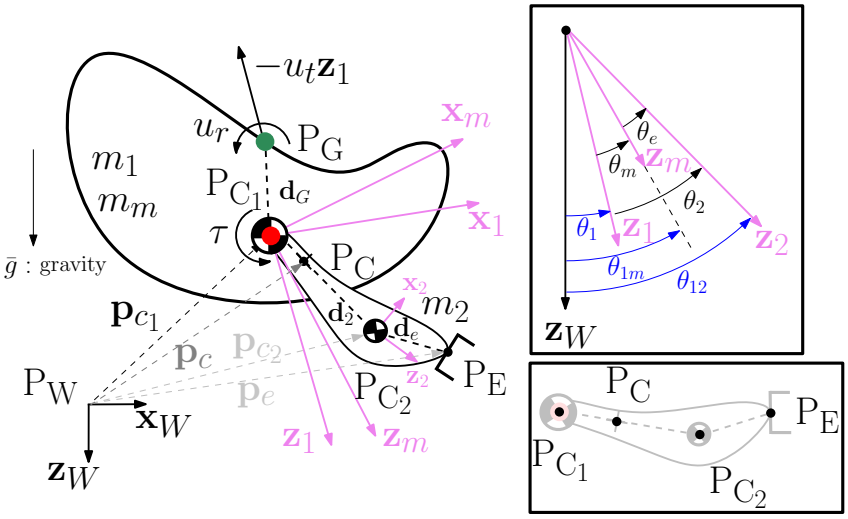

Figure 6.1 – Sketch summarizing the main notations and the relations for the model derived in Sec. 7.1. Left, a sketch of the PVTOL equipped with an actuated link. Notice the offset between the CoM of the PVTOL ($\mathrm{P_{C_1}}$, red point) and the center of actuation ($\mathrm{P_G}$, green point). The rigid link is attached to $\mathrm{P_{C_1}}$, around which the motor rotates and an elastic joint is placed. Right-up: relative and absolute angles of the rigid bodies, where the length of the $\mathbf{z}$ axes are made different to enhance readability. Right-down: locations of important points on the manipulator arm.

The work described in this chapter as been presented at
2016 IEEE/RSJ Int. Conf. on Intelligent Robots and Systems
[Yüksel–2016b][Yüksel–2016c]

6.2 Planar Case Modeling

In this section the kinematics and dynamics of a robot composed of an aerial platform, equipped with an elastic-joint arm are modeled (for the rigid case refer to [Yüksel–2016b]). Similar to previous studies (see, *e.g.*, [Lupashin–2010][Thomas–2013]) the case of a Planar Vertical Take-off and Landing Vehicle (PVTOL) AV is considered. This reduced system still captures the nonlinear features and the underactuation of a 3D system and allows to generalize the obtained results in a later stage. Furthermore, many practical aerial problems are, fundamentally, 2D problems immersed in a 3D world.

The PVTOL with the attached arm is depicted in Fig. 6.1. Denoted with $\mathcal{F}_W : \mathrm{P_W} - \{\mathbf{x}_W, \mathbf{z}_W\}$ and $\mathcal{F}_1 : \mathrm{P_{C_1}} - \{\mathbf{x}_1, \mathbf{z}_1\}$ are the world (inertial) frame and the frame attached to the PVTOL, respectively, where $\mathrm{P_{C_1}}$ is the CoM of the PVTOL (without the arm). Both the motor and the joint of the arm rotate about an axis parallel to $\mathbf{z}_W \times \mathbf{x}_W$ and passing through $\mathrm{P_{C_1}}$. The *motor frame* is defined as $\mathcal{F}_M : \mathrm{P_M} - \{\mathbf{x}_1, \mathbf{z}_1\}$ that is rigidly attached to the motor output shaft. The joint is considered elastic, therefore also a *link frame* $\mathcal{F}_2 : \mathrm{P_{C_2}} - \{\mathbf{x}_2, \mathbf{z}_2\}$ is considered,

where $\mathrm{P}_{\mathrm{C}_2}$ is the CoM of the link. The elastic part of the joint, variable or not, is located between the motor output shaft and the link as depicted in Fig. 6.2. Finally P_{E} denotes the TCP of the EE.

Given an angle $\theta_* \in \mathbf{R}$ between the z-axes of two frames (all the angles are given in Fig. 6.1) the usual rotation matrix definition $\mathbf{R}_* \in \mathrm{SO}(2)$ holds. Therefore, the orientations of $\mathcal{F}_1$ in $\mathcal{F}_W$, $\mathcal{F}_M$ in $\mathcal{F}_1$, $\mathcal{F}_2$ in $\mathcal{F}_1$, and $\mathcal{F}_2$ in $\mathcal{F}_M$ are expressed by the rotation matrices $\mathbf{R}_1$, $\mathbf{R}_m$, $\mathbf{R}_2$ and $\mathbf{R}_e$, respectively. Finally, the absolute motor angle is $\theta_{1m} = \theta_1 + \theta_m$ and absolute link angle is $\theta_{12} = \theta_1 + \theta_2$, as depicted in Fig. 6.1 (right) and Fig. 6.2. Notice that $\theta_e = \theta_2 - \theta_m = \theta_{12} - \theta_{1m}$, which denotes the time varying elongation of the elastic joint.

The constant position of $\mathrm{P}_{\mathrm{C}_1}$ in $\mathcal{F}_2$ is denoted with $-\mathbf{d}_2 = [-d_{2_x} \; -d_{2_z}]^T \in \mathbb{R}^2$. The vector $\mathbf{d}_e = [d_{e_x} \; d_{e_z}]^T \in \mathbb{R}^2$ denotes the constant position of the end-effector P_{E} in $\mathcal{F}_2$. The (time-varying) positions of P_{C} (CoM of the overall system, *i.e.*, {PVTOL+manipulator}), $\mathrm{P}_{\mathrm{C}_1}$, $\mathrm{P}_{\mathrm{C}_2}$ and P_{E} in the world frame $\mathcal{F}_W$ are denoted with $\mathbf{p}_c = [x_c \; z_c]^T \in \mathbb{R}^2$, $\mathbf{p}_{c_1} = [x_1 \; z_1]^T \in \mathbb{R}^2$, $\mathbf{p}_{c_2} = [x_2 \; z_2]^T \in \mathbb{R}^2$ and $\mathbf{p}_e = [x_e \; z_e]^T \in \mathbb{R}^2$, respectively. The mass and moment of inertia of the PVTOL, motor and link are denoted with $m_1 \in \mathbf{R}_+$, $J_1 \in \mathbf{R}_+$; $m_m \in \mathbf{R}_+$, $J_m \in \mathbf{R}_+$; $m_2 \in \mathbf{R}_+$, $J_2 \in \mathbf{R}_+$, respectively. The symbol $\bar{g} \in \mathbb{R}^+$ denotes the the gravitational constant.

The PVTOL is actuated by means of: *i)* a total *thrust force* $-u_t\mathbf{z}_1 \in \mathbb{R}^2$ applied at a point P_G, where $u_t \in \mathbf{R}$ is its magnitude, and *ii)* a *total torque* (moment) $u_r(\mathbf{z}_1 \times \mathbf{x}_1) \in \mathbb{R}^1$ applied at P_G, where $u_r \in \mathbf{R}$ is the torque intensity.[3] Furthermore, a motor is attached to the PVTOL and applies a torque $\tau(\mathbf{z}_1 \times \mathbf{x}_1) \in \mathbb{R}^1$ at $\mathrm{P}_{\mathrm{C}_1}$ to the joint, where $\tau \in \mathbf{R}$ is its intensity. The inputs of the system are gathered in the vector $\mathbf{u} = [u_t \; u_r \; \tau]^T \in \mathbb{R}^3$ and shortly denoted in the following as *thrust*, *PVTOL torque* and *motor torque*. The constant position of P_{G} in $\mathcal{F}_1$ is denoted with $\mathbf{d}_G = [d_{G_x} \; d_{G_z}]^T \in \mathbb{R}^2$.

Remark 6.2.1: *The literature is extended in two directions: first by assuming that* $\mathrm{P}_{\mathrm{C}_1} \not\equiv \mathrm{P}_{\mathrm{G}}$ *(i.e.,* $\mathbf{d}_G$ *is* any *, contrarily to what is typically assumed in the literature, see e.g., [Thomas–2013] where* $\mathbf{d}_G = [0 \; 0]^T$*); and second by also considering, for the first time, the case in which the joint is elastic and not only rigid.*

The system dynamics is written using the Lagrange equation as

$$\ddot{\mathbf{q}} = \mathbf{M}^{-1}(\mathbf{q}) \left(\mathbf{G}(\mathbf{q})\mathbf{u} - \mathbf{c}(\mathbf{q}, \dot{\mathbf{q}}) - \mathbf{g}(\mathbf{q}) + \mathbf{f}_E(\mathbf{q}) + \mathbf{f}_{ext} \right) \tag{6.1}$$

where $\mathbf{q} \in \mathbb{R}^n$ are the considered generalized coordinates ($n = 5$ for the planar elastic joint case at hand here), $\mathbf{M} \in \mathbb{R}^{n \times n}$ is the generalized inertia matrix, $\mathbf{G} \in \mathbb{R}^{n \times 3}$ is the control input matrix, $\mathbf{c} \in \mathbb{R}^n$ is the centrifugal/Coriolis forces, $\mathbf{g} \in \mathbb{R}^n$ represents the gravitational forces and $\mathbf{f}_E \in \mathbb{R}^n$ represents the forces due to the potential energy stored in the elastic joint. Finally, $\mathbf{f}_{ext} \in \mathbb{R}^n$ represents the wrench (composed of a 2D force and 1D torque, in the planar case) applied to the system

[3] For a planar birotor, P_G is the center of two coplanar propellers, u_t the sum of the propeller thrusts and u_r their difference times the distance to P_G.

from external environment. Note that albeit developed in the planar case this models extends to the full 3D case, only the matrices expression and order change.

Input-Output Feedback Linearization Property

Recall, a system is exactly input-output linearizable with a dynamic feedback, if there exists a change of coordinates, possibly including a feedback input transformation, that brings the system in an equivalent linear and controllable form. A sufficient condition to obtain this can be expressed considering the candidate output vector $\mathbf{y}$, then if one derives *w.r.t.* time the components of $\mathbf{y}$ until at least one input appears and the total relative degree matches with the dimension of the system state (taking into account possible additional integrators inserted in the input channels), hence no uncontrolled internal dynamics appears. Then the system is said input-output feedback linearizable for output $\mathbf{y}$, This property is very useful for control purposes, in fact, if one rewrites the vector of derivatives of $\mathbf{y}$ as $\bar{\mathbf{y}}$, one obtains

$$\bar{\mathbf{y}} = \bar{\mathbf{f}}(\bar{\mathbf{x}}) + \bar{\mathbf{G}}(\bar{\mathbf{x}})\bar{\mathbf{u}}, \tag{6.2}$$

where $\bar{\mathbf{x}} \in \mathbb{R}^{\bar{n}}$ is the augmented state of dimension of $\bar{n}$ and $\bar{\mathbf{G}}$ is an invertible decoupling matrix. Then the control law

$$\bar{\mathbf{u}} = \bar{\mathbf{G}}^{-1}(\mathbf{v} - \bar{\mathbf{f}}), \tag{6.3}$$

where $\mathbf{v}$ is a virtual input, brings the system in the form

$$\bar{\mathbf{y}} = \mathbf{v}, \tag{6.4}$$

which is linear and controllable, as long as $\bar{\mathbf{G}}$ is invertible. Once the system is transformed in form (6.4), any outer control loop for stabilizing linear systems can be used to synthesize the control $\mathbf{v}$. Although both concepts sound different, differential flatness is equivalent to exact input-state linearization via dynamic feedback in an open and dense set of the state space and an output is flat if and only if it is exactly linearizing [Martin–2003][De Luca–2002][Fliess–1999]. Hence it is convenient to refer to the exact linearizing outputs are flat outputs as well.

6.3 System Analysis – Exact Feedback Linearization

In this section, it is shown that for the PVTOL with a single elastic-joint arm the output $\mathbf{y} = [\mathbf{p}_{c_1}^T \ \theta_{12}]^T$ is an exactly linearizing (*i.e.*, flat) output, meaning the position of the PVTOL's CoM and the absolute link angle . In order to prove it, let us consider as generalized coordinates $\mathbf{q} = [\mathbf{p}_{c_1}^T \ \theta_1 \ \theta_{12} \ \theta_{1m}]^T \in \mathbb{R}^5$, where the coordinate $\theta_{1m} = \theta_1 + \theta_m$ the absolute motor angle, is introduced to exhibit the elastic-joint particularity. An idealized elastic connection is sketched in Fig. 6.2, where $\theta_2 = \theta_m + \theta_e$. In this case the matrices of the dynamical model (6.1) are,

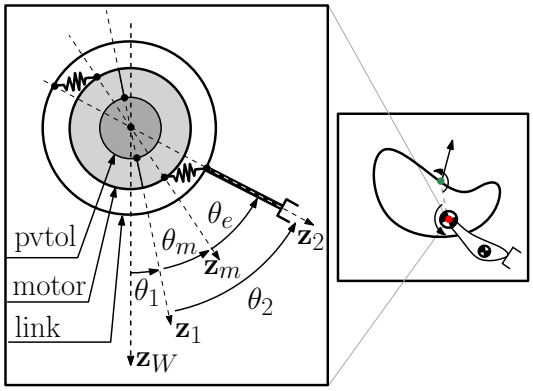

Figure 6.2 – An ideal example of elastic joint between the motor output shaft and link. Proportions are distorted for illustration purposes. The innermost circle, fixed to $\mathcal{F}_1$, the body frame, represents the PVTOL. The middle circle, fixed to $\mathcal{F}_M$, represents the actuator (or motor). The outermost circle is connected to the middle circle via elastic components and is rigidly connected to the link (*i.e.*, fixed to $\mathcal{F}_2$.)

after some algebra,

$$\mathbf{M} = \begin{pmatrix} m_s\mathbf{I}_2 & * & * & * \\ \mathbf{0}_{1\times 2} & J_1 & * & * \\ \boldsymbol{\beta}^T(\theta_{12}) & 0 & m_B - J_m & * \\ \mathbf{0}_{1\times 2} & 0 & 0 & J_m \end{pmatrix} = \mathbf{M}^T \in \mathbb{R}^{5\times 5}, \tag{6.5}$$

$$\mathbf{c}(\mathbf{q}, \dot{\mathbf{q}}) = \begin{bmatrix} \beta_1(\theta_{12})\dot{\theta}_{12}^2 \\ \beta_2(\theta_{12})\dot{\theta}_{12}^2 \\ 0 \\ 0 \\ 0 \end{bmatrix}, \quad \mathbf{g}(\mathbf{q}) = \begin{bmatrix} 0 \\ -m_s\bar{g} \\ 0 \\ g_4(\theta_{12}) \\ 0 \end{bmatrix},$$

$$\mathbf{G}(\mathbf{q}) = \begin{pmatrix} -\sin(\theta_1) & 0 & 0 \\ -\cos(\theta_1) & 0 & 0 \\ d_{G_x} & 1 & -1 \\ 0 & 0 & 0 \\ 0 & 0 & 1 \end{pmatrix}, \quad \mathbf{f}_E(\mathbf{q}) = \begin{bmatrix} 0 \\ 0 \\ 0 \\ f_l(\theta_{1m}, \theta_{12}) \\ f_m(\theta_{1m}, \theta_{12}) \end{bmatrix}. \tag{6.6}$$

Notice that the elastic forces $f_l(\theta_{1m}, \theta_{12})$ and $f_m(\theta_{1m}, \theta_{12})$, respectively acting on the link side and on the motor side, have similar expressions and magnitudes as they describe the same elastic elongation seen from both ends of the spring. These forces can be nonlinear functions of θ_{1m} and θ_{12} depending of the rotational spring mechanical properties. In the linear spring case, or in the nonlinear case but for small deviations around an operating point, both forces can be expressed as proportional to the spring elongation, *i.e.*, $f_l(\theta_{1m}, \theta_{12}) = k_e(\theta_{1m} - \theta_{12})$ and $f_m(\theta_{1m}, \theta_{12}) = k_e(\theta_{12} - \theta_{1m})$, where $k_e > 0$ is the stiffness of the elastic element.

When the spring behavior is nonlinear, the constant k_e is a local description of the the spring behavior. The overall nonlinear spring behavior can be approximated with local linearization for several ranges of operation covering the total range of the elastic element.

Replacing $\mathbf{M}$, $\mathbf{c}$, $\mathbf{g}$, $\mathbf{G}$ and $\mathbf{f}_E$ in (6.1) the explicit dependency of each entry of $\ddot{\mathbf{q}}$ can be derived as

$$\begin{aligned} \ddot{x}_1 &= \xi_1(\theta_1, \theta_{12}, \dot{\theta}_{12}, \theta_{1m}, u_t), \quad \ddot{z}_1 = \xi_2(\theta_1, \theta_{12}, \dot{\theta}_{12}, \theta_{1m}, u_t), \\ \ddot{\theta}_1 &= \xi_3(u_t, u_r, \tau), \qquad\qquad \ddot{\theta}_{12} = \xi_4(\theta_1, \theta_{12}, \dot{\theta}_{12}, \theta_{1m}, u_t), \\ \ddot{\theta}_{1m} &= \xi_5(\theta_{1m}, \theta_{12}, \tau). \end{aligned} \tag{6.7}$$

Considering as output for the feedback linearization $\mathbf{y} = [\mathbf{p}_{c_1}^T \ \theta_{12}]^T$, from (6.7) one can write

$$\ddot{\mathbf{y}} = \boldsymbol{\xi}_1(\theta_1, \theta_{12}, \dot{\theta}_{12}, \theta_{1m}, u_t). \tag{6.8}$$

The total relative degree is $r = 2+2+2 = 6$ and the state dimension is $\bar{n} = 2n = 10$. As recalled in before, exact input-output feedback linearization is achievable when these two quantities are equated. This is achieved by considering as new control inputs $\bar{\mathbf{u}} = [\ddot{u}_t \ u_r \ \tau]^T \in \mathbb{R}^3$ and augmented state $\bar{\mathbf{x}} = [\mathbf{q}^T \ \dot{\mathbf{q}}^T \ u_t \ \dot{u}_t]^T \in \mathbb{R}^{12}$. In fact, differentiating twice *w.r.t.* time and substituting $\ddot{\theta}_{12}$, $\ddot{\theta}_1$, $\ddot{\theta}_{1m}$ from (6.7) yields

$$\mathbf{y}^{(4)} = \boldsymbol{\xi}_3(\theta_1, \theta_{12}, \theta_{1m}, \dot{\theta}_1, \dot{\theta}_{12}, \dot{\theta}_{1m}, u_t, \dot{u}_t, \ddot{u}_t, u_r, \tau),$$

which means that $r = 4 + 4 + 4 = 12$ and $\bar{n} = 12$, as required.

Therefore it is now worth checking if the matrix $\bar{\mathbf{G}}(\bar{\mathbf{x}})$, the decoupling matrix introduced in (6.2), is invertible. The analytical expression of $\bar{\mathbf{G}}(\bar{\mathbf{x}})$ determinant is

$$\det\left(\bar{\mathbf{G}}\right) = -\frac{u_t k_e}{J_1 J_m m_s \left(J_2 m_s + m_2(m_1+m_m)\|\mathbf{d}_2\|_2^2\right)}, \tag{6.9}$$

for more insights the interested reader is referred to [Yüksel–2016b] and [Yüksel–2017]. Therefore $\bar{\mathbf{G}}$ is always invertible, as long as $u_t \neq 0$ and $k_e \neq 0$ As $\bar{\mathbf{G}}(\bar{\mathbf{x}})$ is invertible and knowing that $\bar{\mathbf{y}} = \mathbf{y}^{(4)}$ and $\bar{\mathbf{f}}(\bar{\mathbf{x}}) = \bar{\mathbf{y}} - \bar{\mathbf{G}}(\bar{\mathbf{x}})\bar{\mathbf{u}}$ from (6.2), the controller in the form of (6.3) is exactly linearizing the system for the considered output, *i.e.*, it brings the system to the linear controllable form (6.4). This proves that

Proposition 1: *The vector* $[\mathbf{p}_{c_1}^T \ \theta_{12}]^T$ *is an exactly linearizing output via dynamic feedback for the model with elastic-joint arm , as long as* $u_t \neq 0$ *and* $k_e \neq 0$. *As a consequence, it is also a flat output. Direct proof of the flatness can be found in [Yüksel–2016c].*

Remark 6.3.1: *Contrarily to the grounded manipulator case [De Luca–1996], where the flat outputs are the* relative *orientation of the consecutive links and motors, in the aerial case one has to consider the* absolute *link and motor orientations.*

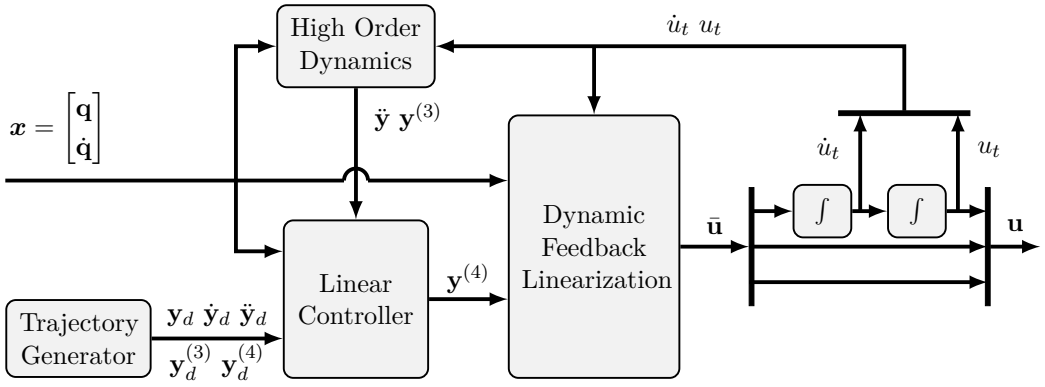

Figure 6.3 – Scheme of the exact linearizing controller. The High Order Dynamics block analytically (*i.e.*, exactly) computes the high order derivatives of the flat outputs $\mathbf{y}$, *i.e.*, $\ddot{\mathbf{y}}$ and $\mathbf{y}^{(3)}$ from the current state $\mathbf{x}$. The Trajectory Generator generates the desired trajectory in C^3, based on a 4-th linear order filter. A Linear Controller, as in (6.10) controls the system in the linear form and tracks the desired outputs and their derivatives. The Dynamic Feedback Linearization block brings the system to the linear controllable form as in (6.3).

This is due to the underactuation of the flying platform that is used as the base of the elastic-joint arm.

6.4 Linear Control Synthesis

The feedback linearizing (nonlinear) controller presented Sec. 6.3, where the flat outputs is $\mathbf{y} = [\mathbf{p}_{c_1}\ \theta_{12}]^T$, brings the system in the decoupled and controllable linear form. Then, given any triplet of desired trajectories of class C^3, $x_1^d(t)$, $z_1^d(t)$, $\theta_{12}^d(t)$ for x_1, z_m and θ_{12} respectively, many classical linear control synthesis techniques can be used as outer control loop. In this work a simple one based on tracking error for C^3 trajectories, is proposed

$$\mathbf{v} = \bar{\mathbf{y}}^d + \mathbf{K}[\mathbf{e}^T\ \dot{\mathbf{e}}^T\ \ddot{\mathbf{e}}^T\ \dddot{\mathbf{e}}^T]^T \in \mathbb{R}^3, \tag{6.10}$$

where $\mathbf{e} = [e_x\ e_z\ e_\theta]^T$ and $e_x = x_1^d - x_1$, $e_z = z_1^d - z_1$, $e_\theta = \theta_{12}^d - \theta_{12}$ and with $\mathbf{K}$ being composed of 3×3 positive definite gain matrices with properly chosen elements to enforce system stability. Additionally, to compensate the errors due to uncertainties and robustify the outer control loop, an integral term of the form $K_{i*} \int_{t_0}^{t_f} e_* dt$ is added for each channel, where $* := \{x, z, \theta\}$ and $K_{i*} \in \mathbb{R}_+$. The whole control scheme, with both the feedback linearization as inner loop and the linear control presented in here as outer loop, is illustrated in Fig. 6.3.

It is worth to notice that the proposed linear control strategy only requires the measurements of $\mathbf{q}$ and $\dot{\mathbf{q}}$, since the derivatives of the outputs present in (6.10) are computed as algebraic functions of $\mathbf{q}$ and $\dot{\mathbf{q}}$, thanks to the model (6.1) and its

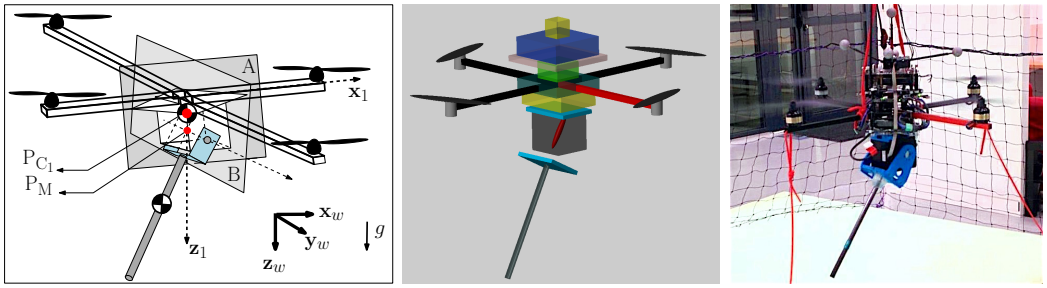

(a) (b) (c)

Figure 6.4 – Evolution from theory to application. *(a)* Conceptual sketch of the model in 3D. The motion in Plane-A is controlled using the controller presented in this chapter. The motion in Plane-B (except the translational motion along $\mathbf{z}_1$) and the rotation around $\mathbf{z}_1$ is controlled using a *near-hovering controller* [Lee–2013]. *(b)* CAD model of the 3D system and a snapshot from *SimMechanics* simulation, where the implemented controllers have been tested. Different colors correspond to the different parts of the real system. The results are given in [video 2–2016]. *(c)* Real system on flight, for details see Fig. B.13. Red ropes are used only for safety reasons, with no tension on them.

analytical derivatives. This fact relieves us from the need for additional, and often noisy, sensors for the higher derivatives of the state.

6.5 Simulation and Experimental Validations

In this section, are presented both extensive numerical simulations and the experimental setup, which consists of a quadrotor equipped with a rigid link that is actuated via a VSA and present preliminary experimental results.

6.5.1 Realistic Numerical Tests

For the sake of completeness the simulation results are succinctly presented here, extensive and realistic simulation results (with parametric uncertainties, measurement noises, sampling errors and actuation limits) are provided in [Yüksel–2016b] and [Yüksel–2016c] and validate the feedback linearizing controllers presented in Sec. 6.3.

In the simulations, the nominal parameters of the system, their deviations and the noise of the measured states are chosen close to real values, see Tab. I and Tab. II in [Yüksel–2016c]. Moreover two important scenarios are investigated: *i)* aerial grasping and *ii)* link velocity amplification. Both rigid joint and elastic joint are compared and it is observed that the rigid-joint design is more suitable for the first scenario (picking), while using an elastic-joint arm is much more advantageous for the second one (explosive task). The detailed explanations of the simulation setups are given in [Yüksel–2016c] and are briefly highlighted hereafter.

The controller, see Fig. 6.3, is tested in a simulation considering the full dynamical 3D model of the system, using the CAD model of the experimental setup in SimMechanics, a realistic physical simulation toolbox provided by Matlab. The proposed 3D system consists of a quadrotor equipped with a qbmove[4] for the elastic joint and mounted with a rigid arm link as pictured in Fig. 6.4). To conduct the simulation the 3D model is split in two planes, Plane-A and Plane-B as shown in Fig. 6.4a. All the motions on Plane-A (including that of the absolute link angle) is controlled using the exact linearizing controller presented above (via thrust, torque around $\mathbf{x}_1$ and torque for the qbmove, see Fig. 6.3). The rest of the quadrotor motion (motion in Plane-B and rotation around the vertical axis $\mathbf{z}_1$) is controlled using a *near-hovering controller*, the details of which can be found in [Lee–2013]. This allows to test the performance of the 2D derived controller in a real experimental scenario, *i.e.*, in 3D. The SimMechanics model is based on a precise CAD model of the real setup, the advantage of using SimMechanics relies in the fact that the dynamic model used for simulation is derived automatically by SimMechanics, hence it guaranties that the model used for the controller and for the plant are derived independently, thus allowing realistic simulation with the addition of noise and parametric uncertainties. The full simulation results are available to the interested reader in [Yüksel–2016b] and [Yüksel–2016c]. They suggest that the rigid-joint design is more suitable for the first scenario (picking), while using an elastic-joint arm is much more advantageous for the second one (explosive task). Which is rather intuitive as for the picking the elastic joint might lack of precision due to its compliant property, while it is clear that for explosive task the elastic component of the joint can be exploited to store and release energy, hence outperforming the rigid-joint case.

6.5.2 Preliminary Experiments

The experimental setup is based on a Mikrokopter[5] quadrotor Vertical Take-off and Landing Vehicle (VTOL) as underactuated AV and a qbmove VSA as elastic-joint, for which the stiffness parameters of the springs in the elastic connections can be tuned. State measurements of the quadrotor are acquired through a 1 kHz Unscented Kalman filter[6] fed by both an on board Inertial Measurement Unit (IMU) and an external MoCap. The controller sketched in Fig. 6.3 is implemented as *C/C++* libraries and ROS nodes, similarly to what is done in [Grabe–2013] and [Lächele–2013]. Table 6.1 recalls the main components of the experimental setup.

Preparation of the qbmove

The use of a VSA prevailed for its wide range of stiffness preset capabilities which allow the user to choose between, *e.g.*, high and low stiffness values, depending on

[4] `http://www.qbrobotics.com/products/qbmove-maker-pro/`
[5] `http://www.mikrokopter.de/en/home`
[6] `http://robotpkg.openrobots.org/robotpkg/localization/libpom/index.html`

Component description	key quantities
VTOL mikrokoprer quadrotor	
total mass (incl. payload)	1.5 kg
max. thrust and torque	28 N, 1.5 Nm
qbmove Variable Stiffness Actuator (VSA)	
max. torque	1.2 Nm
control frequency	500 Hz
Optitrack Motion Capture System (MoCap)	100 Hz
6-axis IMU	1 kHz
Unscented Kalman Filter: IMU+MoCap	1kHz

Table 6.1 – Characteristics of the main components of the setup.

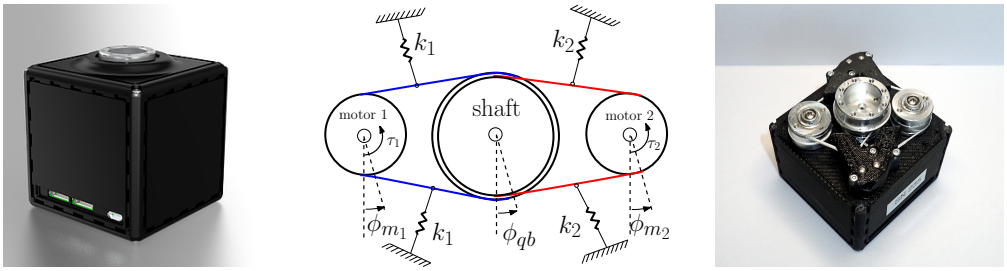

(a) (b) (c)

Figure 6.5 – On the left (a), an external view of the qbmove VSA, a 66 mm cube for 0.260 kg. In the center (b), a sketch of the agonistic/antagonistic mechanism used in the qbmove. And on the right (c), the real system's inside with apparent shafts and pulley.

the task of the AR. Note that, as this work is a preliminary step toward onboard VSA for AR, the full capacity of the VSA were not exploited, *i.e.*, the stiffness variation was not regulated during experiment but remained at a fixed setpoint. The choice of VSA led to the qbmove, an agonistic/antagonistic servo-VSA. Shortly, it consists of two *PD* controlled servo motors, which allow to regulate independently desired stiffness and output-shaft equilibrium, *i.e.*, in the formerly introduced notations k_e and θ_m, respectively. See Fig. 6.5 for a view of the device and a sketch of its working mechanism. This VSA provides state measurements (θ_m, θ_e) at 500 Hz. Its main advantages reside in the lightweight design and the wide range of stiffness preset available.

The working principle of the agonistic/antagonistic mechanism structure chosen for the qbmove are sketched here after. First introduce the notation in Fig. 6.5b, $\phi_{qb} = \theta_m$ denotes the output shaft of the VSA and ϕ_{1m} and ϕ_{2m} denote the motor output angles of each servo composing the mechanism. The output shaft is linked to

the two servos by mean of reasonably non extensible threads (see Fig. 6.5b in blue and red) and these threads are put into tension by four springs, which are assumed of equal stiffness. At constant stiffness, the output shaft motion is obtained by moving the two servos of the same quantity in the same direction, *i.e.*, $\phi_{qb} = \frac{1}{2}(\phi_{1m} + \phi_{2m})$. For example moving the shaft by 10° clockwise, means moving the two servos by 10° clockwise, in this case the bottom spring k_1 and the top spring k_2 are loaded and provide the elastic behavior, while the top spring k_1 and the bottom spring k_2 are inactive, hence the denomination agonistic/antagonistic. Not that at rest, if the output shaft is moved from the load side clockwise, the same springs are activated, and counter-clockwise the opposite springs are activated. At constant output shaft position, the stiffness can be changed by rotating the two servos in opposite direction, *i.e.*, $k_e \propto (\phi_{2m} - \phi_{1m})$. By combining these two modalities the output shaft position, $\phi_{qb} = \theta_m$, and the stiffness k_e can be set independently. Notice that from the nature of the mechanism the actuation time constant of the output shaft is faster than the one of the stiffness, as highlighted in the qbmove datasheet[7].

The meticulous reader will see that no gripper is featured in the described setup, this is mainly due to safety considerations on the maximal deflection supported by the qbmove, indeed in order not to damage the spring it was preferred to have a reduced mass on the output shaft of the VSA, its base being rigidly attached to the VTOL of mass around 1.5 kg.

In order for the controller introduced above to work with qbmove VSA, several extra steps need to be conducted. First of all, a parametric identification of the {qbmove VSA+rigid arm} system has been performed, in order to retrieve the parameters of the equivalent motor studied in [Yüksel–2016b]. The stiffness (and the damping) parameters of the {qbmove+arm} system are identified by first considering it as a simple mass-damper system and then letting the arm swing from an initial condition, without any control action (see [Yüksel–2015] for a similar method). Note that the qbmove features a nonlinear spring, which is considered as a linear spring for deflection in the range of ±20°. Inertial parameters of the system are found using the system geometry. All the identified and computed parameters are available in Table 6.2. The parameters are for a given stiffness, for simplicity no parameter expression based on the stiffness preset where investigated. Moreover, the control framework presented requires a torque-controlled motor, while a qbmove is not proposing this control modality. For this reason the implementation of an outer loop controller around the qbmove device has been required, it translates the desired torque into a desired position through a feedback linearization scheme. This approach requires a precise knowledge of the system parameters: distances, masses and inertia were computed through CAD model, while other parameters where experimentally identified as described above and are given in Table 6.2. This *bridge* between the proposed controller in [Yüksel–2016b] and the qbmove VSA is directly implemented as a ROS node. This approach was devised in order to palliate for the

[7] www.qbrobotics.com/wp-content/uploads/2016/03/45c5a1_792590e00b134129b2b6363a1ea7de45.pdf

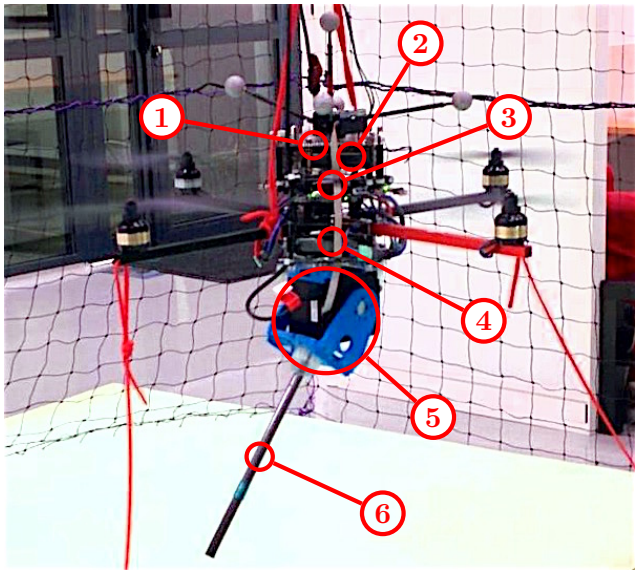

Figure 6.6 – Experimental setup composed of a MikroKopter quadrotor as under-actuated VTOL and a qbmove block as VSA. The sub-components of the platform are: (1) Flight Controller (incl. IMU), (2) the odroid runing the controller, (3) the ESC, (4) the battery pack, (5) the qbmove itself and (6) the manipualtor link connected to the VSA output shaft. Red ropes are used only for safety reasons, with no tension on them.

fact that qbmove is position controlled and that this control modality proved hard at first sight to incorporate in the feedback linearization approach. The outer loop are the VSA is not perfect but provides sufficient performances.

Quadrotor Setup

The experiments are conducted on a AR, see Fig, B.13. The payload of the AR is composed of, from top to bottom, (1) a flight controller (incl. IMU), (2) an Odroid-XU[8] computer running Ubuntu 14.04, (3) four brushless motor controllers with their power board (ESC), (4) a battery pack, (5) a qbmove with its connectors and (6) a rigid arm attached to it. Total weight of the system is 1.5 kg (including safety ropes that are carried by the AR), which corresponds to a total hovering thrust of 14.75 N. Each propeller of the VTOL can generate lift up to 7 N, which allows to carry the described payload and perform flight.

The actual values in the setup of the main quantities introduced in the modeling, Sec. 7.1, are presented in the Tab. 6.2 for the reader to get a grasp on the physical magnitudes of the platform.

[8] http://www.hardkernel.com/main/products/prdt_info.php?g_code=G137510300620

Real Parameters	Notation	Value	Unit
mass of the quadrotor	$\tilde{\mathbf{m}}_1$	1.309	kg
mass of the VSA mechanism	$\tilde{\mathbf{m}}_m$	0.06	kg
mass of the arm	$\tilde{\mathbf{m}}_2$	0.098	kg
dis. vec. betw. $\mathrm{P}_{\mathrm{C}_1}$ & P_{G}	$\tilde{\mathbf{d}}_G$	$[0.0\ 0.0081]^T$	m
dis. vec. betw. $\mathrm{P}_{\mathrm{C}_2}$ & P_{M}	$\tilde{\mathbf{d}}_2$	$[0\ 0.0979]^T$	m
inertia of the PVTOL	$\tilde{J}_1$	0.0154	$\mathrm{kg\,m^2}$
motor inertia	$\tilde{J}_m$	0.4101	$\mathrm{kg\,m^2}$
link inertia	$\tilde{J}_2$	0.0011	$\mathrm{kg\,m^2}$
spring stiffness	$\tilde{k}_e$	3.55	$\mathrm{N\,m\,rad^{-1}}$
spring damping	$\tilde{k}_f$	0.07	$\mathrm{N\,m\,rad^{-1}}$

Table 6.2 – Measured, computed or identified parameters of the setup. The variable $\tilde{*}$ denotes the quantity $*$ for the experimental setup. Notice that $\tilde{k}_f$ is identified but not used in the controller.

Preliminary Experiment of a Quadrotor with a VSA Arm

This section highlights the experimental results obtained with the above described controller and system, see [video 2–2016] for the system in action. In a first experiment the flight quality of the proposed approach is assessed, without motion from the joint. The full system is tested for a trajectory tracking along the z axis while staying at zero on the x axis for the a-plan, while the near-hovering controller for the B-plan is tasked to keep all its controlled quantities constant. Results are given in Fig. 6.7, where the maximum error for both x_1 and z_1 is around 2 cm. This validates good flight performances of the system.

In a second experience performed, the absolute link orientation follows a sinusoidal trajectory, while the PVTOL's CoM follows another trajectory along the z axis and tries to stay at zero on the x axis, this trajectories are meant to highlight the decoupling of the motion. Results are given in Fig. 6.8, where for x_1 and z_1 the maximum errors are around 2cm. This in particular shows that the arm swinging is properly taken into account in the controller and does not affect too much the orientation of the VTOL, which results in no translational motion along x_1.

For both experiments, steady-state errors are observed mainly due to unmodeled effects as, *e.g.*, neglecting the damping of the spring, and the displacement between the $\mathrm{P}_{\mathrm{C}_1}$ and P_M in the real setup (see Fig. 6.4a), while in theory they are considered *coincident* (see Fig. 6.1).

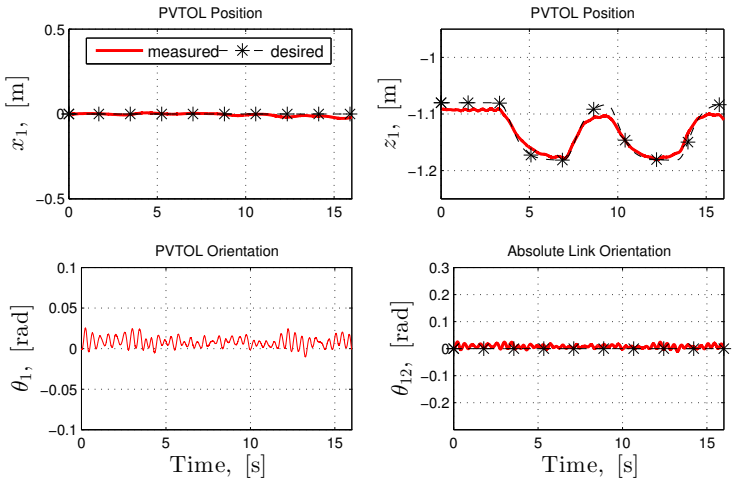

Figure 6.7 – First test on controlling the {quadrotor+VSA} arm position along x and z directions. A step-like trajectory is followed along the z-axis. Notice that negative z is upwards, as per NED convention.

6.6 Discussion and Open Research Directions

In this chapter the dynamic modeling, property analysis and control of a PVTOL system equipped with a single elastic-joint arm is presented. It has been proven that this system is differentially flat for a set of outputs, which are the same a for

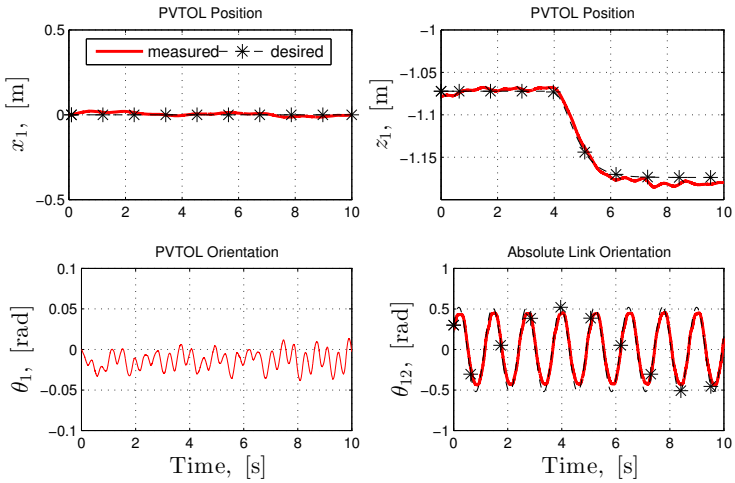

Figure 6.8 – Preliminary results for trajectory tracking with {quadrotor+VSA} arm setup. The arm attached to the qbmove is swinging back and forth (see θ_{12}), while quadrotor VTOL is tracking a stable trajectory along x-direction, and a step-like trajectory along the z-direction. Oscillations on θ_1 are due to the motion of the arm, against which the controller is trying to keep x position constant. Notice that negative z is upward, as per NED convention.

rigid joint, see [Yüksel–2016b], and an exact linearization tracking controllers is provided. Extensive numerical tests, provided in [Yüksel–2016c], show clear differences between the rigid and elastic joint models, rigid-link setup is more advantageous for precisely tracking tasks such as aerial grasping, while elastic-link setup is more suitable for tasks requiring link velocity amplification such as throwing or hammering. Another numerical validation as been performed using the full 3D model of the real setup in SimMechanics and finally preliminary experimental results of controlling a quadrotor VTOL equipped with a qbmove are presented. In fact, a clear trade-off between rigid-link and elastic-link setups directs us to use VSA for a wide range of aerial physical interaction tasks. This work is a bridge between previous experiences [Yüksel–2015] and future studies and extension of the use of VSA for aerial manipulation, which will include: *i)* further experiments using the quadrotor and qbmove setup, *e.g.*, peg-in-hole or throwing, hammering; *ii)* extension of the theory to 3D and/or arms with multiple degrees, see [Yüksel–2016a] for interesting preliminary results; *iii)* use of sensor-based calibration methods as, *e.g.*, in [Censi–2013] to retrieve the system parameters on the fly.

Open Research Directions

The work presented in this chapter was a preliminary investigation about having VSA embedded on AR. As such, the variable stiffness was not fully exploited, possible way to do so are two folds: *i) open-loop*, high level control, a planner could switch between a couple of stiffness preset matching the task at hand, *ii) close-loop*, stiffness trajectory generation and tracking. The first solution seems rather easy to implement, as it has been shown that high stiffness is better suited for precision tasks and low stiffness for compliance or dynamic task (*e.g.*, resonance amplification). Although the results are expected to be more toward a practical application contribution than a theoretical one. The second direction reserves way more open challenges both from the stiffness trajectory generation side than from the low-level fast stiffness control. For the stiffness trajectory generation, and motion trajectory generation at large, the considered task to exhibit the VSA versatility would be an explosive one, like trowing or hammering. A potential application for throwing can be found USAR scenario. Consider a several story tall building semi-demolished after a disaster. In that case exploration for survivors would be difficult for an AR alone, which would be challenged by the unknown and unstructured environment. On the other hand ground robots, such as crawlers, could not climb the stairs and be limited in their exploration of the building. The combination of both could be obtained by considering a rescue mission where a AR mounted with a VSA is tasked to trow a small crawler inside the building higher floors. In this way the crawler can easily explore higher floors, while the AR can bring it where needed. The interest to consider throwing in that case resides in the fact that the transition from outdoor to indoor navigation for AV is an arduous topic. Throwing the crawler in, while remaining outside, avoids this difficulty and still allows to exploit crawlers for the exploration of higher flours in a semi-demolished building. In such a scenario, the

trowing trajectory as to accommodate both the AR spatial constraints and actuation limits, the VSA own actuation limits and the target of the trowing, which makes it a non trivial planning problem.

A part from the exploitation of the variable stiffness, several challenges remain for AR with elastic joints, the flatness property highlighted in the presented work, relies on the assumption that the CoM of the flying platform coincides with the joint, which is hard to met in practice. Moreover, feedback linearization relies on model inversion and, albeit the described experimental results are fairly good, more robust approach could be devised, especially as the control of VSA is leaping forward.

Finally from the hardware point of view, two main directions can be investigated: *i)* improvement of the flying platform and *ii)* improvement of the VSA design and control. Indeed, fully-actuated multi-directional thrust platform, or maybe just more powerful AV, could be of great advantage as they would undoubtedly be closer to a mechanical ground for the loading of the spring. This is motivated by empirical tests conducted along the presented work, where mass where added at the tip of the arm to mimic hammering, a typical use case for VSA. It was clear that the actuation constraint of the quadrotor considered and the use of an agnostic near-hovering position controller were highlighting the system limits. Behavior with the controller presented in this work is improved but the actuation limits are not overcome and are easily violated as the mass/inertia on the VSA output shaft increases. The second direction worth investigating is to devise a possibly improved VSA design. The improvements should be toward a lighter design but more importantly toward a finer identification and control of the used mechanism. Indeed, it appeared that the simple model provided by the manufacturer was not describing the VSA behavior, notably because of dry friction present in the mechanism when velocity is close too zero. Moreover advanced control techniques often consider torque actuation, whereas the qbmove only provides position control of its motors. The presented way to compensate for that is not optimal and relies on several assumptions that should be sought to be relaxed. The best way to improve the qbmove behavior would be to propose a low-level controller relying on a more accurate model of the VSA and finer estimation of its parameters, which is in itself a vast topic.

Chapter 7

Flexibility in MAGMaS Load

Contents

Abstract

This chapter presents preliminary study of the case of a MAGMaS composed of a robotic arm and an AR cooperatively manipulating a flexible beam. The theoretical study of the flexibility is proposed in the vertical plane. The modeling is introduced in Sec. 7.1, followed by the system analysis in Sec. 7.2 and some discussion on the possible extensions in Sec. 7.3. This a work was done in cooperation with Seoul National University.

7.1 Modeling of a MAGMaS with Flexibility

The work described in this chapter as been accepted for
2018 IEEE/RSJ Int. Conf. on Intelligent Robots and Systems
[Yang–2018]

The interest for the flexibility arose from the consideration that in beam manipulation usually the tip of the beam is affected by parasitic motions induced by flexibility and that MAGMaS can counteract these tip motions using an AR to grasp the tip. In practice it also appeared from preliminary experiments on MAGMaS that the flexibility of the beam can be rejected by the AR. To understand the root of this phenomenon, a 2D modeling of MAGMaS with flexibility was conducted.

7.1.1 Beam Flexibility

In order to model the flexibility in the beam, the classical Euler-Bernoulli model was chosen, see [Inmann–2007]. The beam motion is defined as following partial differential equation for the 2D case with a beam section and a density constant over the beam

$$\frac{\partial^2 w(x,t)}{\partial t^2} + \frac{EI}{\rho A}\frac{\partial^4 w(x,t)}{\partial x^4} = f(x,t), \tag{7.1}$$

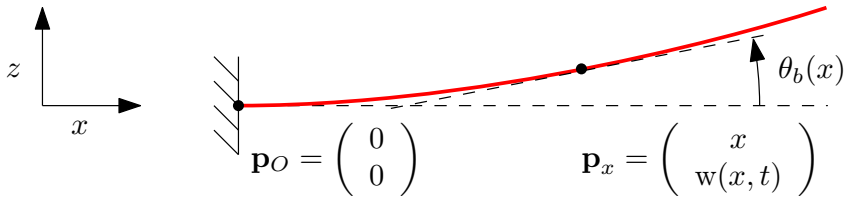

Figure 7.1 – Sketch of a quantilever beam (in red), deflection from the undeformed longitudinal axis (dashed) is exaggerated for illustration. For any point $\mathbf{p}_x$ along the beam its coordinate are x along undeformed longitudinal axis and the deflection $w(x,t)$ along a direction normal to he undeformed longitudinal axis. The beam sketch depicts only a first module deflection for simplicity.

where $w(x,t)$ describes the deflection at an abscissa x along the beam and at a instant t, see Fig. 7.1, and E, I, ρ, A are physical constants related to the beam material and structure, respectively Young modulus, second Inertia moment of the section, density and area of the beam section. Lastly $f(x,t)$ denotes a transverse external force applied along the beam, which is considered to be null if the beam is only subject to its weight. This model relies on the assumption that the beam is subject to lateral load only. Nevertheless this model was chosen to conduct the first study, a more complex model relaxing these assumptions, *e.g.*, Timoshenko's beam model see [Meirovitch–1997], could be chosen for further studies.

The deflection $w(x,t)$ can be described using mode shape formalisms

$$w(x,t) = \sum_{i=1}^{\mu=\infty} \phi_i(x)\delta_i(t) \tag{7.2}$$

where μ is the number of vibration modes, theoretical infinite but chosen finite in practice to get exploitable models, $\phi_i(x) : \mathbb{R}_+ \to \mathbb{R}$ are mode shape functions which describe the temporal evolution of vibration at given spacial location and $\delta_i(t) : \mathbb{R}_+ \to \mathbb{R}$ are functions which describe time varying part of the deflection associated with given mode shape $\phi_i(x)$.
The analytical expression of mode shape functions can be found to be of the form

$$\phi_i(x) = \cosh(\beta_i x) - \cos(\beta_i x) - \sigma_i(\sinh(\beta_i x) - \sin(\beta_i x)) \quad \forall\, i \in 1 \dots \mu \tag{7.3}$$

where β_i, σ_i are coefficients for each mode, derived from Euler-Bernoulli equation's solution. For typical beam constraint like the cantilever beam, these coefficients expression in relation with the beam physical property can be found in handbooks, like [Inmann–2007].

Beam Parameters Identification

In order to retrieve the physical parameters from the beam and verify that the two first modes are sufficient to describe the flexible behavior an experiment exciting

the vibration modes in a flexible wooden beam is conducted. The wooden beam studied was equipped with MoCap markers along its length, to measure its deformation in a discretized way, and was firmly attached by one of its end in what is know to be a cantilever beam configuration. In this configuration the boundary conditions necessary to determine the solution are know and can be used to determine analytically the expressions of the coefficients of the mode shape functions, see [Inmann–2007].

A first observation can be made from the rest equilibrium, the deflection at the tip of the beam is 19.2 cm, for a 244 cm free beam, which corresponds to 7.87 %, validating the small deformation condition. Excitations were performed in 3 different ways: *i)* by imposing a deflection of around 20 cm at the beam tip and realizing it, *ii)* by imposing a small impact at the beam tip with a 200 gr hammer and *iii)* by imposing a larger impact at the beam tip wit the same hammer. Results of the observed energy peaks in the Fast Fourrier Transform (FFT) are summarized in Tab. 7.1, the two first modes correspond to the first peak (1.46 Hz) and second peak (8.98 Hz), which have respective relative error to the theoretical ones of 7.01 % and 9.05 %. These differences can be explained mostly by the variation of the physical properties of wood *w.r.t.* hygrometry, in particular the Young modulus E. Hence this experiments is used to retrieve the physical E of the wooden beam through simple oscillation measurements. Wood is chosen despite this drawback because in practice it offers a compromise between length and cross section necessary to observe flexibility vibrations and is expendable.

Boundary Conditions for MAGMaS

In order to find the constant in the solution of (7.1) one should study the boundary conditions of the beam, the side attached to the ground manipulator is considered as clamped, the side attached to the AR requires further study. Let us consider the case of one AR attached at the tip of the beam, as depicted in fig.7.2, the boundary

experiment		deflection (up)	impact (small)	impact (big)
1^{st} peak	$[Hz]$	1.45	1.44	1.45
2^{nd} peak	$[Hz]$	9.01	8.98	8.95
3^{rd} peak	$[Hz]$	.	26.51	26.38
4^{th} peak	$[Hz]$	.	50.11	49.86

Table 7.1 – Frequency of the peaks observed in FFT analysis of different experimental data of flexibility excitation in a wooden beam of free length 244cm and section 1.3 cm × 3.8 cm.

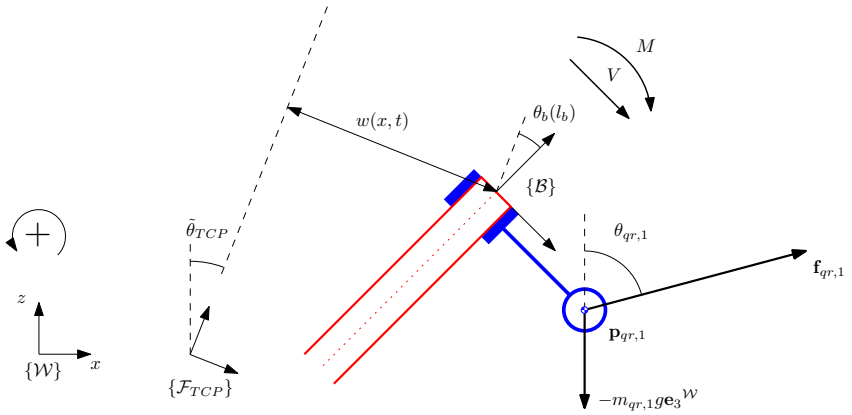

Figure 7.2 – Tip of the beam, with one AR schematized as a point mass with orientable thrust. Both the weight from the AR and the generated thrust have to be taken into account in the boundary conditions.

conditions can be written as follows

$$V(x=l_b) = -m_{qr,1}\ddot{w}(l_b,t) - \ddot{\theta}_b(l_b)m_{qr,1}\left[\mathbf{p}_{qr,1}^{TCP}\right]_x + \left[m_{qr,1}ge_3^{\mathcal{W}} + \mathbf{f}_{qr,1}^{TCP}\right]_x \quad (7.4)$$

$$M(x=l_b) = -I_{qr,1}\ddot{\theta}_b(l_b) - \ddot{w}(l_b,t)m_{qr,1}\left[\mathbf{p}_{qr,1}^{TCP}\right]_x + d_{qr,1}\left[m_{qr,1}ge_3^{\mathcal{W}} - \mathbf{f}_{qr,1}^{TCP}\right]_z \quad (7.5)$$

where $[.]_x$ and $[.]_z$ denote respectively the x and z component of a vector expressed int the TCP-frame, $m_{qr,1}$ the mass of the AR located at position $\mathbf{p}_{qr,1}^{TCP}$ in the TCP-frame, $d_{qr,1}$ denotes the distance between the tip of the beam and $\mathbf{p}_{qr,1}^{TCP}$. Note that this boundary conditions are close to the ones of a cantilever beam with a lumped mass and a force at its end, the later being non-homogeneous, both cases are carefully studied in [Meirovitch–2000b]. From the boundaries conditions, it is possible to determine the exact solution coefficients.

7.1.2 MAGMaS Model

Considering the planar system described in Fig. 7.3, with a fully actuated ground manipulator, a flexible beam with flexibility (exaggerated for illustration) and an underactuated AR attached at the tip of the beam with its rotational decoupled from the rest of the system by a passive joint.

By studying the energy flow in the system under the Euler-Lagrangian formalism and by omitting the decoupled rotational dynamics of the AR, the equations of

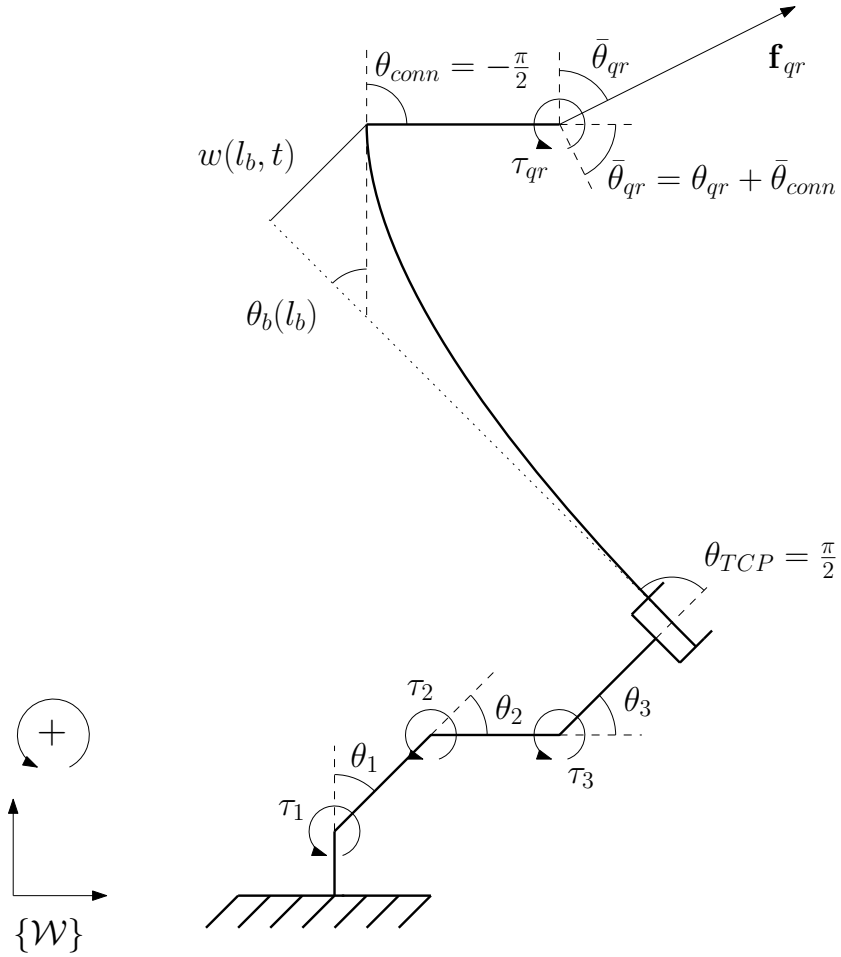

Figure 7.3 – Sketch of flexible MAGMaS composed of a fully actuated ground manipulator, a flexible beam with flexibility (exaggerated for illustration) and an underactuated AR attached at the tip of the beam with its rotational dynamics decoupled from the rest of the system. Important modeling quantities are reported, note that absolute angles are expressed with the notation $\bar{\theta}_{\cdot}$ and relative angles with $\theta_{\cdot}$.

motions of the system can be written as

$$\begin{bmatrix} \boldsymbol{M}_\theta & \boldsymbol{M}_{\theta\delta} \\ \boldsymbol{M}_{\delta\theta} & \boldsymbol{M}_\delta \end{bmatrix} \begin{pmatrix} \ddot{\boldsymbol{\theta}} \\ \ddot{\boldsymbol{\delta}} \end{pmatrix} + \begin{bmatrix} \boldsymbol{C}_\theta & \boldsymbol{C}_{\theta\delta} \\ \boldsymbol{C}_{\delta\theta} & \boldsymbol{0} \end{bmatrix} \begin{pmatrix} \dot{\boldsymbol{\theta}} \\ \dot{\boldsymbol{\delta}} \end{pmatrix} + \begin{pmatrix} \boldsymbol{g}_\theta \\ \boldsymbol{g}_\delta \end{pmatrix} + \ \ldots \tag{7.6}$$

$$\ldots \begin{bmatrix} \boldsymbol{0} & \boldsymbol{0} \\ \boldsymbol{0} & \boldsymbol{K}_\delta \end{bmatrix} \begin{pmatrix} \boldsymbol{\theta} \\ \boldsymbol{\delta} \end{pmatrix} = \begin{bmatrix} \boldsymbol{I} & \boldsymbol{B}_{\theta,qr} \\ \boldsymbol{0} & \boldsymbol{B}_{\delta,qr} \end{bmatrix} \begin{pmatrix} \boldsymbol{\tau}_{arm} \\ \boldsymbol{f}_{qr} \end{pmatrix} \tag{7.7}$$

where $\boldsymbol{\theta} \in \mathbb{R}^n$ stacks the joint angles of the ground manipulator, $\boldsymbol{\delta} \in \mathbb{R}^\mu$ stacks the $\delta_i(t)$ deflection of each vibration mode considered, $\boldsymbol{\tau}_{arm} \in \mathbb{R}^n$ represents the

joint torque in the robotic arm, $\boldsymbol{M}_q \in \mathbb{R}^{n\times n}$, $\boldsymbol{M}_{\theta\delta} \in \mathbb{R}^{n\times\mu}$, $\boldsymbol{M}_{\delta\theta} \in \mathbb{R}^{\mu\times n}$ are inertia matrices and $\boldsymbol{M}_{\theta\delta} = \boldsymbol{M}_{\delta\theta}^{\top}$, $\boldsymbol{C}_q \in \mathbb{R}^{n\times n}$, $\boldsymbol{C}_{q\delta} \in \mathbb{R}^{n\times\mu}$, $\boldsymbol{C}_{\delta q} \in \mathbb{R}^{\mu\times n}$ are Coriolis matrices, $\boldsymbol{K}_\delta \in \mathbb{R}^{m\times m}$ is a stiffness matrix, $\boldsymbol{B}_{q,quad} \in \mathbb{R}^{n\times\mu}$, $\boldsymbol{B}_{\delta,quad} \in \mathbb{R}^{n\times\mu}$ are input mapping matrices from 2-dim AR thrust $\boldsymbol{f}_{qr} = [f_{x,qr}, f_{y,qr}]^{\top}$ to dynamics. Here, note that due to orthogonality between each mode, $\boldsymbol{M}_\delta, \boldsymbol{K}_\delta \in \mathbb{R}^{\mu\times\mu}$ have only diagonal component, see [Meirovitch–2000b].

In order to simplify the expression of these matrices, it is assumed that the CoM of the AR and the connection are considered to be at the tip of the beam, *i.e.*, the AR thrust and torque, and the weight of both the AR and its arm are applied at the tip of the beam. Furthermore, let us assume that the AR and connector weight are not supported by the arm but by the AR. This translates to $\theta_{conn} = 0,\ m_{conn} = 0,\ d_{conn} = 0$ and $m_{qr} = 0$.

The compact expression of the matrices important for the system analysis are explicited here after:

$$\boldsymbol{K}_\delta = \begin{bmatrix} EId_{11} & EId_{12} \\ EId_{12} & EId_{22} \end{bmatrix} \qquad \boldsymbol{M}_\delta = \begin{bmatrix} \rho Aa_{11} & \rho Aa_{12} \\ \rho Aa_{12} & \rho Aa_{22} \end{bmatrix} \tag{7.8}$$

where the terms a_{ij} and d_{ij} are coming from the beam's kinetic and potential energy expressions in the Euler-Lagrangian formalism and can be written as

$$a_{ii} = \int_0^{l_b} \phi_i(x)\phi_j(x)dx \qquad d_{ii} = \int_0^{l_b} \phi_i''(x)\phi_j''(x)dx \tag{7.9}$$

where $\phi_i''(x)$ denotes the second spatial derivative of $\phi_i(x)$. Thanks to the orthogonality property of the modes, see [Meirovitch–2000a], it can be noted that $a_{ij} = 0$ and $d_{ij} = 0$ when $i \neq j \quad \forall(i,j) \in \mathbb{R}^{\mu\times\mu}$. Moreover the part of the control matrix relating the AR thrust and the vibration dynamics can be written

$$\boldsymbol{B}_{\delta,qr} = \begin{bmatrix} f_1(\boldsymbol{\theta},\boldsymbol{\delta}) & 0 \\ f_2(\boldsymbol{\theta},\boldsymbol{\delta}) & 0 \end{bmatrix} \tag{7.10}$$

with

$$f_1(\boldsymbol{\theta},\boldsymbol{\delta}) = \left(w_b \sin(\theta_b)\phi_1'(l_b) + \cos(\theta_b)\phi_1(l_b)\right)\cos(\theta_{qr}) \tag{7.11}$$

$$f_2(\boldsymbol{\theta},\boldsymbol{\delta}) = \left(w_b \sin(\theta_b)\phi_2'(l_b) + \cos(\theta_b)\phi_2(l_b)\right)\cos(\theta_{qr}) \tag{7.12}$$

where $\theta_{qr} = \bar{\theta}_{qr} - (\bar{\theta}_b + \theta_{conn})$, considering the assumption introduced.

7.2 System Analysis

This section exploits the presented model in order to conduct a system analysis on the flexibility in beam manipulated by MAGMaS. By linearizing the vibration model close to the operational point, observability and controllability of the vibration

modes are proven.

7.2.1 Linearized State Space Representation

From (7.6) one can separate the dynamics of the manipulator and the one of the vibration. Furthermore assuming very high tracking performances for the ground manipulator, *i.e.*, $\boldsymbol{\theta} = \boldsymbol{\theta}^d$, on can rewrite the vibration dynamics as

$$\ddot{\boldsymbol{\delta}} = \mathbf{M}_{\delta}^{-1}\left(-\boldsymbol{E} - \boldsymbol{K}\boldsymbol{\delta} - \boldsymbol{g}(\boldsymbol{\theta}^d) + \mathbf{B}_{\delta}\boldsymbol{\tau}_{qr}\right) \tag{7.13}$$

where

$$\boldsymbol{E} = \mathbf{M}_{\theta q}^{\top}\ddot{\boldsymbol{\theta}}^d + \boldsymbol{C}_{\delta\theta}\dot{\boldsymbol{\theta}}^d, \tag{7.14}$$

the term $\boldsymbol{E}$ can be interpreted as kind of energy dissipation with an upper limit and $\mathbf{B}_{\delta}$ is the linearized version of $\boldsymbol{B}_{\delta,qr}$ from (7.10), such that

$$\mathbf{B}_{\delta} = \begin{bmatrix} b_1 & 0 \\ b_2 & 0 \end{bmatrix}. \tag{7.15}$$

Note that $\mathbf{M}_{\theta q}$ is function of $\boldsymbol{\theta}$ and $\boldsymbol{C}_{\delta\theta}$ is function of $\boldsymbol{\theta}$ and $\boldsymbol{\delta}$. It is interesting to then rewrite the state space representation of vibration dynamics.

$$\begin{bmatrix} \ddot{\boldsymbol{\delta}} \\ \dot{\boldsymbol{\delta}} \end{bmatrix} = \begin{bmatrix} \mathbf{0} & -\mathbf{M}_{\delta}^{-1}\boldsymbol{K} \\ \mathbf{I} & \mathbf{0} \end{bmatrix} \begin{bmatrix} \dot{\boldsymbol{\delta}} \\ \boldsymbol{\delta} \end{bmatrix} + \begin{bmatrix} \mathbf{M}_{\delta}^{-1}\mathbf{B}_{\delta} \\ \mathbf{0} \end{bmatrix} \boldsymbol{\tau}_{qr} - \begin{bmatrix} -\mathbf{M}_{\delta}^{-1}\boldsymbol{E} \\ \mathbf{0} \end{bmatrix} \tag{7.16}$$

$$= \underbrace{\begin{bmatrix} \mathbf{0} & -\bar{\boldsymbol{K}} \\ \mathbf{I} & \mathbf{0} \end{bmatrix}}_{A} \begin{bmatrix} \dot{\boldsymbol{\delta}} \\ \boldsymbol{\delta} \end{bmatrix} + \underbrace{\begin{bmatrix} \bar{\mathbf{B}}_{\delta} \\ \mathbf{0} \end{bmatrix}}_{B} \boldsymbol{\tau}_{qr} - \underbrace{\begin{bmatrix} -\bar{\boldsymbol{E}} \\ \mathbf{0} \end{bmatrix}}_{F}, \tag{7.17}$$

with $\mathbf{A} \in \mathbb{R}^{4\times4}$, $\mathbf{B} \in \mathbb{R}^{4\times2}$ and $\boldsymbol{F} \in \mathbb{R}^4$, as in practice only the two first vibration modes are considered, see Sec. 7.1.1. As one expected outcome of the system analysis is to assess if the vibration modes are observable, an output of the state space is represented as

$$\boldsymbol{y} = \underbrace{\begin{bmatrix} \mathbf{0} & \mathbf{I} \end{bmatrix}}_{C} \begin{bmatrix} \dot{\boldsymbol{\delta}} \\ \boldsymbol{\delta} \end{bmatrix}, \tag{7.18}$$

with $\boldsymbol{C} \in \mathbb{R}^{2\times4}$ given the size of $\boldsymbol{\delta}$. The system analysis is conducted on the linearized state space model of the vibration mode just introduced, the observability and controllability of the vibration mode are established.

7.2.2 Observability

One can write the observability matrix of the state space system described by (7.17)-(7.18) as

$$\mathbf{Obs} = \begin{bmatrix} \boldsymbol{C} & \boldsymbol{C}\mathbf{A} & \boldsymbol{C}\mathbf{A}^2 & \boldsymbol{C}\mathbf{A}^3 \end{bmatrix}^\top . \tag{7.19}$$

Clearly this matrix has row rank equal to 4, as $\boldsymbol{C} = \begin{bmatrix} \mathbf{0} & \mathbf{I} \end{bmatrix}$ and $\boldsymbol{C}\mathbf{A} = \begin{bmatrix} \mathbf{I} & \mathbf{0} \end{bmatrix}$, thus the matrix $[\boldsymbol{C}\ \boldsymbol{C}\mathbf{A}]^\top$ is full rank. So the state variables δ_1 and δ_2 are observable.

7.2.3 Controllability

One can write the controllability matrix of the state space system described by (7.17)-(7.18) as

$$\mathbf{Ctrl} = \begin{bmatrix} \mathbf{B} & \mathbf{A}\mathbf{B} & \mathbf{A}^2\mathbf{B} & \mathbf{A}^3\mathbf{B} \end{bmatrix}. \tag{7.20}$$

The rank analysis is not straightforward for the controllability matrix. One can note that, if $\operatorname{rank}\left(\bar{\mathbf{B}_\delta}\right) = 2$ is guaranteed or already proven, then the matrix column rank is 4, as $\mathbf{B} = \begin{bmatrix} \bar{\mathbf{B}_\delta} \\ \mathbf{0} \end{bmatrix}$ and $\mathbf{A}\mathbf{B} = \begin{bmatrix} \mathbf{0} \\ \bar{\mathbf{B}_\delta} \end{bmatrix}$. A general approach to assess the rank of the controllability matrix starts by precising the expression of matrix $\bar{\mathbf{B}_\delta}$ using the expression of (7.8) and (7.15),

$$\bar{\mathbf{B}_\delta} = \mathbf{M}_\delta^{-1}\mathbf{B}_\delta = \frac{1}{\rho A}\operatorname{diag}\left(a_{11}^{-1}, a_{22}^{-1}\right)\begin{bmatrix} b_1 & 0 \\ b_2 & 0 \end{bmatrix} = \frac{1}{A\rho}\begin{bmatrix} \frac{b_1}{a_{11}} & 0 \\ \frac{b_2}{a_{22}} & 0 \end{bmatrix} = \begin{bmatrix} \tilde{b}_1 & 0 \\ \tilde{b}_2 & 0 \end{bmatrix}. \tag{7.21}$$

From here, once noticed that every sub-matrix of **Ctrl** has a zeros column, hence the study of controllability has to be made on the following simplified matrix

$$\mathbf{Ctrl}_s = \begin{bmatrix} \tilde{b}_1 & 0 & -\frac{EId_{11}}{a_{11}\rho A}\tilde{b}_1 & 0 \\ \tilde{b}_2 & 0 & -\frac{EId_{22}}{a_{22}\rho A}\tilde{b}_2 & 0 \\ 0 & \tilde{b}_1 & 0 & -\frac{EId_{11}}{a_{11}\rho A}\tilde{b}_1 \\ 0 & \tilde{b}_2 & 0 & -\frac{EId_{22}}{a_{22}\rho A}\tilde{b}_2 \end{bmatrix}. \tag{7.22}$$

The determinant of this simplified controllability matrix is,

$$\det\left(\mathbf{Ctrl}_s\right) = -\frac{E^2\, I^2\, {b_1}^2\, {b_2}^2\left(a_{11}\, d_{22} - a_{22}\, d_{11}\right)^2}{a_{11}^4\, a_{22}^4\, \rho^6\, A^6}. \tag{7.23}$$

For the system to be controllable the determinant as to be different from zero. Knowing that the physical quantities are all positive, that the product $a_{11}a_{22}$ also is and that M_δ is invertible in order to write the state space representation, one

only needs to study the below expression

$$\det\left(\mathbf{Ctrl}_s\right) = 0 \Leftrightarrow \Gamma = b_1\, b_2\, (a_{11}\, d_{22} - a_{22}\, d_{11}) = 0, \tag{7.24}$$

which maps to three independent cases to be studied: *i)* $b_1 = 0$, *ii)* $b_2 = 0$ and *iii)* $(a_{11}\, d_{22} - a_{22}\, d_{11}) = 0$.

In order to proceed, let us write down the linearization of matrix $\mathbf{B}_\delta$ for $\boldsymbol{\delta} = [0\ 0]^\top$ and $\boldsymbol{\theta} = \boldsymbol{\theta}^d$. Based on (7.11)- (7.12), the linearization yields

$$b_1 = f_1(\boldsymbol{\theta}^d, [0\ 0]^\top) + \left.\frac{\partial f_1}{\partial \delta_1}\right|_{\boldsymbol{\delta}=[0\ 0]^\top} (\delta_1 - 0) + \left.\frac{\partial f_1}{\partial \delta_2}\right|_{\boldsymbol{\delta}=[0\ 0]^\top} (\delta_2 - 0) \tag{7.25}$$

$$b_2 = f_2(\boldsymbol{\theta}^d, [0\ 0]^\top) + \left.\frac{\partial f_2}{\partial \delta_1}\right|_{\boldsymbol{\delta}=[0\ 0]^\top} (\delta_1 - 0) + \left.\frac{\partial f_2}{\partial \delta_2}\right|_{\boldsymbol{\delta}=[0\ 0]^\top} (\delta_2 - 0). \tag{7.26}$$

Expanding the terms leads to the following expressions,

$$b_1 = \phi_1(l_b) \cos\left(\bar{\theta}^d_{qr} - \theta_0 - \theta^d_1 - \theta^d_2 - \theta^d_3 - \theta_{TCP}\right) = \phi_1(l_b) \cos\left(\theta^d_{qr}\right) \tag{7.27}$$

$$b_2 = \phi_2(l_b) \cos\left(\bar{\theta}^d_{qr} - \theta_0 - \theta^d_1 - \theta^d_2 - \theta^d_3 - \theta_{TCP}\right) = \phi_2(l_b) \cos\left(\theta^d_{qr}\right) \tag{7.28}$$

Then the conditions (i) and (ii) for loss of controllability become, $\phi_1(l_b) = 0$ or $\phi_2(l_b) = 0$, *i.e.*, l_b is a node for the vibration modes, or $\theta_{qr} = k\pi + \frac{\pi}{2} \quad k \in \mathbb{Z}$, *i.e.*, the thrust orientation is perpendicular to w_b direction hence can not impact w_b.

The third and last condition for null determinant is $(a_{11}\, d_{22} - a_{22}\, d_{11}) = 0$, were a_{ii} and d_{ii} expressions are recalled in (7.9) and are introduce in the computation of the kinetic and potential energy in the beam. First notice that $a_{ii} \neq 0$ and $d_{ii} \neq 0$, because otherwise

$$\phi_i(x) = 0 \quad \forall x \in [0\ l_b] \tag{7.29}$$

$$\phi_i''(x) = 0 \quad \forall x \in [0\ l_b], \tag{7.30}$$

which means that there are no vibrations along the beam. So the third condition translates to the following equality,

$$\frac{a_{11}}{a_{22}} = \frac{d_{11}}{d_{22}}, \tag{7.31}$$

which can be rewritten as

$$\frac{\rho A a_{11}}{EI d_{11}} = \frac{\rho A a_{22}}{EI d_{22}}. \tag{7.32}$$

The numerators can be seen as the 'inertia' of the two modes and the denominators as 'stiffness' of the modes. Hence the fractions represents the natural spatial frequency of the modes. If they are equal, it means that the two mode are spatially super-imposed, hence not differentiable so it is like there is only one mode.

In conclusion, for the linearized system to be controllable the following must

hold

1) $\phi_1(l_b) \neq 0$, *i.e.*, l_b is not a node for first mode vibration

2) $\phi_2(l_b) \neq 0$, *i.e.*, l_b is not a node for second mode vibration

3) $\theta_{qr} \neq \frac{\pi}{2} + k\pi \quad k \in \mathbb{Z}$, *i.e.*, the thrust of the AR is not orthogonal to the vibration induced deflection

4) $(a_{11}\, d_{22} - a_{22}\, d_{11}) = 0$, *i.e.*, the spatial natural frequency of the two modes are different

The conditions 1) 2) and 4) are always fulfilled by system design in this mechanical system. So the only condition to check to guarantee controllability is that the thrust orientation must remain non-orthogonal to the deflection of the beam.

7.3 Discusssion and Future Works

This exploratory study on the flexibility in MAGMaS, conveys some interesting system properties which require to be tested in simulations and experiments. The modeling of the flexibility in beam manipulated by MAGMaS was the occasion to exhibit the controllability of the vibration modes from a theoretical analysis. This is validating the empirical observation made during the experiments on MAGMaS presented in Chapter 5.

Modeling

The modeling can evolve around three main directions. First, the modeling relies on several assumptions to reduce the expression complexity and provide a simplified model, relaxing these assumptions should be considered to increase the accuracy of the model.

Another way to extend the proposed model is to consider the 3D case, which should make appear more coupling between the vibration modes and the ground manipulator dynamics, due to centrifugal/Coriolis effects.

In the same direction of extending the model, multi-directional thrust AR could be considered instead of underactuated AR, this will make a coupling between the AR rotational dynamics and the flexibility dynamics appear. Lastly considering several AR and different shape of object would also provide a more general model.

Another way to model flexibility is via the finite element methods, see [Meirovitch–2000c], this has not been investigated yet and might provide better results in terms of computational power required to simulate the flexibility. In particular, the addition of several AR along a beam is expected to be easier in the finite element method, as extra forces will be applied in discrete location, than in the continuous method as discrete force exertion corresponds to an in-homogeneous boundary condition, thus complicating the analytical solution.

Control

The linearized model for the vibration modes is controllable and observable. From the control point of view, it implies that separate controllers for the ground manipulator and the AR orientation need to be synthesized and, as the model derived relies on linearization, the vibration linear controller shall emphasis robustness, with approaches like Linear-Quadratic Regulator (LQR) or H_∞ control. At the same time an observer or the vibration mode should be designed, also relying on the linearized model. P otential observers and controllers designed based on the linearized model need to be validated in realistic simulations based on the non-linearized model. Simulations would permit to assess their robustness to the model discrepancies and to parameters variations in a controlled environment.

Chapter 8

Summary and Future Works

Contents

8.1 Summary

Nowadays free-flying MAV are a well developed technology accompanied by various commercial successes in the general public, spanning from crop/structure visual inspection to hobby racing. The next frontier for Aerial Robotics is symbolized by APhI, where MAV are embodied with the capacity to physically interact with their environment; this opens the way to many applications, *e.g.*, contact inspection and cooperative manipulation. The research lines on APhI and AM are fostered by European projects and other national initiatives leading to a rich literature of both original designs and clever control algorithms. The work presented in this thesis is based on a vision of AR as potential *flying companions* for cooperative manipulation with both humans and other robots. The main contribution of this thesis consists in proposing a new concept for cooperative manipulation, MAGMaS composed of both ground and aerial manipulators. While combining two different kind of manipulators to mitigate their respective drawbacks, MAGMaS also open a new research direction with many possible applications. This thesis work laid the foundation of the theory for MAGMaS and demonstrated, through experiments, their feasibility and potential for a breakthrough in the real world. In particular, the first ever cooperative manipulation between a ground and an aerial manipulator was showcased at the Hanover Fair 2017. In the following, an overview of the content and the contributions in the chapters is given.

In Chapter 3, the motivations of the MAGMaS concept are outlined. From a review of available manipulation solutions, it appeared that ground manipulators often suffer from limited workspace around their base and admissible joint torques, but have a satisfying payload and energetic autonomy. The limitations of ground manipulator can be exhibited when manipulating long objects: to satisfy the torque constrains the grasping should be close to the object CoM which is often in conflict with the workspace limitation. On the other hand AR, which have a virtually infinite workspace, are suffering from payload and autonomy limitation. The concept of MAGMaS targets the cooperative manipulation of long objects and proposes to combine ground manipulators and AR to mitigate their respective drawbacks. In particular the addition of a *flying companion* to the ground manipulator permits

to *i)* reduce the torque perceived at the EE and *ii)* suppress vibrations in the load. Application are numerous for industry requiring assembly or disassembly tasks, *e.g.*, construction, plant decommissioning and USAR. The use of robots for these tasks is even more desirable if the environment is hazardous for humans. Based on these motivations and potential applications the general model of MAGMaS is introduced at length. Modeling of the AR in free flight is conducted and this model is then incorporated in the one of MAGMaS. Lastly, ways to extend the proposed model and further possible theoretical studies on MAGMaS are introduced.

In Chapter 4, the control framework necessary for MAGMaS is introduced, with a focus on the AR specific controller. A generic high level controller composed of a basic planner and control allocation scheme is presented. The control allocation splits the desired forces required to move the load for each sub-system of the MAGMaS. At the same time it ensures that every actuation and system constraints are respected and it exploits the redundancy of MAGMaS to maximize the manipulability index of the system. In order to control the AR three components are required, *i)* a low-level geometric controller, *ii)* an external wrench estimator and *iii)* a force based controller, each of which is presented in depth. A particular emphasis is given to the external wrench estimation with two distinct methods presented, one relying on model identification and the other on closed loop motor velocity control. The presented force based controller for AR relies on the external wrench estimator and on classical impedance control techniques.

The experimental validations of the MAGMaS concept are presented in Chapter 5. The first part of the chapter is devoted to numerical simulations and proof of concept experiments and corresponds to the early stage on the work on MAGMaS. In this early stage, the use of a quadrotor with a spherical passive joint was considered, in order to efficiently decouple the rotational dynamics of the manipulated load and the AR. The design and the benefit of such a joint is validated experimentally. Additionally the capacity of MAGMaS to reduce the vibration of the load are highlighted in a comparative experiment. The second part of the chapter is devoted to a massive integration and experimental work developed for the KUKA 2017 Innovation Award; the addition of a tele-presence framework to a MAGMaS and the design of a multi-directional thrust AR are detailed. The implementation and integration of the overall system is covered in depth. This part is concluded with the experimental results for cooperative bar lifting.

In Chapter 7, an on-going exploratory study on the flexibility and its implications in MAGMaS is conducted. A planar model of MAGMaS manipulating a flexible beam is presented, with emphasis put on the flexibility modeling. The proposed system is linearized to conduct a system analysis: both observability and controllability of the first two vibration modes are exhibited.

In parallel to MAGMaS another research direction was investigated during this thesis. The use of elastic joints for AM was explored with the conviction that they could allow safer and more versatile physical interactions with the environment. This field of research is stimulating, but integration of elastic joints and VSA on AR proved tedious in practice due to hardware limitations. The theoretical study of

flatness for elastic joint AR is presented in Chapter 6. The model of an AR with an elastic joint is derived and the analysis conducting to the proof of flatness for a set of output is described. Finally, a feedback linearization based controller is synthesized for the AR with VSA. The approach is validated by extensive numerical simulations comprising noise and parametric uncertainties and by a set of experiments with a VSA mounted on the AR. This chapter is concluded by possible research directions on using elastic joints for AR.

8.2 Future Works and Potential Extensions

8.2.1 MAGMaS: Aerial-Ground Co-manipulation

The original and unique work on MAGMaS presented in this thesis is still in its infancy. Hence the potential future works to develop MAGMaS and their usage is vast and can be articulated around the following directions, in no preferencial order: *i)* theoretical contributions, *ii)* planning and supervision, *iii)* environment perception, *iv)* safe human physical interaction and *v)* system design and integration.

Theoretical Contributions Exploiting the formalization of MAGMaS proposed in this thesis several research directions could be pursued (see Sec. 3.4). During the developments of MAGMaS the following questions were raised and could not be addressed due to resource/time constraints.

- How does the number of ground manipulators and AR impact the MAGMaS overall performance?
- Is there an optimal number of DoFs for the ground manipulator given a MAGMaS structure?
- Are DoFs from a mobile base equivalent in terms of system performances to the one of the ground manipulator? Can the number of DoFs of the ground manipulator be reduced if it is mounted on a mobile base?
- What are the best grasping points for a weirdly shaped object given a MAGMaS structure?
- How to estimate the load inertial parameters with a MAGMaS? How to exploit this information to increase the system performances?
- Can an AR failure be compensated by the MAGMaS at large?

Each of this questions merits a separated theoretical study. Moreover, so far the base of the ground manipulator was assumed fixed, waving this hypothesis and considering a mobile base should trigger new challenges for modeling, planning and control of MAGMaS.

Planning and Supervision In the presented work the planning and supervision solutions proposed are very crude as the focus was more to enable MAGMaS from a lower abstraction level point of view. In particular the task and trajectory for MAGMaS is an open field. A planning brick which should be developed for further use of MAGMaS consists in a collision avoidance scheme taking into account the

manipulated load. Moreover from a supervision point of view, the interface with human operator is paramount. The three main directions that could be investigated for human machine interfaces are: *i)* the visual feedbacks provided by a combination of on-board cameras and a visualizer based on the system state, *ii)* the use of a haptic interface to control the system in tele-presence, in particular a deeper study on the informations to render in order to provide better situational awareness and *iii)* the possibility to directly physically interact with the system, via impedance framework for example, in order to guide or halt the motion of a MAGMaS. For more details see Sec. 5.5.

Environment Perception The presented work made abstractions of the perception challenge inherent to any robotic application. The experiment setup relies heavily on MoCap which provides an accurate position and orientation information for objects equipped with markers, robots or environment parts. Perception is important to maintain knowledge of the systems' environment, *e.g.*, for dynamic obstacle avoidance or grasping, and for the AR state reconstruction. Both usages can be fulfilled with visual perception solutions, some potential directions are detailed in Sec. 5.5. The research group at LAAS–CNRS is currently investigating some visual perception methods for AR. In particular, the use of infra-red stereo-slam is investigated with an Intel Euclide sensor[1] and shows promising results.

Safe Human Physical Interaction A direction unveiled, but not explored in this thesis is the potential to have human physical interactions with the MAGMaS. Although the safe physical interaction with industrial manipulator is well investigated in the literature, safe physical interaction with AR studies are still embryonic in the literature. The recent advances in force estimation and control for AR are a first step towards a safe physical interaction with humans for AR. Nevertheless the techniques developed for ground manipulators (see Sec. 5.5), can not bee applied as such to AR due to the floating base challenge arising from the flying platform. Further developments in that direction will enable the *flying companion* paradigm to take form. Also a unified safe physical interaction for heterogeneous systems, with both ground and aerial manipulators as MAGMaS, should be investigated to allow collaborative part handling and assembly.

System Design and Integration As the MAGMaS concept started from a blank sheet, many design choices had to be made with no comparison point available. With this respect further work on MAGMaS could use the aggregated experience to improve several aspects of the system design. In particular, the *flying companion* is an in-house design tailored for bar lifting and at least two points could be improved. First the design of the grasping mechanism should be at the same time robustified and also made lighter, to better fit the AR paradigms. Another improvement of the AR would consist in a study of the possible propellers' layout in a way to

[1] `https://click.intel.com/intelr-euclidtm-development-kit.html`

create some favorable force exertion direction matching the bar lifting task while conserving the over properties of the multi-directional thrust AV. Moreover, the integration of the MAGMaS was a challenge and was conducted at very fast pace for a dedicated application. Hence it could be beneficial to re-define the different sub-system interfaces to make the system even more modular and allow for easier change of sub-system, *i.e.*, ground manipulator or AR or number of AR or haptic interface. This work, although not mandatory, from a research point of view should prove its importance for further usage of MAGMaS. Lastly an important step towards real life applications of MAGMaS is the increase of the system autonomy, from the energy and perception point of view. This calls for further developments and integration of perceptions solutions for MAGMaS. An idea to increase the energy autonomy of MAGMaS, could be to work towards the integration of an automated charging pod for the AR on the ground manipulator base.

8.2.2 MAGMAS Possible Applications

On top of the presented potential extensions, two major applications remain to be fully demonstrated. On one hand, the full scale demonstration of a MAGMaS in a real case scenario is still missing and should became feasible with the work detailed under the umbrella system design and integration, see previous section and Sec. 5.5. In particular the most promising scenario of use seems to be nuclear plant decommissioning, for the reasons mentioned in the following. First, nuclear plants are very well documented making the environment *a priori* well known for the system and very structured, which should reduce the strain on planning and perception capacities for MAGMaS. The second reason is that part of nuclear plants are hazardous due to their radioactivity, even if small, thus robotic usage is highly sought. Lastly the worldwide aging of nuclear plants calls for decommissioning or refurbishing operations, *e.g.*, average age for nuclear reactors in France is 32 years for an expected lifetime of 40 years and 9 reactors were already undergoing decommissioning in 2013[2].

On the other hand, MAGMaS are opening the way toward human-AR cooperative manipulation. Indeed the developments on AR to make them *flying companions* for humans is already engaged. And once a proper decentralized force control framework would be achieved for cooperative manipulation in MAGMaS the extension to human-AR should become possible and thrilling.

8.2.3 Variable Stiffness Actuators for Aerial Vehicles

During this work, the use of VSA for AR has been investigated. Although successful experiments were conducted, it revealed to be a subject fit for a thesis in itself. As it seems to be currently investigated by other groups specialized in aerial manipulation. In particular foundations on the control and integration of VSA were laid,

[2] `https://www.connaissancedesenergies.org/fiche-pedagogique/parc-nucleaire-francais`

but this topic requires further development in the direction of lightweight VSA, as detailed in Sec. 6.6. From the experimental work it results that the development of VSA for AR should focus on lighter actuators but more importantly on more robust methods for parameters' identification and finer control strategies for the VSA. Once this steps are achieved, the VSA low-level control shall not be a limitation anymore to the use of advanced non-linear control techniques for AR. This should pave the way to interesting applications, like throwing, collision compliance and human APhI, each calling for its specific challenges. The capacities of VSA in these situations should be leveraged by fine planning algorithms and precise control algorithms, for the case at hand, which both need to be devised.

Appendices

Appendix A

Force Estimation: Close Loop Spinning Velocity Control

Contents

Abstract

The work presented in this Appendix is not a personal contribution and is presented here for completeness of the argument.

This appendix details a force estimation approach based on closed-loop spinning velocity control of the propellers, see Sec. A.1. It has been investigated, in a parallel work, at LAAS–CNRS and showed conclusive results for spinning velocity control and APhI applications. Indeed, the precise spinning velocity control allows to use static mapping between the spinning velocity and the wrench generated by the propeller, see Sec. A.2.

A.1 Propeller Spinning Velocity Control

This section outlines the results presented in [Franchi–2017b], on which the work presented in Chapter 5 of this thesis is relying.

Motivations

Recall that the biggest flaw of many low/middle-cost ESC, used in multi-rotor platforms for APhI, is that setpoints or pseudo-setpoints are used to command propeller spinning velocity in a open loop fashion. This relies on the use of look-up table and is clearly not fast nor robust, moreover the pre-calibration effort is non negligible.

Some ESC softwares, like SimonK, BHLHeli and Autoquad ESC32, implement a real closed-loop speed control to solve this problem. The typical approach is to use a proportional integral (PI) in conjunction with a feedforward (FF). This allows to reach good control performances, however pre-calibration remains intensive for the FF term, that is specific for each motor/propeller pair. The introduction of an

integral action provides some robustness, which is kept limited due tot the need of avoiding excessive overshoot and wind-up problems.

The solution to improve spinning velocity control, was to propose and implement a newest and easy low-level spinning velocity control loop on the ESC. This is described at length in [Franchi–2017b], the rest of this section outlines this work and the implications for APhI. The solution developed is different from the classical ESC software presented earlier, as *i)* it does not require any pre-calibration phase, *ii)* it is extremely robust and applicable to a wide set of motor/propeller without the need of gain tunning, *iii)* it can achieve performances that are independent of the battery terminal voltage, the mechanical wearing, the temperature and so on, *iv)* it is amenable to extremely low complexity implementation even when compared with 'supposedly simple' classical controllers.

Problem Setting

Standard BLDC motors are considered with their associated control hardware, in-depth description can be found in [Franchi–2017b].

The basic functioning principle of of such an ESC and BLDC motor is as follows. An equivalent voltage, uV_+ is applied to the motor coils, where $u \in [0,1]$ is the duty cycle of the actual PWM signal used to control the motor and $V_+ \in \mathbb{R}^+$ is the power supply voltage (typically the battery's terminal voltage). For low inductance BLDC motors, fast current dynamics can be neglected, with this approximation the rotor frequency (or speed) of rotation dynamics can be represented as nonlinear differential equation

$$\dot{x} = \bar{f}(x,t) - \bar{f}(x,V_+,t)u \tag{A.1}$$

where both $\bar{f}$ and $\bar{h}$ are unknown nonlinear function of x and the time t. One can see the function $\bar{h}$ as the inverse of the inertia 'seen' by the motor control input, u. While $\bar{f}$ gathers all the possible other possible nonlinear dynamical effects.

The ESC unit contain an inverter which provides the sequential current commutation on the coil, generating the magnetic field that start and sustain the motion of the rotor. Commutation are triggered by a rotor position feedback that comes either from and additional sensor (*e.g.*, an encoder) or, in case of sensorless BLDC, from the detection of the instants of zero crossing of the voltage generated in the unpowered windings. The later approach has been selected, as it is the most common in aerial robotics applications, since it allows for smaller weight, reduced hardware complexity and lower costs. This comes at a cost, the speed information of this method is poor for low speed, which are usually not spawned in typical applications. Considering that (A.1) can be rewritten for the rotor period of rotation $y = 1/x$, its dynamics can be written as

$$\dot{y} = -y^2\bar{f}(1/y,t) - y^2\bar{f}(1/y,V_+,t)u \tag{A.2}$$

$$= f(y,t) - h(y,V_+,t)u \tag{A.3}$$

Problem Statement

The goal of the described control method is to enforce a robust control of the propeller period of rotation. Given that the desired spinning velocity and the measured one are available signals, and that the duty cycle of the PWM voltage is the control input. The goal is to design a feedback control loop, that steers the motor's period of rotation to the desired one, while enforcing:

- **Low Complexity**, the algorithm should be implementable with simple arithmetic operations (additions, subtractions, shift, comparison and simple multiplication) at low resolution;
- **Adaptiveness and Robustness**, the algorithm should be performing for all kind of motor/propeller configuration and for wide range of setpoints without explicit tuning.

An algorithm answering these two requirements has been devised in [Franchi–2017b] and is detailed hereafter.

The ABAG Algorithm

The algorithm proposed is named ABAG, for Adaptive-Bias/Adaptive-Gain algorithm. Its basic loop is composed of four steps;

1. **an error sign low pass filtering**, the low pass filtered error signal is used in the computation of the bias and the gain.
2. **an adaptive bias update**, is necessary to be used in conjunction of the gain update to effectively suppress chattering.
3. **an adaptive gain update**, the idea is to increase the gain only if the tracking quality degrades and to decrease it otherwise
4. **a control input computation**,the control input is computed with the updated gain and bias to track desired speed.

For both the adaptive bias and adaptive gain, during their update phase they are increased/decreased of a given quantity which is a parameter from the controller. Additionally the choice to decrease/increase them is based on comparison with one static threshold for each, leading to two additional parameters for the ABAG controller. Rationals behind this strategy, as well as more details can be found in [Franchi–2017b].

Software Implementation

The aforementioned algorithm has been implement on an ATMega168A, with limited arithmetic capabilities, allowing only 8bits additions, subtractions and multiplications, The full software comprise, *i)* an interface and protocol part, *ii)* a clock synchronization routine, as the main difficulty was to get a precise time measure on the micro-controller that has no quartz oscillator, *iii)* a speed measurement routine with correct noise filtering capabilities not sacrificing filtering delay, *iv)* the ABAG Algorithm, with a recorder longest code path of 27.5 µs at 8 MHz, and *v)* safety features (active breaking, over-current and blockage safeties).

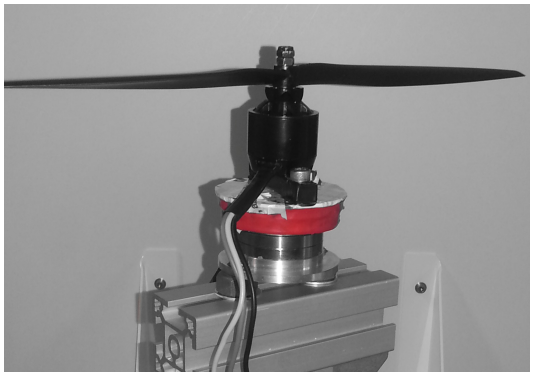

Figure A.1 – Picture of the setup for the propeller aerodynamic coefficients identification. The propeller and its associated BLDC motor are mounted on the 6D F/T sensor. The combination is mounted on a support to ensure that ground effect aerodynamic effect are not affecting the measurements. (From [Bicego–2015])

The small execution time of the ABAG Algorithm is a very important property since the controller, by essence, provide very discontinuous PWM duty cycle, the faster it runs the less chattering will actually be visible from the motor coil.

Performances Evaluations

The performances of the full software have been successfully tested both on test bench and in-flight.

The bench tests, where conducted with several motors and propellers, with the same ABAG parameters, in depth results are presented in [Franchi–2017b]. For step response commands, the response time are very fast with rising time of a few tens of ms and the steady case average error is null. the tracking of time varying chirp is also excellent for all motor/propeller combinations, with performances degrading smoothly with increasing acceleration.

The in-flight tests consist of the usage of this ESC software by the group, *e.g.*, [Tognon–2016b] or [Ryll–2017] and the results presented in Chapter 5 of this thesis.

A.2 Force Controller at Propeller Level

Once the propeller spinning velocity is efficiently regulated, a last step is necessary for force control, identify the maps between spinning velocity and the wrench produced by the propeller (thrust force and the drag moment). Relying on the simplified models presented in Sec. 3.2.1, this translate in identifying two aerodynamic coefficients the aerodynamic thrust coefficient, c_F, and the drag coefficient c_T. This is done by mounting the motor/propeller pair on a *static* 6D F/T-sensor, as depicted in Fig. A.1, and is presented here for completeness as it was investigated in [Bicego–2015].

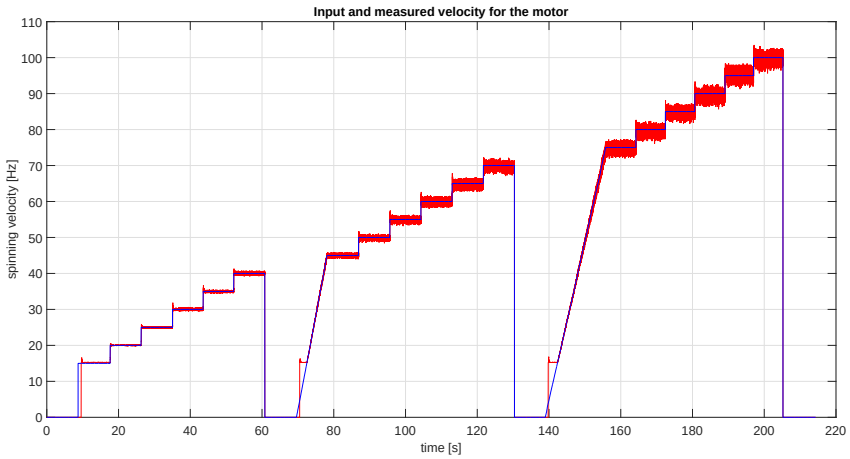

Figure A.2 – Excitation trajectory used for the propeller aerodynamic coefficients identification. Note that below 15 Hz spinning velocity tracking can not be ensured because the velocity measurements are not precise enough. Also the excitation is done in three chunks to prevetn motor overheating. (From [Bicego–2015])

The identification process is as follows, the motor is fed with a spinning velocity trajectory composed of steps spanning its full operation range, the steps are chosen long enough to remove transient behavior, see Fig. A.2. The signal from the 6D F/T-sensor is acquired and post-processed offline, *i.e.*, filtered with a non causal filter. The force and torque measurements in the relevant directions are then synchronized with the recorded spinning velocity. The value of the aerodynamics coefficient are then retrieved using least square methods, under the first order approximation that the relation between the propeller wrench and the squared spinning velocity is linear.

Annexe B

Résumé Long en Français

Sommaire

Organisation

Ce résumé retrace les grandes lignes des travaux de recherche présentés dans cette thèse. Dans un premier temps un rapide panorama du contexte de la thèse, l'interaction physique aérienne entre robots aériens (AR pour *Aerial Robot*) et leur environnement, est présenté dans la section B.1. En particulier, les concepts nécessaires au développement de l'interaction physique aérienne (APhI pour *Aerial Physical Interaction*) sont introduits. Une première contribution relative à l'estimation de force, pré-requis pour l'APhI est présentée dans la section B.2. Dans un deuxième temps, les travaux formant la contribution principale de cette thèse sont introduits. À savoir, le système de co-manipulation hétérogène aérien/terrestre, appelé MAGMaS pour *Multiple Aerial-Ground Manipulator System*. Dans la section B.3, les motivations à l'origine d'un tel système sont détaillées et les principaux résultats de cette thèse sont présentés. Un travail mené en parallèle sur les actionneurs à impédance variable est passé en revu dans la section B.4. Celui-ci représente aussi une contribution dans le domaine des APhI. Enfin les principaux résultats de cette thèse et leurs implications sont synthétisés dans la section B.5.

B.1 Parardigmes de l'interaction aérienne physique

B.1.1 Contexte

Les recherches sur les aéronefs sans pilote (UAVs, pour *unmanned aerial vehicles*) ont connues de rapides développements dans les dernières décennies. Dans les développements suivants, l'accent sera mis sur les applications civiles et les micro aéronefs (MAV, pour *Micro Aerial Vehicle*), définis comme étant « assez petits pour être transporté et utilisé par une personne seule » (voir [Galinsky–2007]), ce qui en

(a) [NASA] (b) [Wikimedia Foundation] (c) [Wikimedia Foundation]

FIGURE B.1 – Divers plateformes MAV : de gauche à droite un aéronef à voilure fixe, un hélicoptère et un multi-rotor.

pratique ce traduit par un poids de 5 à 6 kg et une envergure d'environ 1.2 m, voir figure B.1.

Dans les dernières années, la chutes du prix des composants électroniques a rendu les MAV abordables pour tout type de recherches et d'applications industrielles. Résultant en une variété d'usages et de designs, tant pour les aéronefs à voilure fixe que ce à voilure tournantes. En particulier les services de secours et le domaine de l'agriculture sont intéressés par des applications de surveillance. La chute des prix a aussi permis la démocratisation des usages de loisirs comme la photographie aérienne et les courses de pilotage. Considérant le succès et les résultats de recherche pour les vols sans contact avec l'environnement, *e.g.*, [Mahony–2012] pour un tutoriel complet sur les multi-rotors, un nouveau thème de recherche sur l'interaction physique avec l'environnement (APhI, pour *Aerial Physical Interaction*) a émergé dans les 15 dernières années. Ce thème de recherche étudie les interactions physique avec l'environnement ; de la plus simple, comme pousser contre une surface, à de plus complexes, comme le transport ou la manipulation coopérative d'objets.

B.1.2 Interactions physique avec l'environnement

Le terme APhI regroupe toutes les interactions physique avec l'environnement. Les conditions pour rendre ses interactions possibles pour les MAV sont développées dans cette section. Deux tâches simples pouvant servir d'illustration sont la capacité à exercer des forces le long d'une surface ou à se percher, voir figure B.2. En Europe ces recherches sont encouragées par de nombreux projets ; AIRobots[1], ARCAS[2], AeroWorks[3] et Aeroarms[4].

Applications

Les applications d'APhI, non englobées par la manipulation aérienne (AM, pour *Aerial Manipulation*) détaillée dans la section suivante, consistent à se percher (*per-*

[1] http://airobots.dei.unibo.it/
[2] http://www.arcas-project.eu/
[3] https://www.aeroworks2020.eu/
[4] https://aeroarms-project.eu/

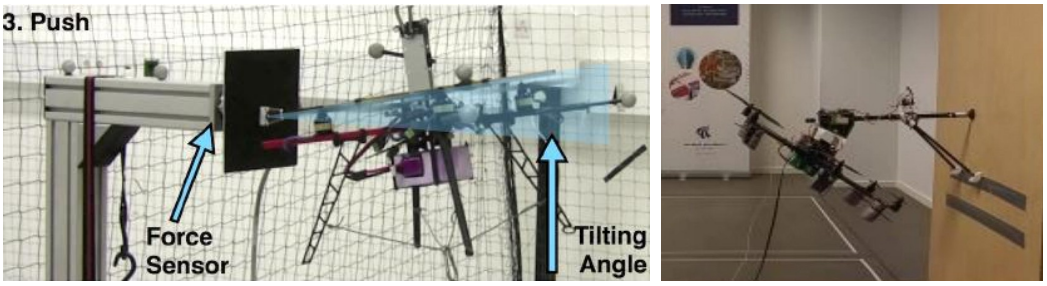

(a) [Gioioso–2014a] (b) [Wopereis–2017a]

FIGURE B.2 – Exemples d'interactions physiques avec l'environement : (a) poussée contre une surface et (b) perching sur un mur.

ching) quand un MAV s'attache temporairement à l'environnement, ou à exercer une force contre une surface, en poussant sur un point ou en glissant le long d'une surface tout en poussant. Les interactions au moyen de câbles sont aussi présentées.

Perching

Le perching est étudié dans le domaine de l'APhI, comme un moyen d'augmenter l'endurance des MAV. En effet, une fois perchés les MAV n'ont plus besoin de résister activement la gravité avec leurs hélices, réduisant ainsi leur consommation d'énergie. Le perching peut être utile pour les réseaux de capteurs, qu'il s'agisse de capteurs de température ou de caméras utilisées pour la surveillance de l'environnement, par exemple pour la surveillance des foules, ou comme relais radio dans un environnement post-catastrophe. Une autre utilisation de la manœuvre de perching est le rechargement de la batterie par énergie solaire, un MAV avec une batterie faible peut se percher et utiliser un panneau solaire pour recharger sa batterie avant de continuer la mission. Dans [Wopereis–2017a], les auteurs étudient le perching pour les multi-rotors, ils proposent un design mécanique pour se percher sur des murs verticaux. Les résultats présentés dans [Pope–2017] vont encore plus loin et proposent une solution pour se percher et grimper sur des surfaces verticales. Dans [Thomas–2016b] une manœuvre de vol agressive pour se percher sur une surface inclinée est étudiée. Des capacités de perching ont également été démontrées avec succès pour de petits avions à voilure fixe, comme dans [Mehanovic–2017] et [Desbiens–2011].

Application de force sur une surface

Une autre tâche souvent décrite dans la littérature des APhI consiste à exercer une force sur une surface, éventuellement le long d'une trajectoire et tout en suivant un profile de force. Cette description se traduit par une action de poussée où le but est d'exercer une force désirée sur un emplacement, soit pour réaliser une mesure via un capteur qui nécessite un contact (type ultrasons) ou soit pour appuyer sur un méca-

(a) [Elistair] (b) [Kondak–2009] (c) [Tognon–2016b]

FIGURE B.3 – APhI par câble : (a) solution commerciale pour une surveillance endurante, (b) transport de charge en collaboration et (c) exploitation du câble pour atterrir sur une surface en pente.

nisme de type interrupteur, ou d'exercer un force le long d'une trajectoire, pour la peinture en hauteur par exemple. Des exemples peuvent être trouvés dans [Gioioso–2014a] avec un contrôleur pour vol quasi-stationnaire utilisé pour exercer des forces 3D sur une surface verticale via un outil monté sur un mécanisme passif, dans [Ryll–2017] un MAV à poussée multidirectionnelle est utilisé pour l'inspection par contact de tuyaux, en appliquant une pression sur les points de mesure, dans [Yüksel–2017] un outil rigide est utilisé sur un plafond inégal ou dans [Alexis–2013] pour pousser sur une surface verticale avec un asservissement via un capteur de force. Un autre design intéressant est proposé dans [Papachristos–2014a], en mettant l'accent sur la force exercée sur la surface en réorientant les hélices. Une autre approche, proposée dans [Wopereis–2017b], pour appliquer une poussée sur l'environnement de magnitude comparables au poids du MAV repose sur le contrôle LQR.

Interactions par câbles

La dernière tâche APhI examinée consiste à relier un MAV au sol au moyen d'un câble. Ils peuvent être utilisés pour transporter de l'énergie ou des données en augmentant ainsi l'autonomie du MAV, voir figure B.3. De plus, le câble peut être utilisée pour améliorer les performances de vol, comme dans [Sandino–2014a], pour survoler ou pour guider l'atterrissage, ou dans [Sandino–2014b]. Et même d'effectuer des manœuvres impossibles sans cette attache, comme un atterrissage en douceur et en toute sécurité sur une surface inclinée [Tognon–2016b]. De telles applications sont désormais disponibles en tant que produit en France [5], avec comme application la surveillance de zone avec capteur visuel ou la surveillance de la qualité de l'air. Les câbles peuvent aussi être utilisés pour le transport collaboratif d'objets, voir [Kondak–2009].

[5] `http://elistair.com/`

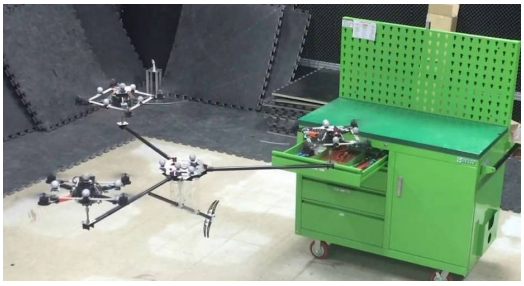
(a) [Nguyen–2015]


(b) [Mellinger–2010]

FIGURE B.4 – Exemples de manipualtion aérienne : (a) ouverture et fermeture d'un tiroir et (b) transport collaboratif d'une charge.

B.1.3 Manipulation aérienne

La manipulation aérienne (AM, pour *Aerial Manipulation*) fait partie des interaction avec l'environnement. Celle-ci regroupe toutes les tâches où un objet doit être transporté par un ou plusieurs MAV, voir figure B.4. Pour ce faire, des développements sont nécessaires tant sur le design mécanique des MAV, que sur leur contrôle et les mécanismes de coopération entre MAV. Ces thèmes sont passés en revue ci-après.

B.1.4 Designs mécaniques

Afin de rendre possibles les différentes tâches d'APhI de nombreux designs mécaniques ont été proposés. Nous nous concentrons sur les plateformes multi-rotor et leurs extensions en robot aérien (AR, pour *Aerial Robot*). Ces plateformes peuvent être séparées en deux grandes catégories, d'une part les designs à poussée unidirectionelle et d'autre part les designs à poussé multi-directionnelle Pour faire de ces plateformes des robots aériens, un manipulateur ou au moins un mécanisme de préhension doit être intégré sur le MAV.

Designs à poussée unidirectionnelle

Une conception dans laquelle tous les plans de rotation des hélices sont coplanaires. C'est le cas de la plateforme MAV la plus connue, le quadrotor planaire, constitué de quatre hélices réparties sur les sommets d'un rectangle (régulier ou non), toutes orientées dans la même direction. La simplicité de la conception mécanique se fait au détriment du sous-actionnement, *i.e.*, du couplage entre les dynamiques de translation et de rotation. L'orientation de la poussée dans l'espace est réalisé via des commandes différentielles pour les hélices. La simplicité et la robustesse de se design l'ont également rendu célèbre parmi les amateurs. Globalement, la conception est toujours bénéfique et est utilisée pour transporter des charges lourdes, par exemple un manipulateur à deux bras de 1.8 kg, comme dans [Suarez–2017a], ou des


(a) [Kondak–2014]

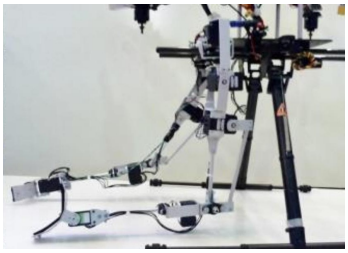
(b) [Suarez–2017a]


(c) [Danko–2015]

FIGURE B.5 – Différents types de manipulateurs aériens : (a) version industrielles à 7 DoFs, (b) manipulateur à doubel bras et (c) manipulateur parallèle monté sous un MAV.

capteurs, dans des appications non APhI, tels que l'ALTA8 de *Free Fly Systems* [6] capables de soulever une charge utile 9.1 kg pour un poids à vide 6.2 kg. Le modèle général du MAV multi-rotors est développé en profondeur dans la Sec. 3.2 de cette thèse, en mettant l'accent sur le cas colinéaire, et une stratégie de contrôle possible pour les APhI est détaillée dansla Sec. 4.2 de cette thèse.

Designs à Poussées Multidirectionnelle

Une tendance récente dans la conception des manipulateurs aériens est l'apparition de MAV totalement actionnés, ce qui signifie que leurs dynamiques de translation et de rotation sont complètement découplées (jusqu'aux limites d'actionnement). Les plates-formes entièrement actionnées sont également appelées plateforme à poussée multidirectionnelle, leur poussée pouvant être orientée dans plusieurs directions. Ces plateformes peuvent suivre des trajectoires arbitraires dans $SE(3)$. Mais plus important encore, aucun changement d'orientation n'est nécessaire pour exercer une force latérale, elles peuvent résister à des perturbations externes tout en suivant une trajectoire dans $SE(3)$. Pour garantir l'actionnement total, la conception mécanique impose une disposition non colinéaire des hélices. De ce fait, l'actionnement total génère des forces internes, qui se traduisent par une perte d'efficacité énergétique. Pour arriver à un tel design, on peut choisir de partir d'une structure sous-actionnée bien connue et de la modifier, comme le travail présenté dans [Rajappa–2015] [Ryll–2017] sur les hexarotors. Un autre travail dans ce sens est présenté dans [Brescianini–2016], où une configuration à huit rotors qui maximise l'agilité du véhicule dans n'importe quelle direction est dérivée basée sur une analyse de force statique et de couple pour des configurations d'actionneur génériques.

Manipulateurs Aériens

Afin de mettre en œuvre les AR, il est nécessaire d'adjoinde aux plateformes volantes un manipulateur qui soit à la fois léger (pour être emporter) et capable de

[6] `http://freeflysystems.com/alta-8/specs`

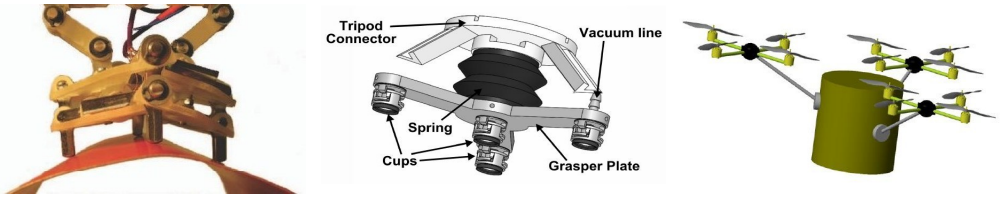

(a) [Gawel–2017] (b) [Kessens–2016] (c) [Mohammadi–2016]

FIGURE B.6 – Different prehensors for AM: (a) magnetic mechanism to grasp non flat ferrous objects, (b) vacuum based prehensor working with an airborne pump and (c) swarm grasping of a cylindrical object.

déplacer une charge suffisante pour être utile. L'idée principale est qu'un manipulateur augmente la dextérité des AR pour les tâches de manipulation, compensant éventuellement pour les plateformes sous-actionnées. Dans la littérature, plusieurs approches différentes sont proposées, voir figure B.5. De grandes catégories, selon le type de manipulateurs, peuvent être retrouver dans la littérature. Les manipulateurs à actionnement au niveau de leurs articulations, qui sont les manipulateurs standard de la robotique simplement monté sous un MAV, par example dans [Kondak–2014]. Les manipulateurs à actionnement déporté (généralement au niveau de leur base), qui utilisent des système de courroies de manière à réduire le moment que génère leur poids sur le MAV. Les manipulateurs parallèles, qui par leur simplicité mécanique et leur actionnement à la base peuvent permettre à un AR d'accomplir des tâches de précisions, voir [Danko–2015]. Les manipulateurs passifs, qui peuvent être utilisés dans certain tâches où le manipulateur ne doit pas nécessairement être actionné. En particulier on peut considérer que pour tous les designs où des câbles sont utilisés pour transporter une charge, ces câbles sont des manipulateurs passifs. Les manipulateurs compliants, qui possèdent une composante élastique, à rigidité variable ou non, qui assure une compliance mécanique en cas de collision avec l'environnement. Les manipulateurs à bras multiples, typiquement deux, qui utilisent plusieurs bras pour augmenter leur dextérité, *e.g.*, dans [Suarez–2017a]. Enfin, certains designs ne comporte pas de manipulateurs à proprement parler mais une extension rigide sur laquelle est fixé une mécanisme de préhension ou avec laquelle l'AR interagit avec l'environnement.

Mécanismes de préhension

Finalement afin de réaliser des tâches de manipulation aérienne, il est nécessaire d'équiper les AR de capacités de préhension. Quelques exemples présentés dans la littérature sont décrit dans la figure B.6. Dans la littérature sur la manipulation aérienne quatre grandes catégories de mécanismes de préhension peuvent être distinguées. Les pinces mécaniques, qui sont les préhenseurs classique de la robotique, composées de doigts qui se referment autour d'un objet. Les préhenseurs utilisant le phénomène de succion, que se soit avec des ventouses ou des pompes créant un vide,

e.g., [Kessens–2016]. Les préhenseurs magnétiques, qui permettent d'agripper des objets ferreux, voir [Gawel–2017]. Et enfin les un mécanisme de préhension reposant sur la coopération de plusieurs AR, qui s'associent pour créer un main volante comme dans [Mohammadi–2016].

B.1.5 Contrôleur géométrique de pose

Le contrôle géométrique des MAV vise à stabiliser le système en vol sans contact (*free-flight*) et à permettre un suivi de trajectoire. La pose du MAV est composée par une position dans $\mathbb{R}^3$ et une rotation de 3-DoF, la pose se trouve donc dans le groupe euclidien spécial $SE(3)$. Dans la littérature, plusieurs représentations d'orientation différentes sont présentes ; *i)* les angles d'Euler prédisposés au blocage de cadran (*Gimbal Lock* en anglais), voir [Mistler–2001] [Spedicato–2016], *ii)* les quaternions ayant une représentation redondante de $SO(3)$, voir [Mayhew–2011], et *iii)* les matrices de rotation qui ne souffrent pas des deux inconvénients précédents mais sont une représentation non compacte, voir [Lee–2010]. La première approche dans la littérature consiste à appliquer des techniques de synthèse classiques à un modèle linéaire approximatif de la dynamique du MAV. Dans [Castillo–2005], le contrôleur linéaire stabilise séquentiellement la poussée puis l'orientation, cette approche séquentielle est également utilisée dans [Spedicato–2016].

Le besoin d'améliorer les performances et la manœuvrabilité a conduit à l'utilisation de stratégies de contrôle non linéaires. Elles s'appuient sur une linéarisation par *feedback dynamic*, voir [Mistler–2001], pour amener le système sous une forme linéaire où des techniques de contrôle linéaire peuvent être appliquées. Dans [Raffo–2010], une approche basée sur le contrôle prédictif du modèle et un contrôleur $\mathcal{H}_\infty$ sont proposés comme stratégie de contrôle robuste non linéaire. Un contrôleur de suivi non linéaire populaire est développé sur le groupe euclidien spécial $SE(3)$ in [Lee–2010], avec l'assurance d'une stabilité quasi globale. Les approches de contrôle non linéaires sont généralement plus gourmandes en calcul, ce qui peut poser problème pour le déploiement intégré. Mais de nos jours, les petits ordinateurs, tels que ceux de la série intel NUC[7], sont assez puissants pour exécuter des algorithmes de commande prédictive et un problème d'optimisation supplémentaire en temps réel, voir *e.g.*, [Baca–2016].

B.1.6 Contrôleur de force

Pour effectuer une tâche d'APhI sûre, le contrôle de suivi de trajectoire n'est pas suffisant et des stratégies de contrôle supplémentaires concernant l'interaction de force sont nécessaires. En effet, dans de telles applications, il est nécessaire pour l'AR d'exercer certaines forces et certains couples sur l'environnement, tout en maintenant un vol stable. Une technique classique repose sur un contrôleur d'admittance/impédance comme dans [Augugliaro–2013] et [Lippiello–2012] [Gioioso–2014a] [Ruggiero–2014] pour l'impédance. D'autres approches reposent sur des consi-

[7] `https://www.intel.com/content/www/us/en/products/boards-kits/nuc.html`

dérations énergétiques. Par exemple, dans [Mersha–2011] en s'appuyant sur la modélisation port-Hamiltonienne et le bond graph, ou [Yüksel–2014b] en s'appuyant sur un schéma de contrôle basé sur la passivité (IDA–PBC).

B.1.7 Estimation des forces externes

Comme indiqué plus haut et détaillé dans le Chapitre 2 de cette thèse, la connaissance de la force exercée sur l'environnement par l'AR est primordiale pour obtenir un contrôle précis de la force d'interaction. De plus, cette information peut également être utilisé en vol libre pour compenser des perturbation externes telles que le vent ou une collision. Pour les raisons développée dans Sec. 2.4.3 de cette thèse, les méthodes d'estimation sont préférées aux capteurs d'efforts. Pour rappel *i)* le rapport entre les performances et le poids/la compacité, *ii)* le fait que les mesures soient localisées et *iii)* le coût, Les capteurs d'efforts 6D ne peuvent pas être intégrés sur des multi-rotors d'entrée et de milieu de gamme. Certains travaux explorent la combinaison d'interrupteurs simples avec la reconstruction de forces basée sur des modèles, *e.g.*, [Rajappa–2017] ou considèrent un mécanisme de mesure de force plus simple, le long d'une unique direction. Ceux-ci résolvent les inconvénients de coût et de poids, mais pas le problème soulevé par les mesures localisées. Cela conduit à choisir des approches basées sur des estimateurs, qui dépendent fortement du modèle du système et de la connaissance de l'effort exercé par la poussée de l'hélice. Ensuite, sur la base du modèle du système, de ses états courants et de la force exercée, il est possible de dériver les forces externes auxquelles l'AR est soumis. La partie essentielle ici est de déterminer la poussée (*thrust*) et le couple de traînée (*drag*) générés par les hélices. Les exigences pour un tel observateur sont *i)* une faible charge de calcul et *ii)* une reproductibilité aisée. Les modèles utilisés dans le processus d'estimation doivent rester aussi simples que possible pour limiter les coûts de calcul tout en capturant toutes les dynamiques essentielles du système afin de produire une estimation fiable. Une fois les modèles définis, leur estimation des paramètres doit être hautement reproductible pour pouvoir être effectuée rapidement après toute modification des systèmes.

B.2 Estimation de force

Dans cette section une solutions pour l'estimation de la force générée par les hélices est introduite, une basée sur l'identification du modèle, pour plus détails voir Sec. 4.4 de cette thèse.

B.2.1 Approche par identification de modèle

Le travail décrit dans cette partie a été présenté à
2015IEEE Int. Conf. on Robotics and Automation [Staub–2015]

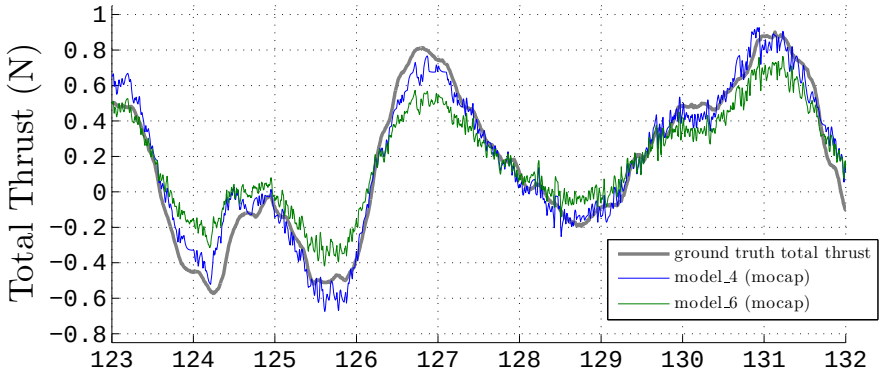

FIGURE B.7 – Comparaison de deux modèles ; l'un incluant la batterie (modèle 6) et l'autre non (modèle 4). Les deux modèles ont le même nombre de paramètres, celui contenant la batterie présente de meilleurs performances.

Cette section présente des travaux préliminaires menés sur l'estimation de la force externe, dans lesquels une nouvelle classe de modèles pour la génération de poussée totale par les MAV à plusieurs rotors est proposée et validée expérimentalement. Cette méthode s'intéresse aux plates-formes à moteurs coplanaires d'entrée et de milieu de gamme, pour lesquelles les capacités sensorielles et de calcul sont limitées. Cette méthode est originale dans le sens où elle diffère des modèles typiques en supposant qu'elle contrôle instantanément la vitesse de rotation du rotor, négligeant ainsi la dynamique des hélices en rotation et de leur moteur associé. Dans la classe de modèles proposée, on considère que la poussée totale a sa propre dynamique et que sa valeur finale dépend explicitement à la fois des commandes (*pseudo-setpoint*) données au contrôleur et de la mesure de la tension des bornes de la batterie. Les différentes instances du modèle sont comparées au sein de la classe en utilisant un dispositif expérimental dans lequel la poussée totale est précisément mesurée en utilisant un système de capture de mouvement comme vérité de terrain, plutôt que des capteurs de force. Les résultats expérimentaux montrent que l'utilisation d'un modèle dynamique incluant également la tension de la borne de la batterie améliore considérablement la capacité de prédiction du modèle en termes de précision, voir figure B.7. Enfin, les résultats expérimentaux montrent comment le modèle proposé peut être identifié en utilisant uniquement des mesures d'accélération embarquées, obtenant une précision étonnamment bonne par rapport à la vérité terrain. L'utilisation du modèle proposé permet une meilleure estimation de la force produite par le MAV, rendant ainsi possible un contrôle de trajectoire plus fin et ouvrant la possibilité d'estimer les forces externes s'appliquant sur le MAV.

B.3 MAGMaS un nouveau système de manipulation

Le travail décrit dans cette partie a été présenté à
2017IEEE Int. Conf. on Robotics and Automation [Staub–2017]
2018IEEE Int. Conf. on Robotics and Automation [Staub–2018]
Et a été accepté pour
Robotic and Automation Magazine [Staub–]
2018 IEEE/RSJ Int. Conf. on Intelligent Robots and Systems [Yang–2018]

L'idée d'un système de manipulation composé de multiples manipulateurs terrestre et aérien (MAGMaS pour *Multiple Aerial-Ground Manipulator System*) provient de l'analyse des limites pratiques des manipulateurs terrestre et aériens. Les MAGMaS sont une solution simple – et encore inexplorée – pour atténuer leurs inconvénients respectifs, car les deux types sont combinés dans un système unique.

Typiquement, pour la manipulation robotisée d'objets, deux approches sont étudiées indépendamment, d'une part l'utilisation de manipulateurs terrestre (potentiellement mobiles) et d'autre part l'utilisation d'AR. La riche littérature sur les manipulateurs terrestre propose des cas d'utilisation avec des systèmes robotiques simples ou multi-robots pour la manipulation d'objets, en particulier pour le transport coopératif [Dumora–2013] [Cehajic–2017a] [Machado–2016] [Dumora–2012], ou la surveillance et manipulation robotique sur des plateformes off-shore [Pfeiffer–2011], ou pour un assemblage coopératif.

Cependant, deux inconvénients majeurs à l'utilisation de robots terrestres peuvent être identifiés. Premièrement, les petits manipulateurs industriels classiques ont des limites de couple de joint relativement basses, ce qui se traduit par un couple Cartésien admissible maximal médiocre au niveau de l'EE. Deuxièmement, les manipulateurs terrestre, mobiles ou non, ont un espace de travail assez restreint autour de leur base, empêchant leurs possibilités de manipulation, notamment dans le sens vertical. Cela peut s'avérer particulièrement problématique pour les manipulations d'objets longs. En effet, si le manipulateur terrestre ne peut pas les saisir par leur CoM en raison des limitations de l'espace de travail, la manipulation nécessiterait un manipulateur capable de générer d'important couple au niveau de son EE. De plus, la manipulation d'objets longs est souvent sujette à une manœuvre de reprise afin de surmonter les limitations de l'espace de travail, ce qui nuit aux performances d'exécution.

Une approche qui gagne en notoriété consiste à utiliser des AR pour la construction et la manipulation de grandes charges. Leur utilisation a été démontrée en tant que groupe pour transporter des charges via câbles dès 2009 dans [Kondak–2009], afin répartir la charge globale entre les membres. Une utilisation intéressante et récente de AR se retrouve aussi dans la construction ou l'assemblage multi-robot [Augugliaro–2014] [Lindsey–2012] [Kim–2013] et [Suarez–2015b]. Un inconvénient majeur de ces plates-formes est la plage d'actionnement limitée, qui se traduit par une capacité de charge utile limitée.

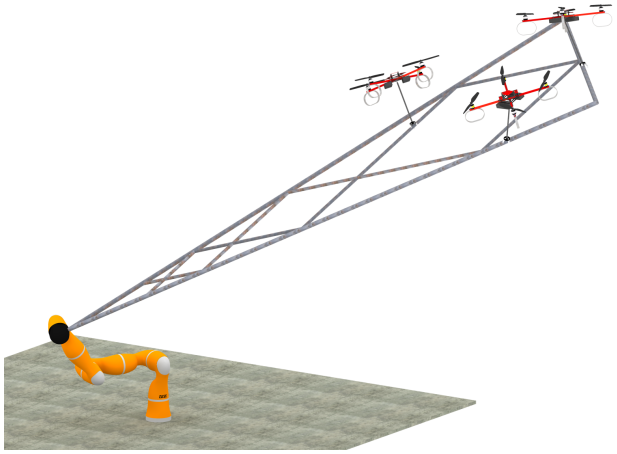

FIGURE B.8 – Vue schématique d'un MAGMaS composé d'un manipulateur terrestre (7 DoF) et de trois AR sous-actionnés, attachés au chargement via des liaisons rotules.

L'originalité de l'approche MAGMaS est de considérer un système multi-robot *hétérogène* composé à la fois de manipulateurs terrestres et aériens, voir figure B.8, pour balancer leurs défauts individuels [Staub–2017]. La faible charge utile d'un AR est compensée par la force du manipulateur terrestre, tandis que l'espace de travail limité et le faible couple au niveau de l'EE du manipulateur terrestre sont compensés par l'espace de travail pratiquement illimité et le levier favorable fourni par les AR. Grâce à leur grand espace de travail, les AR peuvent exercer une force sur la charge afin de réduire le couple induit à l'EE du manipulateur terrestre par le poids de la charge. Dans ce système, les AR peuvent agir en tant que *Compagnons Volants* en aidant le manipulateur terrestre à transporter de longues charges en les saisissant à une autre extrémité et en atténuant le couple généré, permettant ainsi la manipulation de charges d'une manière *coopérative*.

Un autre avantage résultant de l'utilisation de compagnons volants est l'amortissement des oscillations dans la charge transportée. Grâce aux AR, les oscillations de la charge peuvent être supprimées via une stratégie d'asservissement.

B.3.1 Apllications

La manipulation d'objets longs est une tâche courante pour les systèmes robotiques, par exemple pour la construction d'échafaudages ou de tours de transmission, la maintenance d'installations comprenant un réseau de tuyauterie important, telles que des usines de produits chimiques ou des raffineries. Ce sont des exemples où les MAGMaS pourraient être utilisés pour des tâches de type construction, voir figure B.9. Un autre type de tâches identifiées pour les MAGMaS, est leur utilisation pour étendre la portée du manipulateur, utilisant une longue barre (actionné par l'AR) comme dernier lien du bras robotique. Avec pour applications des opérations

(a) (b)

FIGURE B.9 – Cas d'utilisation potentiels pour MAGMaS de composition différente. Reste (a) dans un scénario USAR avec une base mobile et un AR sous-exploité nettoyant les buldings. Droite (b) dans un scénario de mise hors service avec un robot terrestre fixe et une poussée multidirectionnelle manipulant un tube en coopération.

en hauteur, telles que la peinture, le perçage ou le changement d'ampoule. Enfin, un dernier type d'opération identifié pour les MAGMaS se déroule dans des environnements non structurés et consiste à nettoyer des ruines après une catastrophe, par exemple un séisme, où les vestiges de constructions sont souvent des pièces et des structures aux formes complexes. Cette application de recherche et secours en milieu urbain est appelée USAR et est illustrée en figure B.9a

L'intérêt pour la solution robotique est motivé par le niveau de danger pour l'homme. Les tâches de manipulation décrites peuvent avoir lieu dans des environnements potentiellement dangereux tels que, mais sans s'y limiter, *i)* après une catastrophe naturelle ou humaine, par exemple une catastrophe post-séisme ou industrielle, où la vie des sauveteurs est menacée par l'effondrement potentiel des structures, *ii)* en haute altitude ou isolés, comme les sites de construction de montagne, les camps du pôle Sud ou les plates-formes off-shore, où les risques sont multipliés pour les travailleurs en raison de l'accès limité aux soins médicaux, et *iii)* environnements contenant des radiations dues à des activités nucléaires, *e.g.*, démantèlement de centrales nucléaires. Certains de ces environnements sont également dangereux pour la plateforme, comme décrit dans le chapitre 5 de cette thèse, et leur utilisation nécessiterait un durcissement supplémentaire du système, tel que la conformité aux normes ATEX (pour atmosphères explosives) ou un durcissement aux rayonnement pour les environnements nucléaires.

Parmi les applications présentées, la plus prometteuse est le démantèlement des centrales nucléaires pour des MAGMaS entièrement autonomes, notamment parce que les centrales nucléaires sont un environnement hautement structuré, ce qui simplifie les exigences de perception.

B.3.2 Design du système, de son architecture et implementation

Le MAGMaS présenté dans cette section est composé de trois composants robotiques principaux : *i)* le bras LBR-iiwa (*"Leichtbauroboter – intelligent industrial*

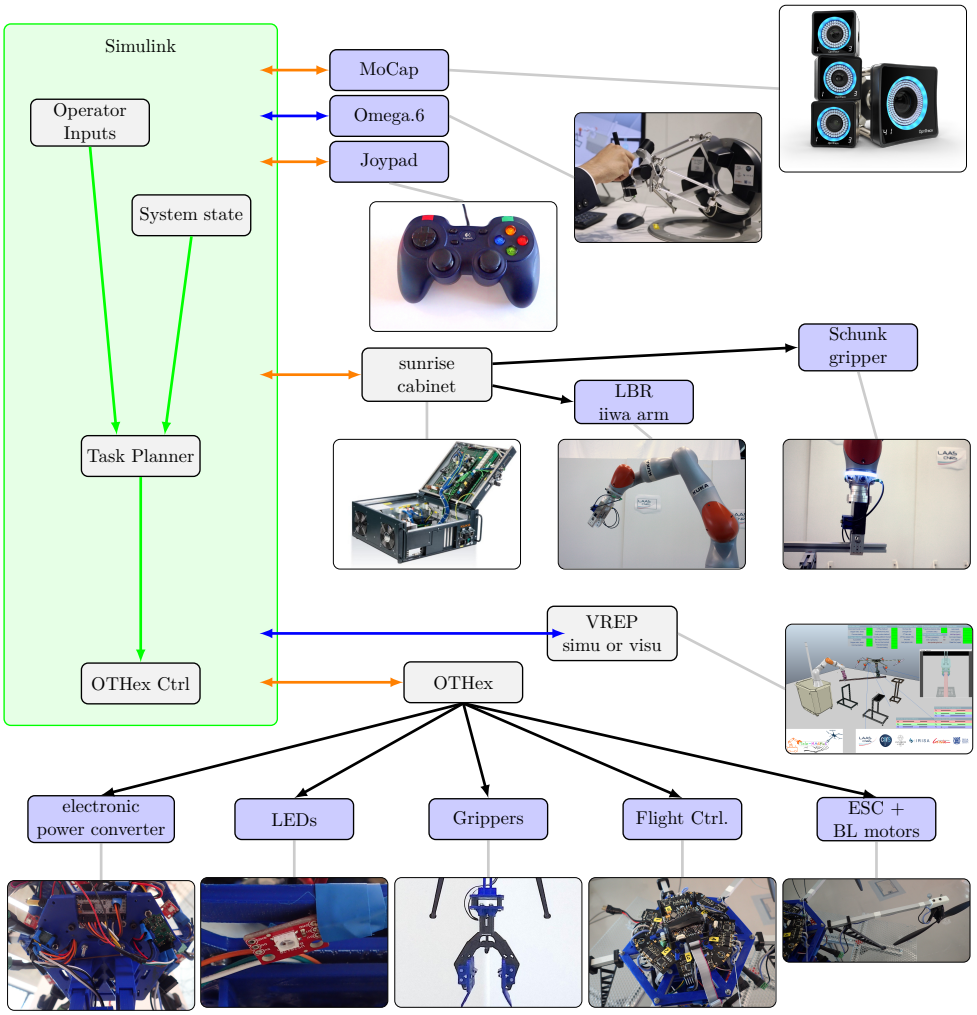

FIGURE B.10 – Description de l'architecture logicielle utilisée dans le projet Tele-MAGMaS, première implémentation et démonstration du concept de companion aérien. Sont représentés en vert les connexions Matlab-Simulink, en bleu les connexions via S-fonction (en C), en orange les connexions via Genom3 et en noir les connexions bas niveau.

work assistant" pour robot léger et cobot industriel intelligent) ; *ii)* le manipulateur aérien OTHex, développé spécialement pour ce projet et *iii)* l'interface haptique Omega.6, une composante nécessaire pour la partie télé-présence. De plus, un simulateur et un visualiseur ont été développés pour faciliter l'intégration du système et fournir un retour visuel à l'opérateur.

Le système expérimental s'appuie sur la couche d'abstraction Genom3[8], qui permet de définir des composants logiciels pour la robotique, indépendamment du middleware qui peut être choisi au moment de la compilation. Les composants

[8] `https://git.openrobots.org/projects/genom3/wiki`

Genom3 peuvent être contrôlés de diverse manières ; script tcl-shell, script Matlab, Matlab-Simulink ou plusieurs middleware (ROS, Pocolibs, Orocos), ce qui permet une grande flexibilité dans le développement et l'utilisation des composants.

L'architecture du logiciel est illustrée dans la figure B.10. Le contrôle de haut niveau du système complet est implémenté dans Matlab-Simulink, qui est lié aux composants matériels via des modules Genom3 ou des pilotes sous forme de S-fonctions Matlab. Cette approche a été choisie car le développement et le test du contrôleur dans Matlab-Simulink peuvent être beaucoup plus rapides qu'en C/C++ pur, par contre Matlab-Simulink est loin d'être temps réel, donc le contrôle bas-niveau du matériel doit être réalisé par des composants Genom3 ou des S-fonctions Matlab, qui sont codée en C.

Dans l'architecture proposée, la partie Matlab-Simulink s'exécute à 500 Hz. Le planificateur de tâche/trajectoire, l'interpréteur des entrées humaines et le contrôleur pour l'OTHex s'exécutent dans Matlab-Simulink. Le processus Matlab-Simulink est lié au périphérique haptique via une S-fonction personnalisée et au simulateur/visualiseur via d'autres S-fonctions. Le Matlab-Simulink est également interfacé avec le sous-systèmes suivants : joystik, Optitrack MoCap, la partie physique de l'OTHex et les composants du LBR-iiwa via Genom3. Ces composants Genom3 sont essentiellement des pilotes pour le matériel, car la majorité de la partie algorithmique est implémentée dans Matlab-Simulink. À l'exception des composants LBR-iiwa, en effet, pour satisfaire aux contraintes de temps réel de la communication avec le LBR-iiwa, la cinématique inverse et d'autres fonctions utilitaires associées sont exécutées dans un composant Genom3.

En outre, cette architecture à base de composants permet de répartir facilement la charge entre les processus et les machines. Dans les expériences présentées, ROS est choisi en tant que middleware, qui fournit suffisamment de «temps réel» pour le but recherché. La conception basée sur les composants permet également un changement aisé des entrées d'interface pour l'opérateur, des composants de perception ou du matériel composant le MAGMaS, chacun étant séparé de la partie algorithmique principale et fournissant des interfaces standard qui ne sont pas spécifiques au matériel.

B.3.3 Résultats expérimentaux

Une série d'expériences a été réalisée avec une co-manipulation réussie d'une barre longue de 2.5 m. La tâche souhaitée consiste à soulever, en coopération, une barre comme illustré dans figure B.11, l'OTHex est piloté manuellement pour saisir la barre à l'une de ses extrémités, tandis que le robot manipulateur terrestre se saisit de manière autonome de l'autre extrémité. Une fois que les deux manipulateurs ont saisi la barre, la co-manipulation est totalement autonome, ils soulèvent la barre de ses supports, la déplacent deux fois le long d'une ligne dans le plan horizontal puis la soulèvent à 30°. Ensuite, les deux manipulateurs ramènent la barre à sa position de départ.

La séquence de l'expérience est représentée dans la figure B.11 et [video 6–2017],

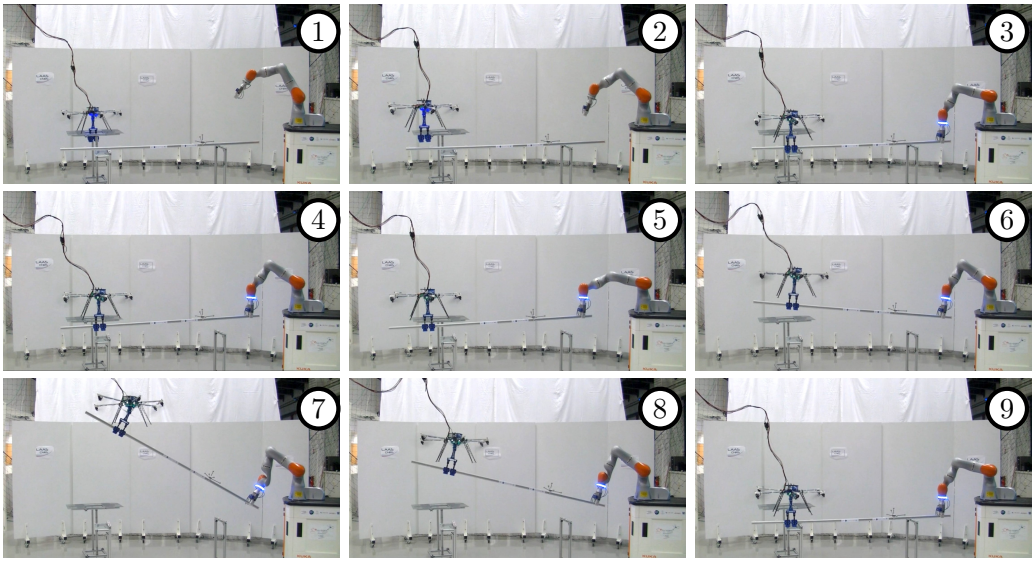

FIGURE B.11 – Séquence d'une tâche de manipulation coopérative réalisée par un MAGMaS. Les deux robots sont dans leur position initiale (1), approchent de la barre (2), saisissent de la barre (3), lèvent la barre en coopérant (4), déplacent la bar latéralement (5), lèvent la barre de manière synchronisé jusqu'à 30° (6-7-8) et reposent la barre sur ses supports (9). La vidéo correspondante de l'expérience est disponible à [video 6–2017].

ce qui met en évidence à la fois la stabilisation des vibrations induite par le OTHex et la faisabilité du MAGMaS.

Prix de l'innovation KUKA "KUKA Innovation Award" Le concept de Tele-MAGMaS a été présenté avec succès lors de la foire de Hanovre en 2017, en tant que finaliste du Prix de l'innovation KUKA 2017 Innovation Award. À cette occasion le Tele-MAGMaS a enchaîné des démonstrations devant les industriels du monde entier. Démontrant la robustesse et la fiabilité du système, en effectuant des démonstrations en dehors d'un environnement de laboratoire et jusqu'à 10 fois par jour pendant une semaine. Au cours de cette démonstration, le système était à la fois télécommandé et autonome pour illustrer les deux modalités de notre architecture. En raison de contraintes d'espace, la barre manipulée était significativement plus courte que dans l'expérience conduite au LAAS–CNRS. Des vidéos mettant en évidence les principales caractéristiques de la démonstration sont disponibles en ligne [video 4–2017] et [video 5–2017].

B.3.4 Étude de la fléxibilité dans les MAGMaS

L'intérêt pour l'étude de la flexibilité dans les MAGMaS est venu de l'observation suivante, dans la manipulation d'une barre part une de ses extrémités l'autre ex-

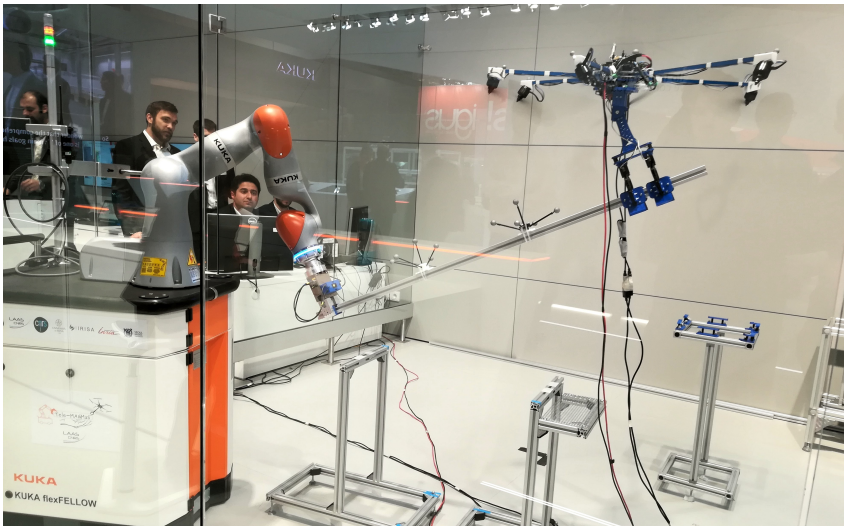

FIGURE B.12 – Illustration de la manipulation coopérative par un Tele-MAGMaS effectuée durant le Prix de l'innovation KUKA 2017 Innovation Award à la Foire de Hanovre, avec 4 opérateurs en arrière-plan.

trémité est affectée par des mouvements parasites induits par la flexibilité. Dans le cas des MAGMaS ses mouvements peuvent être supprimés par les AR. En pratique, les expériences préliminaires sur les MAGMaS ont également montré que la flexibilité de la barre peut être atténuée par un AR. Pour comprendre la racine de ce phénomène, une modélisation 2D d'un MAGMaS et de la flexibilité a été réalisée. Cette étude exploratoire sur la flexibilité des MAGMaS présente des propriétés intéressantes du système, qui doivent être testées dans de futures simulations et expériences. La modélisation de la flexibilité dans la barre manipulée par un MAGMaS a permis d'exposer la contrôlabilité des modes de vibration à partir d'une analyse théorique. Ce qui valide les observations empiriques faites lors des expériences sur les MAGMaS présentées dans le chapitre 5 de cette thèse.

B.4 Actionneur à impedance variable

Le travail décrit dans cette partie a été présenté à
2016 IEEE/RSJ Int. Conf. on Intelligent Robots and Systems
[Yüksel–2016b] [Yüksel–2016c]

Cette section se concentre sur l'utilisation prometteuse mais confidentielle des actionneurs à rigidité variable (VSA pour *Variable Stiffness Actuator*) pour les tâches d'APhI. En effet, dans presque tous travaux disposnibles, AR sont équipés de bras à joints rigides. D'autre part, les manipulateurs à actionneurs compliants (*i.e.*, à faible rigidité) sont de plus en plus largement étudiés pour les robots terrestres comme les humanoïdes et les manipulateurs interagissant physiquement avec les

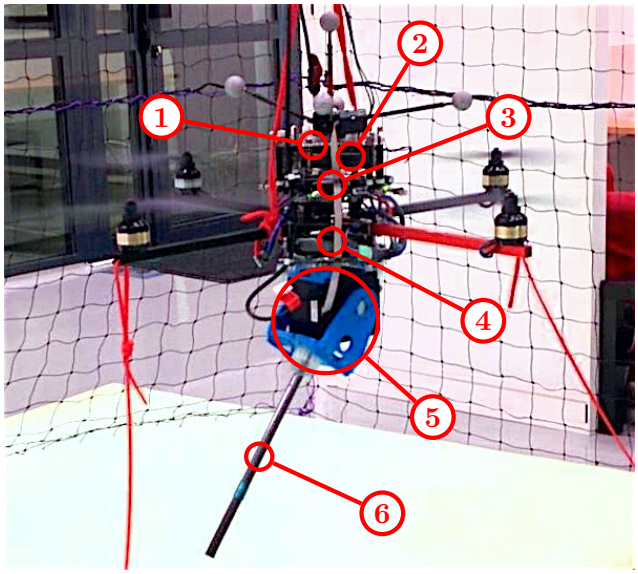

FIGURE B.13 – Configuration expérimentale composée ; d'un quadrotor Mikro-Kopter actionné et d'un bloc qbmove, solution commerciale, de VSA. Les sous-composants de la plateforme sont:(1) contrôleur de vol (incl. IMU), (2) l'odroid exécutant le contrôleur, (3) les ESC, (5) le qbmove lui-même et (6) le lien du manipulateur dirrectement connecté à la sortie du VSA. Les câbles rouges ne sont utilisées que pour des raisons de sécurité, sans être tendus.

humains, voir le projet européen SaPHARI[9]. Ils sont également des outils efficaces pour les tâches de mouvement rapide, exploitant l'élasticité de l'articulation pour effectuer des tâches explosives, comme lancer un objet ou frapper sur une surface, ce qui nécessite de grandes vitesses qu'un bras à joints rigides ne peut pas atteindre [Braun–2013].

Cependant, leur utilisation dans la robotique aérienne et les APhI n'est quasiment pas étudiée. Les travaux récents ont commencé à envisager l'utilisation de l'élasticité pour les AR, comme par exemple [Yüksel–2015] pour un seul manipulateur et [Suarez–2015b][Suarez–2017b] pour manipulateur à double bras.

En particulier, dans le cas de APhI, la possibilité de variée la rigidité peut être exploitée pour le mouvement explosif mais aussi et surtout pour assurer la compliance mécanique du manipulateur aéroporté. En effet, en utilisant le réglage de la rigidité, il est possible d'imposer un comportement très rigide au manipulateur, généralement pour les tâches où un positionnement précis de l'EE est nécessaire, *e.g.*, le ramassage d'objets, tandis qu'un comportement compliant peut être utilisé en cas de mouvement dans un environnement inconnu ou non structuré. Dans ce cas, les effets d'une collision imprévue peuvent être atténués par le comportement compliant du bras. Cela signifie que si le bras entre en collision avec l'environnement, une partie substantielle de la force d'impact sera stockée dans la partie élastique de

[9] `http://www.saphari.eu/`

l'actionneur à rigidité variable au lieu d'être appliquée directement sur la base du MAV, cette propriété mécanique réduit considérablement le taux de défaillance du système. Enfin, en introduisant la souplesse mécanique, le VSA devrait représenter un niveau de sécurité supplémentaire pour les interactions homme-robot. L'implémentation de VSA sur des MAV se heurte à deux défis principaux, *i)* le design mécanique et *ii)* l'analyse et la synthèse d'un contrôleur performant.

Dans le chapitre 6 de cette thèse, nous présentons la modélisation dynamique, l'analyse des propriétés et le contrôle d'un AR équipé d'un seul bras élastique, voir figure B.13. Il a été prouvé que ce système est plat (*flat*) pour un ensemble de sorties, qui sont les mêmes que pour un joint rigide, voir [Yüksel–2016b], et un contrôleur de suivi de trajectoire basé sur la linéarisation exacte par feedback est fourni. Des tests numériques complets, fournis dans [Yüksel–2016c], montrent des différences nettes entre les modèles de joints rigides et élastiques, la configuration par liens rigides est plus avantageuse pour le suivi précis de tâches telles que la saisie d'objets, tandis que les liens élastiques sont plus avantageux pour les tâches nécessitant une amplification de vitesse tel que le lancer ou le martelement. Une autre validation numérique a été effectuée à l'aide du modèle 3D complet de la configuration réelle dans SimMechanics, et des résultats expérimentaux préliminaires de contrôle d'un quadrotor équipé d'un qbmove sont présentés. En fait, un compromis clair entre les configurations à liaison rigide et à liaison élastique nous oblige à utiliser un VSA pour une large gamme de tâches d'interaction physique aérienne.

Ce travail est un pont entre les expériences antérieures [Yüksel–2015] et de futures études sur l'extension de l'utilisation de VSA pour la manipulation aérienne, qui comprendront : *i)* d'autres expériences utilisant la plateforme expérimentale, *e.g.*, lancer, marteler ; *ii)* une extension de la théorie en 3D et/ou à des bras à plusieurs degrés de liberté, voir [Yüksel–2016a] pour des résultats préliminaires intéressants ; *iii)* l'utilisation de méthodes d'étalonnage basées sur des capteurs comme *e.g.*, in [Censi–2013] pour récupérer les paramètres du VSA à la volée.

B.5 Conclusion et panorama de la thèse

B.5.1 Conclusion

De nos jours, les MAV sont une technologie bien développée accompagnée de divers succès commerciaux pour le grand public, allant de l'inspection visuelle aux courses de loisirs. La prochaine frontière pour la robotique aérienne est symbolisée par les APhI, qui se caractérise par la capacité d'interaction physique avec l'environnement pour les MAV. Ceci ouvre la voie à de nombreuses applications. Les recherches sur les APhI et la manipulation aérienne sont encouragées par des projets européens et d'autres initiatives nationales conduisant à une littérature riche à la fois de designs mécaniques originaux et d'algorithmes de contrôle intelligents. Le travail présenté dans cette thèse est basé sur une vision des AR comme potentiel *Compagnons Volants* pour la manipulation coopérative avec des humains et d'autres robots. L'apport principal de cette thèse consiste à proposer un nouveau concept

de manipulation coopérative, MAGMaS composé de manipulateurs terrestres et aériens. En combinant ces deux types de manipulateurs différents, pour atténuer leurs inconvénients respectifs, les MAGMaS ouvrent une nouvelle voie de recherche avec de nombreuses applications possibles. Ce travail de thèse a jeté les bases de la théorie pour les MAGMaS et a démontré, grâce à des expériences, leur faisabilité et leur potentiel de percée dans le monde réel. En particulier, la toute première manipulation coopérative entre un manipulateur terrestre et un manipulateur aérien a été présentée à la foire de Hanovre 2017. Dans ce qui suit, un aperçu du contenu et des contributions par chapitre est donné.

B.5.2 Panorama de la thèse

Le premier chapitre de cette thèse présente les contributions et l'organisation de cette thèse.

Dans le chapitre 2, les paradigmes de l'APhI sont passés en revue. Différentes techniques, méthodes et designs mécaniques sont présentés, afin de contextualiser le travail de cette thèse.

Dans le chapitre 3, les motivations à l'origine du concept de MAGMaS sont décrites. À partir de l'examen des solutions de manipulation existantes, il est apparu que les manipulateurs terrestre souffrent souvent d'un espace de travail limité autour de leur base et les intensités de leurs couples d'actionnement sont faibles, mais possède une charge utile et une autonomie énergétique satisfaisantes. Ces limites des manipulateurs terrestres peuvent être atteintes lors de la manipulation d'objets longs : pour satisfaire aux contraintes de couple, la saisie doit être proche du centre de masse de l'objet, ce qui entre souvent en conflit avec les limites l'espace de travail. D'autre part, les AR, qui ont un espace de travail pratiquement infini, souffrent d'une limitation de leur charge utile et d'autonomie. Le concept de MAGMaS cible la manipulation coopérative des objets longs et propose de combiner les manipulateurs terrestres et les AR pour atténuer leurs inconvénients respectifs. En particulier, l'ajout d'un compagnon volant au manipulateur terrestre permet de *i)* réduire le couple à l'EE et *ii)* supprime les vibrations dans la charge. Les applications sont nombreuses pour les industries nécessitant des tâches d'assemblage ou de désassemblage, par exemple la construction, le démantèlement d'installations. L'utilisation de robots pour ces tâches est encore plus souhaitable si l'environnement est dangereux pour l'homme. Sur la base de ces motivations et applications potentielles, le modèle général d'un MAGMaS est introduit en détail. La modélisation de l'AR en vol sans contact est effectuée puis ce modèle est incorporé dans celui du MAGMaS. Enfin, un moyen d'étendre le modèle et d'éventuelles études théoriques sur MAGMaS sont discutées.

Dans le chapitre 4, la structure de contrôle nécessaire pour un MAGMaS est introduite, en mettant l'accent sur le contrôleur nécessaire pour l'AR. Un contrôleur générique de haut niveau est présenté, il est composé d'un planificateur de tâches et d'un schéma de répartition de l'effort de contrôle. La répartition de l'effort de contrôle divise les forces souhaitées pour déplacer la charge entre chaque

sous-système du MAGMaS. En même temps, elle s'assure du respect de toutes les contraintes d'actionnement et du système et exploite la redondance du MAGMaS pour maximiser l'index de manipulabilité du système.

Les validations expérimentales du concept de MAGMaS sont présentées dans le chapitre 5. La première partie du chapitre est consacrée à des simulations numériques et à des expériences de preuve de concept et correspondent au stade précoce du travail sur les MAGMaS. À ce stade précoce, l'utilisation d'un quadrotor avec une liaison sphérique passive a été envisagée afin de découpler efficacement la dynamique de rotation de la charge manipulée de celle de l'AR. La conception et les bénéfices d'une telle liaison sont validés expérimentalement. De plus, la capacité de MAGMaS à réduire la vibration de la charge est mise en évidence dans une expérience comparative. La deuxième partie du chapitre est consacrée à une intégration massive et à un travail expérimental développé pour le KUKA 2017 Innovation Award, l'ajout d'un cadre de télé-présence à un MAGMaS et la conception d'un AR à poussée multi-directionnelle sont détaillés. L'implémentation et l'intégration de l'ensemble du système sont couvertes en profondeur. Cette partie est conclue par les résultats expérimentaux concernant la manipulation coopérative de barres.

Parallèlement au MAGMaS, une autre direction de recherche a été étudiée au cours de cette thèse. L'utilisation d'actionneurs compliants pour la manipulation aérienne été explorée avec la conviction qu'ils pourraient permettre des interactions physiques plus sûres et plus polyvalentes avec l'environnement. Ce domaine de recherche est stimulant, mais l'intégration de tels actionneurs sur des AR s'est avérée fastidieuse en raison des limitations matérielles. L'étude théorique de la platitude pour les actionneurs élastiques dans les AR est présentée dans le chapitre 6. Le modèle d'AR avec actionneurs élastiques est dérivé et l'analyse conduisant à la preuve de la platitude pour un ensemble de sortie est effectuée et un contrôleur basé sur la linéarisation par dynamic feedback est synthétisé. L'approche est validée par de nombreuses simulations numériques comprenant des incertitudes paramétriques et du bruit. Ainsi que par un ensemble d'expériences avec un VSA monté sur un AR. Ce chapitre est conclu par des pistes de recherche possibles sur l'utilisation d'actionneurs élastiques pour les AR.

Dans le chapitre 7, une étude exploratoire sur la flexibilité dans les objets manipulés par un MAGMaS est menée. Un modèle dans le plan d'un MAGMaS manipulant une barre flexible est présenté, l'accent est mis sur la modélisation de la flexibilité. Le système proposé est linéarisé pour effectuer une analyse du système: à la fois l'observabilité et la contrôlabilité des deux premiers modes de vibration sont prouvés.

Finalement le chapitre 8 regroupe un résumé des contributions de cette thèse ainsi qu'une discution sur de possibles extensions des travaux présentés.

Bibliography

[Adorno–2015] B. V. Adorno, A. P. L. Bó, and P. Fraisse. "Kinematic modeling and control for human-robot cooperation considering different interaction roles". In: *Robotica* 33.2 (2015), pp. 314–331 (cited on page 91).

[Albers–2010] A. Albers, S. Trautmann, T. Howard, M. Frietsch, and C. Sauter. "Semi-autonomous flying robot for physical interaction with environment". In: *2010 IEEE Conf. Robot. Autom. Mechatronics*. June 2010, pp. 441–446 (cited on page 15).

[Alexis–2010] K. Alexis, G. Nikolakopoulos, and A. Tzes. "Constrained-control of a quadrotor helicopter for trajectory tracking under wind-gust disturbances". In: *Melecon 2010 - 2010 15th IEEE Mediterranean Electrotechnical Conference*. Apr. 2010, pp. 1411–1416 (cited on page 21).

[Alexis–2013] K. Alexis, C. Huerzeler, and R. Siegwart. "Unmanned coaxial rotorcraft force and position control for physical interaction through contact". In: *21st Mediterranean Conference on Control and Automation*. June 2013, pp. 179–184 (cited on pages 12, 21 and 142).

[Augugliaro–2013] F. Augugliaro and R. D'Andrea. "Admittance Control for Physical Human-Quadrocopter Interaction". In: *12th European Control Conference*. Zurich, Switzerland, July 2013, pp. 1805–1810 (cited on pages 20, 22, 24, 25 and 146).

[Augugliaro–2014] F. Augugliaro, S. Lupashin, M. Hamer, C. Male, M. Hehn, M. W. Mueller, J. S. Willmann, F. Gramazio, M. Kohler, and R. D'Andrea. "The Flight Assembled Architecture installation: Cooperative construction with flying machines". In: *IEEE Control Systems Magazine* 34.4 (2014), pp. 46–64 (cited on pages 23, 30 and 149).

[Augugliaro–2015] F. Augugliaro, E. Zarfati, A. Mirjan, and R. D'Andrea. "Knot-tying with flying machines for aerial construction". In: *2015*. Sept. 2015, pp. 5917–5922 (cited on page 23).

[Baca–2016] T. Baca and G. Loiannoand M. Saska. "Embedded Model Predictive Control of Unmanned Micro Aerial Vehicles". In: *2016 21st International Conference on Methods and Models in Automation and Robotics (MMAR)*. Miedzyzdroje, Poland, 2016 (cited on pages 20 and 146).

[Backus–2014] S. B. Backus, L. U. Odhner, and A. M. Dollar. "Design of hands for aerial manipulation: Actuator number and routing for grasping and perching". In: *2014*. Sept. 2014, pp. 34–40 (cited on page 18).

[Bähnemann–2017] R. Bähnemann, D. Schindler, M. Kamel, R. Siegwart, and J. Nieto. "A Decentralized Multi-Agent Unmanned Aerial System to Search, Pick Up, and Relocate Objects". In: *arXiv:1707.03734v1 [cs.RO]* (July 2017) (cited on page 19).

[Bangura–2014] M. Bangura, H. Lim, H. J. Kim, and R. Mahony. "Aerodynamic power control for multirotor aerial vehicles". In: *2014*. May 2014, pp. 529–536 (cited on page 54).

[Bartelds–2016] T. Bartelds, A. Capra, S. Hamaza, S. Stramigioli, and M. Fumagalli. "Compliant Aerial Manipulators: Toward a New Generation of Aerial Robotic Workers". In: 1.1 (Jan. 2016), pp. 477–483 (cited on page 17).

[Bellens–2012] S. Bellens, J. De Schutter, and H. Bruyninckx. "A hybrid pose/wrench control framework for quadrotor helicopters". In: *2012 IEEE Int. Conf. on Robotics and Automation*. St.Paul, MN, May 2012, pp. 2269–2274 (cited on page 22).

[Bernard–2011] M. Bernard, K. Kondak, I. Maza, and A. Ollero. "Autonomous transportation and deployment with aerial robots for search and rescue missions". In: *Journal of Field Robotics* 28.6 (2011), pp. 914–931 (cited on pages 17 and 24).

[Bicego–2015] Davide Bicego. "Design, Modeling and Control of a Redundantly Actuated Aerial Robot". Available under request (`davide.bicego@laas.fr`). MA thesis. 2015 (cited on pages 65, 136 and 137).

[Brandi–2011] F. Brandi, R. Chaudhari, S. Hirche, J. Kammerl, E. Steinbach, and I. Vittorias. "Perceptual Haptic Data Reduction in Telepresence and Teleaction Systems". In: *Multimedia Communication Technical Committee E-Letter* 6.1 (2011), pp. 7–10 (cited on page 86).

[Braun–2013] D. J. Braun, F. Petit, F. Huber, S. Haddadin, P. van der Smagt, A. Albu-Schäffer, and S. Vijayakumar. "Robots driven by compliant actuators: Optimal control under actuation constraints". In: 29.5 (2013), pp. 1085–1101 (cited on pages 95 and 156).

[Brescianini–2016] D. Brescianini and R. D'Andrea. "Design, Modeling and Control of an Omni-Directional Aerial Vehicle". In: *2016 IEEE Int. Conf. on Robotics and Automation*. Stockholm, Sweden, May 2016, pp. 3261–3266 (cited on pages 15 and 144).

[Briod–2013] A. Briod, P. Kornatowski, A. Klaptocz, A. Garnier, M. Pagnamenta, J. C. Zufferey, and D. Floreano. "Contact-based navigation for an autonomous flying robot". In: *2013*. Nov. 2013, pp. 3987–3992 (cited on page 10).

[Briod–2014] A. Briod, P. M. Kornatowski, J.-C. Zufferey, and D. Floreano. "A Collision Resilient Flying Robot". In: 31.4 (2014), pp. 469–509 (cited on page 10).

[C Breazeal–2008] A. Takanishi C. Breazeal and T. Kobayashi. *Social Robots that Interact with People*. Ed. by B. Siciliano and O. Khatib. Berlin, Heidelberg: Springer Berlin Heidelberg, 2008, pp. 1349–1369 (cited on page 90).

[Castillo–2005] P. Castillo, R. Lozano, and A. Dzul. "Stabilization of a mini rotorcraft with four rotors". In: *IEEE Control Systems Magazine* 25.6 (2005), pp. 45–55 (cited on pages 20 and 146).

[Cehajic–2017a] D. Cehajic, P. B. gen. Dohmann, and S. Hirche. "Estimating unknown object dynamics in human-robot manipulation tasks". In: *2017*. May 2017, pp. 1730–1737 (cited on pages 29, 90 and 149).

[Cehajic–2017b] D. Cehajic, S. Endo, M. Aggravi, D. Prattichizzo, and S. Hirche. "Spatial guidance of the human arm motion using vibrotactile feedback". In: *Work-In-Progress paper, IEEE World Haptics 2017*. June 2017 (cited on page 91).

[Censi–2013] A. Censi, A. Franchi, L. Marchionni, and G. Oriolo. "Simultaneous Maximum-likelihood Calibration of Odometry and Sensor Parameters". In: 29.2 (2013), pp. 475–492 (cited on pages 110 and 157).

[Chaudhari–2011] R. Chaudhari, E. Steinbach, and S. Hirche. "Towards an Objective Quality Evaluation Framework for Haptic Data Reduction". In: *IEEE World Haptics Conference*. Istanbul, Turkey, 2011 (cited on page 86).

[Cherubini–2015] A. Cherubini, R. Passama, P. Fraisse, and A. Crosnier. "A unified multimodal control framework for human-robot interaction". In: *Robotics and Autonomous Systems* 70 (2015), pp. 106–115 (cited on page 92).

[Cherubini–2016] A. Cherubini, R. Passama, A. Crosnier, A. Lasnier, and P. Fraisse. "Collaborative manufacturing with physical human-robot interaction". In: *Robotics and Computer-Integrated Manufacturing* 40 (July 2016), pp. 1–13 (cited on page 29).

[Danko–2015] T. W. Danko, K. P. Chaney, and P. Y. Oh. "A parallel manipulator for mobile manipulating UAVs". In: *2015 IEEE International Conference on Technologies for Practical Robot Applications (TePRA)*. May 2015, pp. 1–6 (cited on pages 16, 144 and 145).

[De Luca–1996] A. De Luca. "Decoupling and feedback linearization of robots with mixed rigid/elastic joints". In: *1996*. Minneapolis, MN, Apr. 1996, pp. 816–821 (cited on pages 96 and 101).

[De Luca–2002] A. De Luca and G. Oriolo. "Trajectory planning and control for planar robots with passive last joint". In: *The International Journal of Robotics Research* 21.5-6 (2002), pp. 575–590 (cited on page 99).

[De Luca–2007] A. De Luca, G. Oriolo, and P. Robuffo Giordano. "Image-based visual servoing schemes for nonholonomic mobile manipulators". In: *Robotica* 25.2 (2007), pp. 131–145 (cited on page 92).

[De Luca–2010] A. De Luca, G. Oriolo, and P. Robuffo Giordano. "Kinematic control of Nonholonomic mobile manipulators in the presence of steering wheels". In: *2010 icra*. Anchorage, Alaska, USA, May 2010, pp. 1792–1798 (cited on page 50).

[Desbiens–2011] A. L. Desbiens and A. T. Asbeck nd M. R. Cutkosky. "Landing, perching and taking off from vertical surfaces". In: *2011*. Vol. 30. July 2011, pp. 355–370 (cited on pages 12 and 141).

[Dumora–2012] J. Dumora, F. Geffard, C. Bidard, T. Brouillet, and P. Fraisse. "Experimental study on haptic communication of a human in a shared human-robot collaborative task". In: *2012*. Oct. 2012 (cited on pages 29, 90 and 149).

[Dumora–2013] J. Dumora, F. Geffard, C. Bidard, N. A. Aspragathos, and P. Fraisse. "Robot Assistance Selection for Large Object Manipulation with a Human". In: *2013 IEEE International Conference on Systems, Man, and Cybernetics*. Oct. 2013, pp. 1828–1833 (cited on pages 29, 91 and 149).

[Erhart–2013] S. Erhart and S. Hirche. "Adaptive force/velocity control for multi-robot cooperative manipulation under uncertain kinematic parameters". In: *2013 IEEE/RSJ Int. Conf. on Intelligent Robots and Systems*. Tokyo, Japan, Nov. 2013, pp. 307–314 (cited on page 44).

[Erhart–2015] S. Erhart and S. Hirche. "Internal Force Analysis and Load Distribution for Cooperative Multi-Robot Manipulation". In: *IEEE Trans. on Robotics* 21.3 (2015), pp. 1238–1243 (cited on pages 44 and 90).

[Fliess–1999] M. Fliess, J. Lévine, P. Martin, and p. Rouchon. "Some open questions related to flat nonlinear systems". In: *Open Problems in Mathematical Systems and Control Theory*. London: Springer London, 1999, pp. 99–103 (cited on page 99).

[Franchi–2012] A. Franchi, C. Secchi, M. Ryll, H. H. Bülthoff, and P. Robuffo Giordano. "Shared Control: Balancing Autonomy and Human Assistance with a Group of Quadrotor UAVs". In: *, Special Issue on Aerial Robotics and the Quadrotor Platform* 19.3 (2012), pp. 57–68 (cited on page 81).

[Franchi–2014] A. Franchi, A. Petitti, and A. Rizzo. "Distributed Estimation of the Inertial Parameters of an Unknown Load via Multi-Robot Manipulation". In: *53rd*. Los Angeles, CA, Dec. 2014, pp. 6111–6116 (cited on page 45).

[Franchi–2017a] A. Franchi, R. Carli, D. Bicego, and M. Ryll. "Full-Pose Tracking Control for Aerial Robotic Systems with Laterally-Bounded Input Force". In: *Arxiv* (2017). URL: `https://arxiv.org/abs/1605.06645` (cited on page 80).

[Franchi–2017b] A. Franchi and A. Mallet. "Adaptive Closed-loop Speed Control of BLDC Motors with Applications to Multi-rotor Aerial Vehicles". In: *2017*. Singapore, May 2017 (cited on pages 65, 66, 133, 134, 135 and 136).

[Fumagalli–2014] M. Fumagalli, R. Naldi, A. Macchelli, F. Forte, A. Q. L. Keemink, S. Stramigioli, R. Carloni, and L. Marconi. "Developing an Aerial Manipulator Prototype: Physical Interaction with the Environment". In: 21.3 (Sept. 2014), pp. 41–50 (cited on page 14).

[Fumagalli–2016] M. Fumagalli, S. Stramigioli, and R. Carloni. "Mechatronic design of a robotic manipulator for Unmanned Aerial Vehicles". In: *2016*. Oct. 2016, pp. 4843–4848 (cited on page 16).

[Galinsky–2007] C. Galinsky and R. Zbikowski. "Some problems of micro air vehicles development". In: *Bulletin of the Polish Academy of Sciences, Technical Sciences* 55.1 (2007) (cited on pages 8 and 139).

[Gassner–2017] M. Gassner, T. Cieslewski, and D. Scaramuzza. "Dynamic collaboration without communication: Vision-based cable-suspended load transport with two quadrotors". In: *2017 IEEE Int. Conf. on Robotics and Automation*. Singapore, May 2017, pp. 5196–5202 (cited on page 24).

[Gawel–2017] A. Gawel, M. Kamel, T. Novkovic, J. Widauer, D. Schindler, B. P. von Altishofen, R. Siegwart, and J. Nieto. "Aerial picking and delivery of magnetic objects with MAVs". In: *2017*. May 2017, pp. 5746–5752 (cited on pages 18, 19, 24, 145 and 146).

[Gioioso–2014a] G. Gioioso, M. Ryll, D. Prattichizzo, H. H. Bülthoff, and A. Franchi. "Turning a Near-hovering Controlled Quadrotor into a 3D Force Effector". In: *2014*. Hong Kong, China, May 2014, pp. 6278–6284 (cited on pages 9, 12, 20, 141, 142 and 146).

[Gioioso–2014b] G. Gioioso, G. Salvietti, A. Franchi, M. Malvezzi, S. Scheggi, L. Meli, M. Ryll, H. H. Bülthoff, and D. Prattichizzo. "The Flying Hand: a Teleoperation Framework for Cooperative Aerial Grasping and Transportation". In: *Automatica.it 2014, Convegno Annuale dei Docenti e Ricercatori Italiani in Automatica*. Bergamo, Italy, Sept. 2014 (cited on page 19).

[Gonçalves–2016] V. M. Gonçalves, P. Fraisse, A. Crosnier, and B. V. Adorno. "Parsimonious Kinematic Control of Highly Redundant Robots". In: 1.1 (Jan. 2016), pp. 65–72 (cited on page 51).

[Grabe–2013] V. Grabe, M. Riedel, H. H. Bülthoff, P. Robuffo Giordano, and A. Franchi. "The TeleKyb Framework for a Modular and Extendible ROS-based Quadrotor Control". In: *6th*. Barcelona, Spain, Sept. 2013, pp. 19–25 (cited on pages 56, 59, 60 and 104).

[Hirche–2012] S. Hirche and M. Buss. "Human-Oriented Control for Haptic Teleoperation". In: *Proceedings of the IEEE* (2012) (cited on page 23).

[Inmann–2007] D. J. Inmann. "Distributed-Parameter Systems". In: *Engineering Vibration 3rd*. New Jersey: Prentice Hall PTR, 2007, pp. 464–530. ISBN: 0-13-228173-2 (cited on pages 113, 114 and 115).

[Isidori–1995] A. Isidori. *Nonlinear Control Systems, 3rd edition*. Springer, 1995. ISBN: 3540199160 (cited on page 49).

[JimenezCano–2013] A. E. Jimenez-Cano, J. Martin, G. Heredia, A. Ollero, and R. Cano. "Control of an aerial robot with multi-link arm for assembly tasks". In: *2016*. May 2013, pp. 4916–4921 (cited on page 16).

[Kamel–2016] M. Kamel, S. Comari, and R. Siegwart. "Full-Body Multi-Objective Controller for Aerial Manipulation". In: *Mediterranean Conference on Control and Automation (MED)*. June 2016, pp. 659–664 (cited on page 16).

[Keemink–2012] A. Q. L. Keemink, M. Fumagalli, S. Stramigioli, and R. Carloni. "Mechanical design of a manipulation system for unmanned aerial vehicles". In: *2012 IEEE Int. Conf. on Robotics and Automation*. St. Paul, MN, May 2012, pp. 3147–3152 (cited on page 16).

[Kessens–2016] C. C. Kessens, J. Thomas, J. P. Desai, and V. Kumar. "Versatile aerial grasping using self-sealing suction". In: *2016*. May 2016, pp. 3249–3254 (cited on pages 18, 19, 145 and 146).

[Kim–2013] S. Kim, S. Choi, and H. J. Kim. "Aerial manipulation using a quadrotor with a two DOF robotic arm". In: *2013 IEEE/RSJ Int. Conf. on Intelligent Robots and Systems*. Tokyo, Japan, Nov. 2013, pp. 4990–4995 (cited on pages 30 and 149).

[Kim–2017] H. Kim, H. Lee, S. Choi, Y. k. Noh, and H. J. Kim. "Motion planning with movement primitives for cooperative aerial transportation in obstacle environment". In: *2017 IEEE International Conference on Robotics and Automation (ICRA)*. May 2017, pp. 2328–2334 (cited on page 24).

[Kimmel–2015] M. Kimmel and S. Hirche. "Active Safety Control for Dynamic Human-Robot Interaction". In: *2015*. Hamburg, Germany, Oct. 2015, pp. 4685–4691 (cited on page 90).

[Kimmel–2017] M. Kimmel and S. Hirche. "Invariance Control for Safe Human-Robot Interaction in Dynamic Environments". In: *IEEE Transactions on Robotics* (2017) (cited on page 90).

[Klaptocz–2013] A. Klaptocz, A. Briod, L. Daler, J. C. Zufferey, and D. Floreano. "Euler spring collision protection for flying robots". In: *2013*. Nov. 2013, pp. 1886–1892 (cited on pages 10 and 11).

[Knepper–2013] R. A. Knepper, T. Layton, J. Romanishin, and D. Rus. "IkeaBot: An autonomous multi-robot coordinated furniture assembly system". In: *2013 IEEE Int. Conf. on Robotics and Automation*. Karlsruhe, Germany, Oct. 2013, pp. 855–862 (cited on page 29).

[Kondak–2009] K. Kondak, M. Bernard, F. Caballero, I. Maza, and A. Ollero. "Cooperative Autonomous Helicopters for Load Transportation and Environment Perception". In: *Advances in Robotics Research: Theory, Implementation, Application*. Ed. by T. Kröger and F. M. Wahl. Berlin, Heidelberg: Springer Berlin Heidelberg, 2009, pp. 299–310 (cited on pages 13, 17, 30, 142 and 149).

[Kondak–2014] K. Kondak, F. Hubert, M. Schwarzbach, M. Laiacker, D. Sommer, M. Bejar, and A. Ollero. "Aerial manipulation robot composed of an autonomous helicopter and a 7 degrees of freedom industrial manipulator". In: *2014 IEEE Int. Conf. on Robotics and Automation*. Hong Kong, China, May 2014, pp. 2108–2112 (cited on pages 14, 16, 144 and 145).

[Kornatowski–2017] P.M. Kornatowski, S. Mintchev, and D. Floreano. "An Origami-Inspired Cargo Drone". In: *2017*. Sept. 2017 (cited on page 10).

[Lächele–2013] J. Lächele, M. Riedel, P. Robuffo Giordano, and A. Franchi. "SwarmSimX and TeleKyb: Two ROS-integrated Software Frameworks for Single- and Multi-Robot Applications". In: *Int. Work. on Towards Fully Decentralized Multi-Robot Systems: Hardware, Software and Integration, at 2013*. Karlsruhe, Germany, May 2013 (cited on page 104).

[Lee–2010] T. Lee, M. Leoky, and N. H. McClamroch. "Geometric tracking control of a quadrotor UAV on SE(3)". In: *49th IEEE Conf. on Decision and Control*. Atlanta, GA, Dec. 2010, pp. 5420–5425 (cited on pages 20, 51 and 146).

[Lee–2013] D. J. Lee, A. Franchi, H. I. Son, H. H. Bülthoff, and P. Robuffo Giordano. "Semi-Autonomous Haptic Teleoperation Control Architecture of Multiple Unmanned Aerial Vehicles". In: *, Focused Section on Aerospace Mechatronics* 18.4 (2013), pp. 1334–1345 (cited on pages 103 and 104).

[Li–2012] H. Li, J. Park, D. Lee, and H.J. Kim. "Build Your Own Quadrotor: Open-Source Projects on Unmanned Aerial Vehicles". In: 19.3 (2012), pp. 33–45 (cited on page 56).

[Lindsey–2011] Q. Lindsey, D. Mellinger, and V. Kumar. "Construction of Cubic Structures with Quadrotor Teams". In: *2011 Robotics: Science and Systems*. Los Angeles, CA, June 2011 (cited on pages 18, 23 and 24).

[Lindsey–2012] Q. Lindsey, D. Mellinger, and V. Kumar. "Construction with quadrotor teams". In: *Autonomous Robots* 33.3 (2012), pp. 323–336 (cited on pages 30 and 149).

[Lippiello–2012] V. Lippiello and F. Ruggiero. "Exploiting redundancy in Cartesian impedance control of UAVs equipped with a robotic arm". In: *2012 IEEE/RSJ Int. Conf. on Intelligent Robots and Systems*. Vilamoura, Portugal, Oct. 2012, pp. 3768–3773 (cited on pages 20 and 146).

[Ljung–1999] L. Ljung. *System Identification - Theory For the User, 2nd ed.* Upper Saddle River, N.J.: PTR Prentice Hall, 1999 (cited on page 61).

[Lupashin–2010] S. Lupashin, A. Schöllig, M. Sherback, and R. D'Andrea. "A simple learning strategy for high-speed quadrocopter multi-flips". In: *2010 IEEE Int. Conf. on Robotics and Automation*. Anchorage, AK, May 2010, pp. 1642–1648 (cited on page 97).

[Machado–2016] T. Machado, T. Malheiro, S. Monteiro, W. Erlhagen, and E. Bicho. "Multi-constrained joint transportation tasks by teams of autonomous mobile robots using a dynamical systems approach". In: *2016 IEEE Int. Conf. on Robotics and Automation*. Stockholm, Sweden, May 2016, pp. 3111–3117 (cited on pages 29 and 149).

[Mahony–2012] R. Mahony, V. Kumar, and P. Corke. "Multirotor Aerial Vehicles: Modeling, Estimation, and Control of Quadrotor". In: *IEEE Robotics & Automation Magazine* 19.3 (2012), pp. 20–32 (cited on pages 8, 34, 55 and 140).

[Manubens–2013] M. Manubens, D. Devaurs, L. Ros, and J. Cortés. "Motion Planning for 6-D Manipulation with Aerial Towed-cable Systems". In: *2013 Robotics: Science and Systems*. Berlin, Germany, May 2013 (cited on page 17).

[Marino–2017] A. Marino, G. Muscio, and F. Pierri. "Distributed cooperative object parameter estimation and manipulation without explicit communication". In: *2017*. May 2017, pp. 2110–21116 (cited on page 44).

[Martin–2003] P. Martin, R. M. Murray, and P. Rouchon. "Flat systems, equivalence and trajectory generation". In: *2003 CDS Technical Report*. 2003 (cited on page 99).

[Mayhew–2011] C. G. Mayhew, R. G. Sanfelice, and A. R. Teel. "Quaternion-Based Hybrid Control for Robust Global Attitude Tracking". In: *IEEE Transactions on Automatic Control* 56.11 (Nov. 2011), pp. 2555–2566 (cited on pages 20 and 146).

[McArthur–2017] D. R. McArthur, A. B. Chowdhury, and D. J. Cappelleri. "Design of the I-BoomCopter UAV for environmental interaction". In: *2017*. May 2017, pp. 5209–5214 (cited on page 15).

[Medina Hernández–2015] J.R. Medina Hernández, T. Lorenz, and S. Hirche. "Synthesizing Anticipatory Haptic Assistance Considering Human Behavior Uncertainty". In: 31.1 (Feb. 2015), pp. 180–190. DOI: 10.1109/TRO.2014.2387571 (cited on page 90).

[Medina–2017] J. R. Medina, T. Lorenz, and S. Hirche. "Considering Human Behavior Uncertainty and Disagreements in Human–Robot Cooperative Manipulation". In: *Trends in Control and Decision-Making for Human–Robot Collaboration Systems*. Springer, 2017 (cited on page 90).

[Mehanovic–2017] D. Mehanovic, J. Bass, T. Courteau, D. Rancourt, and A. Lussier Desbiens. "Autonomous Thrust-Assisted Perching of a Fixed-Wing UAV on Vertical Surfaces". In: *6th International Conference, Living Machines 2017*. Standford, CA, July 2017 (cited on pages 12 and 141).

[Meirovitch–1997] L. Meirovitch. "Distributed-Parameter Systems". In: *Principles and Techniques of Vibrations*. New Jersey: Prentice Hall PTR, 1997, pp. 361–500. ISBN: 0-13-270430-7 (cited on page 114).

[Meirovitch–2000a] L. Meirovitch. "Distributed-Parameter Systems". In: *Fundamentals of Vibrations*. McGraw-Hill Higher Education, 2000, pp. 280–373. ISBN: 0-07-118174-1 (cited on page 118).

[Meirovitch–2000b] L. Meirovitch. "Distributed-Parameter Systems, Exact Solutions". In: *Fundamentals of Vibrations*. McGraw-Hill Higher Education, 2000, pp. 374–463. ISBN: 0-07-118174-1 (cited on pages 116 and 118).

[Meirovitch–2000c] L. Meirovitch. "The Finite Element Method". In: *Fundamentals of Vibrations*. McGraw-Hill Higher Education, 2000, pp. 549–615. ISBN: 0-07-118174-1 (cited on page 122).

[Mellinger–2010] D. Mellinger, M. Shomin, N. Michael, and V. Kumar. "Cooperative grasping and transport using multiple quadrotors". In: *10th Int. Symp. on Distributed Autonomous Robotic Systems*. Lausanne, Switzerland, Nov. 2010, pp. 545–558 (cited on pages 10 and 143).

[Mersha–2011] A. Y. Mersha, R. Carloni, and S. Stramigioli. "Port-based Modeling and Control of Underactuated Aerial Vehicles". In: *2011 IEEE Int. Conf. on Robotics and Automation*. Shanghai, China, May 2011, pp. 14–19 (cited on pages 20 and 147).

[Michael–2009] N. Michael, J. Fink, and V. Kumar. "Cooperative Manipulation and Transportation with Aerial Robots". In: *2009 Robotics: Science and Systems*. Seattle, WA, June 2009 (cited on page 24).

[Michieletto–2017] G. Michieletto, M.Ryll, and A. Franchi. "Fundamental Actuation Properties of Multi-rotors: Force-Moment Decoupling and Fail-safe Robustness". In: (2017). **Submitted**, hal-01612602. URL: `https://hal.archives-ouvertes.fr/hal-01612602v1` (cited on page 36).

[Mistler–2001] V. Mistler, A. Benallegue, and N. K. M'Sirdi. "Exact linearization and noninteracting control of a 4 rotors helicopter via dynamic feedback". In: *10th IEEE Int. Symp. on Robots and Human Interactive Communications*. Bordeaux, Paris, France, Sept. 2001, pp. 586–593 (cited on pages 20 and 146).

[Mohammadi–2016] M. Mohammadi, A. Franchi, D. Barcelli, and D. Prattichizzo. "Cooperative Aerial Tele-Manipulation with Haptic Feedback". In: *2016*. Daejeon, South Korea, Oct. 2016, pp. 5092–5098 (cited on pages 18, 19, 145 and 146).

[Molina–2017] J. Molina and S. Hirai. "Pruning tree-branches close to electrical power lines using a skew-gripper and a multirotor helicopter". In: *2017 IEEE International Conference on Advanced Intelligent Mechatronics (AIM)*. July 2017, pp. 1123–1128 (cited on page 11).

[Mueller–2011] M. W. Mueller, S. Lupashin, and R. D'Andrea. "Quadrocopter ball juggling". In: *2011*. 2011, pp. 5113–5120 (cited on page 25).

[MunozMorera–2015] J. Munoz-Morera, I. Maza, C. J. Fernandez-Aguera, F. Caballero, and A. Ollero. "Assembly planning for the construction of structures with multiple UAS equipped with robotic arms". In: *2015*. June 2015, pp. 1049–1058 (cited on page 24).

[Navarro–2017] B. Navarro, A. Cherubini, A. Fonte, G. Poisson, and P. Fraisse. "A Framework for Intuitive Collaboration with a Mobile Manipulator". In: *2017*. Sept. 2017 (cited on pages 90 and 91).

[Nguyen–2015] H.-N. Nguyen, S. Park, and D. J. Lee. "Aerial Tool Operation System using Quadrotors as Rotating Thrust Generators". In: *2015 IEEE/RSJ Int. Conf. on Intelligent Robots and Systems*. Hamburg, Germany, Oct. 2015, pp. 1285–1291 (cited on pages 10, 15, 17, 24 and 143).

[Nguyen–2016] T. Nguyen and E. Garone. "Control of a UAV and a UGV cooperating to manipulate an object". In: *2016 American Control Conference*. Boston, MA, July 2016, pp. 1347–1352 (cited on page 24).

[Niemeyer–2008] G. Niemeyer, C. Preusche, and G. Hirzinger. "Telerobotics". In: *Springer Handbook of Robotics*. Ed. by B. Siciliano and O. Khatib. Springer, 2008, pp. 741–757 (cited on page 22).

[Nikou–2015] A. Nikou, G. C. Gavridis, and K. J. Kyriakopoulos. "Mechanical design, modelling and control of a novel aerial manipulator". In: *2015*. May 2015, pp. 4698–4703 (cited on page 15).

[Odelga–2016] M. Odelga, P. Stegagno, and H. H. Bülthoff. "A fully actuated quadrotor UAV with a propeller tilting mechanism: Modeling and control". In: *2016 IEEE International Conference on Advanced Intelligent Mechatronics (AIM)*. July 2016, pp. 306–311 (cited on page 14).

[Orsag–2017] M. Orsag, C. Korpela, S. Bogdan, and P. Oh. "Dexterous Aerial Robots Mobile Manipulation Using Unmanned Aerial Systems". In: *IEEE Transactions on Robotics* PP.99 (2017), pp. 1–14 (cited on page 17).

[Papachristos–2014a] C. Papachristos, K. Alexis, and A. Tzes. "Efficient force exertion for aerial robotic manipulation: Exploiting the thrust-vectoring authority of a tri-tiltrotor UAV". In: *2014*. May 2014, pp. 4500–4505 (cited on pages 12 and 142).

[Papachristos–2014b] C. Papachristos and A. Tzes. "The power-tethered UAV-UGV team: A collaborative strategy for navigation in partially-mapped environments". In: *22nd Mediterranean Conference on Control and Automation*. June 2014, pp. 1153–1158 (cited on page 24).

[Park–2016] S. Park, Jongbeom J. Her, J. Kim, and D. Lee. "Design, Modeling and Control of Omni-Directional Aerial Robot". In: *2016 IEEE/RSJ Int. Conf. on Intelligent Robots and Systems*. Daejeon, South Korea, 2016, pp. 1570–1575 (cited on page 14).

[Passenberg–2010] C. Passenberg, A. Peer, and M. Buss. "A survey of environment, operator, and task-adapted controllers for teleoperation systems". In: *Mechatronics* 20.7 (2010), pp. 787–801 (cited on page 22).

[Petitti–2016] A. Petitti, A. Franchi, D. Di Paola, and A. Rizzo. "Decentralized Motion Control for Cooperative Manipulation with a Team of Networked Mobile Manipulators". In: *2016*. Stockholm, Sweden, May 2016, pp. 441–446 (cited on page 45).

[Pfeiffer–2011] K. Pfeiffer, M. Bengel, and A. Bubeck. "Offshore robotics - Survey, implementation, outlook". In: *2011 IEEE/RSJ Int. Conf. on Intelligent Robots and Systems*. San Francisco, CA, Sept. 2011, pp. 241–246 (cited on pages 29 and 149).

[Pope–2017] M. T. Pope, C. W. Kimes, H. Jiang, E. W. Hawkes, M. A. Estrada, C. F. Kerst, W. R. T. Roderick, A. K. Han, D. L. Christensen, and M. R. Cutkosky. "A Multimodal Robot for Perching and Climbing on Vertical Outdoor Surfaces". In: 33.1 (Feb. 2017), pp. 38–48 (cited on pages 11, 12 and 141).

[Pounds–2014] P. E.I. Pounds and A. M. Dollar. "Stability of Helicopters in Compliant Contact under PD-PID Control". In: 30.6 (2014), pp. 1472–1486 (cited on page 14).

[Prattichizzo–2008] D. Prattichizzo and J. C. Trinkle. "Grasping". In: *Springer Handbook of Robotics*. Ed. by B. Siciliano and O. Khatib. Berlin, Heidelberg: Springer Berlin Heidelberg, 2008 (cited on page 43).

[Raffo–2010] G. V. Raffo, M. G. Ortega, and F. R. Rubio. "An integral predictive/nonlinear H-infinity control structure for a quadrotor helicopter". In: *Automatica* 46.1 (2010), pp. 29–39 (cited on pages 20 and 146).

[Rajappa–2015] S. Rajappa, M. Ryll, H. H. Bülthoff, and A. Franchi. "Modeling, Control and Design Optimization for a Fully-actuated Hexarotor Aerial Vehicle with Tilted Propellers". In: *2015*. Seattle, WA, May 2015, pp. 4006–4013 (cited on pages 14, 36, 78 and 144).

[Rajappa–2017] S. Rajappa, H. H. Bülthoff, and P. Stegagno. "Design and implementation of a novel architecture for physical human-UAV interaction". In: 36 (5-7 June 2017), pp. 800–819 (cited on pages 21, 22, 25, 54 and 147).

[Ritz–2012] R. Ritz, M. W. Mueller, M. Hehn, and R. D'Andrea. "Cooperative quadrocopter ball throwing and catching". In: *2012*. 2012 (cited on page 24).

[Robuffo Giordano–2008] P. Robuffo Giordano, A. Stemmer, K. Arbter, and A. Albu-Schaffer. "Robotic assembly of complex planar parts: An experimental evaluation". In: *2008*. Sept. 2008, pp. 3775–3782 (cited on page 92).

[Rodriguez Salazar–2017] L. Rodriguez Salazar, J. A. Cobano, and A. Ollero. "Small UAS-Based Wind Feature Identification System Part 1: Integration and Validation". In: *Sensors* 17.1 (2017) (cited on page 21).

[Rodriguez–2016] L. Rodriguez, J. A. Cobano, and A. Ollero. "Wind field estimation and identification having shear wind and discrete gusts features with a small UAS". In: *2016*. Oct. 2016, pp. 5638–5644 (cited on page 21).

[Ruggiero–2014] F. Ruggiero, J. Cacace, H. Sadeghian, and V. Lippiello. "Impedance Control of VToL UAVs with a Momentum-based External Generalized Forces Estimator". In: *2014 IEEE Int. Conf. on Robotics and Automation*. Hong Kong, China, Apr. 2014, pp. 2093–2099 (cited on pages 20, 22 and 146).

[Ruggiero–2015] F. Ruggiero, M. A. Trujillo, R. Cano, H. Ascorbe, A. Viguria, C. Peréz, V. Lippiello, A. Ollero, and B. Siciliano. "A multilayer control for multirotor UAVs equipped with a servo robot arm". In: *2015*. May 2015, pp. 4014–4020 (cited on page 16).

[Ryll–2016] M. Ryll, D. Bicego, and A. Franchi. "Modeling and Control of FAST-Hex: a Fully-Actuated by Synchronized-Tilting Hexarotor". In: *2016*. Daejeon, South Korea, Oct. 2016, pp. 1689–1694 (cited on pages 15, 36, 52 and 78).

[Ryll–2017] M. Ryll, G. Muscio, F. Pierri, E. Cataldi, G. Antonelli, F. Caccavale, and A. Franchi. "6D Physical Interaction with a Fully Actuated Aerial Robot". In: *2017*. Singapore, May 2017, pp. 5190–5195 (cited on pages 12, 14, 18, 22, 65, 66, 67, 136, 142 and 144).

[Sa–2012] I. Sa and P. Corke. "System identification, estimation and control for a cost effective open-source quadcopter". In: *2012*. May 2012 (cited on pages 56 and 57).

[Salaan–2017] C. J. Salaan, K. Tadakuma, Y. Okada, E. Takane, K. Ohno, and S. Tadokoro. "UAV with two passive rotating hemispherical shells for physical interaction and power tethering in a complex environment". In: *2017*. May 2017 (cited on page 10).

[Sandino–2014a] L. A. Sandino, M. Bejar, K. Kondak, and A. Ollero. "Advances in Modeling and Control of Tethered Unmanned Helicopters to Enhance Hovering Performance". In: *Journal of Intelligent & Robotics Systems* 73.1-4 (2014), pp. 3–18 (cited on pages 12 and 142).

[Sandino–2014b] L.A Sandino, D. Santamaria, M. Bejar, A. Viguria, K. Kondak, and A. Ollero. "Tether-guided landing of unmanned helicopters without GPS sensors". In: *2014 IEEE Int. Conf. on Robotics and Automation*. Hong Kong, China, May 2014, pp. 3096–3101 (cited on pages 12 and 142).

[Savitzky–1964] A. Savitzky and M. J. E. Golay. "Smoothing and Differentiation of Data by Simplified Least Squares Procedures." In: *Analytical Chemistry* 36.8 (1964), pp. 1627–1639 (cited on page 60).

[Sempere–2014] A. Sempere, D. Llorente, I. Maza, and A. Ollero. "Local Heuristics Analysis in the Automatic Computation of Assembly Sequences for Building Structures with Multiple Aerial Robots". In: *ROBOT2013: First Iberian Robotics Conference: Advances in Robotics*. Ed. by M. A. Armada, A. Sanfeliu, and M Ferre. Vol. 1. Springer International Publishing, 2014, pp. 87–101 (cited on page 24).

[Sheridan–1992] T. B. Sheridan. "Musings on telepresence and virtual presence". In: *Presence: Teleoperators & Virtual Environments* 1.1 (1992), pp. 120–126 (cited on page 84).

[Sieber–2015] D. Sieber, S. Music, and S. Hirche. "Multi-robot manipulation controlled by a human with haptic feedback". In: *2015*. Oct. 2015 (cited on page 84).

[Six–2017] D. Six, S. Briot, A. Chriette, and P. Martinet. "Dynamic Modeling and Trajectory Tracking Controller of a Novel Flying Parallel Robot". In: *20th IFAC World Congress*. Toulouse, France, July 2017 (cited on page 17).

[Soderstrom–1989] T. S. Soderstrom and P. G. Stoica. *System Identification*. Prentice Hall International Series In Systems And Control Engineering. Prentice Hall, 1989 (cited on page 61).

[Son–2013] H. I. Son, A. Franchi, L. L. Chuang, J. Kim, H. H. Bülthoff, and P. Robuffo Giordano. "Human-Centered Design and Evaluation of Haptic Cueing for Teleoperation of Multiple Mobile Robots". In: 43.2 (2013), pp. 597–609 (cited on page 23).

[Spedicato–2016] S. Spedicato, A. Franchi, and G. Notarstefano. "From Tracking to Robust Maneuver Regulation: an Easy-to-Design Approach for VTOL Aerial Robots". In: *2016*. Stockholm, Sweden, May 2016, pp. 2965–2970 (cited on pages 20 and 146).

[Spica–2012] R. Spica, A. Franchi, G. Oriolo, H. H. Bülthoff, and P. Robuffo Giordano. "Aerial Grasping of a Moving Target with a Quadrotor UAV". In: *2012*. Vilamoura, Portugal, Oct. 2012, pp. 4985–4992 (cited on page 24).

[Spica–2013] R. Spica, P. Robuffo Giordano, M. Ryll, H. H. Bülthoff, and A. Franchi. "An Open-Source Hardware/Software Architecture for Quadrotor UAVs". In: *2nd*. Compiegne, France, Nov. 2013 (cited on pages 22, 56, 57 and 60).

[Staub–] N. Staub, M. Mohammadi, D. Bicego, Q. Delamare, H. Yang, D. Prattichizzo, P. Robuffo Giordano, D. J. Lee, and A. Franchi. "Tele-MAGMaS: a Human-assisted Aerial-Ground Manipulator System". In: **Accepted** (cited on pages 4, 5, 76 and 149).

[Staub–2015] N. Staub and A. Franchi. "Battery-aware Dynamical Modeling and Identification for the Total Thrust in Multi-rotor UAVs using only an Onboard Accelerometer". In: *2015*. Seattle, WA, May 2015, pp. 3341–3346 (cited on pages 4, 5, 55, 62, 63 and 147).

[Staub–2017] N. Staub, M. Mohammadi, D. Bicego, D. Prattichizzo, and A. Franchi. "Towards Robotic MAGMaS: Multiple Aerial-Ground Manipulator Systems". In: *2017*. Singapore, May 2017 (cited on pages 3, 5, 30, 51, 69, 83, 85, 149 and 150).

[Staub–2018] N. Staub, D. Bicego, Q. Sablé, V. Arellano, S. Mishra, and A. Franchi. "Towards a Flying Companion Paradigm: the OTHex". In: *2018*. Brisbane, Australia, May 2018 (cited on pages 4, 5, 78 and 149).

[Steich–2016] K. Steich, M. Kamel, P. Beardsley, M. K. Obrist, R. Siegwart, and T. Lachat. "Tree cavity inspection using aerial robots". In: *2016*. Oct. 2016, pp. 4856–4862 (cited on page 16).

[Suarez–2015a] A. Suarez, G. Heredia, and A. Ollero. "Compliant and Lightweight Anthropomorphic Finger Module for Aerial Manipulation and Grasping". In: *Robot 2015: Second Iberian Robotics Conference: Advances in Robotics, Volume 1*. Ed. by L. P. Reis, A. P. Moreira, P. U. Lima, L. Montano, and V. Muñoz-Martinez. Cham: Springer International Publishing, 2015, pp. 543–555 (cited on page 17).

[Suarez–2015b] A. Suarez, G. Heredia, and A. Ollero. "Lightweight compliant arm for aerial manipulation". In: *2015 IEEE/RSJ Int. Conf. on Intelligent Robots and Systems*. Hamburg, Germany, Sept. 2015, pp. 1627–1632 (cited on pages 17, 30, 96, 149 and 156).

[Suarez–2016] A. Suarez, G. Heredia, and A. Ollero. "Lightweight compliant arm with compliant finger for aerial manipulation and inspection". In: *2016*. Oct. 2016, pp. 4449–4454 (cited on page 17).

[Suarez–2017a] A. Suarez, A. E. Jiménez-Cano, V. Vega, G. Heredia, A. Rodriguez-Castaño, and A. Ollero. "Lightweight and Human-Size Dual Arm Aerial Manipulator". In: *2017 Int. Conf. on on Unmanned Aircraft Systems*. Miami, FL, June 2017, pp. 1778–1784 (cited on pages 14, 16, 143, 144 and 145).

[Suarez–2017b] A. Suarez, P. Ramon Soria, G. Heredia, B. Arrue, and A. Ollero. "Anthropomorphic, Compliant and Lightweight Dual Arm System for Aerial Manipulation". In: *2017*. Vancouver, Canada, Sept. 2017 (cited on pages 17, 96 and 156).

[Thomas–2013] J. Thomas, J. Polin, K. Sreenath, and V. Kumar. "Avian-Inspired Grasping for Quadrotor Micro UAVs". In: *2013 ASME Int. Design Engineering Technical Conf. and Computers and Information in Engineering Conf.* Portland, OR, Aug. 2013 (cited on pages 96, 97 and 98).

[Thomas–2016a] J. Thomas, G. Loianno, K. Daniilidis, and V. Kumar. "Visual Servoing of Quadrotors for Perching by Hanging From Cylindrical Objects". In: 1.1 (Jan. 2016), pp. 57–64 (cited on page 18).

[Thomas–2016b] J. Thomas, M. Pope, G. Loianno, E. W. Hawkes, M. A. Estrada, H. Jiang, M. R. Cutkosky, and V. Kumar. "Aggressive Flight for Perching on Inclined Surfaces". In: *Journal of Mechanisms and Robotics* 8.5 (May 2016) (cited on pages 12 and 141).

[Tognon–2016a] M. Tognon, S. S. Dash, and A. Franchi. "Observer-based Control of Position and Tension for an Aerial Robot Tethered to a Moving Platform". In: 1.2 (2016), pp. 732–737 (cited on page 24).

[Tognon–2016b] M. Tognon, A. Testa, E. Rossi, and A. Franchi. "Takeoff and Landing on Slopes via Inclined Hovering with a Tethered Aerial Robot". In: *2016*. Daejeon, South Korea, Oct. 2016, pp. 1702–1707 (cited on pages 12, 13, 65, 66, 136 and 142).

[Tognon–2017] M. Tognon, B. Yüksel, G. Buondonno, and A. Franchi. "Dynamic Decentralized Control for Protocentric Aerial Manipulators". In: *2017*. Singapore, May 2017, pp. 6375–6380 (cited on pages 16 and 96).

[Tomić–2014] T. Tomić and S. Haddadin. "A unified framework for external wrench estimation, interaction control and collision reflexes for flying robots". In: *2014*. Sept. 2014, pp. 4197–4204 (cited on pages 22 and 25).

[Tomić–2015] T. Tomić and S. Haddadin. "Simultaneous estimation of aerodynamic and contact forces in flying robots: Applications to metric wind estimation and collision detection". In: *2015*. May 2015, pp. 5290–5296 (cited on page 22).

[Tomić–2016] T. Tomić, K. Schmid, P. Lutz, A. Mathers, and S. Haddadin. "The flying anemometer: Unified estimation of wind velocity from aerodynamic power and wrenches". In: *2016*. Oct. 2016, pp. 1637–1644 (cited on page 21).

[Tsukagoshi–2015] H. Tsukagoshi, M. Watanabe, T. Hamada, D. Ashlih, and R. Iizuka. "Aerial manipulator with perching and door-opening capability". In: *2015*. May 2015, pp. 4663–4668 (cited on page 11).

[video 1–2015] **video 1**. *Total Thrust Modeling and Identification with Onboard Accelerometer and Battery*. `https://youtu.be/RdL3adVm6sA`. May 2015 (cited on pages 59 and 60).

[video 2–2016] **video 2**. *Aerial Robots with Rigid/Elastic-joint Arms: Controllability Preliminary Experiments*. `https://youtu.be/Gtojd5AyxtY`. Oct. 2016 (cited on pages 103 and 108).

[video 3–2017] **video 3**. *Towards Robotic MAGMaS: Multiple Aerial-Ground Manipulator Systems*. `https://youtu.be/ZW9M4YXLsXw`. May 2017 (cited on pages 73 and 74).

[video 4–2017] **video 4**. *Tele-MAGMaS Hanover System Presentation*. `https://vimeo.com/217252361`. Apr. 2017 (cited on pages 88 and 154).

[video 5–2017] **video 5**. *Tele-MAGMaS Hanover Demonstration*. `https://youtu.be/GRnGSvJGUKk`. Apr. 2017 (cited on pages 76, 88 and 154).

[video 6–2017] **video 6**. *Aerial-ground Cooperative Manipulation of Long Bars*. `https://youtu.be/TrrPEP3CNlY`. July 2017 (cited on pages 87, 153 and 154).

[video 7–2018] **video 7**. *OTHex Bar Lifting*. `https://youtu.be/AikN3_PgYU4`. May 2018 (cited on page 81).

[Vittorias–2010] I. Vittorias, H. B. Rached, and S. Hirche. "Haptic Data Reduction in Multi-DoF Teleoperation Systems". In: *Proceedings of the International Symposium on Haptics Audio-Visual Environments and Games (HAVE)*. 2010 (cited on page 86).

[Vlantis–2015] P. Vlantis, P. Marantos, C. P. Bechlioulis, and K. J. Kyriakopoulos. "Quadrotor landing on an inclined platform of a moving ground vehicle". In: *2015*. May 2015, pp. 2202–2207 (cited on page 24).

[Wilson–2015] D. Wilson, A. Goktogan, and S. Sukkarieh. "Guidance and Navigation for UAV Airborne Docking". In: *Proceedings of Robotics: Science and Systems*. Rome, Italy, July 2015 (cited on page 8).

[Wopereis–2017a] H. W. Wopereis, D. H. Ellery, T. H. Post, S. Stramigioli, and M. Fumagalli. "Autonomous and sustained perching of multirotor platforms on smooth surfaces". In: *2017 25th Mediterranean Conference on Control and Automation (MED)*. July 2017, pp. 1385–1391 (cited on pages 9, 12, 19 and 141).

[Wopereis–2017b] H. W. Wopereis, J. J. Hoekstra, T. H. Post, G. A. Folkertsma, S. Stramigioli, and M. Fumagalli. "Application of substantial and sustained force to vertical surfaces using a quadrotor". In: *2017*. May 2017, pp. 2704–2709 (cited on pages 12 and 142).

[Wu–2014] G. Wu and K. Sreenath. "Geometric Control of Quadrotors Transporting a Rigid-body Load". In: *2014*. Los Angeles, CA, Dec. 2014, pp. 6141–6148 (cited on page 24).

[Yang–2018] H. Yang, N. Staub, A. Franchi, and D. Lee. "Modeling and Control of Multiple Aerial-Ground Manipulator System with Load Flexibility". In: *2018*. Madrid, Spain, Oct. 2018 (cited on pages 4, 5, 113 and 149).

[Yeol–2014] J. W. Yeol and C. H. Lin. "Development of multi-tentacle micro air vehicle". In: *2014 International Conference on Unmanned Aircraft Systems (ICUAS)*. May 2014, pp. 815–820 (cited on page 17).

[Yüksel–2014a] B. Yüksel, C. Secchi, H. H. Bülthoff, and A. Franchi. "A Nonlinear Force Observer for Quadrotors and Application to Physical Interactive Tasks". In: *2014*. Besançon, France, July 2014, pp. 433–440 (cited on page 22).

[Yüksel–2014b] B. Yüksel, C. Secchi, H. H. Bülthoff, and A. Franchi. "Reshaping the Physical Properties of a Quadrotor through IDA-PBC and its Application to Aerial Physical Interaction". In: *2014*. Hong Kong, China, May 2014, pp. 6258–6265 (cited on pages 20 and 147).

[Yüksel–2015] B. Yüksel, S. Mahboubi, C. Secchi, H. H. Bülthoff, and A. Franchi. "Design, Identification and Experimental Testing of a Light-Weight Flexible-joint Arm for Aerial Physical Interaction". In: *2015*. Seattle, WA, May 2015, pp. 870–876 (cited on pages 17, 96, 106, 110, 156 and 157).

[Yüksel–2016a] B. Yüksel, G. Buondonno, and A. Franchi. "Differential Flatness and Control of Protocentric Aerial Manipulators with Any Number of Arms and Mixed Rigid-/Elastic-Joints". In: *2016*. Daejeon, South Korea, Oct. 2016, pp. 561–566 (cited on pages 96, 110 and 157).

[Yüksel–2016b] B. Yüksel, N. Staub, and A. Franchi. "Aerial Robots with Rigid/Elastic-joint Arms: Single-joint Controllability Study and Preliminary Experiments". In: *2016*. Daejeon, South Korea, Oct. 2016, pp. 1667–1672 (cited on pages 4, 5, 97, 101, 103, 104, 106, 110, 155 and 157).

[Yüksel–2016c] B. Yüksel, N. Staub, and A. Franchi. *Explicit Computations and Further Extensive Simulations for Rigid- or Elastic-joint Arm*. Tech. rep. hal-01345564. LAAS-CNRS, July 2016. URL: `https://hal.archives-ouvertes.fr/hal-01345564` (cited on pages 97, 101, 103, 104, 110, 155 and 157).

[Yüksel–2017] Burak Yüksel. "Design, Modeling and Control of Aerial Robots for Physical Interaction and Manipulation". ISBN 978-3-8325-4492-8. PhD thesis. Max Planck Institute for Biological Cybernetics, Tübingen, Institute of Systems Theory, and Automatic Control, University of Stuttgart, Feb. 2017 (cited on pages 12, 101 and 142).

[Zambelli–2015] A. Zambelli, S. Erhart, L. Zaccarian, and S. Hirche. "Dynamic Load Distribution in Cooperative Manipulation Tasks". In: *2015*. Hamburg, Germany, Sept. 2015, pp. 2380–2385 (cited on page 90).

[Zhao–2017] M. Zhao, K. Kawasaki, X. Chen, S. Noda, K. Okada, and M. Inaba. "Whole-body aerial manipulation by transformable multirotor with two-dimensional multilinks". In: *2017*. May 2017, pp. 5175–5182 (cited on pages 18 and 19).